TARDEC

---TECHNICAL REPORT---

No. 13754

1995 Presidential Award for Quality

TARDEC

A Ceramic Armor Material Database

January 1999

By

T. J. Holmquist
A. M. Rajendran
D. W. Templeton
K. D. Bishnoi
U. S. Army Tank Automotive Research,
Development and Engineering Center
(TARDEC) Attn: AMSTA-TR-R (MS 263)
Warren, MI 48397-5000

Approve for public release, distribution unlimited

U. S. Army Tank-Automotive Research,
Development, and Engineering Center
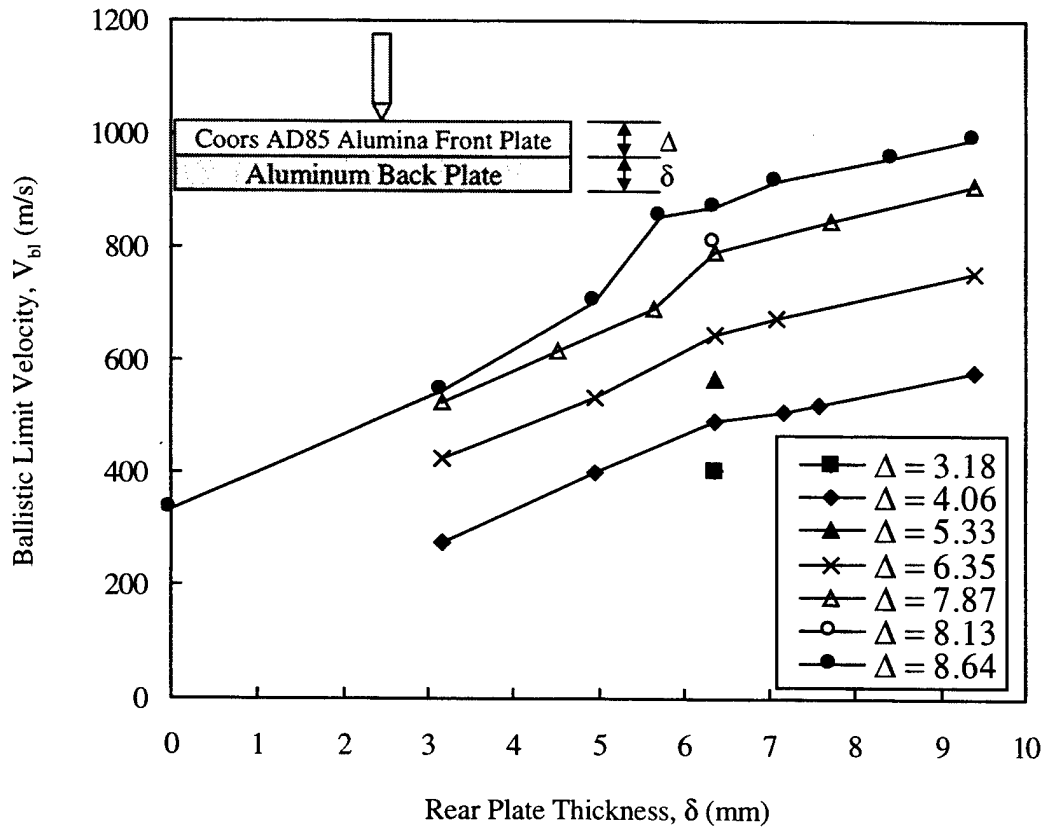Detroit Arsenal
Warren, Michigan 48397-5000

19990506 017

DTIC QUALITY INSPECTED 4

A Ceramic Armor Material Database

By

T. J. Holmquist
A. M. Rajendran
D. W. Templeton
K. D. Bishnoi

REPORT DOCUMENTATION PAGE

1. AGENCY USE ONLY (Leave blank)	2. REPORT DATE January 1999	3. REPORT TYPE AND DATES COVERED Interim

4. TITLE AND SUBTITLE

A Ceramic Armor Material Database

5. FUNDING NUMBERS

Contract Number
DAAH04-95-C-0008

6. AUTHOR(S)

T. J. Holmquist*, A. M. Rajendran**, D. W. Templeton, K. D. Bishnoi

7. PERFORMING ORGANIZATION NAME(S) AND ADDRESS(ES)

U. S. Army TARDEC, AMSTA-TR-R (MS 263)
Warren, MI 48397-5000
**Army Research Laboratory, AMSRL-WM-TD
Aberdeen Proving Ground, MD 21005-5069
*Army High Performance Computing Research Center
Minneapolis, MN 55415

8. PERFORMING ORGANIZATION REPORT NUMBER

TARDEC Technical Report #13754

9. SPONSORING / MONITORING AGENCY NAME(S) AND ADDRESS(ES)

Army High Performance Computing Research Center
1200 Washington Ave. South
Minneapolis, MN 55415

10. SPONSORING / MONITORING AGENCY REPORT NUMBER

11. SUPPLEMENTARY NOTES

12a. DISTRIBUTION / AVAILABILITY STATEMENT

Approved for public release, distribution is unlimited

12b. DISTRIBUTION CODE

13. ABSTRACT (Maximum 200 words)

This report compiles and documents a *Ceramic Armor Material Database*. Experimental data obtained from numerous journals and conference proceedings, by researchers of various disciplines, covering over thirty years are documented in this report. The data include nine different ceramic materials. The ceramics are Silicon Carbide, Boron Carbide, Titanium Diboride, Aluminum Nitride, Silicon Nitride, Aluminum Oxide (85% pure), Aluminum Oxide (high purity), Tungsten Carbide and Glass. For each ceramic material, experimental data are tabulated for the following experiment types; 1)mechanical tests, 2) hydrostatic tests, 3)plate impact tests, 4)semi-infinite penetration tests, 5)depth of penetration (DOP) tests, 6)perforation tests and 7) other tests. The data are documented in tabular form in metric units. A schematic of the experimental configuration, and graphs of the data, are also provided when appropriate. Information about each of the materials tested is also provided including such information as elastic wave velocities, density, grain size, porosity, material processing, elastic modulus, Hugoniot Elastic Limit (HEL) and chemical composition. Although this report was not intended to be an exhaustive search of the literature, an attempt has been made to compile as much data as possible.

14. SUBJECT TERMS

ballistic, ceramic, armor, impact, test, hydrostat, plate impact, penetration, perforation, DOP

15. NUMBER OF PAGES
228

16. PRICE CODE

17. SECURITY CLASSIFICATION OF REPORT UNCLASSIFIED	18. SECURITY CLASSIFICATION OF THIS PAGE UNCLASSIFIED	19. SECURITY CLASSIFICATION OF ABSTRACT UNCLASSIFIED	20. LIMITATION OF ABSTRACT UL

EXECUTIVE SUMMARY

This report is an initial attempt to compile and publish a collection of ceramic material test data available in the open literature. Data for nine ceramic armor materials are presented in this document. Information collected and disseminated in this report is intended for use by model developers, ceramic researchers, and ultimately, armor designers. Although a thorough attempt was made to gather all relevant data, some information was undoubtedly missed or overlooked. This report therefore is only the first edition, and it is intended that future volumes will include additional materials and data (especially pressure-shear plate impact data), as they become available.

iv

ACKNOWLEDGMENT

TABLE OF CONTENTS

1.0 INTRODUCTION

Over the past 30 years a substantial amount of ceramic test data has been generated. The majority of the data was generated over the last fifteen years and has focused primarily on armor development. The data were generated from a wide range of experiments, by researchers of various disciplines. The data are scattered in not easily accessible government and industry reports, journals and conference proceedings making it difficult for the user community, that is in need of the data, to obtain it. Therefore, it was felt that a document that compiled the various experimental data in one report, would be a helpful resource for the armor designer, ceramic researcher, and model developer. This report attempts to gather this data and organize it in a consistent, concise format allowing the researcher easy access and interpretation of the data.

The data collected in this report were obtained exclusively from open literature publications. Although numerous technical journals and conference proceedings were reviewed for this report, it was not an exhaustive search. An attempt was made to gather as much data as possible for each ceramic of interest, although in some instances an intense search of the literature provided only a small amount of data.

The ceramic materials chosen for inclusion in this report have, at one time or another, all been considered for armor applications and represent the primary ceramics considered for armor systems. The ceramics are Silicon Carbide, Boron Carbide, Titanium Diboride, Aluminum Nitride, Silicon Nitride, Aluminum Oxide, Tungsten Carbide and Glass. Glass, although typically not considered an armor grade ceramic for the defeat of kinetic energy penetrators, does exhibit a unique armor capability for the defeat of shaped charge jets. Glass was included in this report not only because of its armor applications, but also because of the extensive experimental database available, and academic interest. The glass material focused on herein is Soda Lime (Float) Glass.

Silicon Nitride ceramic is another material not typically associated with armor grade ceramics, but more commonly associated with high impact and wear resistant applications such as turbine blades. It is included in this report due to both plate impact and ballistic test data available in the literature.

Numerous grades of Alumina have been tested over the years, but the majority of Alumina data fall into one of two categories; either 85% pure Al_2O_3 or purity greater then 99% Al_2O_3. To make the task of gathering and organizing the Alumina data manageable, only two grades of Alumina were considered for this report, 85% pure and high purity Alumina (approximately 99% and above). The behavior of Alumina is influenced by the glassy interface between the grains. Reducing the glassy phase, such as in high purity Alumina, increases the overall performance of the material. Although 85% pure Al_2O_3 ceramic is known to be a poorer armor ceramic than high purity Alumina, it is included in this report due to the extensive testing available that can be used to better understand Alumina based ceramics.

1

To make a report such as this useful, the data must be organized and presented in a manner that is easily used. It was concluded that the most useful format for the researcher was to present the data in tabular form, but wherever possible provide a graphical representation of the data since this format is the most easily and quickly understood.

As was stated earlier, this report was not intended to be an exhaustive search of the literature, although an attempt was made to gather as much data as possible. If we missed some important data, it was not intentional, and please let us know for inclusion in future editions. We hope this report proves easy to use and is helpful in your research endeavors.

2.0 TEST DATA

The organization of the test data will be discussed in some detail in this section. The test data cover a wide range of testing, from uniaxial compression tests to ballistic impact tests.

At the top level, the test data are organized by material. There are nine materials for which test data are provided, and are listed below in the order in which they appear in this report.

1. Silicon Carbide
2. Boron Carbide
3. Titanium Diboride
4. Aluminum Nitride
5. Silicon Nitride
6. Aluminum Oxide (85% pure)
7. Aluminum Oxide (high purity)
8. Tungsten Carbide
9. Glass

The second level, or subsection level, provides the organizational framework for the test data. For each material eight subsections are provided. Each subsection houses a specific class of test data or material information. The eight subsections have descriptive titles that describe the data and are listed below in the order presented in the report.

1. Material Description
2. Mechanical Test Data
3. Hydrostatic Test Data
4. Plate Impact Test Data
5. Penetration (semi-infinite) Test Data
6. DOP Test Data
7. Perforation Test Data
8. Other Test Data

Within each subsection the data are documented in tabular form in SI units. When stresses are listed, they are considered positive in compression and negative in tension. Each test is given a four digit "test number" that uniquely identifies it among all other tests within the database. The test number can also be used to quickly identify the material and test it represents. The first digit identifies the material; the second digit identifies the type of test and the last two digits represent the entry number in the table. For example, the test number 3428 is the 28th entry in the table, documenting a plate impact test (4), for Titanium Diboride (3).

3

Different subsections could have been chosen, but it was concluded that the test data fell nicely into one of the above eight categories. Also included is a Material Description subsection that gives a description of each material tested. The following gives a brief description of each of the eight subsections.

Material Description_ This subsection provides information about each of the materials tested. We felt it was important to provide as much information on the materials as possible since there always seems to be the question "exactly what material was tested". This subsection lists all the material information provided by the respective experimentalist and is presented in tabular form. The material information listed in this section include the manufacturer, trade name, processing, grain size, density, porosity, elastic wave velocities, elastic modulus, and Poison's ratio. Nominal values of the compressive strength, spall strength, tensile strength and Hugoniot Elastic Limit (HEL) are also included when available. In a few cases the chemical composition of the material is known and is also included. Blanks in the table indicate the experimentalist did not provide the data. We did not add any information to the table that was not provided in the reference or obtained directly from the author, other than calculating elastic wave speeds and modulus from the given data. Each material is given a "material number" that identifies it and a reference number where the information was obtained. Material numbers are used throughout the report to identify the specific material being tested.

Mechanical Test Data_ This subsection presents test data that we have identified as "mechanical test data". The data are typically quasi-static or Hopkinson bar uniaxial compression data, although some multiaxial data are listed. The data are presented in tabular form listing the material number, the stress state at failure, and the average strain rate of the test. If other information is provided, such as temperature, it is also listed. Stresses are considered positive in compression and negative in tension, which is consistent throughout the report. At the bottom of each table are a list of comments that provide additional information on the test data if further explanations are warranted. Lastly, on the right side of the table is the name of the first author, and corresponding reference number identifying the publication containing the test data.

Hydrostatic Test Data_ This subsection presents the hydrostatic response of the material. Typically the data are generated using a Diamond Anvil Cell. This test technique involves applying a mechanical load to a fluid that surrounds the specimen of interest. The pressure is determined from a calibrated material immersed in the fluid and the material volume is determined by x-ray diffraction methods. The data are presented in tabular form listing the material number, pressure and volume or density. At the bottom of each table are a list of comments that provide additional information on the individual test data if further explanations are required. Lastly, on the right side of the table is the name of the first author, and corresponding reference number identifying the publication containing the test data. A graphical representation of the data is also provided where the pressure is plotted as a function of volume.

Plate Impact Test Data_ This subsection presents plate impact test data. Plate impact experiments are performed to investigate material behavior at high pressures and high

strain rates. The most frequently reported experimental technique is based on a configuration in which a circular disk of smaller thickness impacts, in a planar manner, a stationary circular disk of larger thickness. The impactor is often called the flyer plate and the stationary disk the target plate. The target plate is always made of the material of interest. In a symmetric impact, both plates are made of the same material. In a non-symmetric impact the flyer plate is made of a different material. The stress state in the plates is triaxial and the strain state is one dimensional. The diagnostic measurements include: (1) the use of a velocity interferometry (VISAR) to record the material particle velocity history at the back of the target plate, and (2) the use of a stress gauge between the target plate and a plastic window to record the stress vs. time history. The diagnostic measurements are used in the construction of the "Hugoniot Curve."

In a plate impact experiment, compressive stresses are produced and transmitted immediately from the plane of impact to the adjacent stress free areas of the material in the form of a stress pulse. If the stress pulse is great enough, the elastic limit of the material is exceeded and permanent (plastic) deformation will occur. The elastic limit is referred to as the Hugoniot Elastic Limit (HEL) of the material and is the maximum principal stress component under one-dimensional strain at strain rates of approximately $10^5 s^{-1}$. The compressive strength (Y) of the material, under plate impact conditions, can be determined straightforwardly using following relationship:

$$Y = HEL\{2G/(K + 4/3G)\}$$

where the HEL is the Hugoniot Elastic Limit and K and G are the bulk and shear moduli, respectively.

Measurement of the free surface velocity at the rear of the target provides data for the loading (compression) and unloading (release) paths. When the release waves interact, tensile stresses of high amplitudes under a triaxial tensile stress state are created, subsequently leading to failure of the material. The magnitude of the principal tensile stress is often referred to as the spall strength of the material. In metals, such failure occurs only when the shock stress exceeds the HEL; in ceramics, however, tensile failure can occur even at stress levels below the HEL.

The data that are documented for plate impact experiments vary from researcher to researcher. In some cases the particle (mass) and wave (shock) velocities for both the elastic and plastic waves are measured from which both the HEL and peak Hugoniot state are determined. Some researchers use Manganin gauges imbedded in the material and measure the stress states directly. While still others use laser interferometry techniques to measure the complete particle velocity time history profile of the material. Because of these various experimental techniques used for data acquisition the format in which the data is documented in this section also varies. (Note: "plastic" may not be the correct nomenclature when discussing the deformation wave in ceramics but it will be used here due to the general understanding that plastic refers to the behavior of the material after exceeding the HEL.)

For each set of experiments a figure describing the initial geometry is presented, followed by a table listing the results. The format of the table is determined by the documented results of the respective experimentalist, which varies as discussed above. The table typically lists the material number, initial conditions, elastic response and deformational response. For both the elastic and deformational regime the table will list the particle and shock velocity, stress and density, if available. At the bottom of each table are a list of comments that provide additional information on the individual test data if further explanations are required. In some cases the particle velocity time histories (wave profiles) are provided and are presented in graphical form following the table.

Penetration (semi-infinite) Test Data_ This subsection presents ballistic penetration test data. What is required of the data, to fall into this subsection, is that nearly all of the penetration must occur in the ceramic material. The only non-ceramic material penetrated, if any, is typically a thin metallic cover plate. For each set of experiments a figure describing the initial geometry of the penetrator and target is presented, followed by a graphical representation of the results. Finally, a table listing the results is provided. The table typically lists the material number, specific penetrator and target characteristics, impact velocity, and penetration. At the bottom of each table is a list of comments that provide additional information on the individual test data if further explanations are required.

DOP Test Data_ This subsection presents ballistic penetration test data where the target is in the Depth-of-Penetration (DOP) configuration. The DOP test has been used to investigate the ballistic performance of ceramic tiles since approximately 1986 [68]. The DOP test is probably the most widely used ballistic test to evaluate ceramic materials. The typical DOP configuration consists of a ceramic tile placed on a steel base target. A penetrator impacts and perforates the ceramic tile and continues into the base target. The penetration into the base target is generally referred to as the residual penetration and is used to determine the ceramic ballistic mass efficiency. A common equation to determine the mass efficiency of the ceramic, for a given velocity, is shown in equation 1[86].

$$E_m = (P_{RHA} - P_r)\rho_{RHA} / (t_c\ \rho_c)$$ (1)

Where: E_m = ceramic ballistic mass efficiency
P_{RHA} = penetration depth into steel with no ceramic
P_r = residual penetration into steel base target after perforating ceramic
ρ_{RHA} = density of the steel
t_c = ceramic thickness
ρ_c = density of ceramic

For each set of experiments in this subsection, a figure describing the initial geometry of the penetrator and target is presented. Typically a graphical representation of the results are also presented. Finally a table listing the results is provided. The table typically lists the material number, specific penetrator and target characteristics, impact velocity, and

residual penetration. In some cases the penetrators penetration capability into the base target only (no ceramic) is also provided which is required to determine the ceramic ballistic mass efficiency as described in equation 1. At the bottom of each table are a list of comments that provide additional information on the test data if further explanations are warranted.

Perforation Test Data_ This subsection presents ballistic test data where the target is generally perforated by the penetrator. Targets are typically comprised of a ceramic front layer and a metallic rear layer and are commonly used in light armor applications. Typical test data extracted from the experiments are the residual penetrator characteristics after exiting the target. In some cases the ballistic limit velocity, V_{bl}, is provided for a specific penetrator and target. The ballistic limit velocity is defined as the velocity of a penetrator, where if shot 100 times at a specific target at the same velocity, 50 would be stopped in the target and 50 would perforate the target.

For each set of experiments a figure describing the initial geometry of the penetrator and target is presented, followed by a table listing the results in tabular form. The table typically lists the material number, specific penetrator and target characteristics and ballistic limit velocity, V_{bl}. At the bottom of each table are a list of comments that provide additional information on the test data if further explanations are warranted.

Other Test Data_ This subsection is a catch all for other experimental data that does not fall into one of the previous six. There are generally very little data in this subsection and for some materials there are no data at all. Some examples of test data that are presented in this subsection include impact response of ceramic bars, prefractured ceramic behavior and evaluation of fracture propagation. Generally, for each experiment documented in this subsection, a figure describing the initial test set up is presented, followed by a table summarizing the results.

The data documented in this report reflects experimental work obtained from over ninety references. Although, a large amount of data was gathered for this report, not all of the ceramic materials had a complete set of test data. Table 2.1 shows what data were available for each ceramic and what references the data were obtained from. This table shows that for some ceramics there is a wealth of data while for others there is very little.

7

Table 2.1   Experiments for Numerous Ceramic Materials with Corresponding References.

	Test	Material								
		SiC	B_4C	TiB_2	AlN	Si_3N_4	Al_2O_3 (85%)	Al_2O_3 (high purity)	WC	Glass
Mechanical Testing	Uniaxial/Multiaxial Compression	3, 4, 5, 10, 92	26, 46	46	12, 13, 83, 84	3	11	13, 14, 26		7
	Hopkinson Bar	3, 5, 4, 92	46	46	12, 83, 84	3				7
	Hydrostatic Testing	2		19	18, 71			15, 16, 17		
Plate Impact	Hugoniot Longitudinal Stress	1, 52, 94, 95	25, 30, 90	1, 64, 82	51, 52, 72	44, 49	30, 38, 50, 65	25, 29, 30, 48, 52, 65	52, 75	7, 62, 80
	Hugoniot Transverse Stress	93, 95		87	51		50			80
	Wave Profile	52	52	52, 82	52	52, 49		52	52	7
	Spall	52, 81	52, 81	52, 59, 81	52	52	73	48, 52	52	47
Ballistic Testing	Penetration (semi-infinite)	6	22, 89		21			35, 42		7, 9
	DOP Data	33, 39, 85, 91	85, 91	39, 41, 85, 91	33, 85, 91	44	32, 39, 41, 66, 85	31, 34, 37, 40, 41, 67, 86		41
	Perforation	26	24, 26, 27	26			23-28	21, 26, 36, 78	26	43

2.1 SILICON CARBIDE

2.1.1 Material Description for Silicon Carbide

Descriptions for the Silicon Carbide materials used throughout Section 2.1 are presented in Table 2.1.1.1. The data were obtained directly from the corresponding reference. When specific information was not available it was left blank. Each material is given a specific material number which is used throughout Section 2.1 to identify it when being tested. The strength values, (Compressive, Tensile, HEL and Spall), are nominal values and are included in the table for comparison purposes. Occasionally researchers will determine the chemical composition of the material being tested to further characterize the material, Table 2.1.1.1 includes this data when available.

Table 2.1.1.1 Description of the Silicon Carbide Materials Tested

		Material Number							
		101	102	103	104	105	106	107	108
Reference		1	2, 3, 5, 10	4	6	26	52, 54	52	69
Manufacturer		Carborundum	Carborundum		Cercom	Carborundum	Eagle Picher	Cercom	Cercom
Trade Name/Description		KT-SiC	α-SiC		SiC-B	KT-SiC		SiC-B	SiC-B
Processing		Hot Pressed	Sintered		Hot Pressed*		Hot Pressed	Hot Pressed	Hot Pressed*
Average Grain Size	(μm)		3		2		7	4	2
Density	(kg/m³)	3090	3200	3100	3220	3090	3177	3150	3180
Void Fraction		0.040					0.01		
Longitudinal Velocity	(m/s)	11400	12120			11000	12060	12220	12250
Shear Velocity	(m/s)	7270	7500			7200	7670	7620	7765
Bulk Velocity	(m/s)	7710	8480			8050	8190	8480	8350
Young's Modulus, E	(GPa)	378	428	380	427	378	434	433	427
Shear Modulus, G	(GPa)	163	180	157		160	187	183	195
Bulk Modulus, K	(GPa)	184	230	218		200	213	227	223
Poisson Ratio		0.157	0.19	0.21		0.18	0.161	0.182	0.14
Compressive Strength	(GPa)		3.9						3.41
Tensile Strength	(GPa)		0.345						
HEL	(GPa)	8.0				8.0	15.0		
Spall Strength	(GPa)						0.35		
Impurities	(%wt)								
B		0.3							
Al₂O₃		0.02							
TiO₂		0.1							
VO		0.02							
CrO₃		0.02							
MnO		0.05							
Fe₂O₃		0.3							
NiO		0.02							

* Pressure Assisted Densified (PAD)

Table 2.1.1.1 Description of the Silicon Carbide Materials Tested, Continued.

		Material Number						
		109	110	111	112	113	114	115
Reference		81	85	52	52	91	92, 95	92, 95
Manufacturer			Dow	Cercom	Cercom			
Trade Name/Description				SiC-N[1]	SiC-C[2]			
Processing		Hot Pressed		Hot Pressed	Hot Pressed		Reaction Bonded	PS[3]
Average Grain Size	(μm)			4	1		1.16	4.48
Density	(kg/m³)	3190	3160			3150	3210	3163
Void Fraction								
Longitudinal Velocity	(m/s)	12110	11760				11890 +-10	11940 +-10
Shear Velocity	(m/s)	7650	7510				7450 +-10	7570 +-10
Bulk Velocity	(m/s)	8284	7943				8210	8130
Young's Modulus, E	(GPa)	437	412			430	420	420
Shear Modulus, G	(GPa)	187	178				178	181
Bulk Modulus, K	(GPa)	219	199				216	209
Poisson Ratio		0.168	0.156				0.18	0.16
Compressive Strength	(GPa)					2.5	4.5	5.2
Tensile Strength	(GPa)							
HEL	(GPa)	13.0-14.7					13.2+-0.3	13.5+-0.3
Spall Strength	(GPa)	0.58-1.07						

[1]This material is an improvement of the SiC-B material (material #107) in which a wet milling process is used to achieve a high homogeneity in the chemistry and microstructure.

[2] This material is yet a further improvement of the SiC-N material (material #111) in which the nominal grain size of the ceramic is reduced to approximately 1μm.

[3]Pressureless Sintered

Table 2.1.1.1 Description of the Silicon Carbide Materials Tested, Concluded.

		Material Number						
		116	117	118				
Reference		92, 95	93, 94	39				
Manufacturer			Cercom					
Trade Name/Description			SiC-B[5]					
Processing		PAD[4]	PAD[4]					
Average Grain Size	(μm)	2.90	4.0					
Density	(kg/m³)	3238	3214+-14	3170				
Void Fraction			~0					
Longitudinal Velocity	(m/s)	12340 +-10	12180+-90					
Shear Velocity	(m/s)	7780 +-10	7740+-50					
Bulk Velocity	(m/s)	8460	8275					
Young's Modulus, E	(GPa)	459	448					
Shear Modulus, G	(GPa)	196	193					
Bulk Modulus, K	(GPa)	232	220					
Poisson Ratio		0.17	0.16					
Compressive Strength	(GPa)	5.2						
Tensile Strength	(GPa)							
HEL	(GPa)	15.7+-0.3	11.5					
Spall Strength	(GPa)							

[4]Pressure Assisted Densification

[5]Crystal structure is α-SiC type 6H

2.1.2 Mechanical Test Data for Silicon Carbide

The following section presents mechanical test data for various Silicon Carbide materials. A typical test specimen showing the stress configuration is shown in Figure 2.1.2.1. Compression is taken as positive and tension as negative. Loading is generally uniaxial compression in the z direction and is increased until the material fails, although some researchers use more complex loading techniques to vary the stress state at failure.

Mechanical test data performed by Lankford [3, 5, 10] are presented in Table 2.1.2.1. The stress state at failure is given as a function of average strain rate, $\dot{\varepsilon}$, and temperature. Both quasi-static and Hopkinson bar experiments were performed.

Hopkinson bar data performed by Anderson *et al.* [4] are presented in Table 2.1.2.1. The normal stress σ_z at failure is given as a function of lateral confinement, σ_x, σ_y, and average strain rate, $\dot{\varepsilon}$.

Mechanical test data performed by Pickup and Barker [92] are also presented in Table 2.1.2.1. Both quasistatic and Hopkinson bar experiments were performed on three different Silicon Carbide materials. The objective of the experimental program was to investigate both low and high rate compressive strength as a function of material processing. Reaction bonding (material #114), pressureless sintered (material #115), and pressure assisted densification (material #116) were the processing techniques investigated.
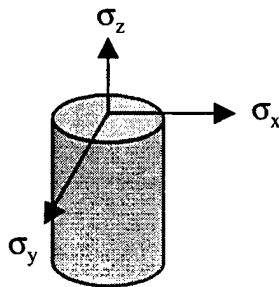
Figure 2.1.2.1 Description of a Typical Mechanical Test Specimen

Table 2.1.2.1 Summary of Experimental Results for Silicon Carbide

Silicon Carbide							
Test Number	Material Number	σ_z (GPa)	σ_x (GPa)	σ_y (GPa)	$\sim \dot{\varepsilon}$ (s^{-1})	Temperature (degrees C)	Reference
1201	102	3.82	0	0	7×10^{-5}	-200	3, 5, 10 (Lankford)
1202	102	3.59	0	0	7×10^{-5}	-200	
1203	102	3.83	0	0	7×10^{-5}	Ambient	
1204	102	3.94	0	0	7×10^{-5}	Ambient	
1205	102	4.11	0	0	7×10^{-5}	570	
1206	102	2.17	0	0	7×10^{-5}	800	
1207	102	3.89	0	0	2×10^{-1}	Ambient	
1208	102	3.98	0	0	2×10^{-1}	Ambient	
1209	102	4.73	0	0	3×10^{2}	Ambient	
1210	102	5.67	0	0	1×10^{3}	Ambient	
1211	102	6.28	0	0	2×10^{3}	Ambient	
1212	103	5.12	0	0	1.8×10^{3}	Ambient	4 (Anderson)
1213	103	5.91	0.10	0.10	1.8×10^{3}	Ambient	
1214	103	7.02	0.20	0.20	1.8×10^{3}	Ambient	
1215	114	4.48+-.18	0	0	1×10^{-3}	Ambient	
1216	114	6.72+-.27	0	0	1×10^{3}	Ambient	92 (Pickup)
1217	115	5.21+-.50	0	0	1×10^{-3}	Ambient	
1218	115	7.47+-.32	0	0	1×10^{3}	Ambient	
1219	116	5.15+-.35	0	0	1×10^{-3}	Ambient	
1220	116	8.17+-.16	0	0	1×10^{3}	Ambient	

Test 1201-1211: the test data is from work by Lankford. Compressive strength was investigated for both quasi-static and Hopkinson bar experiments. Quasi-static experiments were also performed as a function of temperature.

Test 1212-1214: the test data is from work by Anderson. Compressive strength was investigated as a function of confining pressure using the Hopkinson pressure bar.

Test 1215-1220: the test data is from work by Pickup and Barker[92]. Quasi-static and Hopkinson bar experiments were performed on three Silicon Carbide materials. The primary difference in the materials was how they were processed.

2.1.3 Hydrostatic Test Data for Silicon Carbide

This section presents the hydrostatic response for Silicon Carbide. The experimental data were obtained using a Diamond Anvil Cell by Bassett et al.[2] and are presented graphically in Figure 2.1.3.1 and in tabular form in Table 2.1.3.1. The table presents the material tested, the pressure, P, the relative volume, V/V_0, where V is the measured volume and V_0 is the initial volume, and the density, ρ, for each measurement recorded.
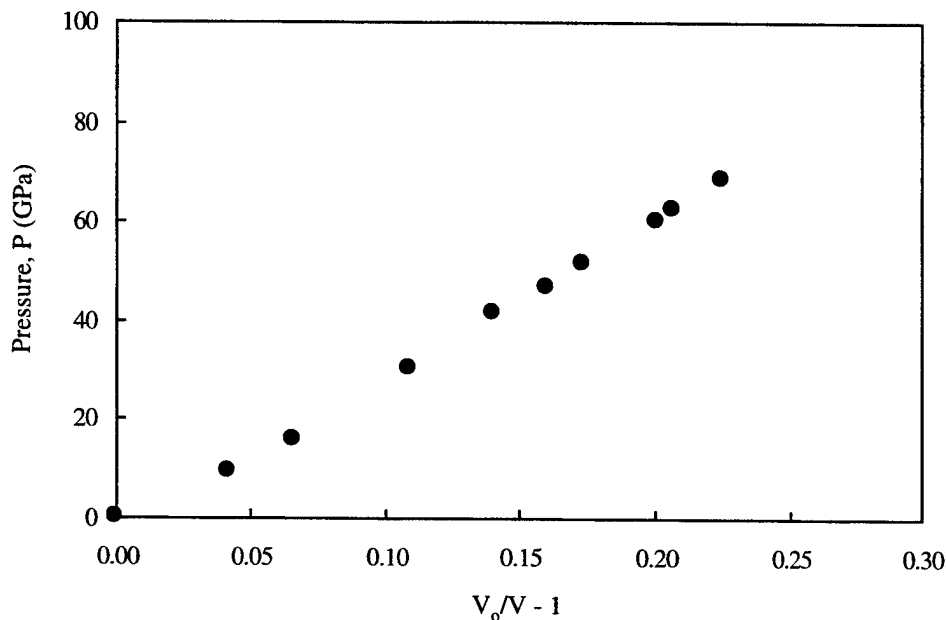
Figure 2.1.3.1 Pressure vs. Volume Relationship for Silicon Carbide, Bassett et al.[2].

Table 2.1.3.1 Summary of Experimental Results Documenting the Hydrostatic Response of Silicon Carbide, Bassett et al. [2].

Silicon Carbide				
Test Number	Material Number	P (GPa)	V/V_0	ρ (kg/m^3)
1301	102	0	1.0	3200
1302	102	9.4	0.960	3333
1303	102	15.8	0.938	3412
1304	102	30.4	0.902	3548
1305	102	41.6	0.877	3649
1306	102	46.9	0.862	3712
1307	102	51.6	0.852	3756
1308	102	60.1	0.833	3842
1309	102	62.6	0.829	3860
1310	102	62.6	0.829	3860
1311	102	68.4	0.817	3917
Test 1301-1311: the test data is from work by Bassett. the data was obtained using a diamond anvil cell. NaCl was used as the pressure medium. An energy dispersive method was used to collect diffraction data.				

2.1.4 Plate Impact Test Data for Silicon Carbide

This section presents plate impact results, performed by numerous researchers, using various Silicon Carbide materials. A typical plate impact test configuration is presented in Figure 2.1.4.1. The peak stress, σ_z, occurs in the z-direction and is generally measured for both the elastic and plastic response. The lateral stresses, σ_x and σ_y, occur due to the uniaxial strain configuration of the experiment, and are typically not measured. The peak stress for the elastic regime is referred to as the Hugoniot Elastic Limit (HEL) and has become a fundamental property of ceramics. The peak stress for the plastic response is generally referred to as the peak Hugoniot stress. The particle velocity and wave velocity for both the elastic and plastic waves are typically measured and documented herein. In some cases the entire particle velocity time history is measured using laser velocity interferometry techniques (VISAR). VISAR traces provide direct information on the material response and are included in this section when available.

The results from Gust et al. [1] are summarized in Table 2.1.4.1. The shock velocity, particle velocity, peak stress, σ_z, and density, ρ, for both the elastic and plastic waves are presented.

A description of the plate impact test configuration used by Grady and Moody [52] is presented in Figure 2.1.4.2. Four Silicon Carbide materials were investigated. The specific test dimensions and some limited results are summarized in Table 2.1.4.2. Compression and release behavior of the Silicon Carbide was measured by monitoring the ceramic-window interface velocity using laser velocity interferometry techniques (VISAR). The interface velocity profiles reflect the uniaxial strain loading and unloading behavior of the material and are presented in Figures 2.1.4.3-5 .

A description of the plate impact test configuration used by Winkler and Stilp [81] is presented in Figure 2.1.4.6. The objective of this experimental study was to investigate spall as a function of peak compressive stress. The specific test dimensions and the results are summarized in Table 2.1.4.3. Only one experiment exceeded the HEL. Compression and release behavior of the Silicon Carbide was measured by monitoring the ceramic free surface velocity using laser velocity interferometry techniques (VISAR). The interface velocity profiles for three experiments are presented in Figure 2.1.4.7 where the pullback representing the spall behavior is clearly shown.

Descriptions of the plate impact test configurations used by Feng et al. [93, 94] are presented in Figure 2.1.4.8. The objective of this experimental program was to investigate material strength as a function of peak longitudinal stress. Two experimental programs were performed, one to obtain longitudinal stress states[94] and the other to obtain transverse stress states [93]. When both the longitudinal and transverse stress states are known, the hydrostatic, deviatoric and shear response can be obtained. The same Silicon Carbide material was used for both test series. The peak stress and density, for all the experiments, are presented in Table 2.1.4.4. Since references [93, 94] only document peak stress and density, Table 2.1.4.4 does not attempt to list elastic and plastic components, but simply lists the peak stress and density as presented in the references.

A description of the plate impact test configuration used by Bourne et al. [95] is presented in Figure 2.1.4.9a. The objective of this experimental program was to investigate material strength as a

14

function of peak longitudinal stress for three Silicon Carbide materials. Plate impact experiments were performed using both longitudinal and transverse manganin gauges. For most of the experiments the transverse gauge indicated the occurrence of a failure wave. Typical gauge signals are presented schematically in Figure 2.1.4.9b. The transverse stress state was obtained before and after the arrival of the failure wave and is presented in tabular form in Table 2.1.4.5, also included are the longitudinal stresses.
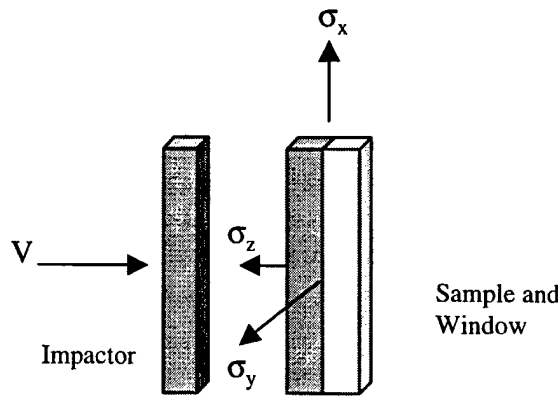
Figure 2.1.4.1 Description of a Typical Plate Impact Test Configuration including Stress Orientations

Table 2.1.4.1 Summary of Experimental Plate Impact Results from Gust et al.[1].

Silicon Carbide											
Test Number	Material Number	Initial Density ρ_o (kg/m^3)	Elastic Regime (HEL)				Plastic Regime				Ref.
			Shock Velocity (m/s)	Particle* Velocity (m/s)	σ_z (GPa)	ρ (kg/m^3)	Shock Velocity (m/s)	Particle# Velocity (m/s)	σ_z (GPa)	ρ (kg/m^3)	
1401	101	3084	11650	121	4.4	3119	8600	593	17.4	3224	1 (Gust)
1402	101	3059	11350	130	4.5	3094	8790	704	19.5	3313	
1403	101	3108	11600	269	9.7	3183	9390	677	20.8	3332	
1404	101	3109	11890	269	9.9	3182	8890	811	24.8	3376	
1405	101	3059	11730	273	9.8	3132	8770	859	25.4	3364	
1406	101	3087	11900	205	7.5	3141	8920	1070	31.3	3520	
1407	101	3108	11240	217	7.6	3170	8530	1345	37.3	3612	
1408	101	3049	11640	301	10.6	3130	8440	1475	40.8	3661	
1409	101	3069					9510	2050	61.5	3917	
1410	101	3090					9630	2080	62.8	3920	
1411	101	3056					10130	2470	77.9	4068	
1412	101	3111					10710	2820	94.0	4223	
1413	101	3069					10500	2860	92.1	4218	
1414	101	3103					10660	2720	90.1	4168	

Test 1401-1414: the test data is from work by Gust. As is shown there is a large scatter in the HEL. Ref. 1 documents the HEL as 8.0 + - 3.0 GPa.

* The elastic particle velocity presented here is half the measured free surface velocity ($U_p = 1/2U_{fs}$).

In Reference 1 the plastic particle velocity was calculated by $U_p = 1/2U_{fs}$ and by impedance matching. The particle velocity presented here is an average of the two.
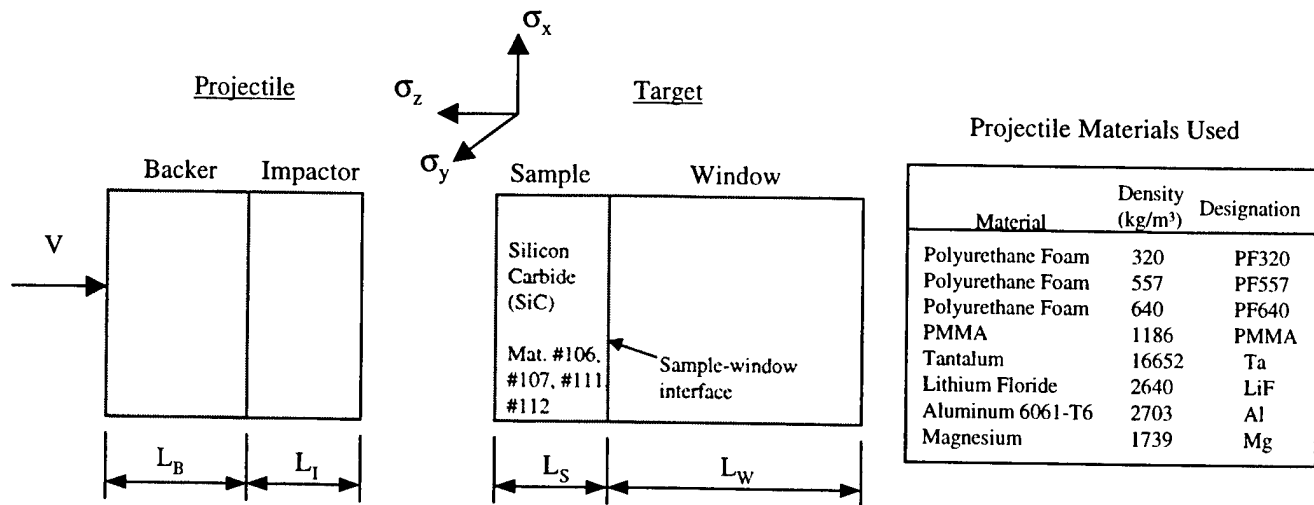
Figure 2.1.4.2 Description of the Plate Impact Test Configuration used by Grady and Moody [52] including the Stress Orientation and Materials used for the Projectile.

Table 2.1.4.2 Summary of Experimental Plate Impact Initial Conditions and Results from Grady and Moody [52].

Silicon Carbide														
		Initial Conditions									Hugoniot Results			
		Projectile				Target								
Test Number	Material Number	V (m/s)	Backer Material	L_B (mm)	Impactor Material	L_I (mm)	Sample Density (kg/m³)	L_S (mm)	Window Material	L_W (mm)	Elastic Regime (HEL) σ_z (GPa)	ρ (kg/m³)	Plastic Regime σ_z (GPa)	ρ (kg/m³)
1415	106	1542	PF320	6.0	SiC	3.987	3177	8.939	LiF	25.4	14.8	3272	27.6	3409
1416	106	2100	PF640	6.0	SiC	3.995	3177	8.940	LiF	25.4	15.3	3276	36.5	3519
1417	106	2118	PF640	6.0	Ta	1.516	3177	8.956	LiF	25.4	14.9	3273	48.7	3658
1418	106	612	PF320	6.0	SiC	4.958	3177	9.841	LiF	25.4				
1419	106	2206	Ta	1.510	LiF	3.297	3177	4.963	LiF	25.4				
1420	107	535	PMMA	6.35	Al	0.990	3221	4.035	LiF	9.196				
1421	107	1566	PF320	8.0	SiC	4.490	3220	9.014	LiF	25.4				
1422	107	2259	PF557	8.0	SiC	4.516	3220	8.993	LiF	25.4				
1423	111	485	PF640	8.04	Mg	0.5974	3227	4.512	PMMA	24.2				
1424	111	1596	PF328	8.0	SiC	4.503	3220	9.012	LiF	25.4				
1425	111	2352	PF640	8.0	SiC	4.504	3230	8.998	LiF	25.4				
1426	112	2385	PF640	8.0	SiC	4.527	3216	8.995	LiF	25.4				
1427	112	489	PMMA	6.35	Mg	0.60	3244	4.025	LiF	9.20				
1428	112	485	PF640	8.03	Al	1.042	3226	4.527	PMMA	24.2				
1429	112	1605	PF320	8.0	SiC	4.506	3220	9.013	LiF	25.4				

Test 1415-1429: the test data is from work by Grady. Material #106 is Silicon Carbide manufactured by Eagle Picher, having a nominal initial density = 3177kg/m³. Material #107 is Silicon Carbide manufactured by Cercom having an initial density = 3150kg/m³. The above table primarily provides the initial conditions for the plate impact experiments, although the elastic and plastic stress-density states are provided when available.
Test 1415-1417: the HEL and peak Hugoniot stress and density obtained from Ref. 54-57.
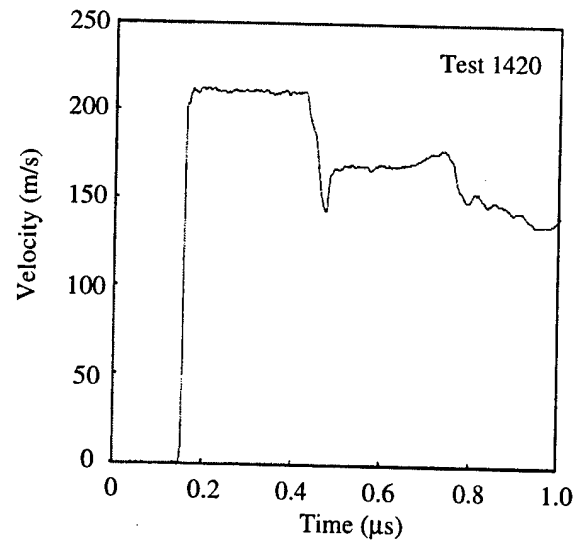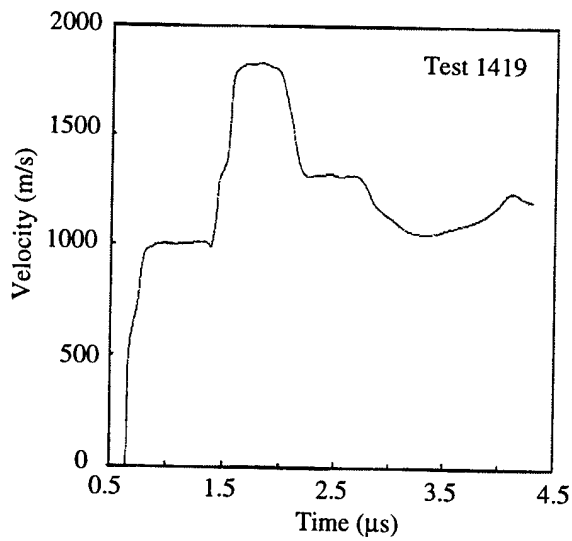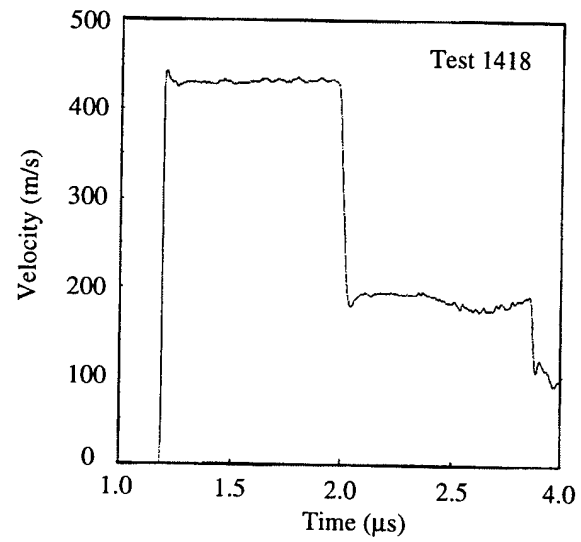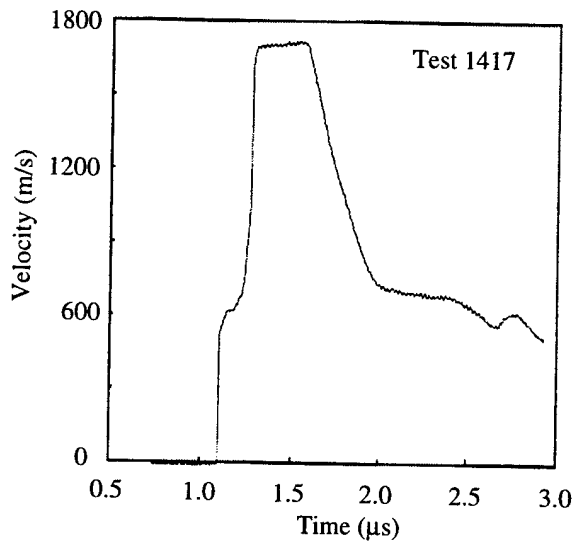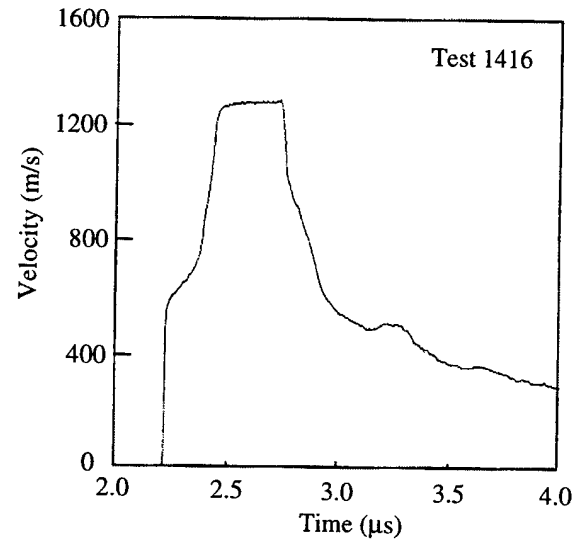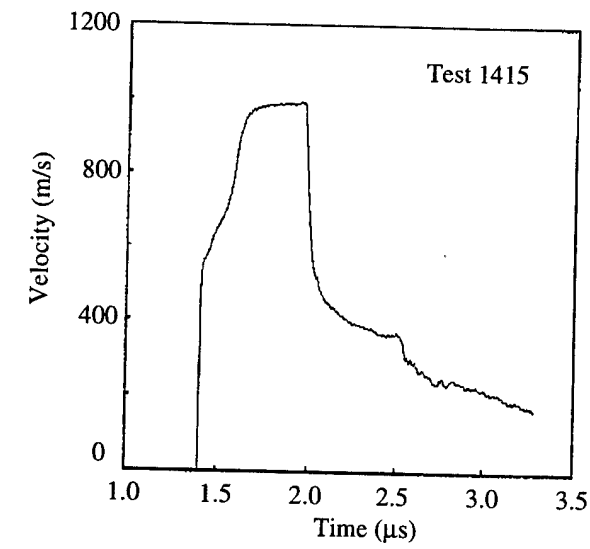
Figure 2.1.4.3 Ceramic-Window Interface Velocity Profiles from Grady and Moody [52] for Tests 1415-1420.

17
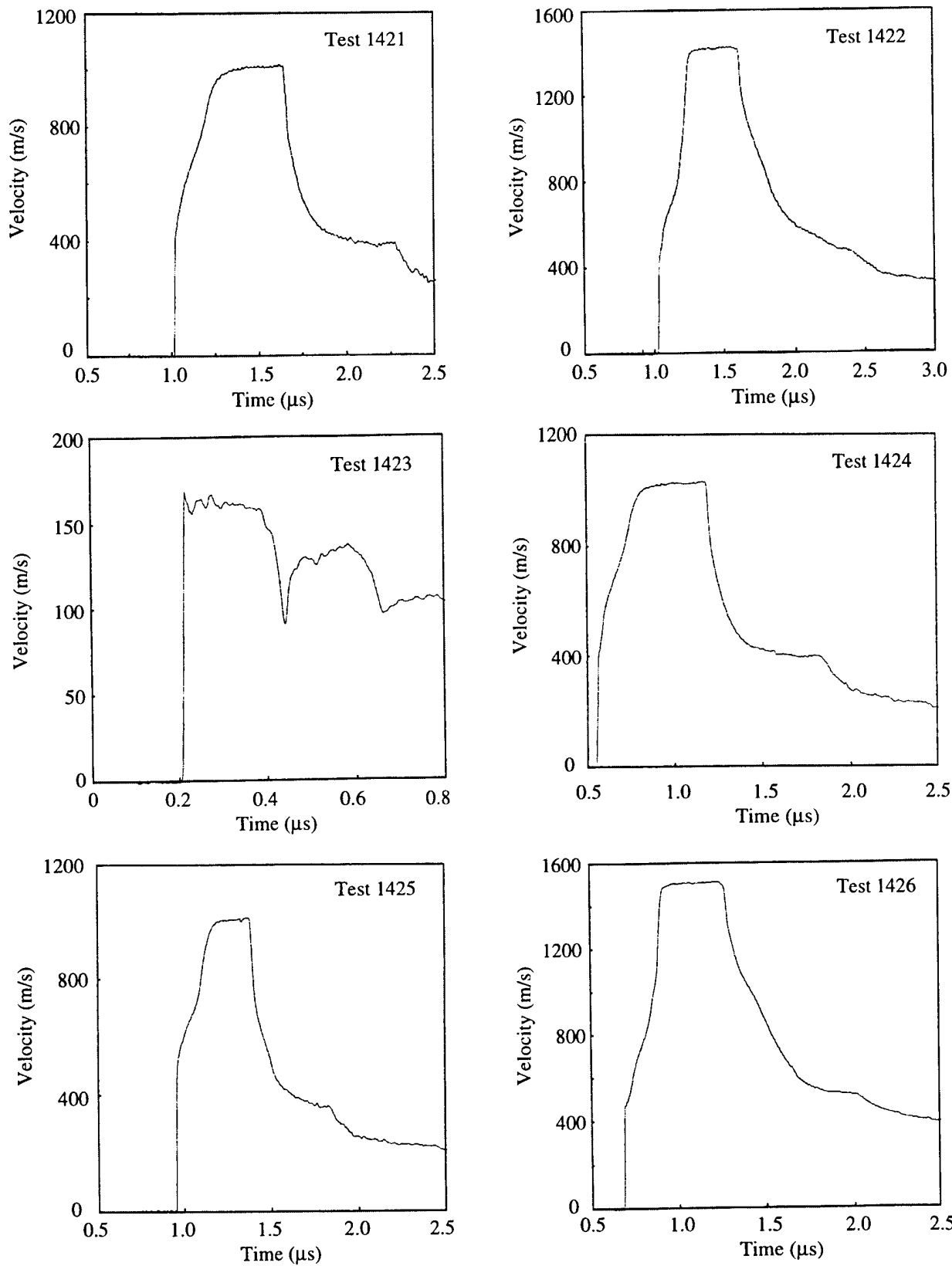
Figure 2.1.4.4 Ceramic-Window Interface Velocity Profiles from Grady and Moody [52] for Tests 1421-1426.

18
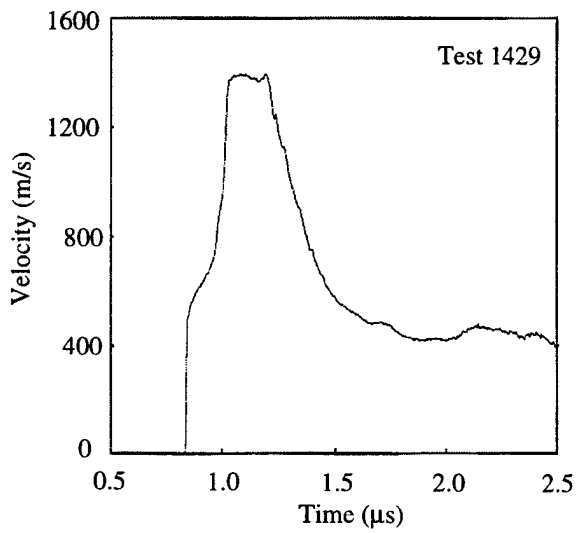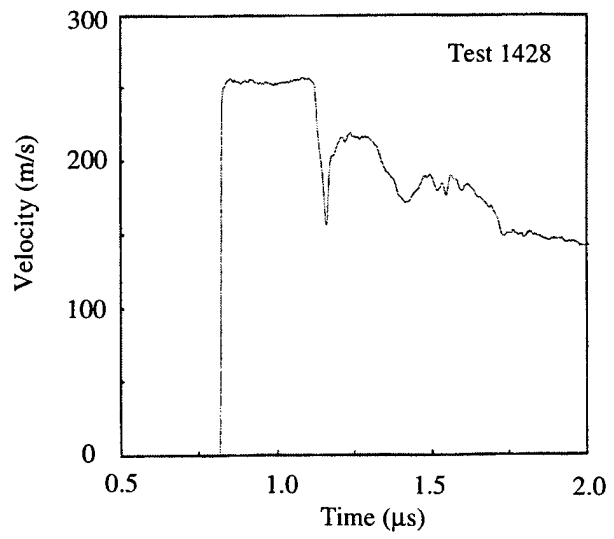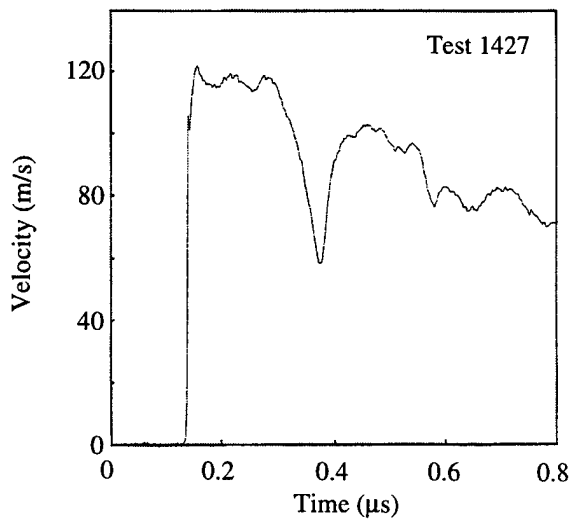
Figure 2.1.4.5 Ceramic-Window Interface Velocity Profiles from Grady and Moody [52] for Tests 1427-1429.
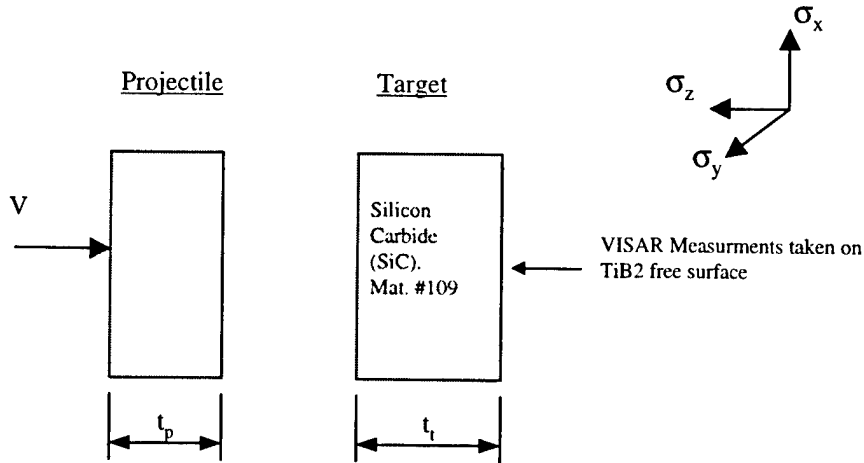
Figure 2.1.4.6   Description of the Plate Impact Test Configuration, Winkler and Stilp [81].

Table 2.1.4.3   Summary of Experimental Plate Impact Initial Conditions and Results, Winkler and Stilp [81].

Silicon Carbide									
Test Number	Material Number	Test Configuration			Elastic Compression		Plastic Compression		Spall Stress (GPa)
		Projectile Material	t_p (mm)	t_t (mm)	Stress σ_z (GPa)	Density ρ (kg/m³)	Stress σ_z (GPa)	Density ρ (kg/m³)	
1430	109	PMMA	0.7	5.7	0.4				No spall
1431	109	PMMA	0.7	6.0	0.7				0.58
1432	109	Aluminum	1.6	5.7	1.3				0.72
1433	109	Armco Iron	1.5	6.0	3.4				0.74
1434	109	Armco Iron	1.5	5.9	4.4				0.79
1435	109	Armco Iron	1.6	5.7	7.8				1.07
1436	109	Armco Iron	0.9	6.0	11.4				1.07
1437	109	Armco Iron	0.9	6.0	12.1				0.48
1438	109	Armco Iron	1.0	5.5	13.8		19.6		0.70

Test 1430-1438: the test data is from work by Winkler and Stilp [81]. The SiC was hot pressed having an initial density = 3190kg/m³. Only the elastic and plastic stresses were documented.
Test 1438: the only experiment to exceed the HEL. The documented HEL for this material is 13.0-14.7 GPa. The HEL of 13.8 GPa in the table is the median of 13.0 and 14.7GPa.

20
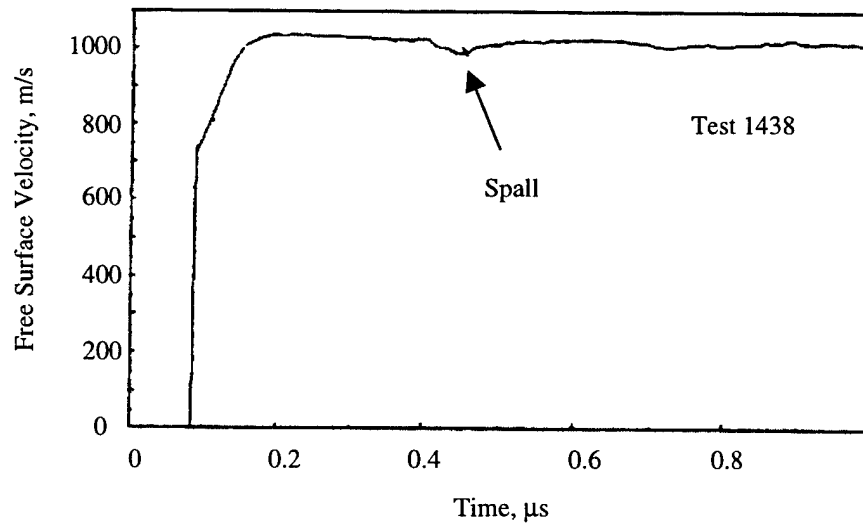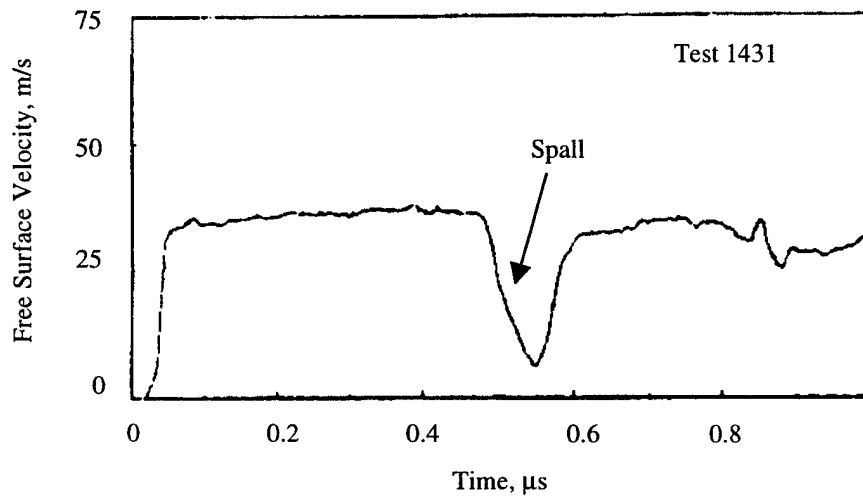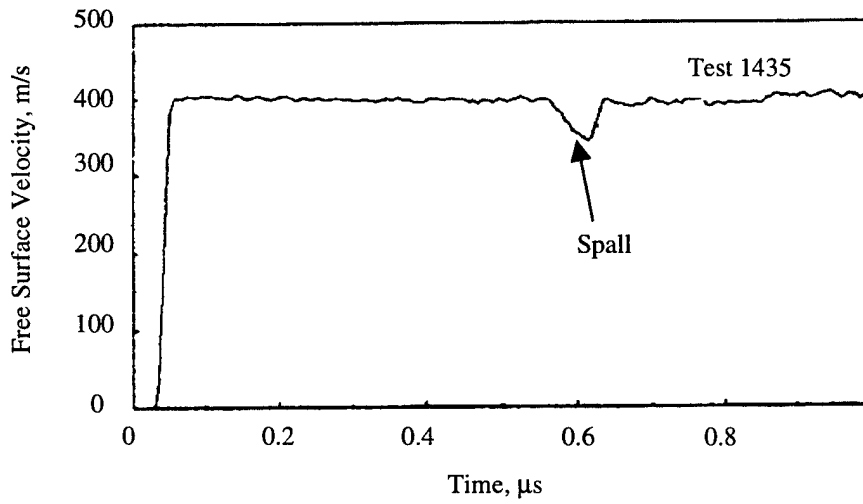
Figure 2.1.4.7 Ceramic Free Surface Velocity Profiles Investigating Spall Behavior, Winkler and Stilp [81].

Copper
Impactor

Silicon Carbide
Sample

| Silicon Carbide (SiC). Mat. #117 | Silicon Carbide (SiC). Mat. #117 |

σ_x

σ_z

σ_y

Copper or
Tantalum
Impactor

Target

| Silicon Carbide (SiC). Mat. #117 |

V

V

Manganin
Gauge for longitudinal
Stress measurement

Manganin
Gauge for transverse
Stress measurement

a) Longitudinal stress measurement, σ_z

b) Transverse stress measurement, $\sigma_x = \sigma_y$
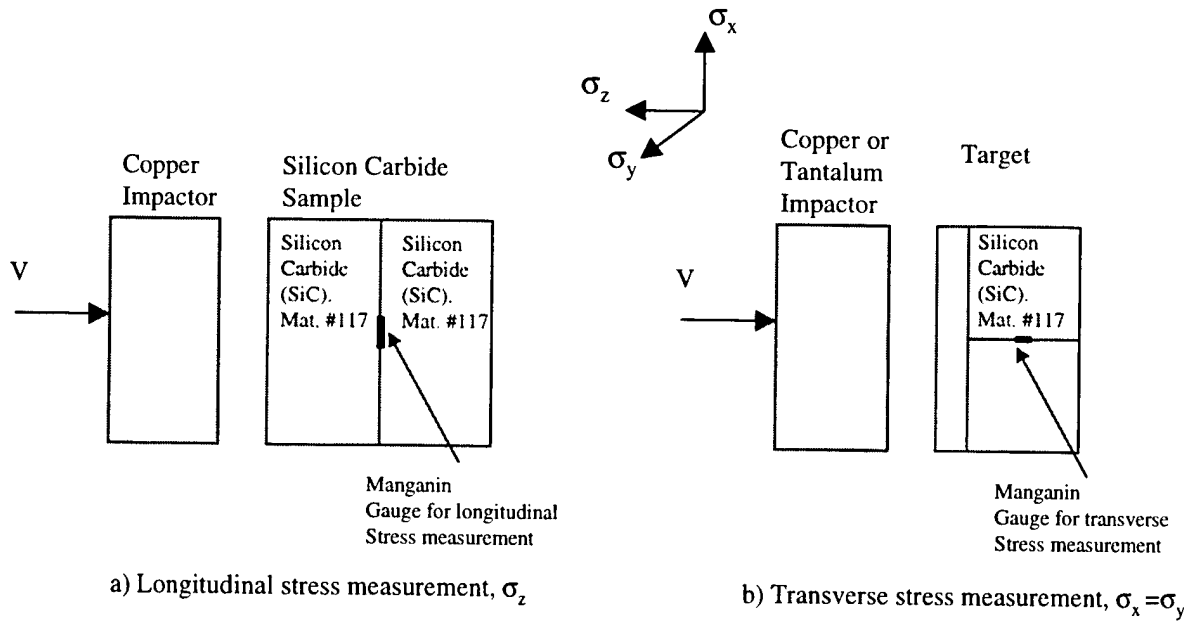
Figure 2.1.4.8   Description of Plate Impact Test Configurations for: a) Longitudinal Stress Measurements, Feng *et al.* [94] and b) Transverse Stress Measurements, Feng *et al.* [93].

Table 2.1.4.4   Summary of Experimental Plate Impact Results by Feng *et al.* [93, 94].

Silicon Carbide					
Test Number	Material Number	Peak Hugoniot Stress			Reference
		σ_z (GPa)	$\sigma_y = \sigma_x$ (GPa)	ρ (kg/m³)	$\mu = \rho/\rho_o - 1$	
1439	117	7.3		3262	0.0149	94 (Feng)
1440	117	10.7		3281	0.0208	
1441	117	13.6		3300	0.0268	
1442	117	16.1		3322	0.0337	
1443	117	17.6		3342	0.0397	
1444	117	23.0		3397	0.0570	
1445	117		1.9	3281	0.0208	93 (Feng)
1446	117		2.3	3299	0.0263	
1447	117		3.4	3314	0.0312	
1448	117		3.6	3320	0.0332	
1449	117		5.0	3345	0.0407	
1450	117		6.9	3367	0.0476	
1451	117		10.3	3408	0.0605	

Test 1439-1444: the test data is from work by Feng *et al.*[94]. In-material Manganin gauge was used to determine the stress in the longitudinal direction only (σ_z). The peak stress and density were measured as listed above. The data was obtained from Figure 2 in Reference [93].
Test 1445-1451: the test data is from work by Feng *et al.* [93]. In-material Manganin gauge was used to determine the stress in the transverse direction only ($\sigma_x = \sigma_y$). The peak stress and density were measured as listed above. The data was obtained from Figure 2 in Reference [93]. The documented HEL for this material = 11.5 GPa with a corresponding density = 3290kg/m³. Test 1439, 1440, 1445: these tests were elastic, not exceeding the HEL.

a) Plate impact test configuration

b) Typical Gauge signals
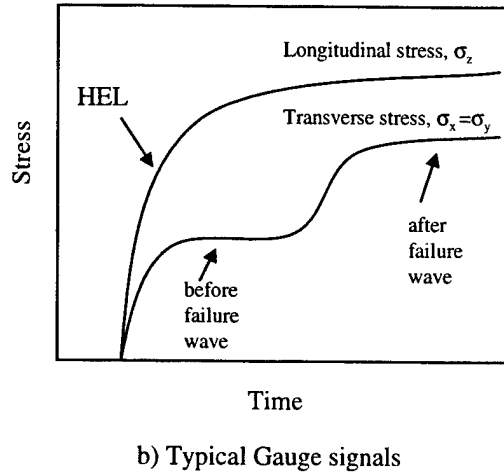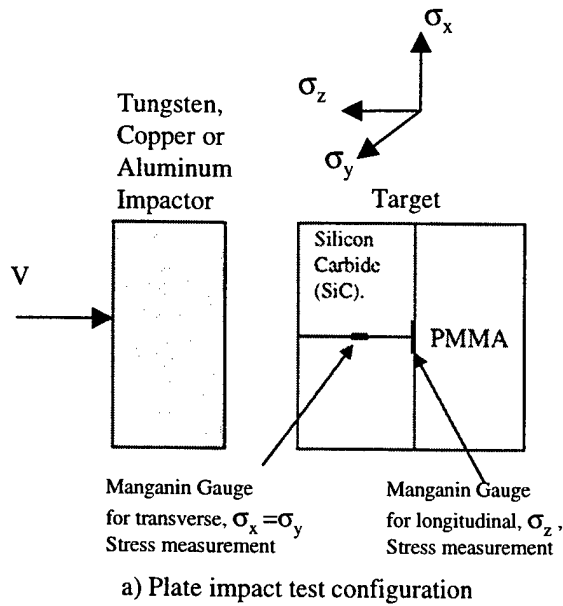
Figure 2.1.4.9 a) Description of Plate Impact Test Configuration for both Longitudinal and Transverse Stress Measurements, b) Typical Gauge Signals, Bourne *et al.* [95].

Table 2.1.4.5 Summary of Experimental Plate Impact Results, Bourne *et al.* [95].

Silicon Carbide				
Test Number	Material Number	σ_z (GPa)	Before Failure Wave $\sigma_y = \sigma_x$ (GPa)	After Failure Wave $\sigma_y = \sigma_x$ (GPa)
1452	114	14.7	3.1	3.5
1453	114	16.6	3.8	6.6
1454	114	18.7	4.7	7.1
1455	115	13.8	2.2	2.2
1456	115	15.7	2.7	5.7
1457	115	18.6	4.4	9.0
1458	116	16.6	3.4	3.4
1459	116	21.2	4.2	5.4
1460	116	23.4	6.8	7.4

Test 1452-1460: the test data is from work by Bourne *et al.*[95]. In-material Manganin gauges were used to determine the stress in the longitudinal and transverse directions. The transverse stress, $\sigma_y = \sigma_x$, was measured before and after the arrival of the failure wave. All test were shocked above the HEL of the material. The data listed above was obtained from Figure 7 in Reference [95].
Test 1452-1454: HEL = 13.2GPa (Material #114)
Test 1455-1457: HEL = 13.5GPa (Material #115)
Test 1457-1460: HEL = 15.7GPa (Material #116)
Test 1455, 1458: no indication of failure wave, transverse wave is flat

23

2.1.5 Penetration (semi-infinite) Test Data for Silicon Carbide

This section presents ballistic penetration results into semi-infinite Silicon Carbide targets. Orphal and Franzen [6] performed penetration experiments into Silicon Carbide over a velocity range of 1500m/s to 4500m/s. The targets and penetrators used are described in Figure 2.1.5.1. The penetration results are presented graphically in Figure 2.1.5.2 and in tabular form in Table 2.1.5.1. Both primary and total penetration are given. Primary penetration is the depth penetrated when the penetrator is just consumed. Total penetration is the total depth penetrated when the penetration event is complete.

Long Target (Test 1501-1522) Short Target (Test 1523-1525)

Impact Location   3.18mm

Aluminum Cover

Titanium sleeve

SiC (Mat. #104)   48.26mm

Aluminum   15.24mm
3.18mm

23.62mm
28.58mm

Impact Location   3.18mm

Aluminum Cover

Titanium sleeve

SiC (Mat. #104)   38.1mm

Aluminum   6.35mm
3.18mm

23.62mm
28.58mm

Penetrator

Tungsten (99.95%)
$\rho = 19,300 kg/m^3$
L = 15.24mm or
    11.43mm
D = 0.762mm
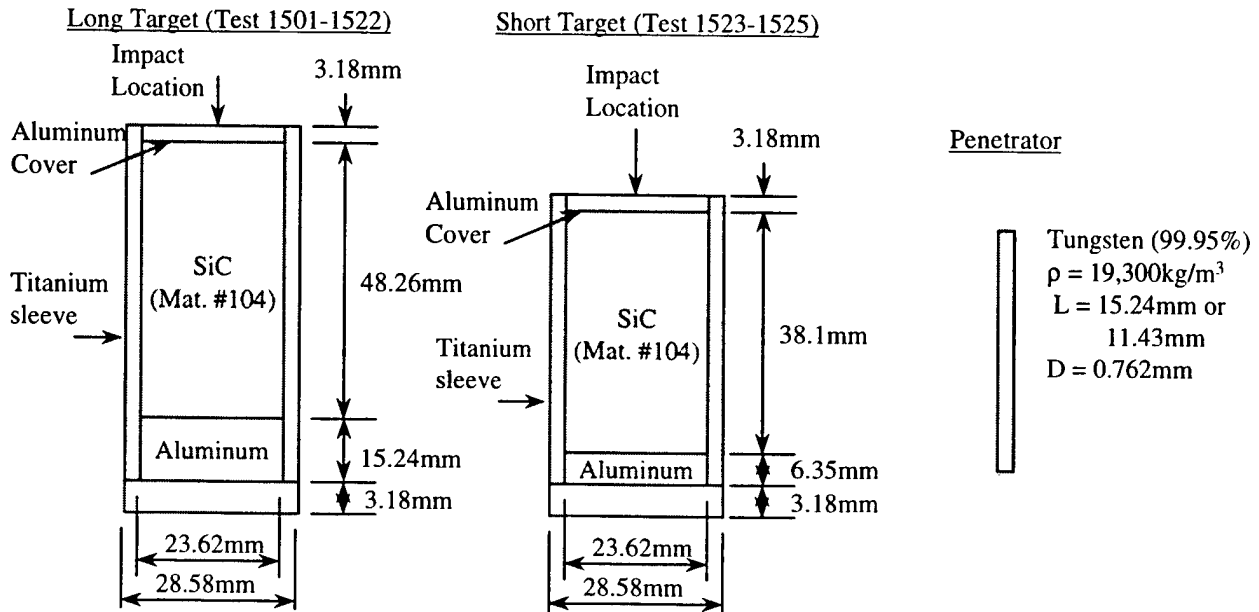
Figure 2.1.5.1 Silicon Carbide Target and Penetrator Descriptions, Orphal and Franzen [6].
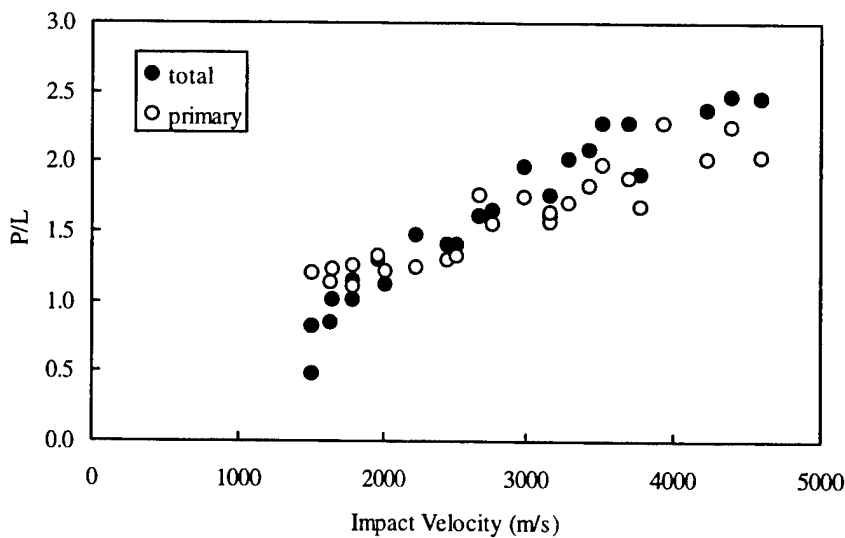
Figure 2.1.5.2 Primary Penetration and Total Penetration vs. Impact Velocity for Tungsten Penetrators Impacting Confined Silicon Carbide Targets [6].

Table 2.1.5.1 Summary of Penetration Results, Orphal and Franzen [6].

Silicon Carbide							
Test Number	Material Number	Penetrator		Target Configuration	Impact Velocity (m/s)	$P_{primary}/L$	P_{total}/L
		D (mm)	L (mm)				
1501	104	0.762	15.24	Long	1520	1.19	0.80
1502	104	0.762	15.24	Long	1520		0.47
1503	104	0.762	15.24	Long	1650	1.12	0.83
1504	104	0.762	15.24	Long	1660	1.21	0.99
1505	104	0.762	15.24	Long	1800	1.09	0.99
1506	104	0.762	15.24	Long	1800	1.24	1.13
1507	104	0.762	15.24	Long	1980	1.31	1.28
1508	104	0.762	15.24	Long	2030	1.20	1.11
1509	104	0.762	15.24	Long	2250	1.23	1.46
1510	104	0.762	15.24	Long	2470	1.28	1.39
1511	104	0.762	15.24	Long	2530	1.31	1.39
1512	104	0.762	15.24	Long	2690	1.75	1.59
1513	104	0.762	15.24	Long	2780	1.54	1.63
1514	104	0.762	15.24	Long	3000	1.73	1.95
1515	104	0.762	15.24	Long	3170	1.56	1.59
1516	104	0.762	15.24	Long	3180	1.62	1.74
1517	104	0.762	15.24	Long	3300	1.69	2.01
1518	104	0.762	15.24	Long	3450	1.82	2.07
1519	104	0.762	15.24	Long	3540	1.96	2.26
1520	104	0.762	15.24	Long	3710	1.87	2.26
1521	104	0.762	15.24	Long	3790	1.66	1.90
1522	104	0.762	15.24	Long	3940	2.27	2.26
1523	104	0.762	11.43	Short	4240	2.01	2.36
1524	104	0.762	11.43	Short	4410	2.24	2.46
1525	104	0.762	11.43	Short	4610	2.02	2.44

Test 1501-1525: the test data is from work by Orphal and Franzen[6]. Two penetrator lengths and two target configurations were used. The penetration includes the 3.18mm cover. In some cases, at the lower velocities, the primary penetration exceeds the total penetration. This is not reality, but is a reflection of how the primary penetration is calculated. The penetration and erosion rates are determined from the x-rays. These rates are assumed to be constant and are used to determine when the penetrator is consumed, and at what depth. At the lower impact velocities the rates are not constant, thus larger primary penetration depths are calculated. A more in depth discussion of this is provided in Reference 6.

2.1.6 Depth-Of-Penetration (DOP) Test Data for Silicon Carbide

This section presents depth-of-penetration (DOP) experiments for numerous Silicon Carbide materials. The DOP test has been used to investigate the effectiveness of ceramics for a number of years. The typical DOP configuration consists of a ceramic tile place on, or within, a steel or aluminum base target. A penetrator impacts and perforates the ceramic tile and continues into the base target. The penetration into the base target is generally referred to as the residual penetration, P_r, and is used to determined the ceramic mass efficiency as discussed in Section 2.0.

The target and penetrator description for the DOP experiments by Franzen et al.[33] is presented in Figure 2.1.6.1. The objective of the experiments was to investigate the ballistic effectiveness of Silicon Carbide as a function of impact velocity and ceramic thickness. The results are presented in tabular from in Table 2.1.6.1. No information was provided for the Silicon Carbide used in these experiments.

The target and penetrator description for the DOP experiment by Rosenberg and Tsaliah [39] is presented in Figure 2.1.6.2. The result is presented in tabular form in Table 2.1.6.2. No information was provided for the Silicon Carbide used in the experiment other than the density.

The target and penetrator description for the DOP experiments by Reaugh et al. [85] is presented in Figure 2.1.6.3. The objective of the experimental program was to investigate the ballistic efficiency of Silicon Carbide as a function of ceramic thickness, impact velocity and impact angle. The results are presented in tabular form in Table 2.1.6.3. Also included in the table are penetration results into the 4340 Steel base target with no ceramic .

The target and penetrator description for the DOP experiments by Rosenberg et al. [91] is presented in Figure 2.1.6.4. The objective of the experimental program was to investigate the ballistic efficiency of Silicon Carbide as a function of ceramic thickness. The results are presented graphically in Figure 2.1.6.5 and in tabular form in Table 2.1.6.3. Also included in the table are penetration results into the steel base target with no ceramic .

26

V

Tungsten penetrator
L =
D =

Silicon Carbide

t_c

RHA
base target

P_r = residual penetration
into RHA base target

Comments:
- ceramic is silicon carbide
- no information was given on any of the materials
- P_r = residual penetration into the RHA steel base
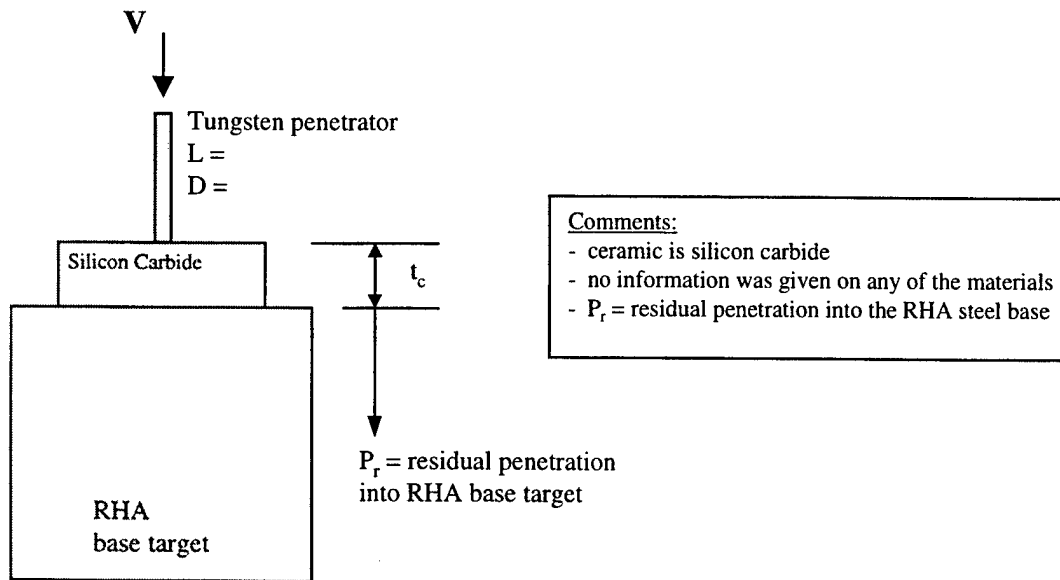
Figure 2.1.6.1 Target and Penetrator Descriptions for Silicon Carbide DOP Experiments, Franzen et al.[33].

Table 2.1.6.1 Summary of Experimental Results for Silicon Carbide DOP Tests, Franzen et al. [33].

Silicon Carbide							
Test Number	Material Number	Impact Velocity (m/s)	Penetrator		Ceramic Thickness t_c (mm)	P_r (mm)	P_r/L (mm)
			L (mm)	D (mm)			
1601		1498	81.8	8.18	25.6	22.5	0.28
1602		1532	107.4	7.16	25.6	52.6	0.49
1603		1509	81.8	8.18	38.2	13.5	0.17
1604		1518	81.8	8.18	38.2	17.6	0.22
1605		1505	81.8	8.18	51.0	0	0
1606		1503	107.4	7.16	51.0	25.1	0.23
1607		2037	62.0	6.2	70.0	3.4	0.05
1608		2038	62.0	6.2	70.0	6.7	0.11
1609		2449	62.0	6.2	80.0	13.9	0.22
1610		2458	62.0	6.2	80.0	3.4	0.05
1611		1990	75.0	7.5	80.0	21.5	0.29
1612		2005	75.0	7.5	80.0	14.2	0.19
1613		2459	75.0	7.5	90.0	22.7	0.30
1614		2449	75.0	7.5	90.0	9.7	0.13
1615		1997	75.0	7.5	30.0	52.0	0.69

Test 1601-1615: the test data is from work by Morris et al. And Wilkins et al. and documented in Reference 33. The ceramic material is silicon carbide and no information on the material was provided in Ref. 33.

27

Tungsten Alloy
penetrator
$\rho = 17800kg/m^3$
L = 80mm
D = 8mm

Silicon Carbide
(Mat. #118)

12.7mm

Ceramic is bonded to the
RHA base target

P_r = residual penetration into
RHA base target

RHA
base target
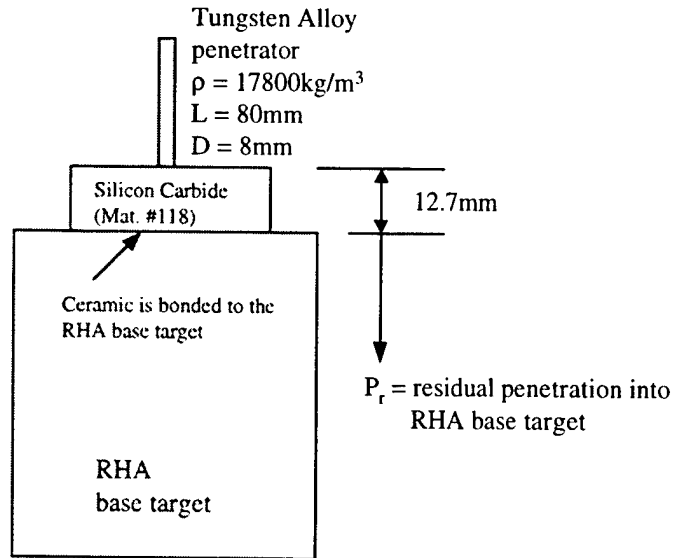
Figure 2.1.6.2 Target and Penetrator Description for DOP Experiment, Rosenberg and Tsaliah [39].

Table 2.1.6.2 Summary of Experimental DOP Result, Rosenberg and Tsaliah [39].

Silicon Carbide						
Test Number	Material Number	Impact Velocity (m/s)	Target Configuration		P_r (mm)	P_r/L (mm)
			t_c (mm)	Base Target		
1616	118	1300	12.7	RHA	37	0.46

Test 1616: the test data is from work by Rosenberg and Tsaliah [39]. The ceramic material used is Silicon Carbide with initial density = $3170kg/m^3$, no other material information was provided.
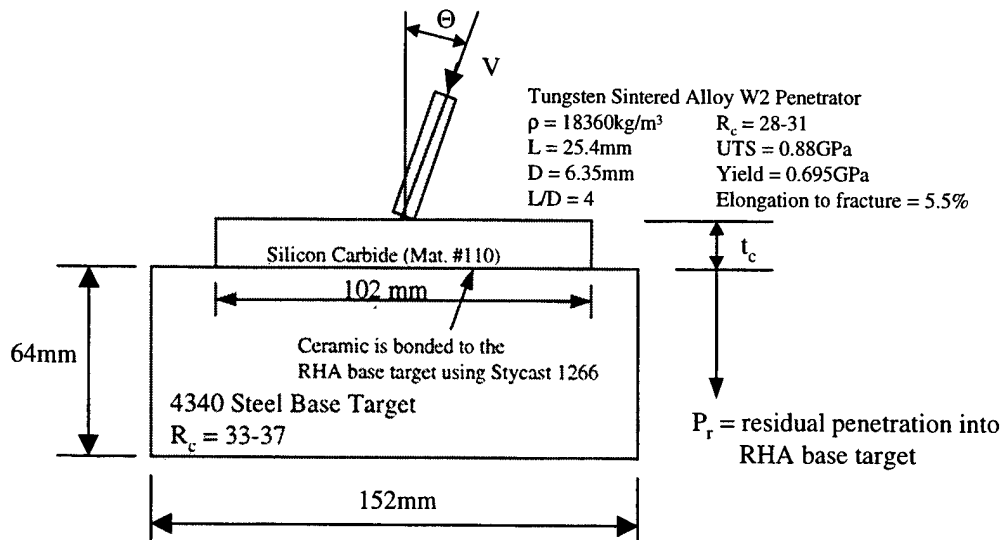
Figure 2.1.6.3 Target and Penetrator Description for DOP Experiment, Reaugh *et al.* [85].

Table 2.1.6.3 Summary of Experimental DOP Results, Reaugh *et al.* [85].

Silicon Carbide					
Test Number	Material Number	Impact Velocity (m/s)	Ceramic t_c (mm)	Impact Angle[#] Θ (degrees)	P_r[&] (mm)
1617	110	1370	10.0	0	13.9
1618	110	1360	15.1	0	2.0
1619	110	1370	20.0	0	0.0
1620	110	1310	30.1	0	0.0
1621	110	1690	20.0	0	14.3
1622	110	1750	20.0	0	14.5
1623	110	1770	29.5	0	5.7
1624	110	1700	30.2	0	2.4
1625	110	1740	40.0	0	0.0
1626	110	1750	15.0	30	14.9
1627	110	1780	31.3	30	1.0
1628	110	1710	15.1	45	8.2
1629	110	1810	25.0	45	0.0
1630	110	1700	10.1	60	6.6
1631	110	1800	14.9	60	1.9
1632	110	1690	20.0	60	0.0
1633	110	2620	30.1	0	18.2
1634	110	2680	39.9	0	15.6
1635	110	2640	59.7	0	0.0
1636		1340	0	0	27.0
1637		1350	0	0	27.8
1638		1350	0	0	28.5
1639		1770	0	0	36.0
1640		2500	0	0	43.8
Test 1617-1640: the test data is from work by Reaugh et al. (Ref. 85). #the angle between the penetrator flight axis and the normal to the tile. & the residual penetration measured normal to the impact surface. Test 1622: Two 10.0mm ceramic tiles used. Test 1636-1640: tests into 4340 steel target only (no ceramic used).					
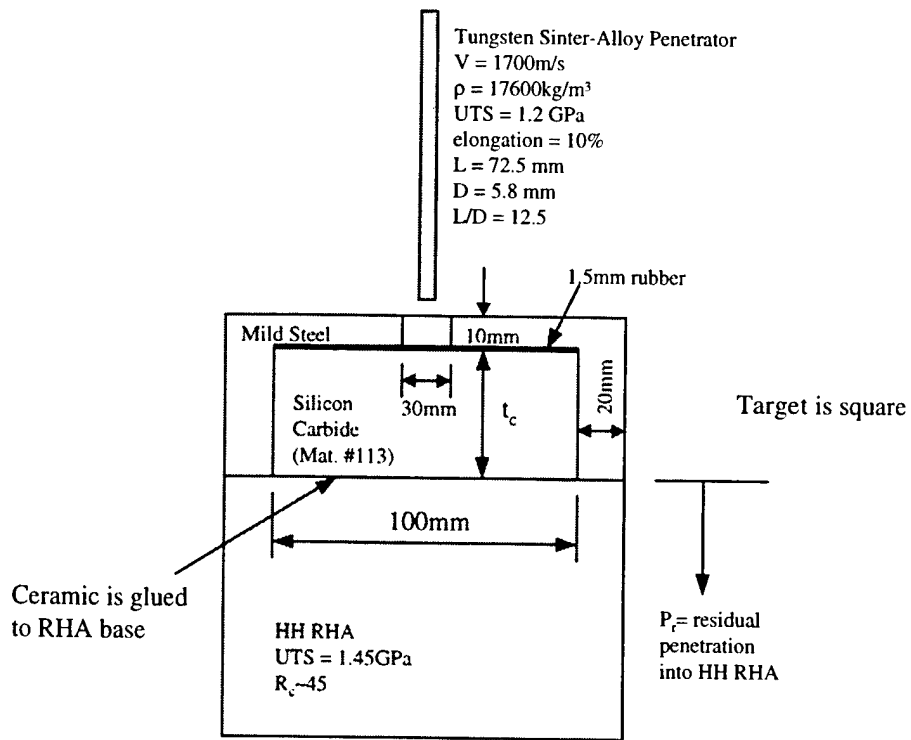
Figure 2.1.6.4 Target and Penetrator Description for DOP Experiment, Rosenberg *et al.* [91].
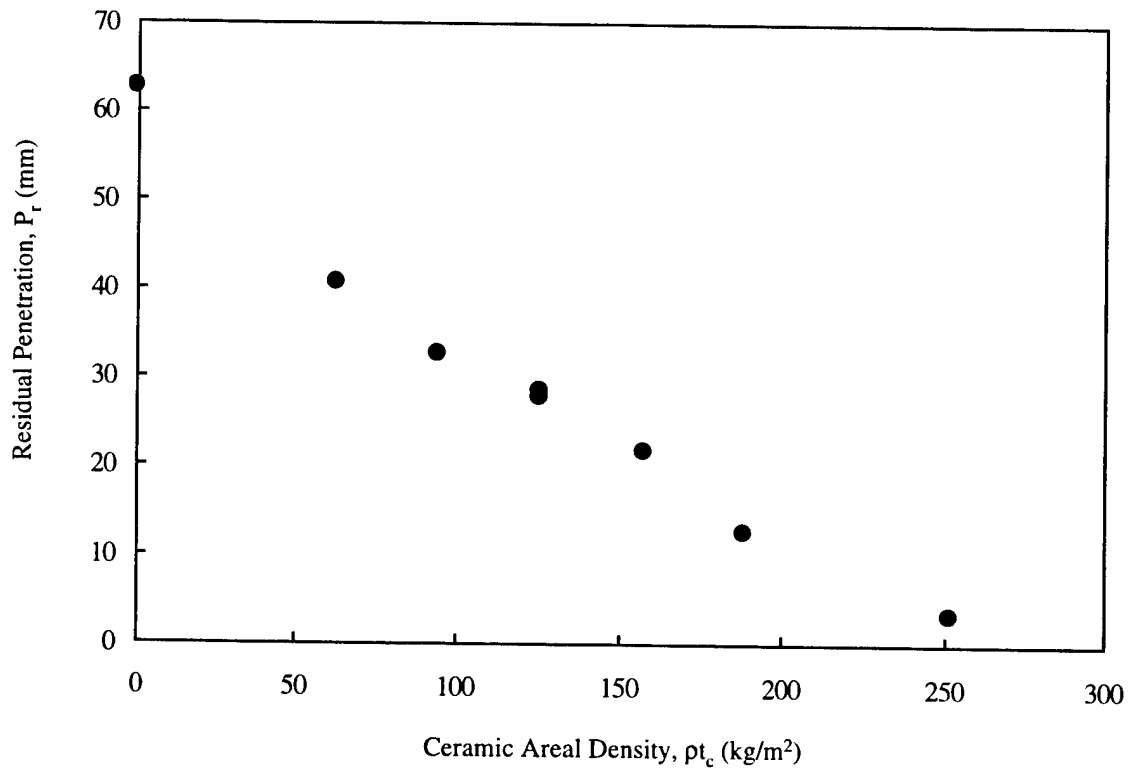
Figure 2.1.6.5 Residual Penetration as a Function of Cermaic Areal Density, Rosenberg *et al.* [91].

Table 2.1.6.4 Summary of Experimental DOP Results, Rosenberg *et al.* [91].

Silicon Carbide					
Test Number	Material Number	Impact Velocity (m/s)	Ceramic t_c (mm)	ρt_c (kg/m^2)	P_r (mm)
1641	113	1700	20	63	40.5
1642	113	1700	30	94.5	32.4
1643	113	1700	40	126	28.4
1644	113	1700	40	126	27.5
1645	113	1700	50	157.5	21.4
1646	113	1700	60	189	12.4
1647	113	1700	80	252	3.2
1648		1700	0	0	62.4

Test 1641-1648: the test data is from work by Rosenberg *et al.* [91]. The tabulated data listed above was obtained from Figure 1 in Reference [91].
All targets were square
$\rho = 3150 kg/m^3$ (density of ceramic)
Test 1648: tests into steel base target only (no ceramic used).

2.1.7 Perforation Test Data for Silicon Carbide

This section presents perforation experiments where the target is usually perforated by the penetrator. Targets are typically comprised of a ceramic front layer and a metallic rear layer and are commonly used in light armor applications. The most common piece of data extracted from perforation experiments is the target ballistic limit, V_{bl}, previously defined in Section 2.0.

The target and penetrator description for the perforation experiments by Wilkins *et al.* [26]. is presented in Figure 2.1.7.1. The results of the experiments are summarized in Table 2.1.7.1 were the ballistic limit velocity, V_{bl}, is provided.
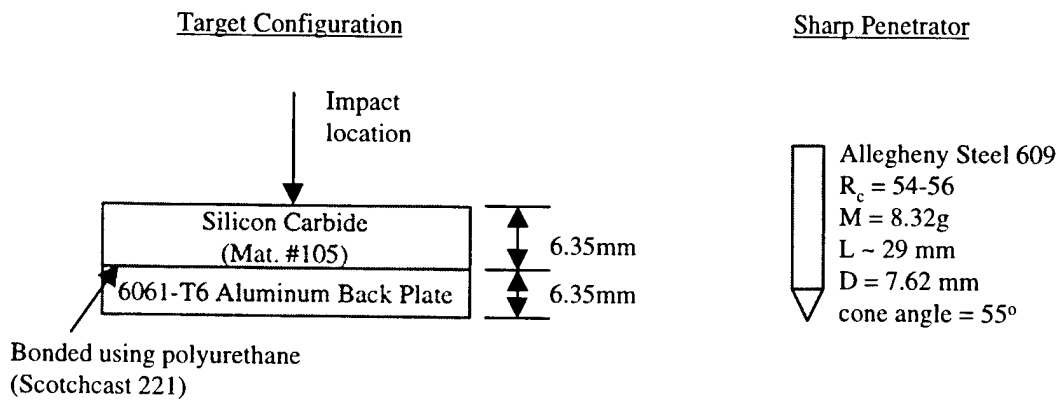
Figure 2.1.7.1 Target and Penetrator Description for Perforation Experiment, Wilkins *et al.* [26].

Table 2.1.7.1 Ballistic Limit Velocity for a Sharp Penetrator against a Silicon Carbide Target, Wilkins *et al.*[26].

Silicon Carbide					
Test Number	Material Number	Penetrator	Target Configuration		Ballistic Limit Velocity, V_{bl} (+- 20m/s)
			Δ (mm)	δ (mm)	
1701	105	Sharp	6.35	6.35	660
Test 1701: the test data is from work by Wilkins *et al.* [26].					

2.1.8 Other Test Data for Silicon Carbide

This section presents experiments that don't fit into one of the previous six experimental categories.

Experiments performed by Strassburger et al. [69] were designed to investigate the fracture propagation in the ceramic. The damage velocity, V_d, was measured as a function of projectile impact velocity, V_p. The target and projectile descriptions are presented in Figure 2.1.8.1. The results of the experiments are summarized in Table 2.1.8.1 where the projectile impact velocity and damage velocity are tabulated. Figure 2.1.8.2 presents the results graphically. The damage velocity is defined as the fastest observed fracture velocity in the Silicon Carbide ceramic. The fracture propagation was observed by means of a Cranz-Schardin camera and photos of this process are presented in Reference 69.
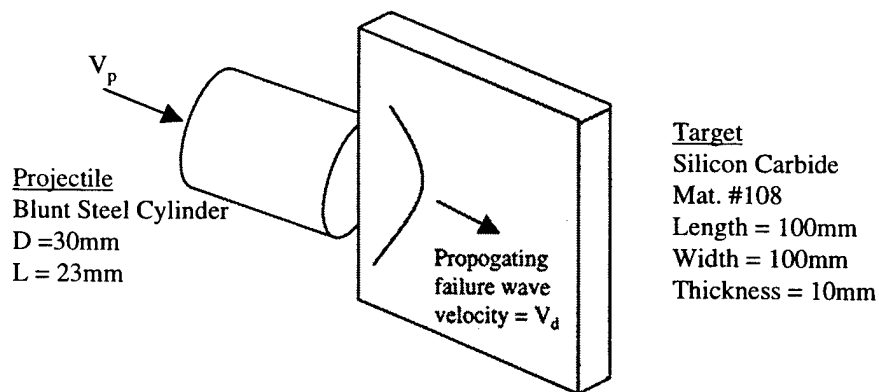
Figure 2.1.8.1 Target and Projectile Description for Fracture Experiment, Strassburger et al. [69].
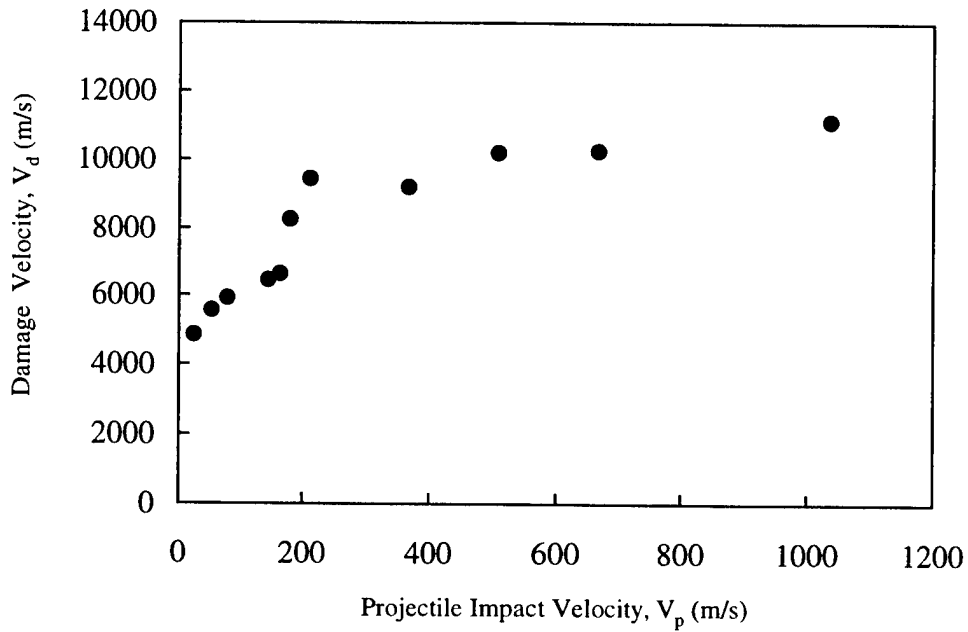
Figure 2.1.8.2 Damage Velocity in Ceramic vs. Projectile Impact Velocity, Strassburger *et al.* [69].

Table 2.1.8.1 Summary of Damage Velocity in Silicon Carbide as a Function of Projectile Impact Velocity, Strassburger *et al.*[69].

Silicon Carbide			
Test Number	Material Number	Projectile Impact Velocity, V_p (m/s)	Damage Velocity V_d (m/s)
1801	108	28	4770
1802	108	56	5510
1803	108	84	5830
1804	108	150	6360
1805	108	167	6570
1806	108	185	8170
1807	108	216	9330
1808	108	370	9120
1809	108	513	10080
1810	108	670	10180
1811	108	1040	11030
Test 1801-1811: the test data is from work by Strassburger *et al.* [69]. The data were obtained from Figure 9a in Ref. 69.			

2.2 BORON CARBIDE

2.2.1 Material Description for Boron Carbide

The purpose of this section is to provide as much information as possible on the materials tested. Descriptions for each of the Boron Carbide materials used in Section 2.2 are presented in Table 2.2.1.1. Each material is given a material number which is used throughout Section 2.2 to identify it. The data listed in Table 2.2.1.1 were obtained directly from the corresponding reference. When specific information was not available it was left blank. The strength values listed, (Compressive, HEL and Spall), are nominal values and are included for comparison purposes. Occasionally researchers will determine the chemical composition of the material being tested to further characterize it, Table 2.2.1.1 includes this data when available.

Table 2.2.1.1   Description of the Boron Carbide Materials Tested

	Material Number						
	201	202	203	204	205	206	207
Reference	22	26, 27	30	46	52	52, 54	81
Manufacturer	Norton Co.		Norton Co.	Dow Chemical	Eagle Picher	Dow Chemical	
Processing	Hot Pressed		Hot Pressed				Hot Pressed
Average Grain Size (μm)	9	30		3	10	3	
Density (kg/m³)	2510	2500	2500	2506	2517	2506	2512
Void Fraction		0.035	0.02			0.01	
Longitudinal Velocity (m/s)		13300	13780	14070	14040	14070	14070
Shear Velocity (m/s)		8600	8540	8870	8900	8870	8810
Bulk Velocity (m/s)		8850	9630	9650	9570	9650	9720
Young's Modulus, E (GPa)		422	432	461	463	461	
Shear Modulus, G (GPa)		185	182	197	199	197	195
Bulk Modulus, K (GPa)		196	232	233	231	233	237
Poisson Ratio		0.14	0.188	0.17	0.164	0.17	0.177
Compressive Strength (GPa)		1.3		5.9			
HEL (GPa)		15.0	15.1			19.0	16.7
Spall Strength (GPa)						0.45	0.59-0.77
Impurities (%wt)							
Al$_2$O$_3$			0.1-0.5				
CaO			0.1				
MgO			0.02				
SiO$_2$			0.08				
NiO			0.01-0.05				

Table 2.2.1.1 Description of the Boron Carbide Materials Tested Continued.

	Material Number						
	208	209	210	211	212	213	214
Reference	85	89	90	90	90	90	90
Manufacturer	Dow	AC Cerama AB	Dow	Dow	Dow	Dow	Dow
Processing							
Average Grain Size (μm)			2.09+-0.57	2.43+-0.74	2.48+-0.85	2.59+-0.75	
Density (kg/m³)	2510	2490	2130	2250	2330	2430	2520
Void Fraction			0.163	0.100	0.048	0.025	0.000
Longitudinal Velocity (m/s)	13830		11850	12520	12800	13020	13420
Shear Velocity (m/s)	8720		7600	8220	8470	8730	8900
Bulk Velocity (m/s)	9480		7960	8165	8257	8240	8630
Young's Modulus, E (GPa)	447		288	359	394	437	468
Shear Modulus, G (GPa)	191		123	152	167	185	200
Bulk Modulus, K (GPa)	226		135	150	159	165	188
Poisson Ratio	0.170		0.17	0.18	0.18	0.18	0.17
Compressive Strength (GPa)							
HEL (GPa)			9.6+-0.3	13.7+-0.3	16.3+-0.4	17.1+-0.4	19.4+-0.3
Spall Strength (GPa)							

Table 2.2.1.1 Description of the Boron Carbide Materials Tested Concluded.

	Material Number						
	215						
Reference	91						
Manufacturer							
Processing							
Average Grain Size (μm)							
Density (kg/m³)	2500						
Void Fraction							
Longitudinal Velocity (m/s)							
Shear Velocity (m/s)							
Bulk Velocity (m/s)							
Young's Modulus, E (GPa)	450						
Shear Modulus, G (GPa)							
Bulk Modulus, K (GPa)							
Poisson Ratio							
Compressive Strength (GPa)	4.50						
HEL (GPa)							
Spall Strength (GPa)							

2.2.2 Mechanical Test Data for Boron Carbide

The following section presents mechanical test data, performed by numerous researchers, for Boron Carbide. A typical test specimen showing the stress configuration is shown in Figure 2.2.2.1. Compression is taken as positive and tension as negative. Loading is generally uniaxial in the z direction and is increased until the material fails, although some researchers use more complex loading techniques to vary the stress state at failure.

Mechanical test data performed by Wilkins et al. [26] are presented in Table 2.2.2.1. The objective of the test program was to determine the strength of Boron Carbide as a function of confining pressure before and after fracture. Wilkins measured the virgin material strength at fracture and the residual strength after fracture for each experiment. The residual strength experiments are identified by an, f, after the test number.

Mechanical test data performed by Lankford [46] are presented in Table 2.2.2.1. The objective of the test program was to determine the strength of Boron Carbide as a function of strain rate. Both quasi-static and Hopkinson bar experiments were performed. The normal stress, σ_z, at failure is given as a function of average strain rate, $\dot{\varepsilon}$.

Mechanical test data performed by Meyer and Faber [88] are presented in Table 2.2.2.2. The objective of this work was to determine the strength of fractured ceramic as a function of pressure and strain rate. These tests were performed using pre-factured ceramic. The pre-fractured ceramic was obtained from plate impact debris having an average particle size of 1.3mm. The ceramic particles were placed inside a steel tube providing confinement in the radial and tangential directions, $\sigma_x = \sigma_y$. An axial load, σ_z, was applied until yielding of the steel tube occurred. Different combinations of tube wall thickness and strength were used to vary the confining stress. The bulk density of the ceramic when place in the tube was approximately 50%. No information on the Boron Carbide material was provided in Reference [88] and thus it was not given a material number.
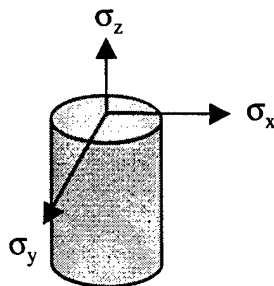
Figure 2.2.2.1 Description of a Typical Mechanical Test Specimen.

Table 2.2.2.1 Summary of Experimental Results.

Boron Carbide						
Test Number	Material Number	σ_z (GPa)	σ_x (GPa)	σ_y (GPa)	$\sim \dot{\varepsilon}$ (s^{-1})	Ref.
2201	202	1.30	0	0	1x10^{-4}	26 (Wilkins)
2202	202	5.42	0.10	0.10	1x10^{-4}	
2203	202	6.26	0.20	0.20	1x10^{-4}	
2204	202	6.73	0.42	0.42	1x10^{-4}	
2205	202	8.17	0.72	0.72	1x10^{-4}	
2206	202	7.02	0.90	0.90	1x10^{-4}	
2207	202	9.18	1.58	1.58	1x10^{-4}	
2201f	202	0	0	0	1x10^{-4}	
2202f	202	0.73	0.10	0.10	1x10^{-4}	
2203f	202	2.01	0.20	0.20	1x10^{-4}	
2204f	202	2.74	0.42	0.42	1x10^{-4}	
2205f	202	3.56	0.72	0.72	1x10^{-4}	
2206f	202	3.90	0.90	0.90	1x10^{-4}	
2207f	202	5.42	1.58	1.58	1x10^{-4}	

Test 2201: uniaxial compressive strength.
Test 2202-2207: compressive strength as a function of confining pressure.
Test 2201f-2207f: these tests are continuations of tests 2101-2107. These results measure the residual ceramic strength after fracture.

2208	204	6.00	0	0	1.09x10^{-4}	46 (Lankford)
2209	204	4.15	0	0	1.08x10^{-4}	
2210	204	6.81	0	0	5.30x10^{-2}	
2211	204	6.59	0	0	5.19x10^{-2}	
2212	204	4.26	0	0	4.87x10^{-1}	
2213	204	6.63	0	0	4.70x10^{-1}	
2214	204	4.86	0	0	1.57x10^3	
2215	204	5.92	0	0	2.09x10^3	
2216	204	6.24	0	0	2.26x10^3	
2217	204	7.69	0	0	3.12x10^3	

Test 2208-2217: the test data is unpublished by Lankford. Compression tests were performed to obtain the compressive strength as a function of strain rate. The highest strain rate testing was on a Hopkinson bar system. The Boron Carbide was manufactured by Dow Chemical Co. having an initial density = 2506kg/m^3.

Table 2.2.2.2   Summary of Experimental Results, Meyer and Faber[88].

Boron Carbide						
Test Number	Material Number	σ_z (GPa)	σ_x (GPa)	σ_y (GPa)	$\sim \dot{\varepsilon}$ (s^{-1})	Ref.
2218		0.87	0.13	0.13	5x10^{-4}	88
2219		1.69	0.43	0.43	5x10^{-4}	(Meyer)
2220		2.53	0.61	0.61	5x10^{-4}	
2221		1.16	0.16	0.16	7.7x10^{1}	
2222		2.22	0.36	0.36	7.7x10^{1}	
2223		3.06	0.62	0.62	7.7x10^{1}	

Test 2218-2223: This work was performed by Meyer and Faber [88]. The above listed data were obtained from Figures 5 and 6 in Reference [88]. Confinement was provided by steel cylinders of various thickness and strength. Axial loads were applied until the cylinder yielded. The axial stress, σ_z, was measured directly and the lateral stresses, $\sigma_x = \sigma_y$ were obtained using strain gauges. The axial stress, σ_z, listed above is the maximum stress obtained for the corresponding confining stress, $\sigma_x = \sigma_y$. No material information was provide in Reference [88] thus no material number is given.

2.2.4 Plate Impact Test Data for Boron Carbide

The following section presents plate impact results performed by numerous researchers using Boron Carbide. A typical plate impact test configuration is presented in Figure 2.2.4.1. The peak stress, σ_z, occurs in the z-direction and is generally measured for both the elastic and plastic response. The lateral stresses, σ_x and σ_y, occur due to the uniaxial strain configuration of the experiment, and are typically not measured. The peak stress for the elastic regime is referred to as the Hugoniot Elastic Limit (HEL) and has become a fundamental property of ceramics. The peak stress for the plastic response is generally referred to as the peak Hugoniot stress. The particle velocity and wave velocity for both the elastic and plastic waves are typically measured and documented herein. In some cases the entire particle velocity time history is measured using laser velocity interferometry techniques (VISAR). VISAR traces provide direct information on the material response and are included in this section when available.

The results from Wilkins [25] are summarized in Table 2.2.4.1. The peak stress, σ_z, and density, ρ, for both the elastic and plastic waves are presented.

The results from Gust and Royce [30] are presented in Table 2.2.4.2. The shock velocity, particle velocity, peak stress, σ_z, and density, ρ, for both the elastic and plastic waves are presented.

A description of the plate impact test configuration used by Grady and Moody [52] is presented in Figure 2.2.4.2. The specific test dimensions and some limited results are summarized in Table 2.2.4.3. Compression and release behavior were measured by monitoring the ceramic-window interface velocity using laser velocity interferometry techniques (VISAR). The interface velocity profiles reflect the uniaxial strain loading and unloading behavior of the material and are presented in Figures 2.2.4.3-4.

A description of the plate impact test configuration used by Winkler and Stilp [81] is presented in Figure 2.2.4.5. The objective of this experimental study was to investigate spall as a function of peak compressive stress. The specific test dimensions and the results are summarized in Table 2.2.4.4. None of the experiments exceeded the HEL. Compression and release behavior of the Boron Carbide was measured by monitoring the ceramic free surface velocity using laser velocity interferometry techniques (VISAR). The interface velocity profiles for three experiments are presented in Figure 2.2.4.6. Test 2443 demonstrates the elastic ringing in the target when no spall occurs. Tests 2445 and 2448 show the pullback in the wave profile indicating that spall has occurred.

A description of the plate impact test configuration used by Brar et al.[90] is presented in Figure 2.2.4.7. The objective of this study was to determine the effect of porosity on the HEL and plastic wave velocity. Five plate impact experiments were performed using Boron Carbide samples with porosity's ranging from 0 to 16 percent. Measurements were made with manganin gauges placed at the back surface of the Boron Carbide specimen and backed by a thick PMMA plate. The HEL and plastic wave velocity was determined for each specimen using the manganin gauge records and are summarized in Table 2.2.4.5.
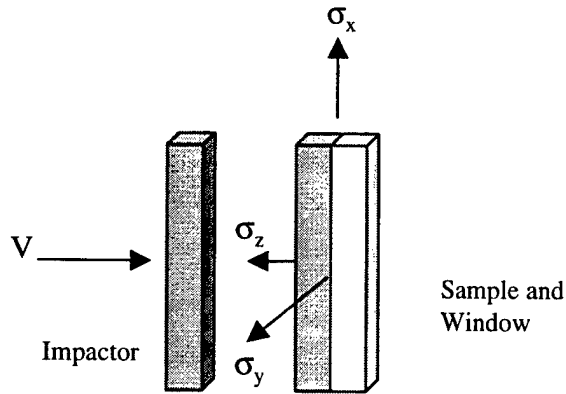
Figure 2.2.4.1 Description of a Typical Plate Impact Test Configuration including Stress Orientations

Table 2.2.4.1 Summary of Experimental Plate Impact Results, Wilkins[25].

Boron Carbide										
Test Number	Material Number	Initial Density ρ_o (kg/m³)	Elastic Regime (HEL)				Plastic Regime			
			Shock Velocity (m/s)	Particle Velocity (m/s)	σ_z (GPa)	ρ (kg/m³)	Shock Velocity (m/s)	Particle Velocity (m/s)	σ_z (GPa)	ρ (kg/m³)
2401	202	2500			13.6	2574			21.1	2666
2402	202	2500			14.0	2578			21.5	2667
2403	202	2500			14.5	2577			22.4	2659
2404	202	2500			14.8	2580			24.0	2695
2405	202	2500			15.1	2582			24.3	2692
2406	202	2500			15.4	2584			27.1	2721
2407	202	2500			15.7	2587			27.5	2714
2408	202	2500			16.3	2591			28.4	2729
2409	202	2500							38.6	2830
2410	202	2500							39.7	2845
2411	202	2500							43.8	2894
Test 2401-2411: the test data is from work by Wilkins [25]. The data was obtained from Figure A7 in Reference 25. The HEL data does not necessarily correspond to the associated peak hugoniot stress shown here.										

Table 2.2.4.2 Summary of Experimental Plate Impact Results, Gust and Royce[30].

			Elastic Regime (HEL)				Deformational Regime			
Test Number	Material Number	Initial Density ρ_o (kg/m^3)	Shock Velocity (m/s)	Particle# Velocity (m/s)	σ_z (GPa)	ρ (kg/m^3)	Shock Velocity (m/s)	Particle* Velocity (m/s)	σ_z (GPa)	ρ (kg/m^3)
2412	203	2498	13880	438	15.2	2579	8030	705	20.4	2672
2413	203	2491	13840	457	15.7	2577	9400	695	21.2	2646
2414	203	2488	13930	389	13.5	2560	9200	705	20.4	2650
2415	203	2511	13790	487	16.8	2603	9340	905	26.6	2733
2416	203	2510	13790	491	17.0	2603	9140	925	27.0	2740
2417	203	2512	13790	479	16.6	2603	10770	955	29.4	2729
2418	203	2512	13740	469	16.2	2601	9790	965	28.4	2748
2419	203	2498	13790	417	14.3	2576	9790	930	26.8	2724
2420	203	2493	13790	428	14.7	2573	9510	915	26.2	2718
2421	203	2510	13740	408	14.1	2587	9160	800	23.1	2710
2422	203	2510	13680	389	13.4	2583	9620	800	23.7	2704
2423	203	2498	13960	380	13.2	2568	10260	880	26.1	2714
2424	203	2509	13790	502	17.3	2603	9190	1000	28.6	2763
2425	203	2509	13810	449	15.5	2593	10050	1305	37.0	2849
2426	203	2509	13740	472	16.2	2598	10020	1330	37.6	2849
2427	203	2496	13900	448	15.5	2583	11070	1420	42.4	2849
2428	203	2486	13880	419	14.4	2564	10250	1485	41.3	2878
2429	203	2505	13790		15.3			1985	59.3	3022
2430	203	2508	13790		15.3			2525	78.4	3155
2431	203	2506	13790		15.3			2885	91.7	3259
2432	203	2502	13790		15.3			2790	87.0	3225

Test 2412-2432: the test data is from work by Gust and Royce [30].

elastic particle velocity obtained using $U_p = 1/2U_{fs}$ where U_{fs} is the free surface velocity.

* plastic particle velocity obtained using $U_p = 1/2U_{fs}$ and by impedance matching. The particle velocity listed here is the average of the two.

Projectile σ_z Target σ_x σ_y

Backer   Impactor   Sample   Window

V

Boron Carbide (B$_4$C)

Mat. #205 or Mat. #206

Sample-window interface

L_B L_I L_S L_W

Materials Used

Material	Density (kg/m³)	Designation
Polyurethane Foam	160	PF160
Polyurethane Foam	320	PF320
Polyurethane Foam	640	PF640
PMMA	1186	PMMA
Tantalum	16659	Ta
Lithium Floride	2640	LF
Aluminum	2703	Al
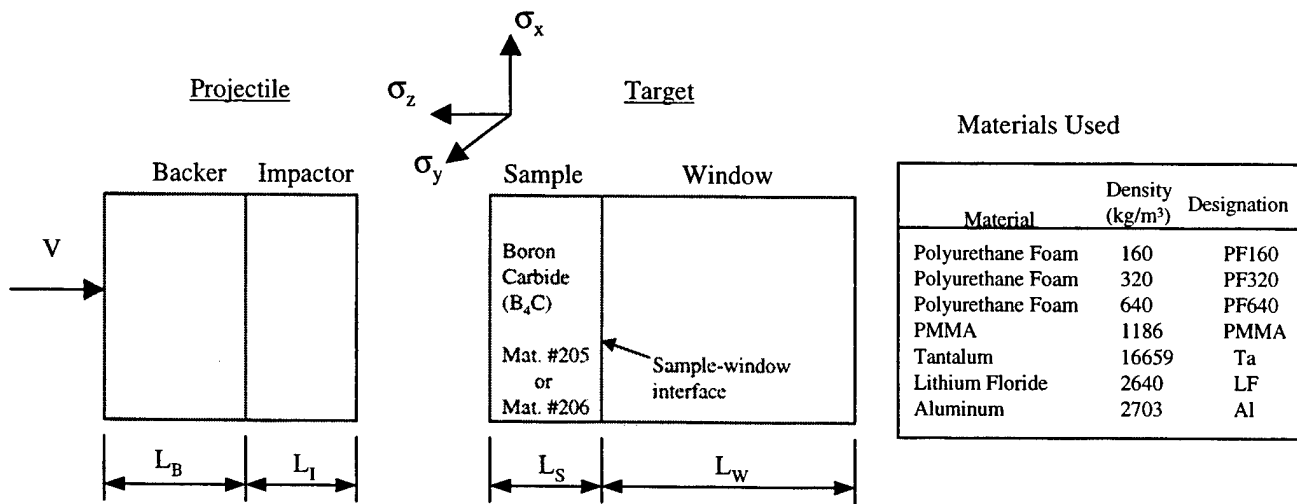
Figure 2.2.4.2 Description of Grady and Moody [52] Plate Impact Test Configuration.

Table 2.2.4.3 Summary of Experimental Plate Impact Results by Grady and Moody [52].

Boron Carbide														
Test Number	Material Number	Projectile				Target				Hugoniot Results				
			Backer		Impactor		Sample		Window		Elastic Compression		Plastic Compression	
		V (m/s)	Material	L_B (mm)	Material	L_I (mm)	Density (kg/m³)	L_S (mm)	Material	L_W (mm)	σ_z (GPa)	ρ (kg/m³)	σ_z (GPa)	ρ (kg/m³)
2433	205	1546	PF320	6.0	B$_4$C	3.902	2517	9.044	LF	25.4	14.8		22.8	
2434	205	2210	PF640	6.0	B$_4$C	3.917	2517	9.033	LF	25.4	14.0		31.4	
2435	206	370	PF320	6.0	B$_4$C	4.924	2506	9.694	PMMA	25.4	6.6			
2436	206	1633	PF320	6.0	B$_4$C	4.831	2506	10.322	LF	25.4			23.6	2711
2437	206	2076	PF640	6.0	B$_4$C	4.815	2506	10.346	LF	25.4			28.6	2788
2438	206	913	PF160	8.0	PMMA	2.004	2506	10.526	PMMA	24.2				
2439	206	2059	PF640	6.0	Ta	1.515	2506	9.680	LF	25.4	16.4		40.0	2921
2440	206	1162	PF160	8.0	PMMA	2.009	2506	10.487	PMMA	24.2				
2441	206	2320	Ta	1.505	LF	3.080	2506	4.761	LF	25.4				
2442	206	3980	PMMA	0.990	B$_4$C	2.016	2506	2.992	LF	18.9	20.0		57.8	3048

Test 2433-2442: the test data is from work by Grady. Material #205 is Boron Carbide manufactured by Eagle Picher, having a nominal initial density = 2517kg/m³. Material #206 is Boron Carbide manufactured by Coors Co. having an initial density = 2506kg/m³. The above table primarily provides the initial conditions for the plate impact experiments, although the elastic and plastic stress-density states are provided when available.
Test 2433, 2434: the HEL and peak hugoniot stress obtained from Ref. 54, 55.
Test 2435: the peak elastic stress (below the HEL threshold) obtained from Ref. 76.
Test 2439,2442: the HEL stress obtained from Ref. 54.
Test 2436,2437,2439, 2442: the Hugoniot state obtained from Figure 6.4 in Ref. 54, and Figure 4 in Ref. 56.
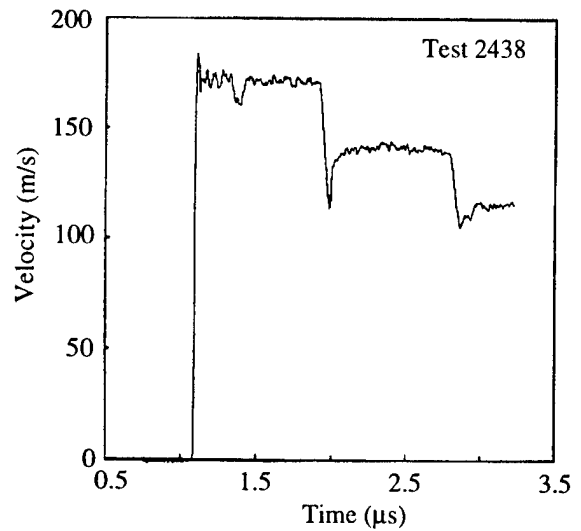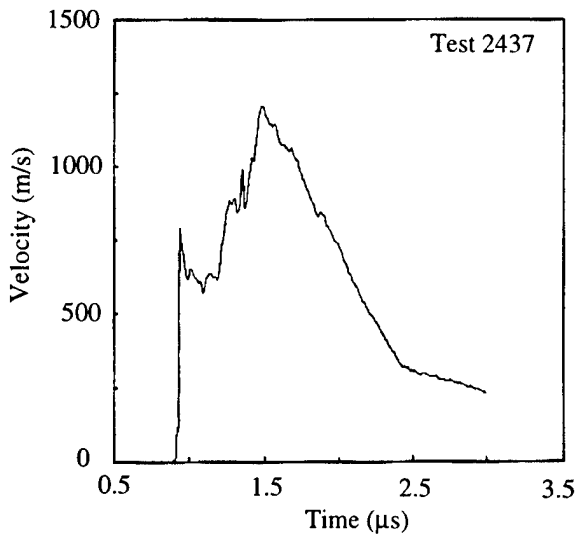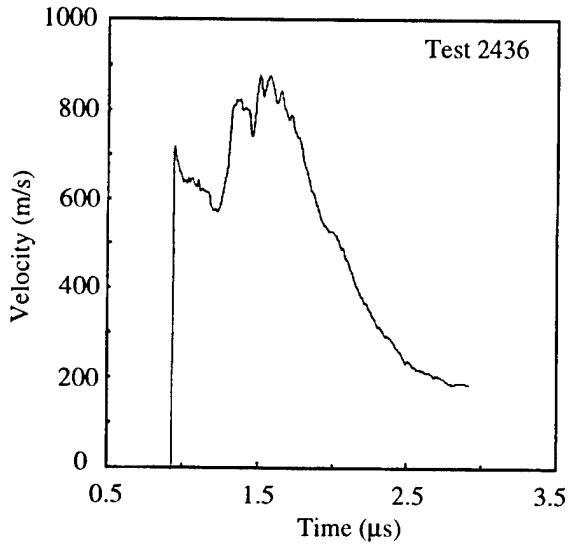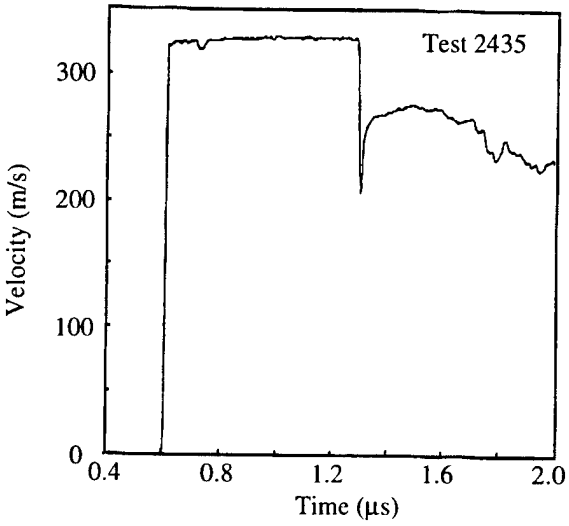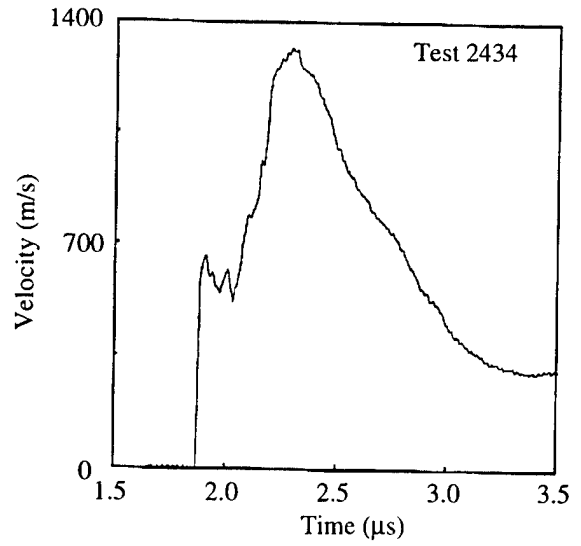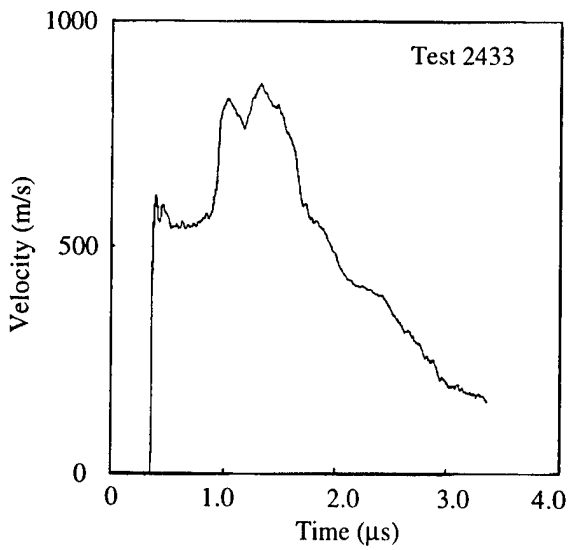
Figure 2.2.4.3 Ceramic-Window Interface Velocity Profiles from Grady and Moody [52] for Tests 2433-2438.
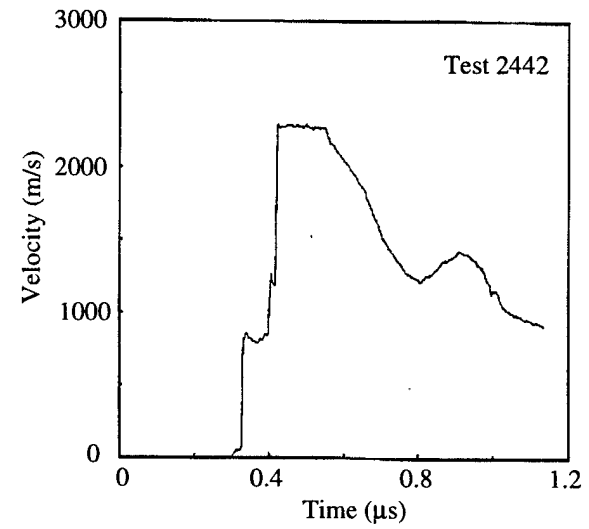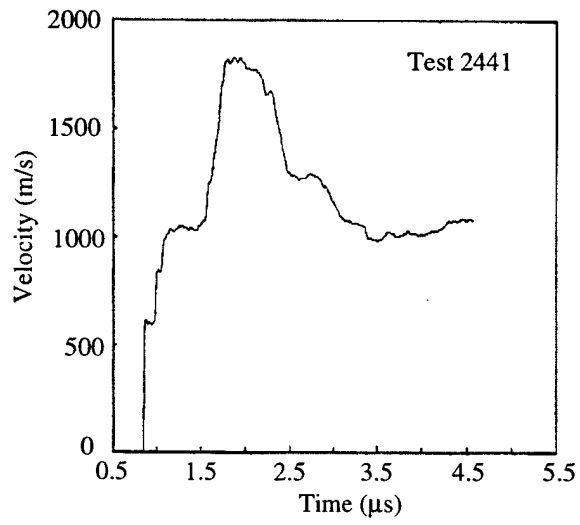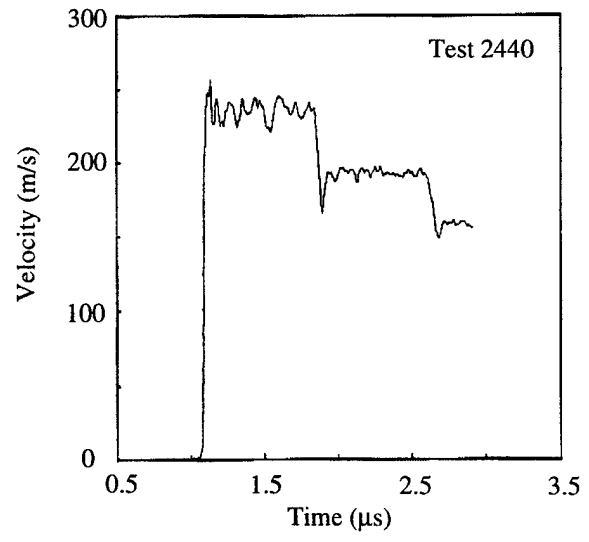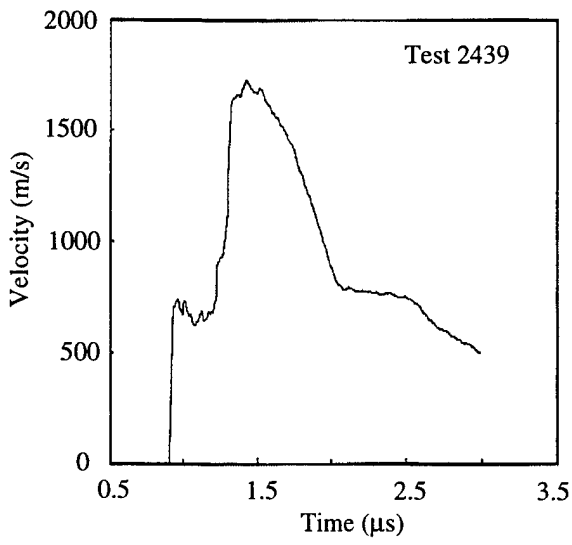
Figure 2.2.4.4 Ceramic-Window Interface Velocity Profiles from Grady and Moody [52] for Tests 2439-2442.
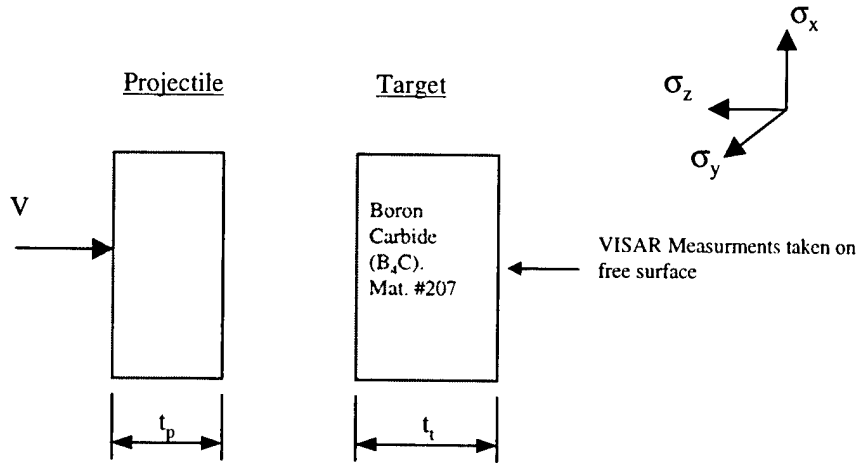
Figure 2.2.4.5   Description of the Plate Impact Test Configuration, Winkler and Stilp [81].

Table 2.2.4.4   Summary of Experimental Plate Impact Initial Conditions and Results, Winkler and Stilp [81].

Boron Carbide									
		Test Configuration			Elastic Compression		Plastic Compression		Spall Stress (GPa)
Test Number	Material Number	Projectile Material	t_p (mm)	t_t (mm)	Stress σ_z (GPa)	Density ρ (kg/m³)	Stress σ_z (GPa)	Density ρ (kg/m³)	
2443	207	PMMA	0.7	5.7	0.4				No spall
2444	207	PMMA	0.7	5.6	0.4				No spall
2445	207	Aluminum	1.5	5.7	1.0				0.59
2446	207	Armco Iron	1.5	5.7	3.1				0.66
2447	207	Armco Iron	1.0	5.7	10.4				0.66
2448	207	Armco Iron	1.5	5.7	10.8				0.77

Test 2443-2448: the test data is from work by Winkler and Stilp [81]. The Boron Carbide was hot pressed having an initial density = 2512kg/m³. None of the experiments exceeded the HEL thus only the elastic stresses are documented. The documented HEL, from reference 81, is at least 16.7 GPa.
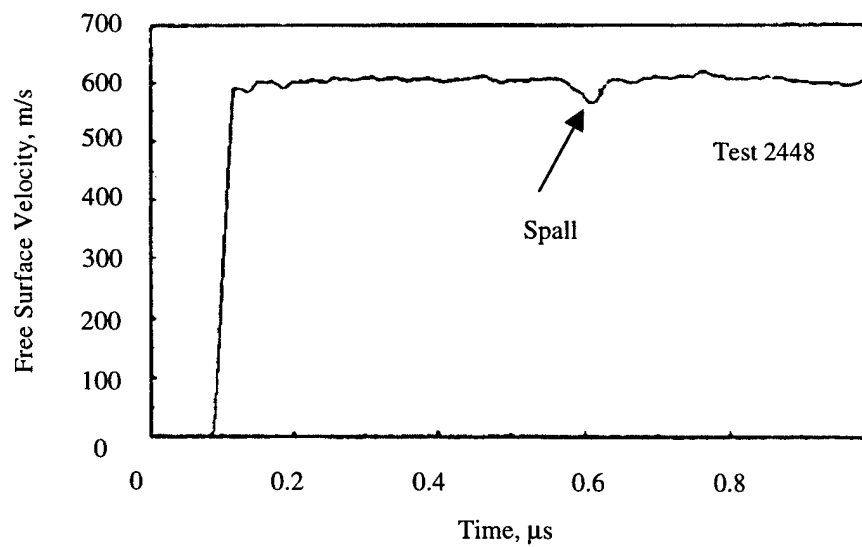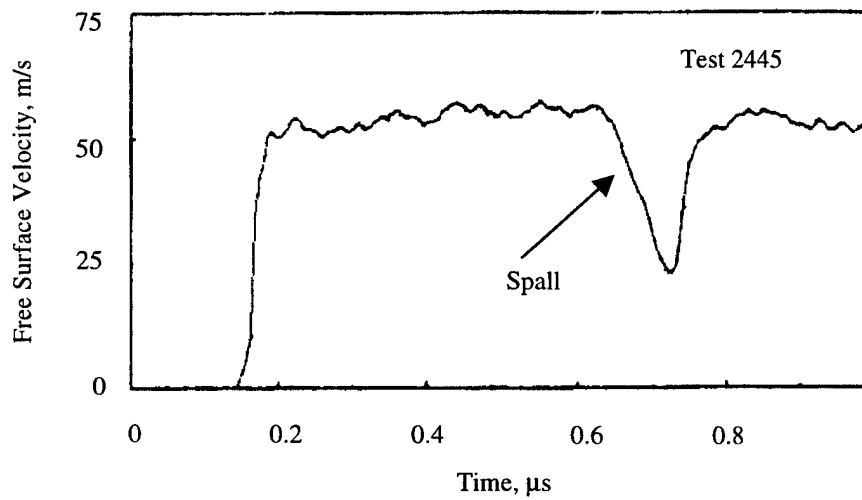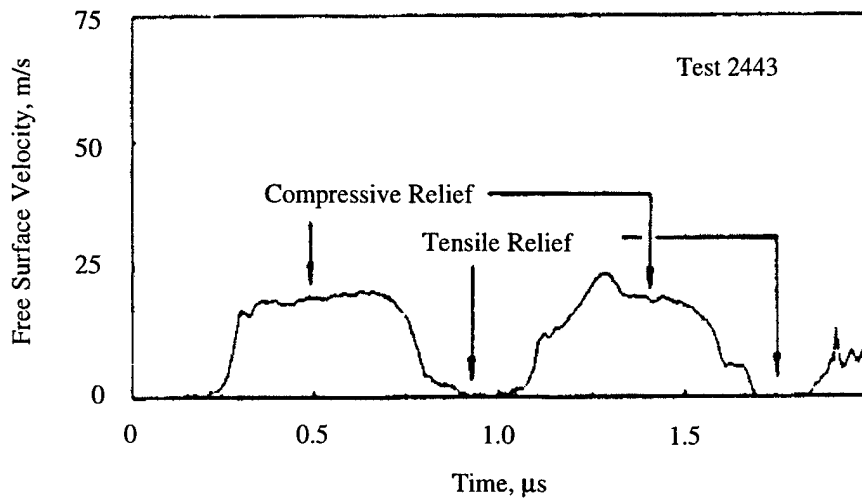
Figure 2.2.4.6 Ceramic Free Surface Velocity Profiles Investigating Spall Behavior, Winkler and Stilp [81].
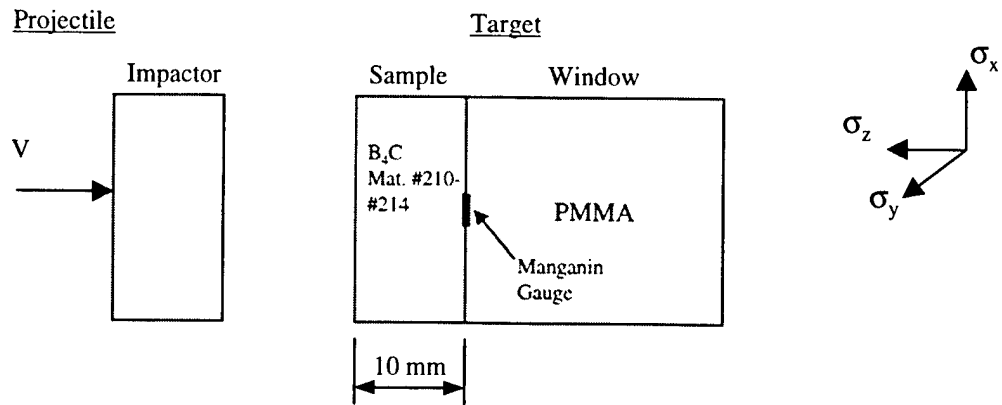
Figure 2.2.4.7 Description of Plate Impact Test Configuration, Brar *et al.* [90].

Table 2.2.4.5 Summary of Experimental Plate Impact Results, Brar *et al.* [90].

Boron Carbide					
Test Number	Material Number	Initial Density ρ_o (kg/m^3)	Porosity (%)	Results	
				HEL σ_z (GPa)	Plastic Wave Velocity (m/s)
2449	210	2130	16.3	9.6 +-0.3	6170
2450	211	2250	10.0	13.7 +-0.3	7100
2451	212	2330	4.8	16.3 +-0.4	7700
2452	213	2430	2.5	17.1 +-0.4	7900
2453	214	2520	0	19.4 +-0.3	9400
Test 2449-2453: The test data is from work by Brar *et al.* [90]. The data shows the effect of porosity on the HEL and the plastic wave velocity. The experimental data were obtained by using manganin gauges embedded at the back surface of the specimen and backed by a thick PMMA plate.The only information presented in Reference [90] were the HEL and plastic wave velocities as tabulated above.					

48

2.2.5 Penetration (semi-infinite) Test Data for Boron Carbide

Penetration results, into semi-infinite Boron Carbide, are presented in this section.

Orphal *et al.* [22] performed penetration experiments into Boron Carbide over a velocity range of 1500m/s to 4500m/s. The targets and penetrators used are described in Figure 2.2.5.1. The penetration results are presented graphically in Figure 2.2.5.2 and in tabular form in Table 2.2.5.1. Both primary and total penetration are given. Primary penetration is the depth penetrated when the penetrator is just consumed. Total penetration is the total depth penetrated when the penetration event is complete.

The target and penetrator configurations used in the penetration experiments performed by Lundberg *et al.* [89] are presented in Figure 2.2.5.3. The objective of the experimental program was to investigate penetration velocity as a function of lateral confinement and impact velocity. Cylindrical targets were fabricated with 1mm, 2mm and 4mm thick steel tubes confining a solid Boron Carbide cylinder. The Boron Carbide core was pre-confined by shrink fitting the steel confinement tube and torqueing the front and rear plugs to 24 Nm. The experiments were performed reverse ballistically. Impact velocities ranged from approximately 1450m/s to 2550m/s. Five x-rays were taken for each of the eleven experiments performed. The location of the penetrator tip was determine for each x-ray. The results are presented graphically in Figure 2.2.5.4 and in tabular form in Table 2.2.5.2.
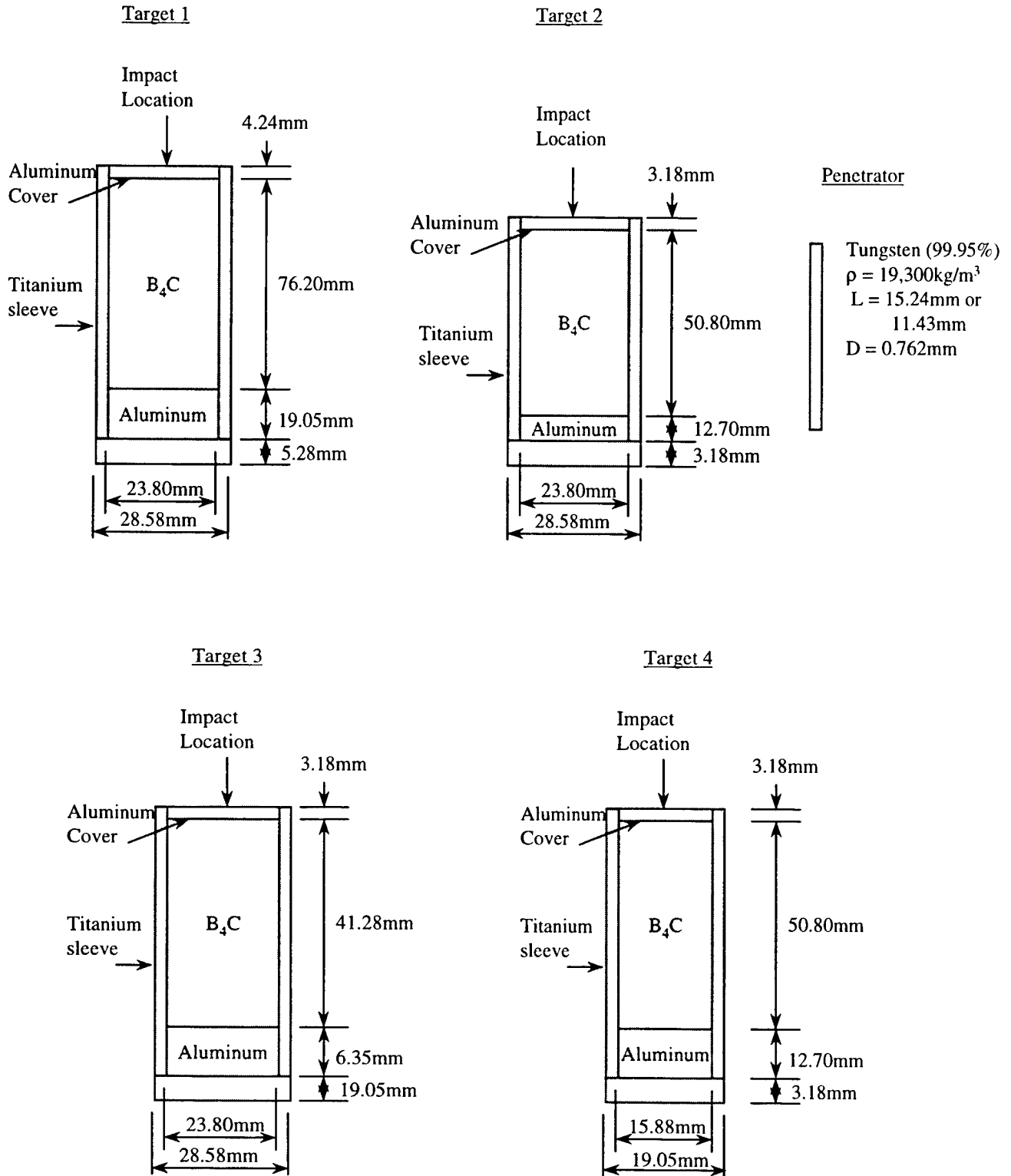
Figure 2.2.5.1 Boron Carbide Target and Penetrator Descriptions, Orphal *et al.* [22].
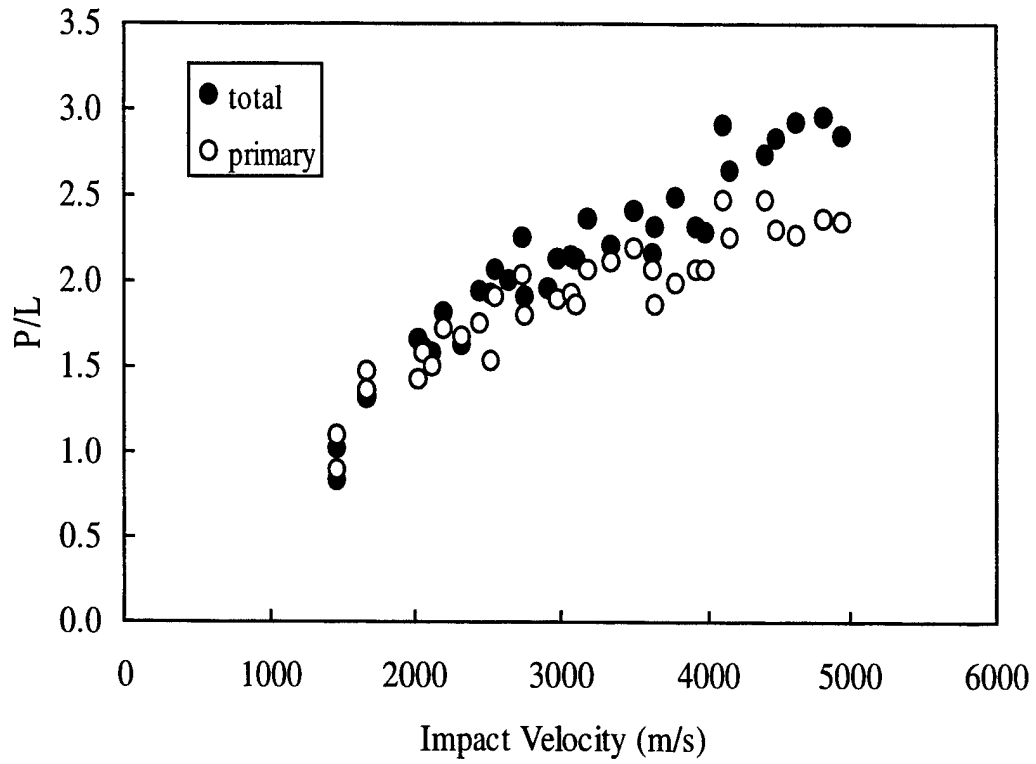
Figure 2.2.5.2   Normalized Total Penetration and Primary Penetration vs. Impact
Velocity for Tungsten Penetrators Impacting Confined Boron
Carbide Targets, Orphal *et al*. [22].

Table 2.2.5.1 Summary of Penetration Results, Orphal *et al.* [22]

Boron Carbide							
Test Number	Material Number	Penetrator		Target Configuration	Impact Velocity (m/s)	$P_{primary}/L$	P_{total}/L
		D (mm)	L (mm)				
2501	201	1.02	20.40	2	1490	0.88	0.82
2502	201	1.02	20.40	2	1490	1.08	1.00
2503	201	1.02	20.40	2	1690	1.46	1.31
2504	201	1.02	20.40	2	1700	1.34	1.29
2505	201	1.02	20.40	2	2040	1.40	1.64
2506	201	1.02	20.40	2	2070	1.57	1.59
2507	201	1.02	20.40	2	2130	1.48	1.56
2508	201	1.02	20.40	2	2220	1.71	1.80
2509	201	0.762	15.24	1 or 2	2340	1.65	1.61
2510	201	1.02	20.40	1 or 2	2470	1.73	1.92
2511	201	0.762	15.24	1 or 2	2540	1.51	1.90
2512	201	1.02	20.40	1 or 2	2570	1.89	2.05
2513	201	0.762	15.24	1 or 2	2670		1.99
2514	201	1.02	20.40	1 or 2	2770	2.01	2.23
2515	201	0.762	15.24	1	2780	1.78	1.89
2516	201	0.762	15.24	1	2940		1.93
2517	201	0.762	15.24	1	3000	1.88	2.11
2518	201	0.762	15.24	1	3100	1.90	2.12
2519	201	0.762	15.24	1	3130	1.85	2.11
2520	201	0.762	15.24	1	3200	2.04	2.34
2521	201	0.762	15.24	1	3360	2.10	2.19
2522	201	0.762	15.24	1	3520	2.17	2.39
2523	201	0.762	15.24	1	3640	2.04	2.14
2524	201	0.762	15.24	1	3660	1.84	2.30
2525	201	0.762	15.24	1	3800	1.97	2.47
2526	201	0.762	15.24	1	3940	2.05	2.30
2527	201	0.762	15.24	1	4000	2.05	2.27
2528	201	0.762	15.24	1	4130	2.45	2.89
2529	201	0.762	15.24	1	4180	2.24	2.62
2530	201	0.762	15.24	3 or 4	4430	2.45	2.72
2531	201	0.762	15.24	3 or 4	4510	2.28	2.81
2532	201	0.762	11.43	3 or 4	4650	2.25	2.90
2533	201	0.762	11.43	3 or 4	4840	2.35	2.93
2534	201	0.762	11.43	3 or 4	4960	2.33	2.83

Test 2501-2534: the test data is from work by Orphal *et al.* [22]. Three penetrator lengths and four target configurations were used. The impact velocity and P/L listed here were obtained from Figure 8 in Ref. 22. The penetration includes the 3.18mm cover. In some cases, at the lower velocities, the primary penetration exceeds the total penetration. This is not reality, but is a reflection of how the primary penetration is calculated. The penetration and erosion rates are determined from the x-rays. These rates are assumed to be constant and are used to determine when the penetrator is consumed, and at what depth. At the lower impact velocities the rates are not constant, thus larger primary penetration depths are calculated. A more in depth discussion of this is provided in Reference 22.

Impact
Location

4.0 mm

B₄C
Mat #209

39.6 mm

4.0 mm

19.0 mm

t

D

Sintered Tungsten Penetrator
DX 2 HCMF from Pechiney
ρ = 17600kg/m³
flow stress = 1.05 GPa
L = 150mm
D = 2.0 mm

Comments:
- Target confinement is tempered steel SIS 2541-3 comparable to AISI/SAE 4340.
- Target is axisymmetric
- B₄C ceramic is preconfined due to shrink fit of steel case by heating steel cylinder prior to insertion of ceramic.
- Confinement was varied by using steel cylinders of various outer diameter, D = 21, 23 & 27mm.

Figure 2.2.5.3 Boron Carbide Target and Penetrator Descriptions, Lundberg *et al.* [89].
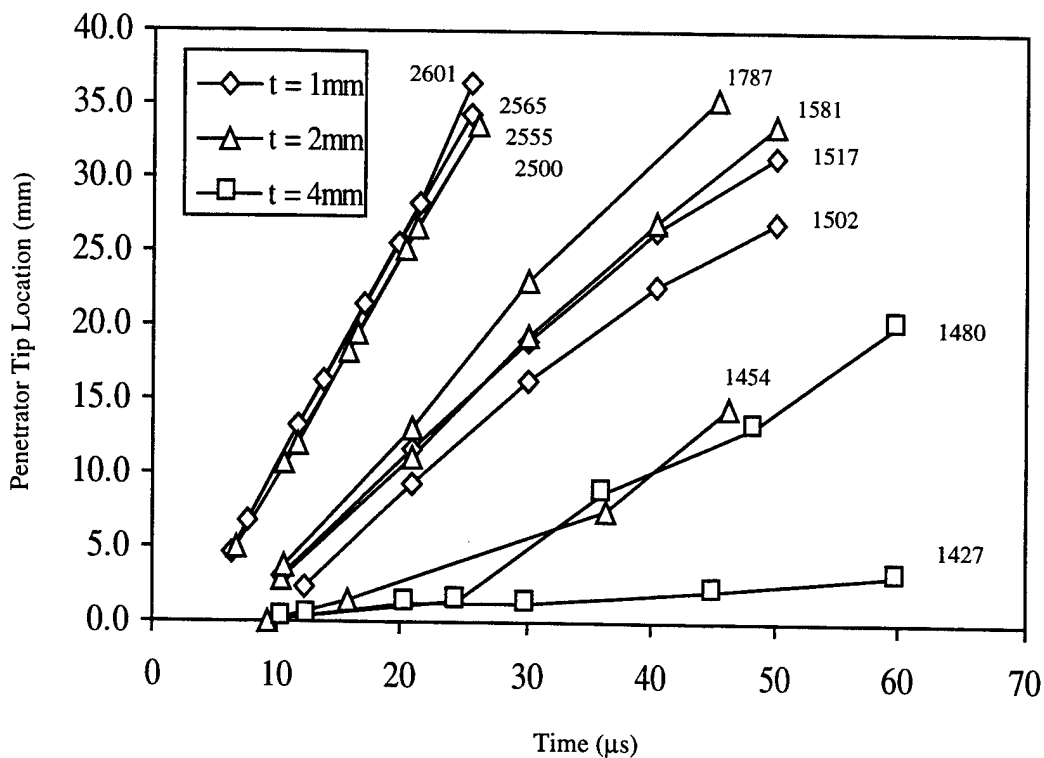
Figure 2.2.5.4   Penetration vs. Time for various confinements and impact velocities, Impact velocities shown for each test, Lundberg *et al.* [89].

53

Table 2.2.5.2 Summary of Penetration Results, Lundberg *et al.* [89]

Test Number	Material Number	Target Outer Diameter, D (mm)	Confinement t (mm)	Impact Velocity (m/s)	X-ray Time (μs)	Penetrator Tip Location* (mm)	Penetration Velocity Linear Fit (m/s)
						Boron Carbide	
2535	209	21	1	1502	12.3	2.4	632
					20.8	9.2	
					30.1	16.2	
					40.3	22.6	
					50.1	26.9	
2536	209	21	1	1517	10.4	3.1	720
					20.8	11.6	
					30.1	18.9	
					40.3	26.4	
					50.1	31.5	
2537	209	21	1	2565	6.4	4.7	1521
					11.7	13.3	
					13.8	16.2	
					19.7	25.6	
					25.5	34.2	
2538	209	21	1	2601	7.7	6.7	1581
					11.7	13.3	
					17.0	21.4	
					21.4	28.2	
					25.5	36.5	
2539	209	23	2	1454	9.3	0	271 (711)
					15.7	1.5	
					36.3	7.5	
					46.2	14.4	
2540	209	23	2	1581	10.4	2.9	770
					20.8	11.1	
					30.1	19.2	
					40.3	26.0	
					50.1	33.6	
2541	209	23	2	1787	10.6	3.7	920
					20.8	13.1	
					30.1	23.1	
					45.2	35.4	
2542	210	23	2	2500	6.8	5.0	1487
					11.7	11.9	
					16.5	19.4	
					21.2	26.6	
					26.1	33.6	
2543	211	23	2	2555	10.6	10.7	1448
					15.7	18.3	
					20.4	25.2	
					26.1	33.6	

Table 2.2.5.2 Summary of Penetration Results, Lundberg *et al.* [89] Concluded.

Boron Carbide							
Test Number	Material Number	Target Outer Diameter, D (mm)	Confinement t (mm)	Impact Velocity (m/s)	X-ray Time (μs)	Penetrator Tip Location* (mm)	Penetration Velocity Linear Fit (m/s)
2544	209	27	4	1427	10.6	0.2	59
					20.6	1.2	
					30.1	1.2	
					45.0	2.1	
					60.0	3.2	
2545	209	27	4	1480	12.7	0.3	511 (97)
					24.6	1.4	
					36.1	8.7	
					48.4	13.3	
					60.0	20.2	

Test 2535-2545: The test data is from work by Lundberg *et al.* [89]. Five 450kV x-ray flashes were taken for each experiment. The data listed above were obtained from Figure 3 and Table 1 in Reference [89].
* The penetrator tip location is measured from the boron carbide-steel interface.
The uncertainty in penetration depths is +-0.15mm
Test 2539, 2545: The penetration velocity in parentheses was obtained excluding the first and last penetration measurements.

2.2.6 Depth-Of-Penetration (DOP) Test Data for Boron Carbide

This section presents depth-of-penetration (DOP) experiments for numerous Boron Carbide materials. The DOP test has been used to investigate the effectiveness of ceramics for a number of years. The typical DOP configuration consists of a ceramic tile place on, or within, a steel or aluminum base target. A penetrator impacts and perforates the ceramic tile and continues into the base target. The penetration into the base target is generally referred to as the residual penetration, P_r, and is used to determined the ceramic mass efficiency as discussed in Section 2.0.

The target and penetrator description for the DOP experiments by Reaugh et al. [85] is presented in Figure 2.2.6.1. The objective of the experimental program was to investigate the ballistic efficiency of Boron Carbide as a function ceramic thickness, impact velocity and impact angle. The results are presented in tabular form in Table 2.2.6.1. Also included in the table are penetration results into the 4340 Steel with no ceramic .

The target and penetrator description for the DOP experiments by Rosenberg et al. [91] is presented in Figure 2.2.6.2. The objective of the experimental program was to investigate the ballistic efficiency of Boron Carbide as a function ceramic thickness. The results are presented in in Table 2.2.6.2. Also included in the table are penetration results into the steel base target with no ceramic .
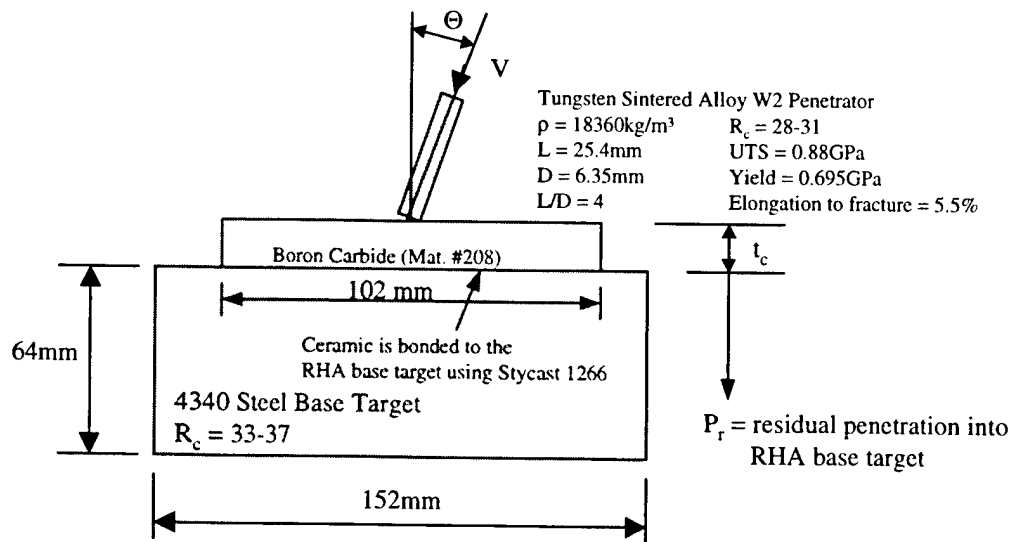
Figure 2.2.6.1 Target and Penetrator Description for DOP Experiment, Reaugh et al. [85].

Table 2.2.6.1 Summary of Experimental DOP Results, Reaugh *et al.* [85].

Boron Carbide					
Test Number	Material Number	Impact Velocity (m/s)	Ceramic t_c (mm)	Impact Angle# Θ (degrees)	P_r& (mm)
2601	208	1790	10.4	0	28.3
2602	208	1740	19.3	0	19.8
2603	208	1780	28.8	0	9.8
2604	208	1790	28.0	30	3.3
2605	208	1770	17.6	60	2.2
2606	208	1280	10.4	0	13.3
2607	208	1220	15.2	0	3.8
2608	208	1290	19.2	0	0.0
2609	208	2610	38.9	0	14.5
2610	208	2610	58.6	0	5.6
2611		1340	0	0	27.0
2612		1350	0	0	27.8
2613		1350	0	0	28.5
2614		1770	0	0	36.0
2615		2500	0	0	43.8

Test 2601-2615: the test data is from work by Reaugh *et al.* [85].
#the angle between the penetrator flight axis and the normal to the tile.
& the residual penetration measured normal to the impact surface.
Test 2611-2615: tests into 4340 steel target only (no ceramic used).
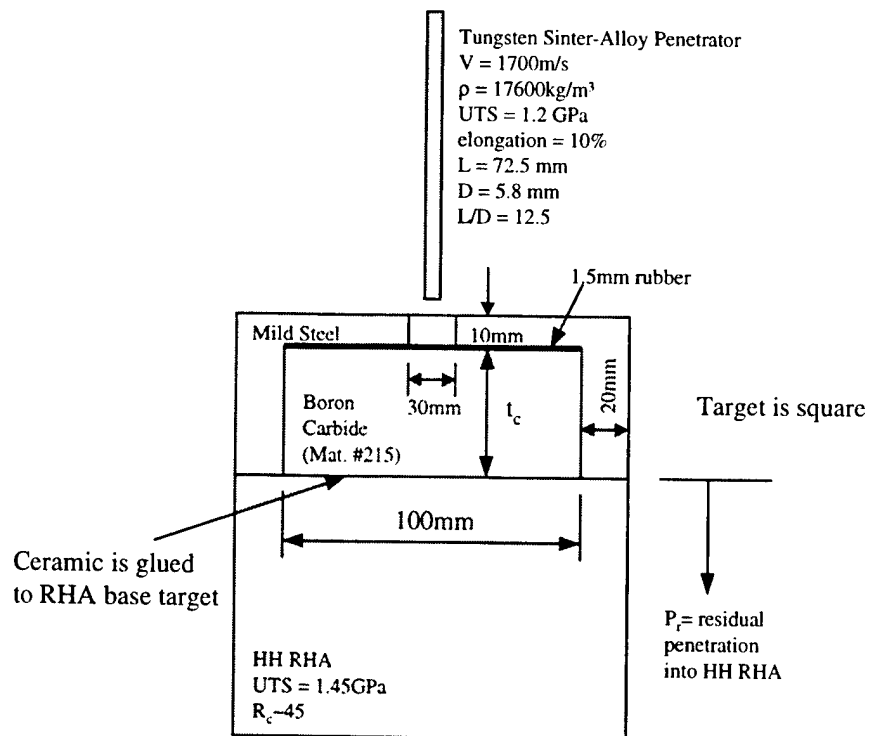
Figure 2.2.6.2 Target and Penetrator Description for DOP Experiment, Rosenberg *et al.* [91].

Table 2.2.6.2 Summary of Experimental DOP Results, Rosenberg *et al.* [91].

Boron Carbide					
Test Number	Material Number	Impact Velocity (m/s)	Ceramic t_c (mm)	ρt_c (kg/m^2)	P_r (mm)
2616	215	1700	46.4	116	32.2
2617	215	1700	82.8	207	7.4
2618		1700	0	0	62.4
Test 2616-2618: the test data is from work by Rosenberg *et al.* [91]. The tabulated data listed above was obtained from Figure 1 in Reference [91]. All targets were square ρ = 2500kg/m^3 (density of ceramic) Test 2618: test into steel base target only (no ceramic used).					

2.2.7 Perforation Test Data for Boron Carbide

This section presents perforation experiments where the target is usually perforated by the penetrator. Targets are typically comprised of a ceramic front layer and a metallic rear layer and are commonly used in light armor applications. The most common piece of data extracted from perforation experiments is the target ballistic limit, V_{bl}, previously defined in Section 2.0.

The target and penetrator descriptions for the perforation experiments by Wilkins *et al.* [24, 26, 27] are presented in Figure 2.2.7.1. The objective of the experiments was to determine the ballistic limit velocity as a function of ceramic front plate thickness and penetrator geometry. The results are presented graphically in Figure 2.2.7.2 where the ballistic limit velocity of the sharp projectile is plotted vs. target rear plate thickness for various ceramic front plate thicknesses. Figure 2.2.7.3 presents the ballistic limit velocity for both the sharp and blunt projectile. The results are also presented in tabular from in Table 2.2.7.1.

Target Configuration

Impact location

Boron Carbide	Δ
6061-T6 Aluminum Back Plate	δ

Bonded using polyurethane
(Scotchcast 221)

Sharp Penetrator

Allegheny Steel 609
$R_c = 54$-56
$M = 8.32g$
$L \sim 29$ mm
$D = 7.62$ mm
cone angle = 55°

Blunt Penetrator

Allegheny Steel 609
$R_c = 54$-56
$M = 8.32g$
$L \sim 24$ mm
$D = 7.62$ mm
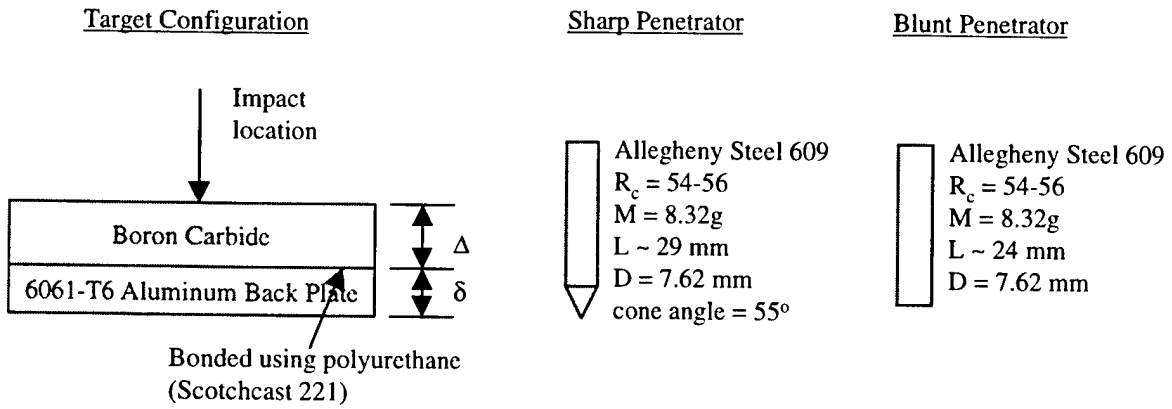
Figure 2.2.7.1   Target and Penetrator Descriptions, Wilkins *et al.* [24, 26, 27].

Sharp Penetrator Impacting:
Boron Carbide Front Plate
6061-T6 Aluminum Rear Plate

Boron Carbide
Ceramic Thickness, mm

- ■ $\Delta = 5.33$
- ◆ $\Delta = 5.72$
- ▲ $\Delta = 6.35$
- ✕ $\Delta = 7.24$
- △ $\Delta = 7.37$
- ○ $\Delta = 7.62$
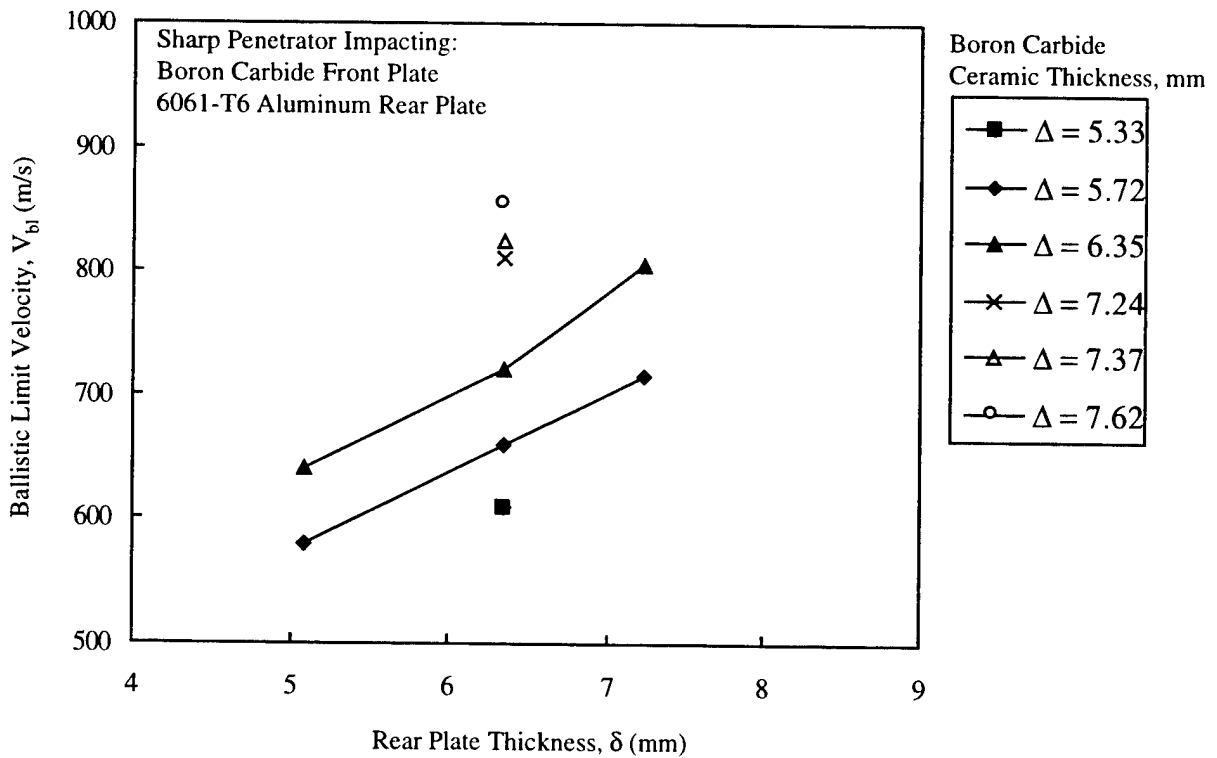
Figure 2.2.7.2   Sharp Penetrator Ballistic Limit Velocity as a function of Boron Carbide ceramic Thickness and 6061-T6 Aluminum Rear Plate Thickness, Wilkins *et al.*[24, 26, 27].
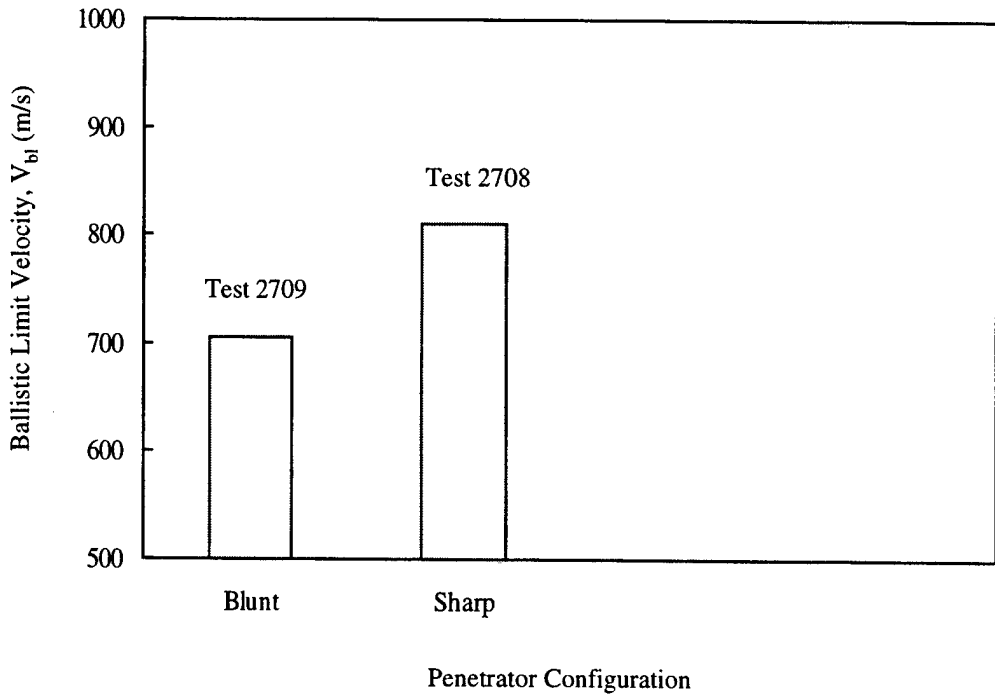
Figure 2.2.7.3   Ballistic Limit Velocity for Sharp and Blunt Projectile Impacting a 7.24mm
Boron Carbide Front Plate and a 6.35mm 6061-T6 aluminum Rear Plate
Target, Wilkins *et al.* [24, 26, 27].

Table 2.2.7.1   Ballistic Limit Velocities for Two Penetrator types against Various Boron
Carbide Target Configurations, Wilkins *et al.* [24, 26, 27].

Boron Carbide					
Test Number	Material Number	Penetrator	Target Configuration		Ballistic Limit Velocity, V_{bl} (+- 15m/s)
			Δ (mm)	δ (mm)	
2701	202	Sharp	5.33	6.35	610
2702	202	Sharp	5.72	5.08	580
2703	202	Sharp	5.72	6.35	660
2704	202	Sharp	5.72	7.24	715
2705	202	Sharp	6.35	5.08	640
2706	202	Sharp	6.35	6.35	720
2707	202	Sharp	6.35	7.24	805
2708	202	Sharp	7.24	6.35	810
2709	202	Blunt	7.24	6.35	705
2710	202	Sharp	7.37	6.35	825
2711	202	Sharp	7.62	6.35	855

Test 2701-2711: the test data is from work by Wilkins *et al.*[24, 26, 27]. Two penetrator
configurations were used, a sharp and blunt. Target configurations consisted of a
Boron Carbide front plate bonded to a 6061-T6 aluminum rear plate.The ballistic limit
velocity was experimentally determined for each target configuration within a +-15m/s
error.

2.3 TITANIUM DIBORIDE

2.3.1 Material Description for Titanium Diboride

The purpose of this section is to provide as much information as possible on the materials tested. Descriptions for each of the Titanium Diboride materials used in Section 2.3 are presented in Table 2.3.1.1. Each material is given a material number which is used throughout Section 2.3 to identify it. The data listed in Table 2.3.1.1 were obtained directly from the corresponding reference. When specific information was not available it was left blank. The strength values listed, (Tensile, Compressive, HEL and Spall), are nominal values and are included for comparison purposes. Titanium Diboride exhibits two cusps when shock loaded and are referred to as the lower and upper HEL. Occasionally researchers will determine the chemical composition of the material being tested to further characterize it, Table 2.3.1.1 includes this data when available.

Table 2.3.1.1   Description of the Titanium Diboride Materials Tested

	Material Number					
	301	302	303	304	305	306
Reference	1	26	4 1	46	52, 55, 59	52, 54, 59
Manufacturer	Union Carbide		Ceradyne	Cercom	Eagle Picher	Cercom
Trade Name/Description						
Processing	Hot Pressed					
Average Grain Size (µm)				30	12	30
Density (kg/m³)	4510	4520	4520	4509	4452	4509
Void Fraction	~0				>0.01	
Longitudinal Velocity (m/s)	11210	11300		10790	10930	10790
Shear Velocity (m/s)	7250	7300		7430	7300	7430
Bulk Velocity (m/s)	7460	7580		6540	6960	6540
Young's Modulus, E (GPa)	541	552	414	522	520	522
Shear Modulus, G (GPa)	237	241		248	237	249
Bulk Modulus, K (GPa)	251	260		193	216	193
Poisson's Ratio	0.141	0.146		0.049	0.098	0.049
Compressive Strength (GPa)			~5.7	3.75		
Tensile Strength (GPa)						
HEL (lower yield) (GPa)	8.6+-3.0	5.4			4.7-5.2	
HEL (upper yield) (GPa)					13.1-13.7	17.0
Spall Strength (GPa)						0.4-0.5
Impurities (%wt)						
SiO$_2$	0.04					
Al$_2$O$_3$	0.04					
CaO	0.01					
CrO$_3$	0.2					
MnO	0.01					
Fe$_2$O$_3$	1.0					
NiO	0.2					

Table 2.3.1.1 Description of the Titanium Diboride Materials Tested, Continued.

	307	308	309	310	311	312	313
	Material Number						
Reference	52, 59	52	64	64	69	81, 82	85
Manufacturer	Ceradyne		Cercom	Ceradyne	Cercom		Dow
Trade Name/Description							
Processing	Hot Pressed				Hot Pressed*	Hot Pressed	
Average Grain Size (μm)							
Density (kg/m³)	4490	4360	4470	4450	4430	4360	4490
Void Fraction	0.009						
Longitudinal Velocity (m/s)	11230	10800	11160	11470	11285	10790	11080
Shear Velocity (m/s)	7410	7300			7430	7240	7430
Bulk Velocity (m/s)	7270	6750			7250	6820	7010
Young's Modulus, E (GPa)	550	501			537	499	540
Shear Modulus, G (GPa)	247	232			249	229	248
Bulk Modulus, K (GPa)	237	199			233	203	220
Poisson's Ratio	0.114	0.079			0.11	0.09	0.090
Compressive Strength (GPa)					4.82		
Tensile Strength (GPa)							
HEL (lower yield) (GPa)	5.9		7.1	7.2-7.9		4.2-4.9	
HEL (upper yield) (GPa)	13.5					9.0	
Spall Strength (GPa)	0.30-0.35					0.43-0.53	
Impurities (%wt)							
W	0.83						
C	0.3						
Co	0.2						
N	0.37						
O	0.32						

* Pressure Assisted Densified (PAD)

Table 2.3.1.1 Description of the Titanium Diboride Materials Tested, Concluded.

	314	315					
	Material Number						
Reference	87	91					
Manufacturer	Cercom						
Trade Name/Description							
Processing	Hot Pressed						
Average Grain Size (μm)							
Density (kg/m³)		4450					
Void Fraction							
Longitudinal Velocity (m/s)							
Shear Velocity (m/s)							
Bulk Velocity (m/s)							
Young's Modulus, E (GPa)		570					
Shear Modulus, G (GPa)							
Bulk Modulus, K (GPa)							
Poisson's Ratio							
Compressive Strength (GPa)		3.0					
Tensile Strength (GPa)							
HEL (lower yield) (GPa)							
HEL (upper yield) (GPa)							
Spall Strength (GPa)							

2.3.2 Mechanical Test Data for Titanium Diboride

The following section presents mechanical test results for Titanium Diboride. A typical test specimen showing the stress configuration is shown in Figure 2.3.2.1. Compression is taken as positive and tension as negative. Loading is generally uniaxial in the z direction and is increased until the material fails, although some researchers use more complex loading techniques to vary the stress state at failure.

Mechanical test data performed by Lankford [46] are presented in Table 2.3.2.1. The objective of the experiments was to determine the strength of Titanium Diboride as a function of strain rate. The stress state at failure is given as a function of average strain rate, $\dot{\varepsilon}$, in Table 2.3.2.1. Both Hopkinson bar and quasi-static experiments were performed.

Mechanical test data performed by Meyer and Faber [88] are presented in Table 2.3.2.2. The objective of this work was to determine the strength of fractured ceramic as a function of pressure and strain rate. These tests were performed using pre-fractured ceramic. The pre-fractured ceramic was obtained from plate impact debris having an average particle size of 2.0 mm. The ceramic particles were placed inside a steel tube providing confinement in the radial and tangential directions, $\sigma_x = \sigma_y$. An axial load, σ_z, was applied until yielding of the steel tube occurred. Different combinations of tube wall thickness and strength were used to vary the confining stress. The bulk density of the ceramic when place in the tube was approximately 50%. No information on the Titanium Diboride material was provided in Reference [88] and thus it was not given a material number.
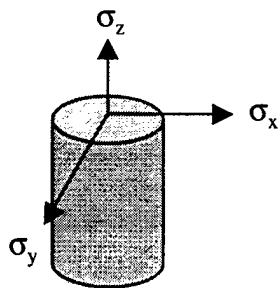

Figure 2.3.2.1 Description of a Typical Mechanical Test Specimen.

65

Table 2.3.2.1 Summary of Experimental Results, Lankford [46].

			Titanium Diboride		
Test Number	Material Number	σ_z (GPa)	σ_x (GPa)	σ_y (GPa)	$\sim \dot{\varepsilon}$ (s^{-1})
3201	304	3.76	0	0	6.92×10^{-5}
3202	304	3.99	0	0	9.15×10^{-5}
3203	304	3.85	0	0	4.48×10^{-2}
3204	304	3.41	0	0	4.56×10^{-2}
3205	304	4.01	0	0	4.08×10^{-1}
3206	304	4.03	0	0	4.09×10^{-1}
3207	304	4.18	0	0	1.15×10^{3}
3208	304	4.46	0	0	1.18×10^{3}
3209	304	4.44	0	0	1.30×10^{3}
3210	304	5.60	0	0	1.95×10^{3}
3211	304	4.69	0	0	2.13×10^{3}

Test 3201-3211: the test data is unpublished by Lankford. Compression tests were performed to obtain the compressive strength as a function of strain rate. The highest strain rate testing used a Hopkinson bar system. The Titanium Diboride was manufactured by Cercom Inc. having an initial density = 4509kg/m^3.

Table 2.3.2.2 Summary of Experimental Results, Meyer and Faber[88].

			Titanium Diboride			
Test Number	Material Number	σ_z (GPa)	σ_x (GPa)	σ_y (GPa)	$\sim \dot{\varepsilon}$ (s^{-1})	Ref.
3212		0.97	0.09	0.09	5×10^{-4}	88
3213		1.89	0.31	0.31	5×10^{-4}	(Meyer)
3214		2.56	0.58	0.58	5×10^{-4}	
3215		1.01	0.25	0.25	7.7×10^{1}	
3216		2.01	0.43	0.43	7.7×10^{1}	
3217		3.22	0.56	0.56	7.7×10^{1}	

Test 3212-3217: This work was performed by Meyer and Faber [88]. The above data was obtained from Figures 5-6 in Reference [88]. Confinement was provided by steel cylinders of various thickness and strength. Axial loads were applied until the cylinder yielded. The axial stress, σ_z, was measured directly and the lateral stresses, $\sigma_x = \sigma_y$ were obtained using strain gauges. The axial stress, σ_z, listed above is the maximum stress obtained for the corresponding confining stress, $\sigma_x = \sigma_y$. No information was given for the material in Reference [88] and thus was not given a material number.

2.3.3 Hydrostatic Test Data for Titanium Diboride

The hydrostatic response for Titanium Diboride is presented in this section. The pressure - volume response was obtained by Akella [19] using a diamond anvil cell. The data is presented graphically in Figure 2.3.3.1 and summarized in Table 2.3.3.1 where P is the pressure and V/V_o is the relative volume, where V is the measured volume and V_o is the initial volume. Very little information was provided on the material, thus the material was not given a specific material number. As can be seen in Figure 2.3.3.1 the material exhibits a response much stiffer than would be expected from a hydrostatic environment. A possible explanation is that the loading environment was not truly hydrostatic, but rather included inadvertently induced deviator stresses [96].
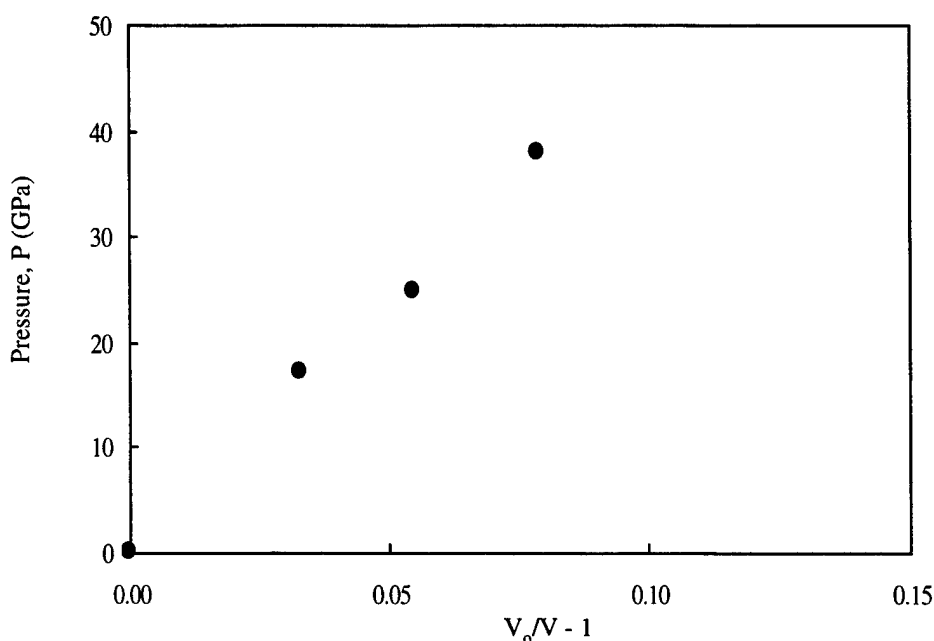
Figure 2.3.3.1 Pressure vs. Volume Relationship, Akella [19].

Table 2.3.3.1 Summary of the Hydrostatic Experimental Results, Akella [19].

Titanium Diboride				
Test Number	Material Number	P (GPa)	V/V_o	$V_o/V - 1$
3301		0	1.0	0
3302		17.1	0.968	0.033
3303		24.8	0.948	0.055
3304		38.0	0.927	0.079
Test 3301-3304: this data was obtained using a diamond anvil cell. No information on the material was provided, thus it was not given a material number. This work is unpublished performed by Akella [19]. The work was performed for Steinberg (Ref. 20) where it is briefly discussed.				

2.3.4 Plate Impact Test Data for Titanium Diboride

The following section presents plate impact results performed by various researchers using various Titanium Diboride materials. A typical plate impact test configuration is presented in Figure 2.3.4.1. The peak stress, σ_z, occurs in the z-direction and is generally measured for both the elastic and plastic response. The lateral stresses, σ_x and σ_y, occur due to the uniaxial strain configuration of the experiment, and are typically not measured. The peak stress for the elastic regime is referred to as the Hugoniot Elastic Limit (HEL) and has become a fundamental property of ceramics. The peak stress for the plastic response is generally referred to as the peak Hugoniot stress. The particle velocity and wave velocity for both the elastic and plastic waves are typically measured and documented herein. In some cases the entire particle velocity time history is measured using laser velocity interferometry techniques (VISAR). VISAR traces provide direct information on the material response and are included in this section when available.

The results from Gust et al. [1] are summarized in Table 2.3.4.1. The shock velocity, particle velocity, peak stress, σ_z, and density, ρ, for both the elastic and deformational waves are presented.

A description of the plate impact test configuration used by Grady and Moody [52] is presented in Figure 2.3.4.2. The specific test dimensions are summarized in Table 2.3.4.2. Compression and release behavior of the Titanium Diboride was measured by monitoring the ceramic-window interface velocity using laser velocity interferometry techniques (VISAR). The interface velocity profiles reflect the uniaxial strain loading and unloading behavior of the material and are presented in Figures 2.3.4.3-6 .

A description of the impact experiment performed by Dandekar et al. [59] to investigate the spall behavior of Titanium Diboride is presented in Figure 2.3.4.7. Two types of spall experiments were performed. Conventional symmetric impact (Test 3441-3448) and a experiment that induced a shock-release cycle prior to inducing a tensile stress (Test 3449-3450). The results are summarized in Table 2.3.4.3.

A description of the impact experiments performed by Yaziv et al. [64] to investigate the HEL and spall of Titanium Diboride are presented in Figure 2.3.4.8. The results are summarized in Table 2.3.4.4.

A description of the impact experiments performed by Winkler and Stilp [81, 82] is presented in Figure 2.3.4.9. The objective of the experimental program was to investigate the HEL, Hugoniot and spall behavior of TiB_2. The results are summarized in Table 2.3.4.5. Compression and release behavior of the Titanium Diboride was measured by monitoring the ceramic free surface velocity using laser velocity interferometry techniques (VISAR). The free surface velocity profiles of selected experiments are presented in Figure 2.3.4.10.

A description of the impact experiments performed by Rosenberg et al. [87] is presented in Figure 2.3.4.11. The objective of the experiments was to investigate the shear strength behavior of TiB_2 above the HEL. A Manganin gauge was used to measure the transverse stress in the material and was the only stress measured. The longitudinal stress was inferred from Hugoniot data from previous researchers[52, 54, 64]. The results are summarized in Table 2.3.4.6.
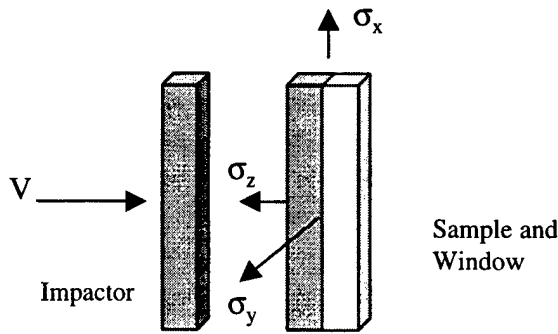
68

σ_x

V →

Impactor

σ_z

σ_y

Sample and Window

Figure 2.3.4.1 Description of a Typical Plate Impact Test Configuration including Stress Orientations

Table 2.3.4.1 Summary of Experimental Plate Impact Results from Gust *et al.*[1].

		Initial Density ρ_o (kg/m^3)	Elastic Regime (HEL)				Plastic Regime			
Test Number	Material Number		Shock Velocity (m/s)	Particle* Velocity (m/s)	σ_z (GPa)	ρ (kg/m^3)	Shock Velocity (m/s)	Particle# Velocity (m/s)	σ_z (GPa)	ρ (kg/m^3)
3401	301	4516	11530	71	3.7	4548	9920	310	14.4	4659
3402	301	4516	11220	173	8.7	4585	9790	321	14.8	4652
3403	301	4518	11760	170	9.0	4585	10070	319	15.8	4655
3404	301	4516	10840	134	6.5	4572	9630	538	24.2	4780
3405	301	4515	11750	265	14.0	4617	9980	505	35.0	4736
3406	301	4513	11400	180	9.3	4585	9640	520	24.0	4757
3407	301	4512	10990	228	11.3	4608	9630	675	30.6	4838
3408	301	4517	11180	115	5.8	4564	9300	729	31.6	4895
3409	301	4516	11210	215	10.9	4602	9140	727	32.0	4882
3410	301	4514	11400	227	11.7	4606	9840	715	33.2	4851
3411	301	4517	11520	158	8.2	4581	9580	992	43.9	5023
3412	301	4515	11630	103	5.4	4554	9420	994	43.1	5039
3413	301	4513	11200	147	7.4	4575	9510	1235	53.6	5118
3414	301	4509	11450	127	6.6	4562	9690	1200	53.4	5139
3415	301	4518	11010	181	9.0	4591		1300	56.6	5233
3416	301	4517					9950	1690	75.9	5441
3417	301	4513					10190	1730	79.7	5441
3418	301	4515					10220	2040	93.9	5640
3419	301	4517					10440	2350	111.0	5834

Test 3401-3419: the test data is from work by Gust *et al.* [1]. As is shown there is a large scatter in the HEL. Reference 1 documents the HEL as 8.6 + - 3.0 GPa.

* The elastic particle velocity presented here is half the measured free surface velocity ($U_p=1/2U_{fs}$).

In Reference 1 the deformational particle velocity was calculated by $U_p=1/2U_{fs}$ and by impedance matching. The particle velocity presented here is an average of the two.
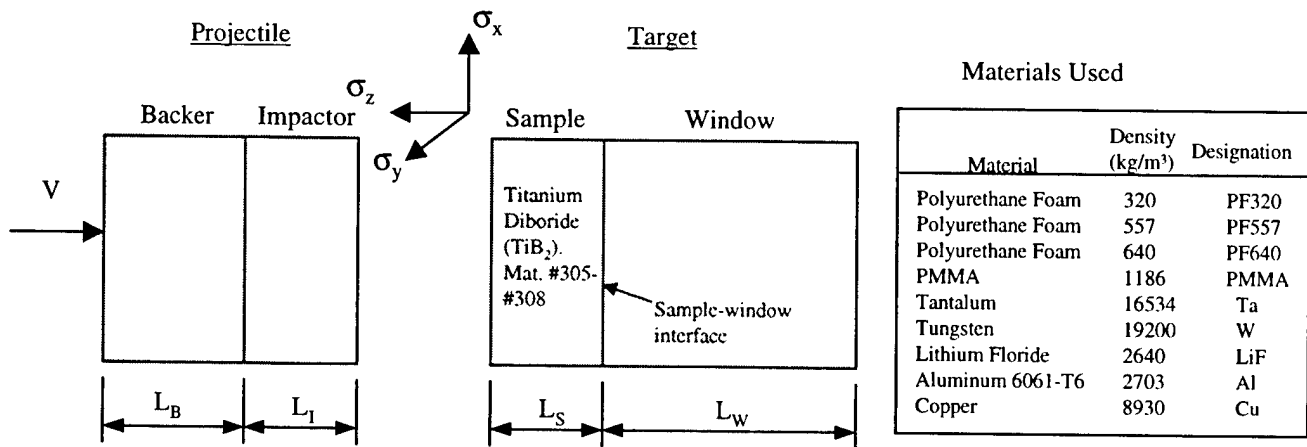
69

Figure 2.3.4.2 Description of the Plate Impact Test Configuration used by Grady and Moody [52] including the Stress Orientation and Materials used for the Projectile.

Materials Used

Material	Density (kg/m³)	Designation
Polyurethane Foam	320	PF320
Polyurethane Foam	557	PF557
Polyurethane Foam	640	PF640
PMMA	1186	PMMA
Tantalum	16534	Ta
Tungsten	19200	W
Lithium Floride	2640	LiF
Aluminum 6061-T6	2703	Al
Copper	8930	Cu

Table 2.3.4.2 Summary of Experimental Plate Impact Initial Conditions and Results from Grady and Moody [52].

Test Number	Material Number	Projectile V (m/s)	Backer Material*	Backer L_B (mm)	Impactor Material	Impactor L_I (mm)	Sample Density (kg/m³)	Sample L_S (mm)	Window Material	Window L_W (mm)	Elastic Compression $\sigma_z^\#$ (GPa)	Elastic Compression ρ (kg/m³)	Plastic Compression σ_z (GPa)	Plastic Compression ρ (kg/m³)
3420	305	2113	PF640	6.0	TiB$_2$	3.337	4452	10.747	LiF	25.4	4.7/13.1		48.5	
3421	305	2253	PF640	6.0	Ta	1.506	4452	10.055	LiF	25.4				
3422	305	1515	PF320	6.0	TiB$_2$	3.972	4452	10.804	LiF	25.4	5.2/13.7		31.0	
3423	306	1503	PF320	6.0	TiB$_2$	2.501	4509	5.011	LiF	25.4				
3424	306	1503	PF320	6.0	TiB$_2$	5.146	4509	10.097	LiF	25.4				
3425	306	367	PF320	6.0	TiB$_2$	4.899	4509	10.091	PMMA	25.4				
3426	306	1112	PF320	6.0	TiB$_2$	5.100	4509	10.193	LiF	25.4				
3427	306	2293	PF640	6.0	TiB$_2$	5.161	4509	10.165	LiF	25.4				
3428	306	741	PF160	6.0	PMMA	2.018	4509	10.088	PMMA	25.4				
3429	306	1155	PF160	8.0	PMMA	2.000	4509	10.347	PMMA	24.1				
3430	306	1439	PF160	8.0	PMMA	2.002	4509	10.246	PMMA	24.21				
3431	306	1708	PF139	7.9	PMMA	2.001	4509	10.126	LiF	25.4				
3432	306	1469	PF420	8.0	TiB$_2$	2.985	4509	5.016	LiF	19.0				
3433	306	1110	PF390	8.0	TiB$_2$	3.000	4509	4.906	LiF	18.9				
3434	306	604	PF330	6.3	TiB$_2$	5.514	4509	5.356	LiF	25.4				
3435	306	552	PF340	6.4	TiB$_2$	5.377	4509	10.352	LiF	25.4				
3436	307	1073	PF394	7.9	TiB$_2$	5.012	4490	9.039	LiF	18.9				
3437	307	1805	PF419	7.9	TiB$_2$	5.008	4490	9.028	LiF	18.9				
3438	307	1972	PMMA	6.340	Ta	1.507	4490	9.031	LiF	19.02				
3439	307	2221	PMMA	6.34	W	1.51	4490	9.036	LiF	19.12				
3440	308	1458	Air	-----	Cu	9.424	4380	4.521	LiF	19.2				

Test 3420-3440: the test data is from work by Grady and Moody [52]. Four different materials were tested. The above table provides the initial conditions for the plate impact experiments, and the associated interface wave profiles can be found on the following pages. Limited stress states are provided here, although further discussion on the data is given in Ref. 54, 55, 57, 58, 59, 77.

Test 3420, 3422: Hugoniot results obtained from Ref. 77.

lower yield/upper yield

*The three numbers following the PF identify the density of the Polyurethane Foam in Kg/m³.

70
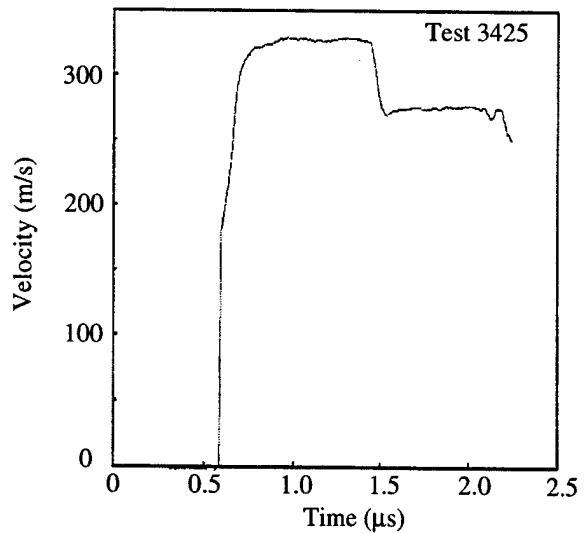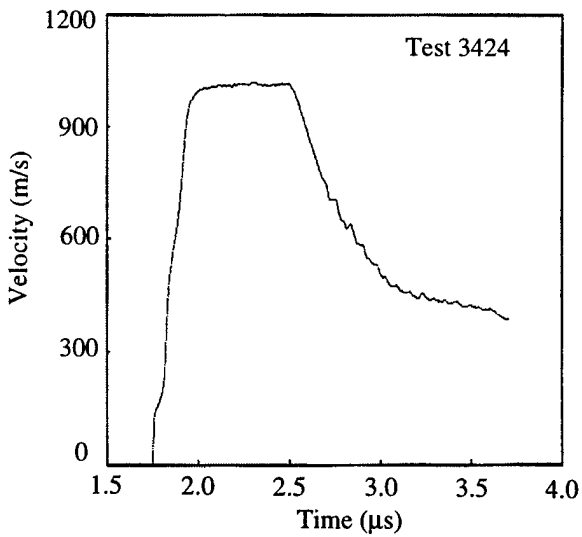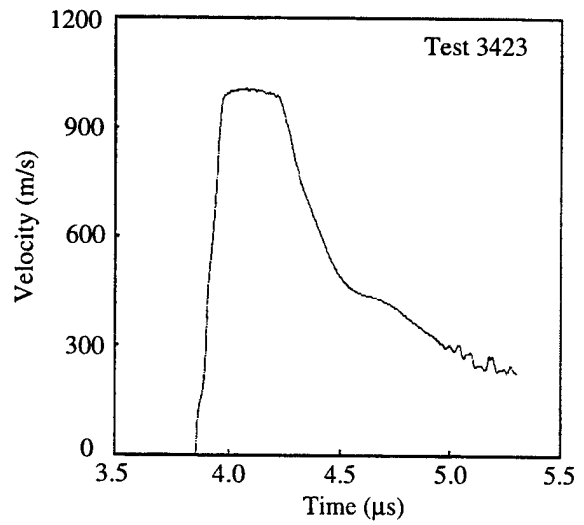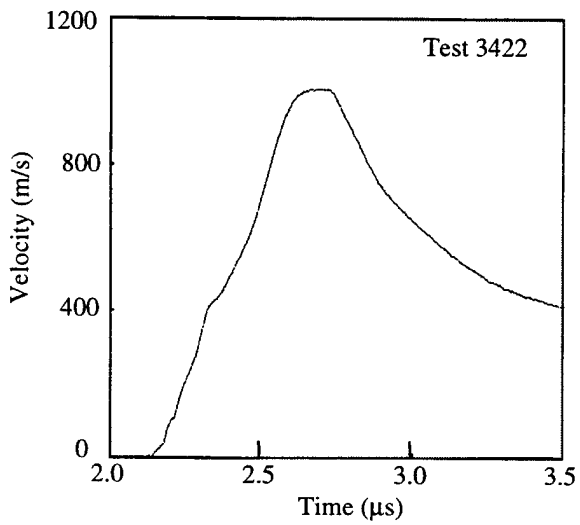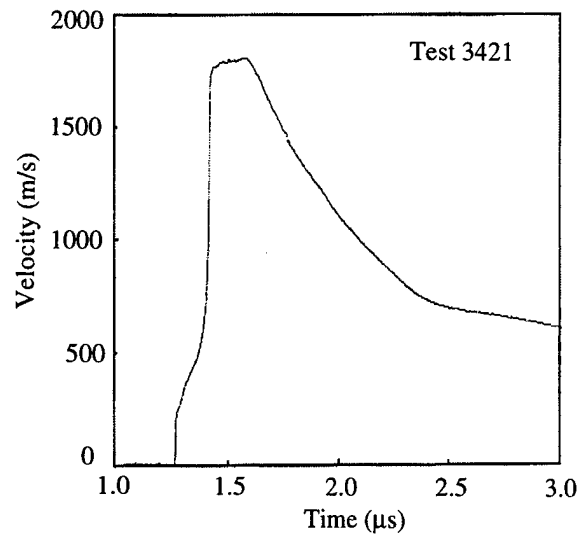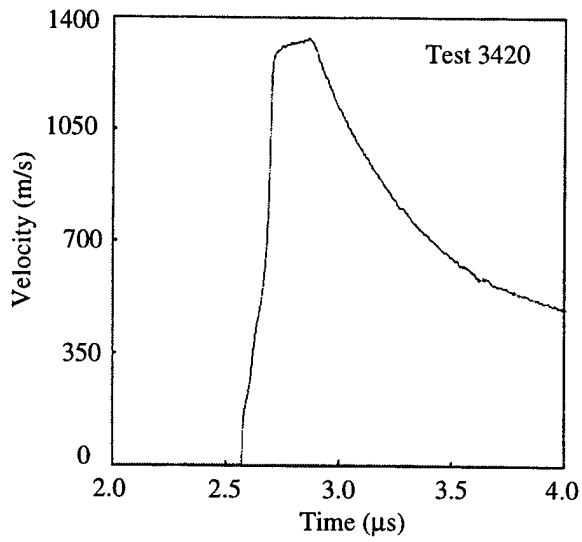
Figure 2.3.4.3 Ceramic-Window Interface Velocity Profiles from Grady and Moody [52] for Tests 3420-3425.

71
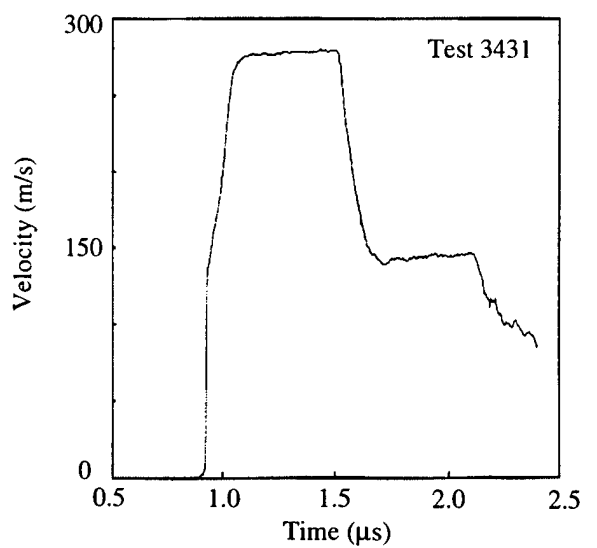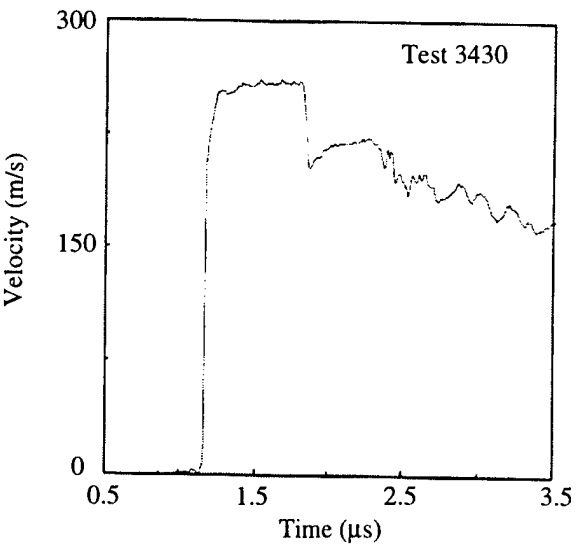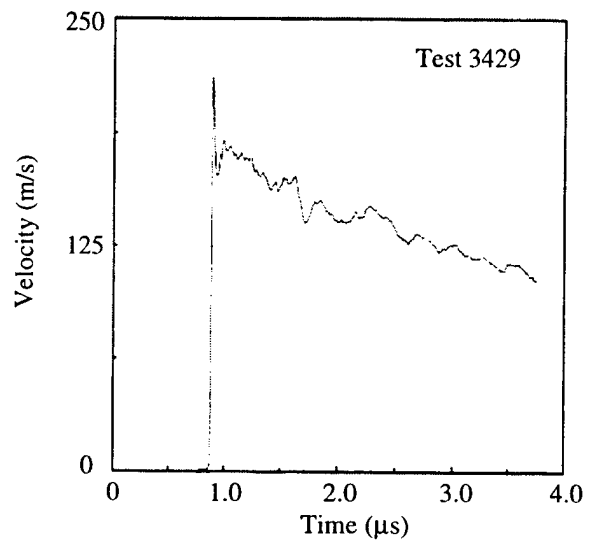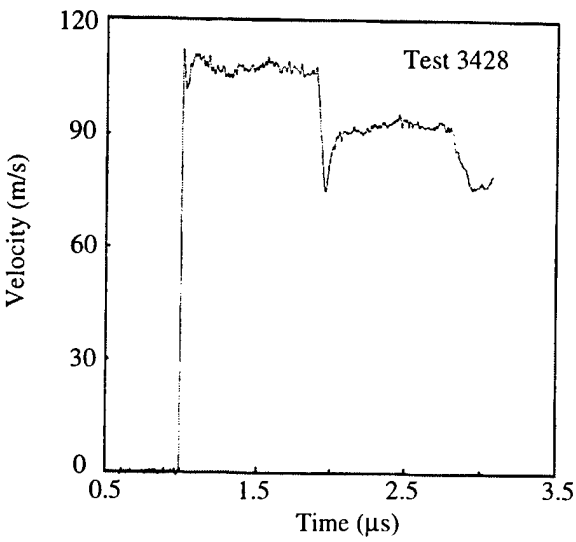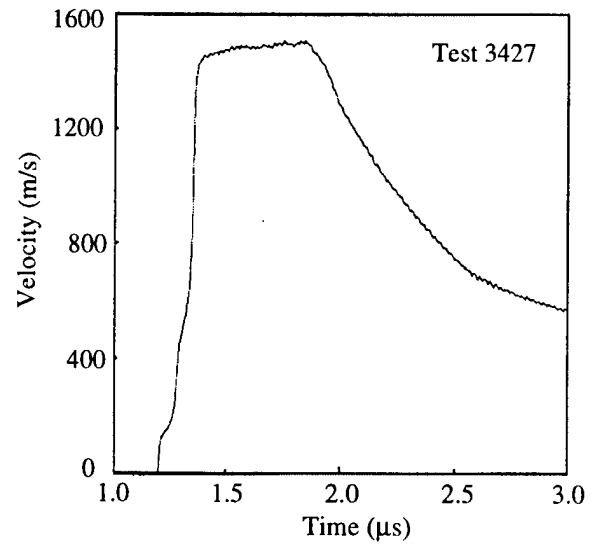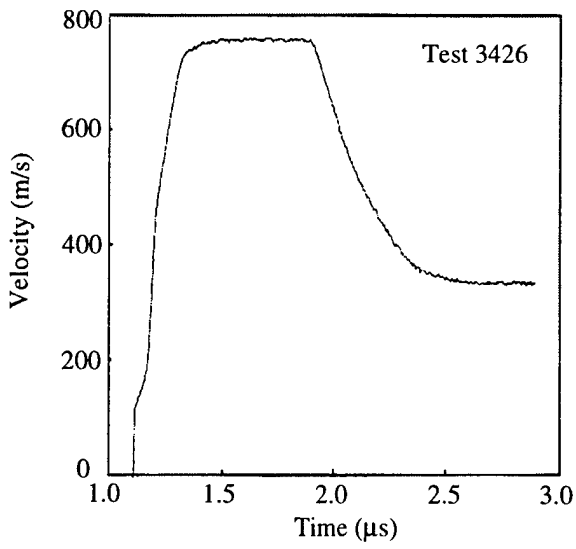
Figure 2.3.4.4 Ceramic-Window Interface Velocity Profiles from Grady and Moody [52] for Tests 3426-3431.
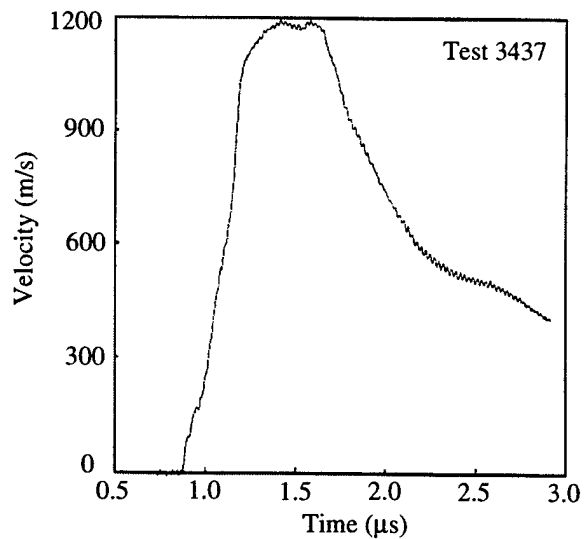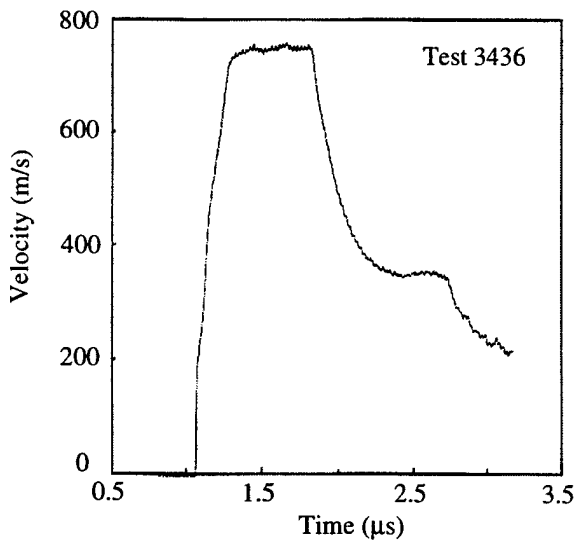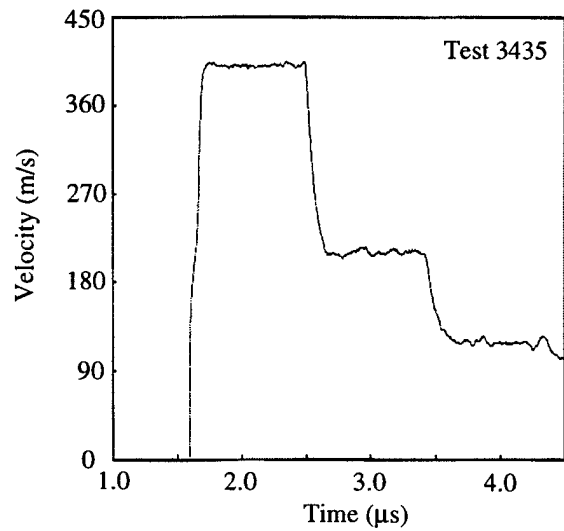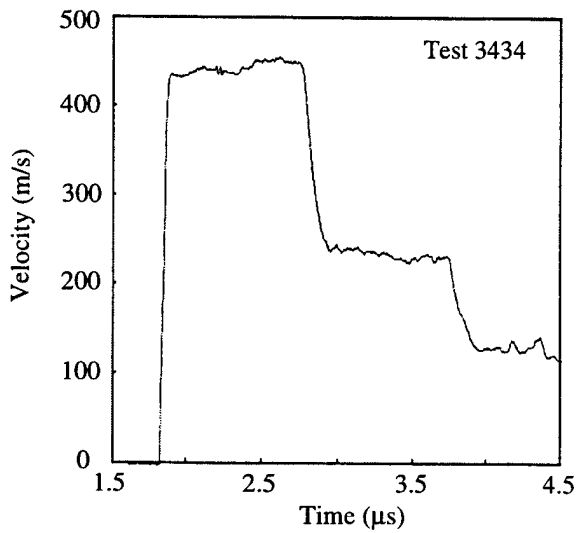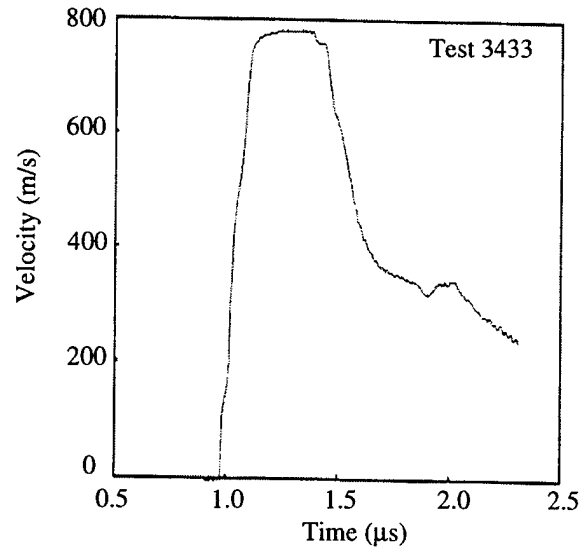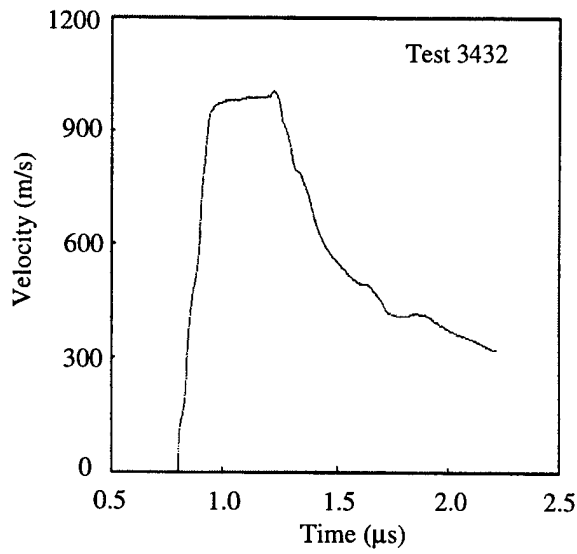
Figure 2.3.4.5 Ceramic-Window Interface Velocity Profiles from Grady and Moody [52] for Tests 3432-3437.

73
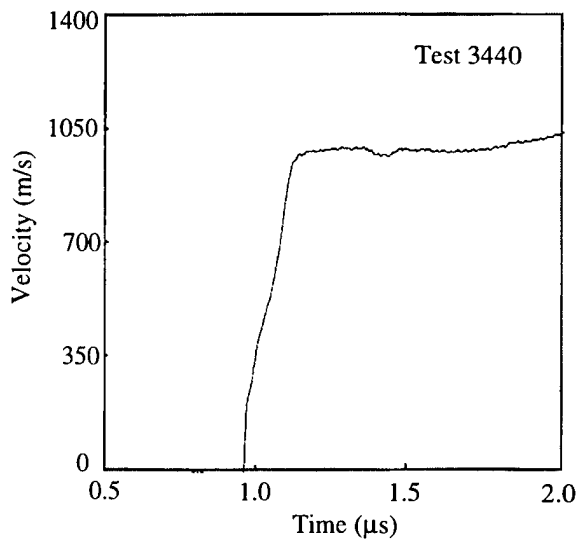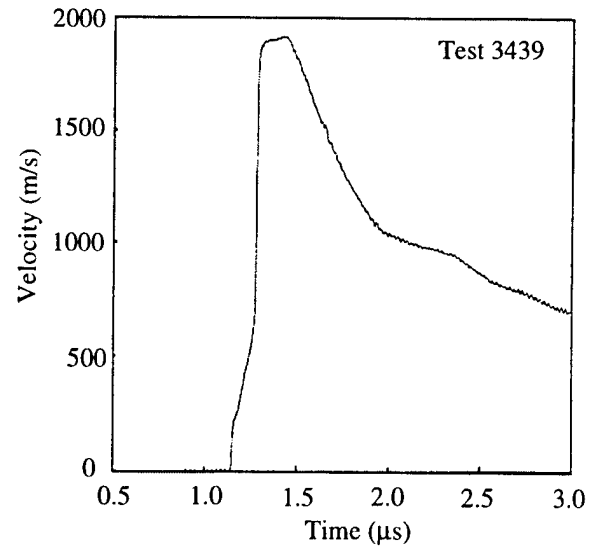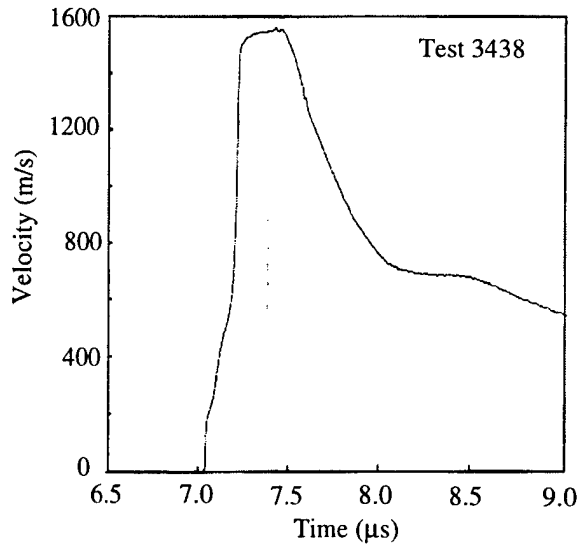
Figure 2.3.4.6 Ceramic-Window Interface Velocity Profiles from Grady and Moody [52] for Tests 3438-3440.
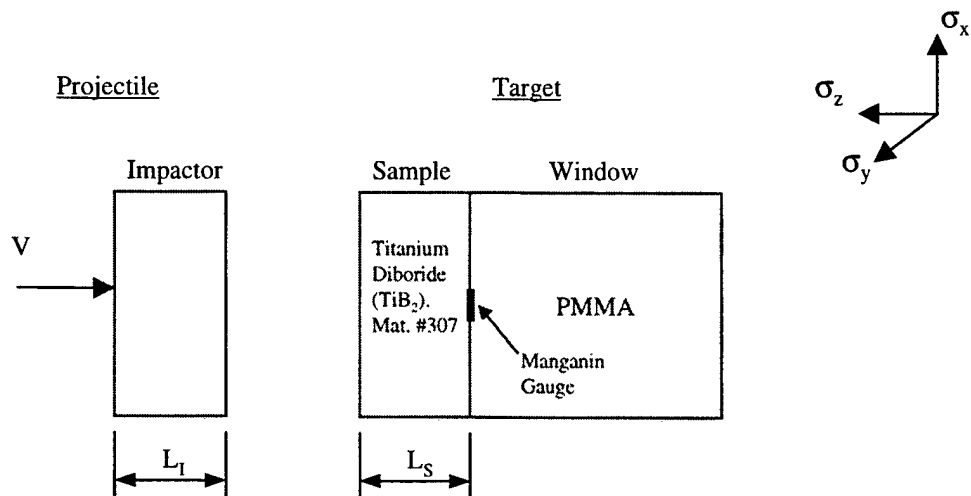
Figure 2.3.4.7   Description of the Plate Impact Test Configuration used by Dandekar and Benfanti [59].

Table 2.3.4.3   Summary of Experimental Plate Impact Initial Conditions and Results, Dandekar and Benfanti [59].

| Titanium Diboride										
		Projectile			Target	Results				
Test Number	Material Number	V (m/s)	Impactor		Sample	First Shock (GPa)	First Release (GPa)	Second Shock (GPa)	Second Release (GPa)	Spall Threshold (GPa)
			Material	L_I (mm)	L_S (mm)					
3441	307	504+-5	TiB$_2$	4.064	8.039	12.84				0.06
3442	307	502+-5	TiB$_2$	1.962	5.995	12.79				0.10
3443	307	354+-1	TiB$_2$	0.999	2.176	9.12				0.14
3444	307	265+-1	TiB$_2$	2.047	4.043	6.68				0.24
3445	307	210+-3	TiB$_2$	2.047	4.043	5.28				0.34
3446	307	88+-1	TiB$_2$	4.038	12.715	2.41				0.32
3447	307	83+-2	TiB$_2$	2.054	4.048	2.09				0.31
3448	307	84+-2	TiB$_2$	2.044	4.046	2.11				0.33
3449	307	229+-9	Cu	2.555	3.970	4.89	0.690	1.11	0.761	0.335
3450	307	239+-3	Cu	2.503	3.995	5.11	0.727	1.16	0.814	0.346

Test 3441-3450: the test data is from work by Dandekar [59] to investigate spall threshold for Titanium Diboride.

Test 3441-3448: Conventional spall experiments conducted through symmetric impact.

Test 3449-3450: Experiments using a copper impactor or z-cut sapphire impactor where thicknesses were chosen to put the specimen through a series of shock-release cycles. The results assess the effect of any damage induced during the first shock-release cycle on the spall threshold.

Further discussions on the results can be found in Ref. 60, 61.

75

Projectile　　　　　　　　　Target

Impactor　　　　Sample　　Window

Copper　　　Titanium Diboride (TiB₂). Mat. #309-#310　　PMMA

Manganin Gauge

σ_x　σ_z　σ_y

V

L_I　　L_S

Figure 2.3.4.8　Description of the Plate Impact Test Configuration used by Yaziv *et al.* [64].

Table 2.3.4.4　Summary of Experimental Plate Impact Initial Conditions and Results, Yaziv *et al.* [64].

Titanium Diboride												
		Test Configuration			Elastic Compression			Plastic Compression				
Test Number	Material Number	V (m/s)	L_I (mm)	L_S (mm)	Particle Velocity (m/s)	Stress σ_z (GPa)	Density (kg/m³)	Particle Velocity (m/s)	Shock Velocity (m/s)	Stress σ_z (GPa)	Density (kg/m³)	Spall Threshold (GPa)
3451	309	692	1.52	10.2	142	7.1	4528*	300	10480	14.5	4597*	
3452	309	614	1.54	5.1				271	10957*	13.5	4582*	
3453	309	543	1.53	5.1				235	10211*	11.4	4570*	
3454	309	163	1.57	5.1	70*	3.5	4498*					
3455	309	195	1.53	5.1	78*	3.9	4501*					0.2
3456	310	719	2.54	12.7	141*	7.2	4505*	302	10870	15.1	4573*	
3457	310	452	1.53	12.7	155*	7.9	4511*	192	10670	9.7	4527*	

Test 3451-3457: the test data is from work by Yaziv *et al.*[64]. Two materials were investigated. Material #309 was manufactured by Cercom having an initial density = 4470kg/m³ and Material #310 was manufactured by Ceradyne having an initial density = 4450kg/ m³.
Plastic Particle Velocities obtained from Figure 6 in Ref. 64.
*Calculated from the data given in Ref. 64.

76
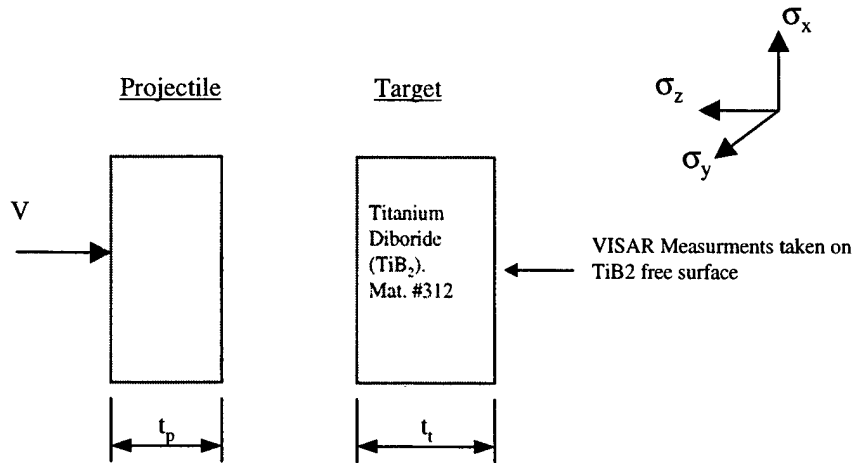
Figure 2.3.4.9   Description of the Plate Impact Test Configuration, Winkler and Stilp [81, 82].

Table 2.3.4.5   Summary of Experimental Plate Impact Initial Conditions and Results, Winkler and Stilp [81, 82].

|		Test Configuration			Elastic Compression		Plastic Compression		Spall Stress (GPa)
Test Number	Material Number	Projectile Material	t_p (mm)	t_t (mm)	Stress σ_z (GPa)	Density ρ (kg/m^3)	Stress σ_z (GPa)	Density ρ (kg/m^3)	
3458	312	Aluminum	1.5	5.5	0.6				0.53
3459	312	Aluminum	1.5	5.5	1.4				0.44
3460	312	Armco Iron	1.5	6.0	3.4				0.45
3461	312	Armco Iron	1.5	5.6	4.0				-----
3462	312	Armco Iron	1.5	6.0	5.1				0.43
3463	312	Armco Iron	2.0	5.5	4.3		6.0		-----
3464	312	Armco Iron	0.9	5.7	4.9		8.6		0.28
3465	312	Armco Iron	1.6	7.5	4.2		10.0		0.26
3466	312	Armco Iron	2.0	6.0			10.5		-----
3467	312	Armco Iron	2.0	5.7	4.4		10.6		0.00
3468	312	TiB2	3.7	7.5	4.7		10.7		0.23
3469	312	Armco Iron	1.6	7.5	4.4		10.8		0.33
3470	312	Armco Iron	1.6	7.5	4.2		11.9		0.19
3471	312	TiB2	3.7	5.7			13.3		-----
3472	312	Armco Iron	1.5	5.6	4.4		14.2		0.28

Test 3458-3472: the test data is from work by Winkler and Stilp [81, 82]. The TiB2 was hot pressed having an initial density = 4360kg/m^3. Only the elastic and plastic stresses were documented.

Test 3458-3462: the peak stress did not exceed the HEL.

Test 3463-3472: the peak stress exceeded the HEL.

Test 3467: this was the only test that exhibited a three wave structure (ie. a lower and upper HEL). The lower HEL=4.4 GPa and the upper HEL=9.0GPa.
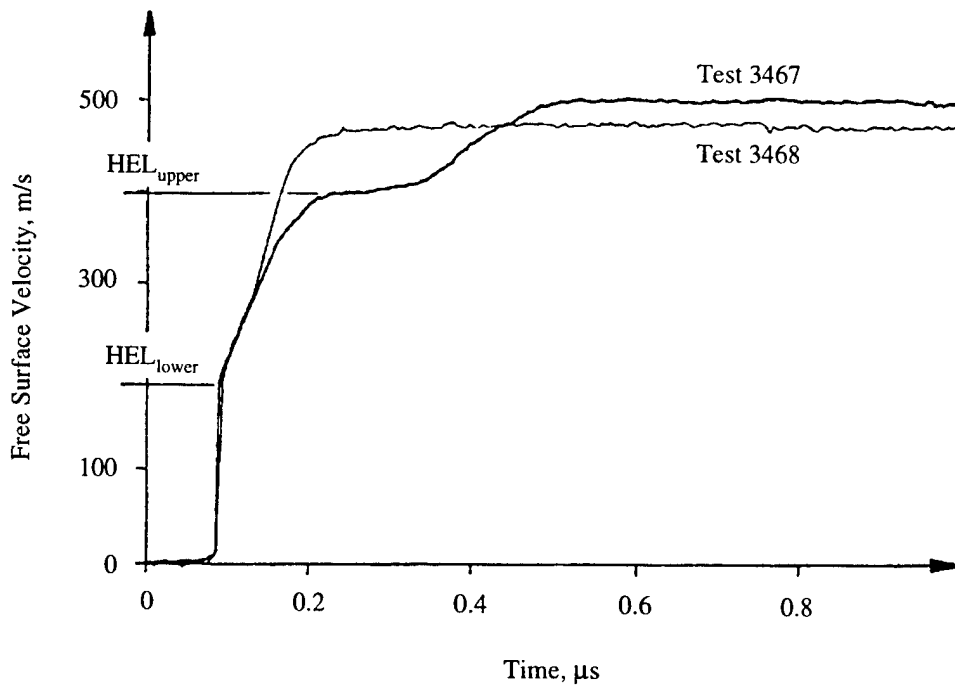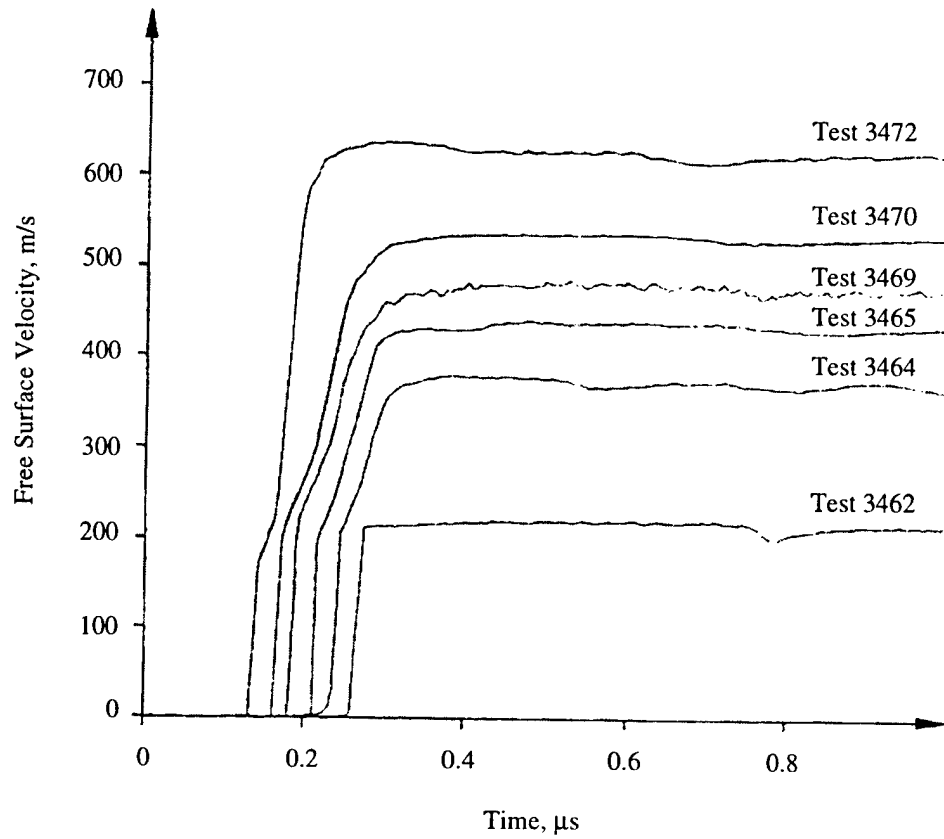
Figure 2.3.4.10   Ceramic Free Surface Velocity Profiles, Winkler and Stilp [81, 82].

Impactor   Target   Manganin gauge

V

copper

TiB₂
Mat. #314

σ_x

σ_z

σ_y

10mm
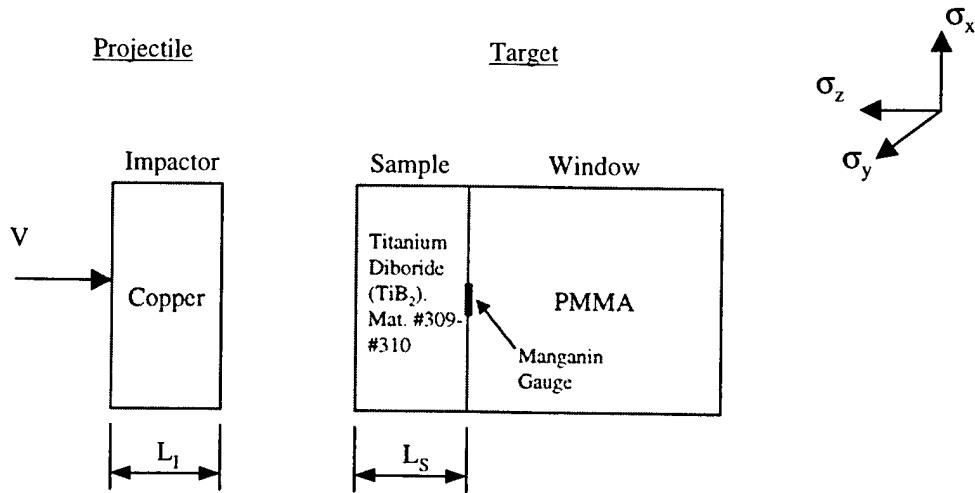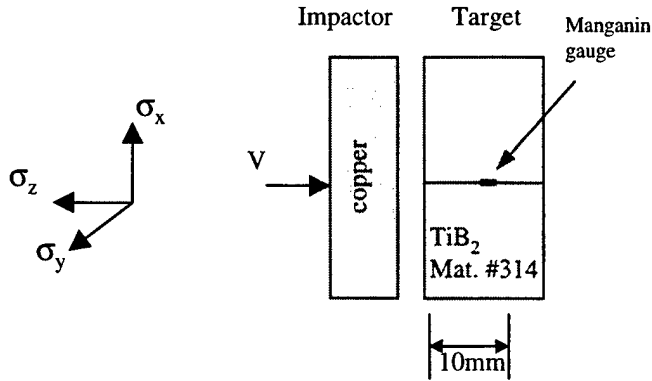
Figure 2.3.4.11   Description of Plate Impact Test Configuration, Rosenberg *et al.* [87].

Table 2.3.4.6   Summary of Experimental Plate Impact Results by Rosenberg *et al.* [87].

Titanium Diboride							
Test Number	Material Number	Elastic Regime			Deformational Regime		
		σ_z (GPa)	$\sigma_y = \sigma_x$ (GPa)	ρ (kg/m³)	σ_z (GPa)	$\sigma_y = \sigma_x$ (GPa)	ρ (kg/m³)
3473	314	6.8	0.9				
3474	314	7.5	0.8		10.0	1.6	
3475	314	7.5	0.8		19.5	7.1	
3476	314	7.5	0.8		19.5	6.1	
3477	314	7.5	0.8		24.0	8.9	

Test 3473-3477: the test data is from work by Rosenberg *et al.*[87]. In-material Manganin gauge was used to determine the stress in the transverse direction only ($\sigma_y = \sigma_x$). The longitudinal stress, σ_z, was obtained from Hugoniot data by Yaziv and Brar[64] and Grady [52, 54]. The above tabulated data was obtained from Figure 3 in Reference 87.
Test 3473: Peak stress below the HEL
The documented HEL for this work = 7.5+-0.4 GPa from Yaziv and Brar[64].

79

2.3.6 Depth-Of-Penetration (DOP) Test Data for Titanium Diboride

This section presents depth-of-penetration (DOP) experiments for numerous Titanium Diboride materials. The DOP test has been used to investigate the effectiveness of ceramics for a number of years. The typical DOP configuration consists of a ceramic tile place on, or within, a steel or aluminum base target. A penetrator impacts and perforates the ceramic tile and continues into the base target. The penetration into the base target is generally referred to as the residual penetration, P_r, and is used to determined the ceramic mass efficiency as discussed in Section 2.0.

The target and penetrator descriptions for the DOP experiments by Rosenberg and Tsaliah [39] are presented in Figure 2.3.6.1. The objective of the experiment was to investigate the ballistic effectiveness of Titanium Diboride. Only one experiment was performed and is presented in Table 2.3.6.1. No information was provided for the Titanium Diboride used in the experiment.

The target and penetrator descriptions for the DOP experiment by Woodward *et al.* [41] are presented in Figure 2.3.6.2. The objective of the experiment was to investigate the ballistic effectiveness of Titanium Diboride. Only one experiment was performed and is presented in Table 2.3.6.2.

The target and penetrator description for the DOP experiments by Reaugh *et al.* [85] is presented in Figure 2.3.6.3. The objective of the experimental program was to investigate the ballistic efficiency of Titanium Diboride as a function of ceramic thickness, impact velocity and impact angle. The results are presented in Table 2.3.6.3. Also included in the table are penetration results into the 4340 Steel with no ceramic .

The target and penetrator description for the DOP experiments by Rosenberg *et al.* [91] is presented in Figure 2.3.6.4. The objective of the experimental program was to investigate the ballistic efficiency of Titanium Diboride as a function of ceramic thickness and lateral dimensions. The results are presented graphically in Figure 2.3.6.5 and in tabular form in Table 2.3.6.4. Also included in the table are penetration results into the steel base target with no ceramic .
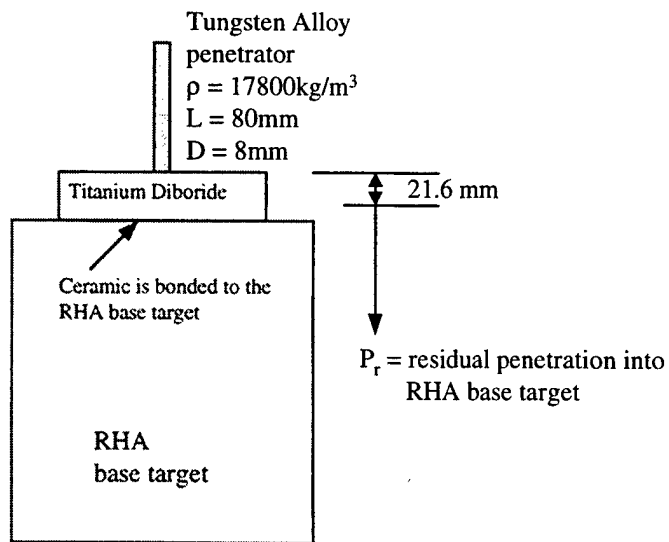
Figure 2.3.6.1 Target and Penetrator Description for DOP Experiment, Rosenberg and Tsaliah [39].

Table 2.3.6.1 Tabulated Experimental Result for DOP Test, Rosenberg and Tsaliah [39].

Titanium Diboride					
Test Number	Material Number	Impact Velocity (m/s)	Target Configuration		P_r (mm)
			t_c (mm)	Base Target	
3601		1366	21.6	RHA	29.5
Test 3601: the test data is from work by Rosenberg and Tsaliah [39]. The ceramic material used is Titanium Diboride with initial density = 4480kg/m³, no other material information was provided.					

81
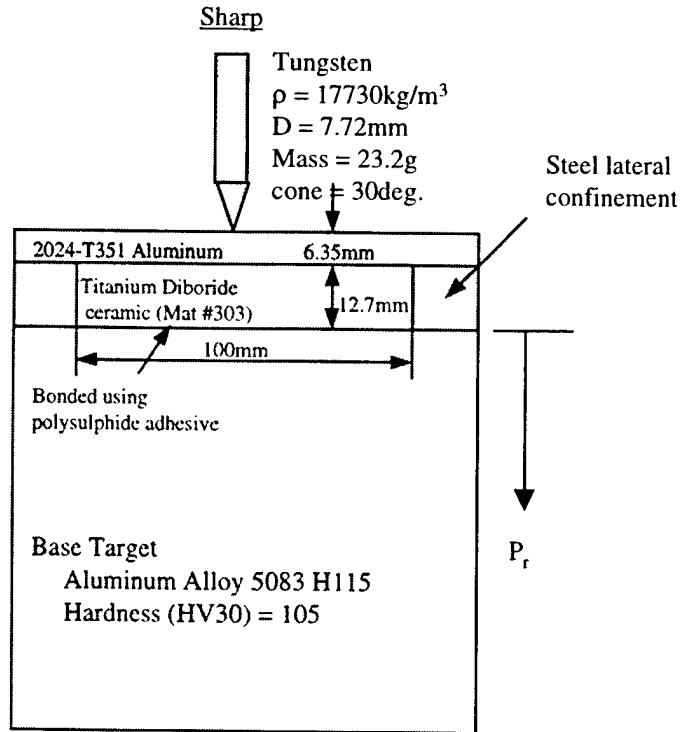
Figure 2.3.6.2 Target and Penetrator Description for DOP Experiment, Woodward *et al.* [41].

Table 2.3.6.2 Tabulated Experimental Result for DOP Test, Woodward *et al.* [41].

Titanium Diboride					
Test Number	Material Number	Impact Velocity (m/s)	Penetrator Geometry	P_r (mm)	P* (mm)
3602	303	1209	Sharp	38.0	265
* This is the semi-infinite penetration into Aluminum. Test 3602: the test data is from work by Woodward *et al.* [41]. The ceramic material used is Titanium Diboride manufactured by Ceradyne with an initial density = 4520 kg/m³.					

Θ

V

Tungsten Sintered Alloy W2 Penetrator
$\rho = 18360 kg/m^3$ $R_c = 28\text{-}31$
$L = 25.4mm$ $UTS = 0.88GPa$
$D = 6.35mm$ $Yield = 0.695GPa$
$L/D = 4$ $Elongation\ to\ fracture = 5.5\%$

Titanium Diboride (Mat. #313)

102 mm

t_c

64mm

Ceramic is bonded to the
RHA base target using Stycast 1266

4340 Steel Base Target
$R_c = 33\text{-}37$

P_r = residual penetration into
RHA base target

152mm
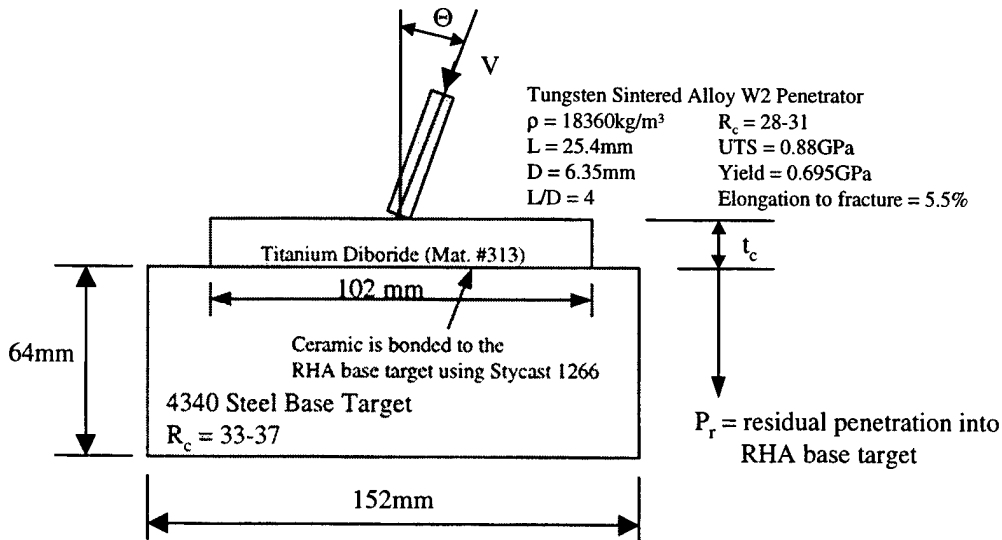
Figure 2.3.6.3 Target and Penetrator Description for DOP Experiment, Reaugh *et al.* [85].

Table 2.3.6.3   Summary of Experimental DOP Results, Reaugh *et al.* [85].

Titanium Diboride					
Test Number	Material Number	Impact Velocity (m/s)	Ceramic t_c (mm)	Impact Angle[#] Θ (degrees)	P_r [&] (mm)
3603	313	1380	7.9	0	12.2
3604	313	1310	10.0	0	3.7
3605	313	1360	15.0	0	0.0
3606	313	1370	20.0	0	0.0
3607	313	1690	10.1	0	22.1
3608	313	1700	14.9	0	7.3
3609	313	1720	20.1	0	1.1
3610	313	1690	30.0	0	0.0
3611	313	1700	10.1	30	19.5
3612	313	1800	25.0	30	0.0
3613	313	1730	7.7	45	15.4
3614	313	1690	20.0	45	0.0
3615	313	1800	7.8	60	5.6
3616	313	1810	15.0	60	0.0
3617	313	2630	20.1	0	34.5
3618	313	2690	24.9	0	29.8
3619	313	2630	30.3	0	17.8
3620	313	2630	40.0	0	9.6
3621		1340	0	0	27.0
3622		1350	0	0	27.8
3623		1350	0	0	28.5
3624		1770	0	0	36.0
3625		2500	0	0	43.8

Test 3603-3625: the test data is from work by Reaugh *et al.* [85].
[#]the angle between the penetrator flight axis and the normal to the tile.
[&] the residual penetration measured normal to the impact surface.
Test 3621-3625: tests into 4340 steel target only (no ceramic used).
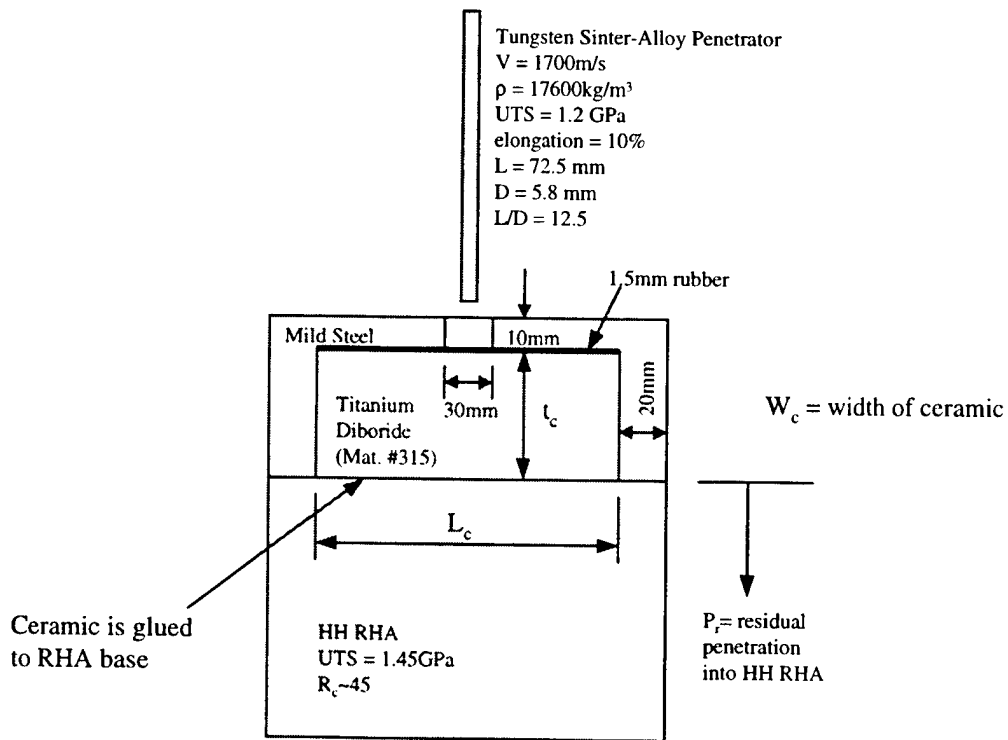
Figure 2.3.6.4 Target and Penetrator Description for DOP Experiment, Rosenberg *et al.* [91].
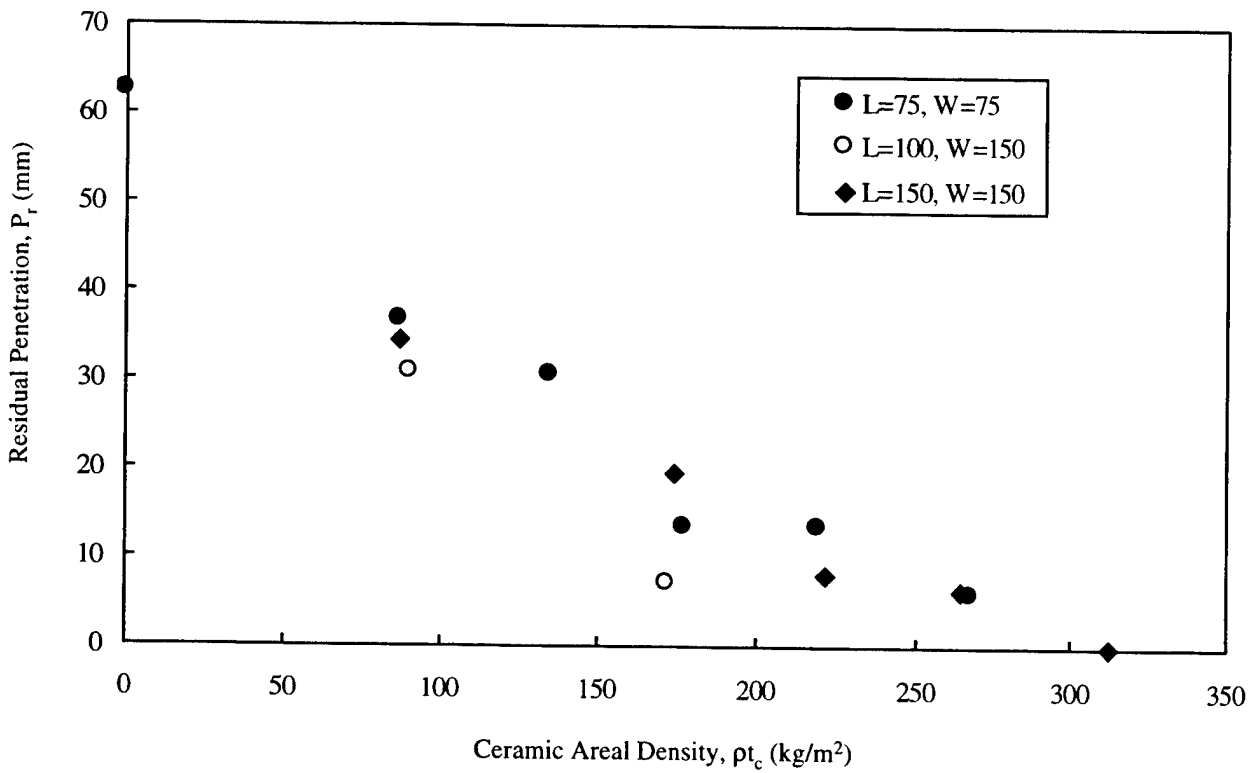
Figure 2.3.6.5 Residual Penetration as a Function of Ceramic Areal Density and Ceramic Tile Width, W, Rosenberg *et al.* [91].

Table 2.3.6.4 Summary of Experimental DOP Results, Rosenberg *et al.* [91].

Titanium Diboride							
Test Number	Material Number	Impact Velocity (m/s)	Ceramic Dimensions			ρt_c (kg/m^2)	P_r (mm)
			Thickness t_c (mm)	Length L_c, (mm)	Width W_c, (mm)		
3626	315	1700	19.6	75	75	87.1	36.5
3627	315	1700	30.3	75	75	134.9	30.6
3628	315	1700	39.9	75	75	177.6	13.5
3629	315	1700	49.5	75	75	220.2	13.5
3630	315	1700	60.2	75	75	268.0	5.9
3631	315	1700	20.3	100	150	90.5	30.8
3632	315	1700	38.7	100	150	172.4	7.0
3633	315	1700	19.6	150	150	87.1	34.4
3634	315	1700	39.1	150	150	174.1	19.6
3635	315	1700	49.9	150	150	222.0	8.1
3636	315	1700	59.5	150	150	264.6	6.3
3637	315	1700	70.2	150	150	312.4	0
3638		1700	0			0	62.4

Test 3626-3638: the test data is from work by Rosenberg *et al.* [91]. The tabulated data listed above was obtained from Figure 1 in Reference [91].
$\rho = 4450$kg/m^3 (density of ceramic)
Test 3638: test into steel base target only (no ceramic used).

2.3.7 Perforation Test Data for Titanium Diboride

This subsection presents results for perforation experiments using Titanium Diboride. Targets are typically comprised of a ceramic front layer and a metallic rear layer and are commonly used for light armor applications. The most common piece of data extracted from perforation experiments is the target ballistic limit, V_{bl}, previously defined in Section 2.0.

The target and penetrator description for the perforation experiments by Wilkins et al. [26] is presented in Figure 2.3.7.1. The objective of the experiments was to determine the ballistic limit velocity for a specific target configuration and penetrator geometry. The results are presented in Table 2.3.7.1.
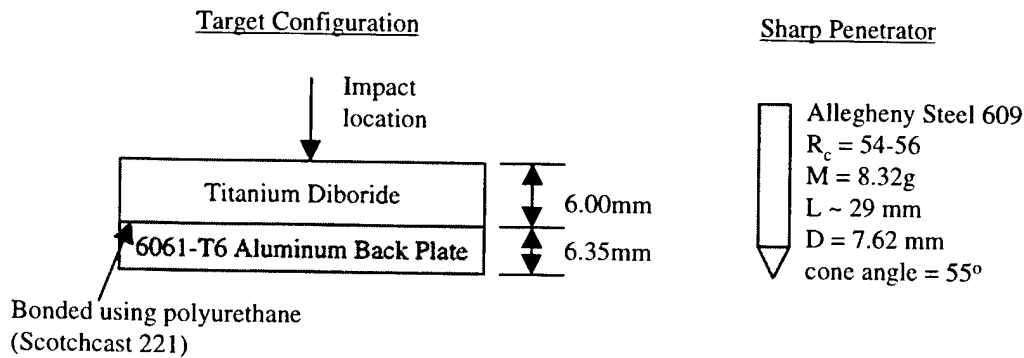
Figure 2.3.7.1 Target and Penetrator Description for Perforation Experiments, Wilkins et al. [26].

Table 2.3.7.1 Ballistic Limit Velocity for a Sharp Penetrator against a Titanium Diboride Target, Wilkins et al. [26].

Titanium Diboride					
Test Number	Material Number	Penetrator	Target Configuration		Ballistic Limit Velocity, V_{bl} (+- 15m/s)
			Δ (mm)	δ (mm)	
3701	302	Sharp	6.00	6.35	690
Test 3701: the test data is from work by Wilkins et al. [26].					

2.3.8 Other Test Data for Titanium Diboride

This subsection presents test data for experiments that do not fit into any of the previous subsections. Typically the experiments that are reported in this subsection are more theoretical and unique in design than those reported in the previous subsections. The following briefly discusses the experiments presented in this subsection.

Experiments by Strassberger et al. [69] were designed to investigate the fracture propagation in ceramics. The damage velocity, V_d, was measured as a function of projectile impact velocity, V_p. The target and projectile descriptions are presented in Figure 2.3.8.1. The results of the experiments are presented graphically in Figure 2.3.8.2 where the damage velocity is shown as a function of penetrator impact velocity. The results are also summarized in Table 2.3.8.1. The damage velocity is defined as the fastest observed fracture velocity in the ceramic. The fracture propagation was observed by means of a Cranz-Schardin camera and photos of this process are presented in Reference 69.
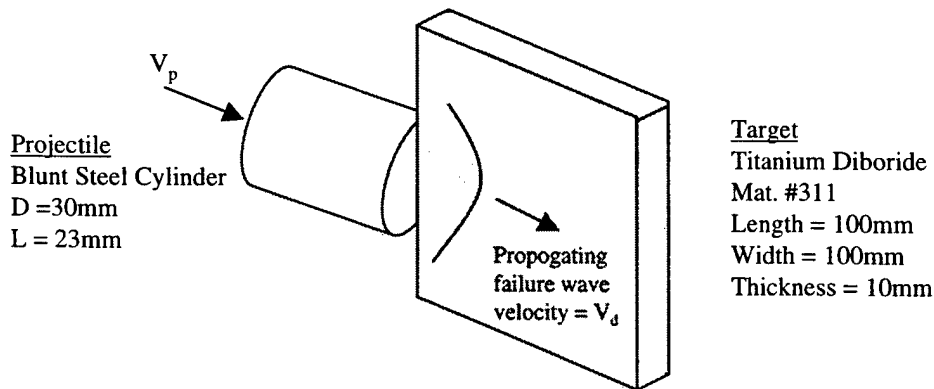
Figure 2.3.8.1 Target and Projectile Description for Fracture Experiment, Strassburger et al. [69].
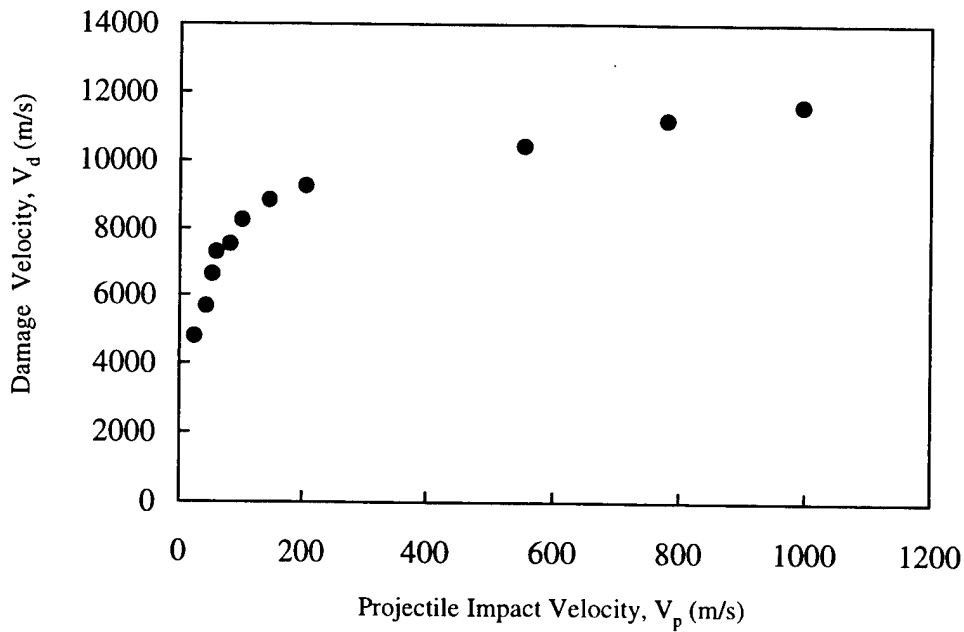
Figure 2.3.8.2 Damage Velocity in Ceramic vs. Projectile Impact Velocity, Strassburger *et al.* [69].

Table 2.3.8.1 Summary of Damage Velocity in Titanium Diboride as a Function of Projectile Impact Velocity, Strassburger *et al.*[69].

Titanium Diboride			
Test Number	Material Number	Projectile Impact Velocity, V_p (m/s)	Damage Velocity V_d (m/s)
3801	311	28	4740
3802	311	49	5600
3803	311	56	6570
3804	311	64	7220
3805	311	85	7430
3806	311	106	8180
3807	311	148	8720
3808	311	210	9150
3809	311	560	10340
3810	311	784	11090
3811	311	1000	11520
Test 3801-3811: the test data is from work by Strassburger *et al.* [69]. The data were obtained from Figure 9b in Ref. 69.			

88

2.4 ALUMINUM NITRIDE

2.4.1 Material Description for Aluminum Nitride

The purpose of this section is to provide as much information as possible on the materials tested. Descriptions for each of the Aluminum Nitride materials used in Section 2.4 are presented in Table 2.4.1.1. Each material is given a material number which is used throughout Section 2.4 to identify it. The data listed in Table 2.4.1.1 were obtained directly from the corresponding reference. When specific information was not available it was left blank. The strength values listed, (Compressive, Tensile, HEL and Spall), are nominal values and are included for comparison purposes. The purity (% AlN) or chemical composition of the material is also included in Table 2.4.1.1 when available.

Table 2.4.1.1 Description of Aluminum Nitride Materials Tested

	Material Number					
	401	402	403	404	405	406
Reference	12*	13	21	51, 52, 54	52	72
Manufacturer			Dow Chemical	Dow Chemical	Sumitomo Electric	Sumitomo Electric
Trade Name/Description			Rocklite 500			
Processing		Hot Pressed	Hot Pressed	Hot Pressed		Sintered
Average Grain Size (μm)		4	1.5	2.0		
Density (kg/m³)	3260	3270	3250	3226	3236	3200
Void Fraction		<0.01		0.01	0.005-0.007	0.013-0.016
Longitudinal Velocity (m/s)	10700		10700	10720	10800	10790
Shear Velocity (m/s)	6310		6300	6270	6340	
Bulk Velocity (m/s)	7830		7900	7890	7940	
Young's Modulus, E (GPa)	320		320	314	322	
Shear Modulus, G (GPa)	130		129	127	130	
Bulk Modulus, K (GPa)	200		203	201	204	
Poisson's Ratio	0.23		0.237	0.238	0.237	
Compressive Strength (GPa)	1.45	3.0	3.8	4.0		
Tensile Strength (GPa)						
HEL (GPa)			9.2	9.4		8.5
Spall Strength (GPa)				0.5-0.6		
Purity (%)		>95	>98			

* Steinberg [12] documented unpublished work by Lankford. It was assumed the material properties documented by steinberg, and listed here, are representative of the material tested by Lankford.

Table 2.4.1.1 Description of Aluminum Nitride Materials Tested Concluded.

	Material Number				
	407	408	409	410	
Reference	83	84	85	91	
Manufacturer	Dow	Dow	Dow		
Trade Name/Description					
Processing	Sintered	Hot Pressed			
Average Grain Size (μm)		2-3			
Density (kg/m³)	3200	3250	3250	3230	
Void Fraction		<0.01			
Longitudinal Velocity (m/s)	10714	10700	10760		
Shear Velocity (m/s)	6300	6300	6330		
Bulk Velocity (m/s)	7866	7903	7896		
Young's Modulus, E (GPa)	313	320	321	310	
Shear Modulus, G (GPa)	127	129	130		
Bulk Modulus, K (GPa)	198	203	203		
Poisson's Ratio	0.237	0.24	0.236		
Compressive Strength (GPa)	2.5	2.8		2.1	
Tensile Strength (GPa)					
HEL (GPa)					
Spall Strength (GPa)					
Impurities (%wt)					
O		1			
C		0.3			
Ca		500(p.p.m.)			
Si		200(p.p.m.)			
Fe		50(p.p.m.)			

2.4.2 Mechanical Test Data for Aluminum Nitride

The following section presents mechanical test results for Aluminum Nitride. A typical test specimen showing the stress configuration is shown in Figure 2.4.2.1. Loading is generally uniaxial in the z direction and is increased until the material fails, although some researchers use more complex loading techniques to vary the stress state at failure.

Mechanical test data performed by Steinberg [12], Heard and Cline [13] and Chen and Ravichandran [83] are presented in Table 2.4.2.1. Mechanical test data performed by Subhash and Ravichandran [84] are presented in Table 2.4.2.2. The stress state at failure is typically given as a function of average strain rate, $\dot{\varepsilon}$. Information on failure strain is also provided if available. Compression is taken as positive and tension as negative.

Steinberg [12] documents unpublished data by Lankford where the compressive strength was obtained as a function of strain rate.

Heard and Cline [13] investigated the effect of confinement on compressive strength. The lateral confining stresses (σ_x, σ_y) were induced by applying a copper or lead jacket on the ceramic specimen. The lateral stresses are thus a function of the applied axial stress. The three normal stresses in the table represent the stress state at failure. The failure strain (ε_z) is the total axial strain measured at catastrophic failure.

Chen and Ravichandran [83] investigated the effect of confining stress and strain rate on compressive strength of a sintered Aluminum Nitride. Lateral confining stresses (σ_x, σ_y) were induced by applying a copper, brass, tool steel or stainless steel jacket on the ceramic specimen. The jacket was heated prior to the insertion of the ceramic specimen. When the jacket cooled an initial confining stress was induced into the ceramic specimen. It is believed that the lateral confining stresses (σ_x, σ_y) listed in Table 2.4.1.1 are the initial confining stresses and not the stress at fracture. The axial stress, (σ_z), is the stress at fracture.

Subhash and Ravichandran [84] investigated the effect of strain rate on the uniaxial compressive strength of hot pressed Aluminum Nitride. The tests were uniaxial compression using either an MTS machine (quasi-static) or a Hopkinson bar apparatus (high rate data). The listed failure strains (ε_z) are the total axial strain measured at catastrophic failure.
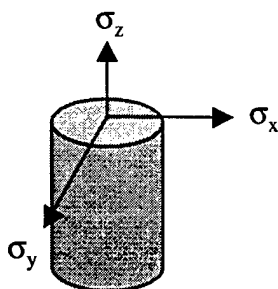
Figure 2.4.2.1 Description of a Typical Mechanical Test Specimen.

91

Table 2.4.2.1 Summary of Experimental Results.

Test Number	Material Number	σ_z (GPa)	σ_x (GPa)	σ_y (GPa)	$\sim \dot{\varepsilon}$ (s^{-1})	Axial strain, ε_z at failure	Ref.
			Aluminum Nitride				
4201	401	1.33	0	0	1.0×10^{-4}	N. A	12 (Steinberg)
4202	401	1.56	0	0	1.0×10^{-4}	N. A.	
4203	401	1.67	0	0	0.9	N. A	
4204	401	1.89	0	0	0.9	N. A.	
4205	401	2.33	0	0	1.0×10^{3}	N. A	
4206	401	2.56	0	0	1.0×10^{3}	N. A.	
4207	402	3.30	0.10	0.10	5.0×10^{-5}	0.031	13 (Heard)
4208	402	4.26	0.30	0.30	5.0×10^{-5}	0.030	
4209	402	4.57	0.30	0.30	5.0×10^{-5}	0.030	
4210	402	4.73	0.49	0.49	5.0×10^{-5}	0.074	
4211	402	4.90	0.60	0.60	5.0×10^{-5}	0.110	
4212	402	5.35	0.70	0.70	5.0×10^{-5}	>0.110	
4213	402	5.54	0.82	0.82	5.0×10^{-5}	>0.110	
4214	407	2.50	0	0	4.0×10^{-4}	N. A	83 (Chen)
4215	407	3.03	0.05	0.05	4.0×10^{-4}	N. A.	
4216	407	3.17	0.12	0.12	4.0×10^{-4}	N. A	
4217	407	3.50	0.15	0.15	4.0×10^{-4}	N. A.	
4218	407	3.77	0.23	0.23	4.0×10^{-4}	N. A	
4219	407	4.4	0	0	5.0×10^{2}	N. A.	
4220	407	4.1	0.05	0.05	5.0×10^{2}	N. A	
4221	407	4.97	0.12	0.12	5.0×10^{2}	N. A.	
4222	407	5.37	0.15	0.15	5.0×10^{2}	N. A	
4223	407	5.07	0.23	0.23	5.0×10^{2}	N. A.	

Tests 4201-4206: the tests are unpublished data by Lankford. The data was obtained from Figure 1, Reference 12.

Tests 4207-4213: the test data is from work be Heard and Cline [13]. The lateral confining stresses (σ_x, σ_y) were induced by applying a copper or lead jacket on the ceramic specimen. The lateral stresses are thus a function of the applied axial stress. The three normal stresses in the table represent the stress state at failure. The failure strain (ε_z) is the total axial strain measured at catastrophic failure. The data was obtained from Figure 7, Reference 13.

Tests 4214-4223: the test data is from work be Chen and Ravichandran [83]. The lateral confining stresses (σ_x, σ_y) were induced by applying a copper, brass, tool steel or stainless steel jacket on the ceramic specimen. The jacket was heated prior to the insertion of the ceramic specimen. When the jacket cooled an initial confining stress was induced into the ceramic specimen. It is believed that the lateral confining stresses (σ_x, σ_y) listed above are the initial confining stresses and not the stress at fracture. The axial stress, (σ_z), is the stress at fracture. The data was obtained from Figure 7, Reference 83.

Table 2.4.2.2 Summary of Experimental Results.

Aluminum Nitride							
Test Number	Material Number	σ_z (GPa)	σ_x (GPa)	σ_y (GPa)	$\sim \dot{\varepsilon}$ (s^{-1})	Axial strain, ε_z at failure	Ref.
4224	408	2.79	0	0	3.89×10^{-6}	N. A	84 (Subhash)
4225	408	2.85	0	0	2.84×10^{-5}	0.0082	
4226	408	2.72	0	0	3.63×10^{-5}	N. A	
4227	408	2.85	0	0	2.24×10^{-2}	N. A.	
4228	408	2.79	0	0	2.45×10^{-2}	N. A	
4229	408	3.57	0	0	1.20×10^{2}	N. A.	
4230	408	3.76	0	0	1.66×10^{2}	N. A	
4231	408	3.79	0	0	1.82×10^{2}	N. A.	
4232	408	3.63	0	0	2.75×10^{2}	N. A	
4233	408	3.73	0	0	2.95×10^{2}	N. A.	
4234	408	3.68	0	0	3.09×10^{2}	N. A	
4235	408	3.47	0	0	3.20×10^{2}	0.0130	
4236	408	3.89	0	0	4.17×10^{2}	N. A	
4237	408	4.15	0	0	4.47×10^{2}	N. A.	
4238	408	4.44	0	0	9.00×10^{2}	0.0141	
4239	408	4.54	0	0	1.02×10^{3}	N. A	
4240	408	4.51	0	0	1.41×10^{3}	N. A	
4241	408	5.25	0	0	2.00×10^{3}	N. A.	

Tests 4224-4241: the test data is from work by Subhash and Ravichandran [84]. The tests were uniaxial compression tests using either an MTS machine (quasi-static) or a Hopkinson bar (high rate data). The failure strain (ε_z) is the total axial strain measured at catastrophic failure. The data was obtained from Figure 2, Reference 84.

2.4.3 Hydrostatic Test Data for Aluminum Nitride

This section presents the hydrostatic response for Aluminum Nitride. The experimental data were obtained using a diamond Anvil Cell performed by Xia *et al.* [18] and Ueno *et al.* [71] and are presented graphically in Figure 2.4.3.1 and summarized in Table 2.4.3.1. Table 2.4.3.1 presents the pressure, P, the relative volume, V/V_o, and V_o/V -1 where V is the measured volume and V_o is the initial volume. Very little information on the materials was provided in the references, thus the materials were not given a specific material number. All the material information is presented in the comment section directly following the tabulated data in Table 2.4.3.1. It is very evident from Figure 2.4.3.1 that Aluminum Nitride exhibits a phase transformation from the wurtzite phase to a rocksalt phase and is consistent between two researchers.
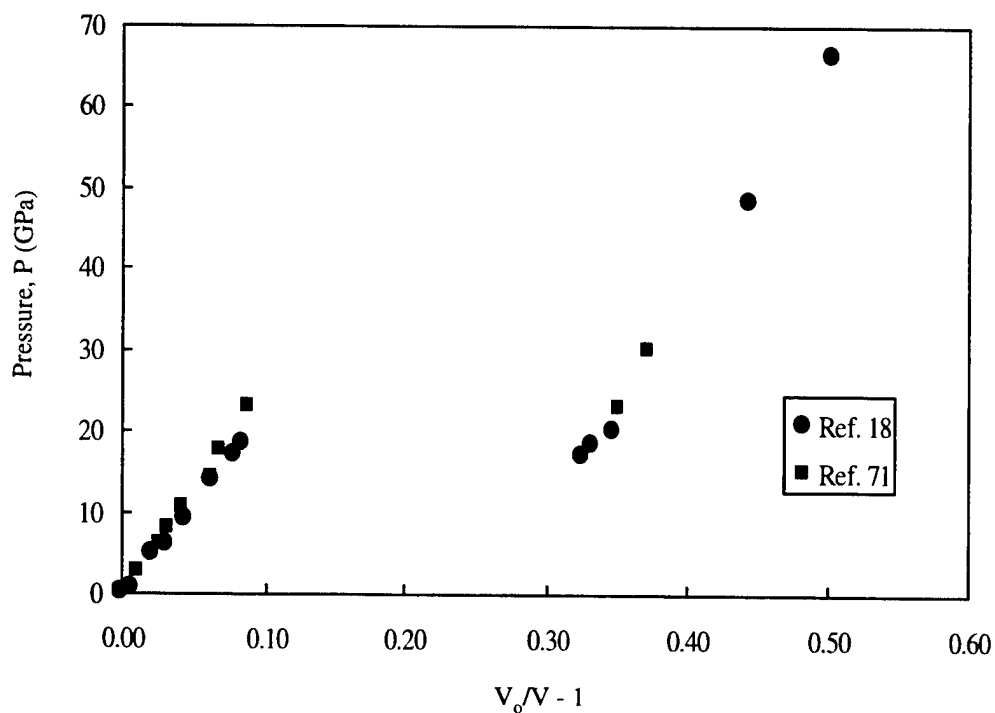
Figure 2.4.3.1 Pressure vs. Volume Relationship for Aluminum Nitride, Xia *et al.*[18] and Ueno *et al.*[71].

Table 2.4.3.1 Summary of Experimental Results Documenting the Hydrostatic Response of
Aluminum Nitride

Aluminum Nitride					
Test Number	Material Number	P (GPa)	V/V_o	V_o/V-1	Ref.
4301		0	1.0	0	18
4302		0.6	0.993	0.007	(Xia)
4303		4.9	0.979	0.021	
4304		5.8	0.970	0.031	
4305		8.9	0.958	0.044	
4306		13.8	0.942	0.062	
4307		17.0	0.928	0.078	
4308		18.4	0.923	0.083	
4309		17.0	0.755	0.325	
4310		18.4	0.751	0.332	
4311		20.0	0.742	0.348	
4312		48.3	0.692	0.445	
4313		66.2	0.666	0.502	

Test 4301-4313: the data were obtained using a diamond-anvil cell. The polycrystalline AlN sample was 99.99% pure, no other material information was provided. The observed phase transformation from the wurtzite phase to a rocksalt phase begins at a pressure of 14 GPa and completes at a pressure of 20 GPa. The above tabulated data was obtained from Figure 2, Ref. 18.

4314		0	1.0	0	71
4315		2.4	0.989	0.011	(Ueno)
4316		5.8	0.974	0.027	
4317		7.8	0.968	0.033	
4318		10.4	0.959	0.043	
4319		14.0	0.942	0.062	
4320		17.4	0.936	0.068	
4321		22.8	0.919	0.088	
4322		22.8	0.739	0.353	
4323		30.0	0.728	0.374	

Test 4314-4323: the data were obtained using a diamond-anvil cell. The AlN sample was > 99% pure, commercially obtained from Tochiba Ceramics, no other material information was provided. The observed phase transformation from the wurtzite phase to the rocksalt phase begins at a pressure of 18 GPa and completes at approximately 23 GPa. The measured initial bulk modulus was 208 GPa, this was the only material information provided in Ref. 71. The above tabulated data was obtained from Figure 3, Ref. 71.

2.4.4 Plate Impact Test Data for Aluminum Nitride

This section presents plate impact results performed by numerous researchers using various Aluminum Nitride materials. A typical plate impact test configuration is presented in Figure 2.4.4.1. The peak stress, σ_z, occurs in the z-direction and is generally measured for both the elastic and plastic response. The lateral stresses, σ_x and σ_y, occur due to the uniaxial strain configuration of the experiment, and are typically not measured. The peak stress for the elastic regime is referred to as the Hugoniot Elastic Limit (HEL) and has become a fundamental property of ceramics. The peak stress for the plastic response is generally referred to as the peak Hugoniot stress. The particle velocity and wave velocity for both the elastic and plastic waves are typically measured and documented herein. In some cases the entire particle velocity time history is measured using laser velocity interferometry techniques (VISAR). VISAR traces provide direct information on the material response and are included in this section when available.

A description of the plate impact test configurations used by Rosenberg et al. [51] are presented in Figure 2.4.4.2. Three different target configurations were used where in-material Manganin gauges were placed in the target to measure the lateral stress and in some cases the transverse stress. The results are summarized in Table 2.4.4.1.

A description of the plate impact test configurations used by Grady and Moody [52] are presented in Figure 2.4.4.3. Two materials were investigated. The specific test dimensions and some limited results are summarized in Table 2.4.4.2. Compression and release behavior was measured by monitoring the ceramic-window interface velocity using laser velocity interferometry techniques (VISAR). The interface velocity profiles reflect the uniaxial strain loading and unloading behavior of the material and are presented in Figures 2.4.4.4-6.

The results from Nakamura et al. [72] are summarized in Table 2.4.4.3. The peak stress, σ_z, and density, ρ, for both the elastic and plastic waves are presented.
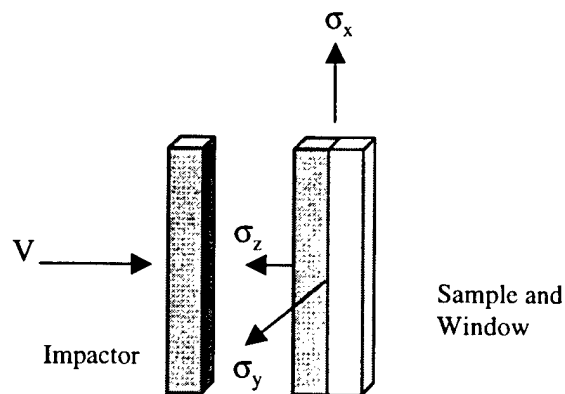
Figure 2.4.4.1 Description of a Typical Plate Impact Test Configuration including Stress Orientations

Configuration 1 — Impactor (copper), Target (Aluminum Nitride, PMMA), Manganin gauge

Configuration 2 — Impactor (copper), Target (Aluminum Nitride, Aluminum Nitride), Manganin gauge

Configuration 3 — Impactor (copper), Target (AlN, AlN), Manganin gauges

σ_x, σ_z, σ_y
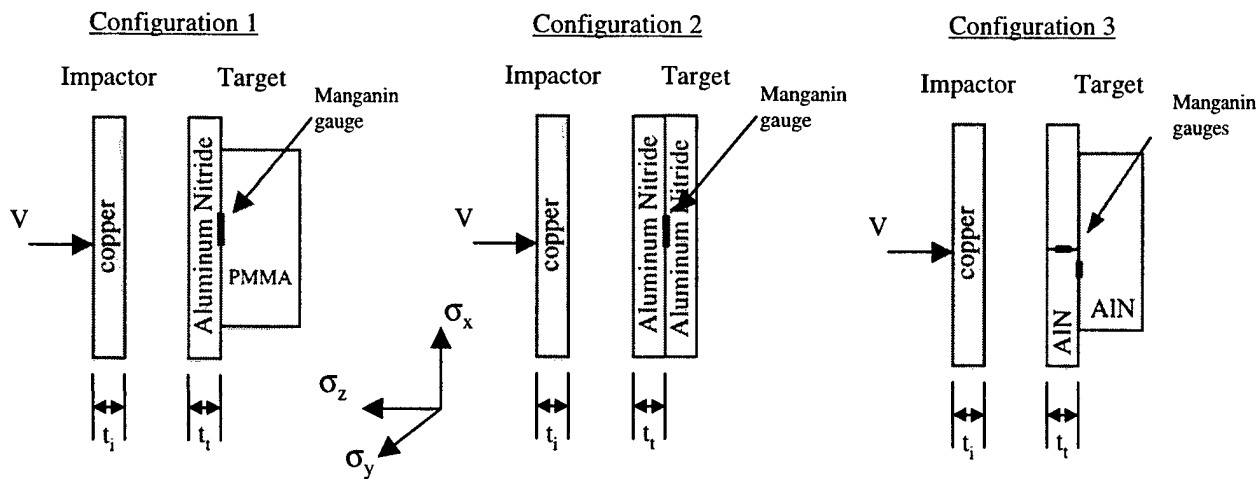
Figure 2.4.4.2 Description of Plate Impact Test Configuration, Rosenberg et al. [51].

Table 2.4.4.1 Summary of Experimental Plate Impact Results by Rosenberg et al. [51].

Aluminum Nitride												
Test Number	Material Number	Test Configuration				Elastic Regime (HEL)		Plastic Regime				
		Config	V (m/s)	t_i (mm)	t_t (mm)	σ_z (GPa)	ρ (kg/m³)	σ_z (GPa)	$\sigma_y = \sigma_x$ (GPa)	ρ (kg/m³)	U_p (m/s)	U_s (m/s)
4401	404	1	590	4	6.96	9.2+-.2	3308					
4402	404	1	739	8	6.96	9.3+-.2	3309					
4403	404	1	984	3	13.0	9.6+-.2	3312					
4404	404	3	990	8	10.3	9.3+-.4	3309	16.8+-.3	8.8+-.1			
4405	404	3	930	8	10.3	9.4+-.4	3310	16.1+-.3	8.7+-.1			
4406	404	2	569	8	5.5			10.6+-.2		3315	296	
4407	404	2	649	6	3.2			11.7+-.2		3342	354	
4408	404	2	706	6	5.5			12.5+-.2		3370	401	
4409	404	2	763	8	6.96			13.4+-.2		3380	430	
4410	404	2	859	6	3.2			14.7+-.3		3415	494	
4411	404	2	1010	8	9.2			17.0+-.3		3478	605	
4412	404	2	1178	8	9.2			18.5+-.5		3583	730	
4413	404	3	550	8	10.3			10.0+-.3	3.0+-.1			9300+-200
4414	404	3	760	8	10.3			13.3+-.3	6.4+-.2			8900+-200
4415	404	3	626	8	9.1			11.5+-.2	4.5+-.1	3334	335	8700+-200
4416	404	3	378	10	8.0			6.7+-.1	1.7+-.1			8300+-200
4417	404	3	410	3	13.0			7.5+-.1	2.6+-.1			
4418	404	3	433	3	13.0			8.0+-.1	2.2+-.2			

Test 4401-4418: the test data is from work by Rosenberg. The material is hot pressed Aluminum Nitride manufactured by Coors, having an initial density = 3226kg/m3. Three target configurations were used and both longitudinal and transverse stresses were measured using in-material manganin gauges. Densities calculated from conservation equations.
Test 4404,4505,4413,4414: Longitudinal stress inferred from Hugoniot because longitudinal gauge failed before reaching peak stress.
Test 4406-4412,4415: Longitudinal stress measured directly.
Test 4416-4418: Longitudinal stress derived from impedance matching in the elastic range
Test 4412: Questionable data due to possible gauge malfunction
Further discussions on the data can be found in Ref. 63.

97

Projectile Materials Used

Material	Density (kg/m³)	Designation
Polyurethane Foam	139	PF139
Polyurethane Foam	320	PF320
Polyurethane Foam	640	PF640
PMMA	1186	PMMA
Tantalum	16659	Ta
Tungsten	19289	W
Aluminum 6061-T6	2703	Al
OFHC Copper	8930	Cu
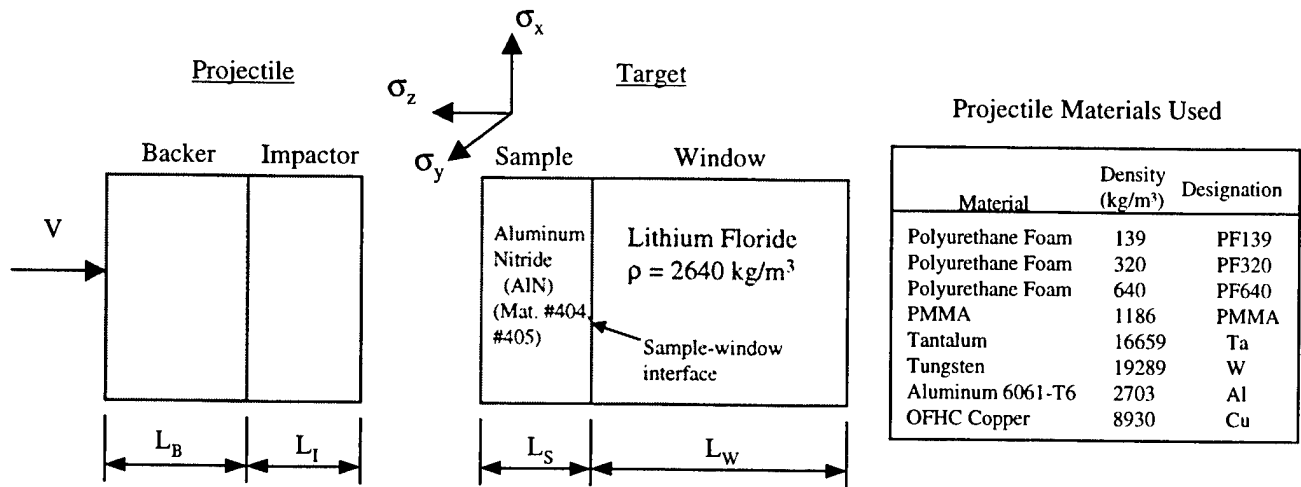
Figure 2.4.4.3 Description of Grady and Moody [52] Plate Impact Test Configuration.

Table 2.4.4.2 Summary of Experimental Plate Impact Results by Grady and Moody [52].

Test Number	Material Number	V (m/s)	Backer Material	L_B (mm)	Impactor Material	Impactor Density (kg/m³)	L_I (mm)	Sample Density (kg/m³)	L_S (mm)	Window L_W (mm)	Elastic Compression σ_z (GPa)	Elastic Compression ρ (kg/m³)	Plastic Compression σ_z (GPa)	Plastic Compression ρ (kg/m³)
4419	404	1780	PF320	8.0	AlN	3258	4.971	3261	9.952	25.4				
4420	404	2277	PF640	8.0	AlN	3260	4.923	3259	9.952	25.4				
4421	404	1263	PF320	8.0	AlN	3258	4.968	3262	9.554	25.4				
4422	404	589	PF320	8.0	AlN	3256	4.975	3255	9.954	25.4				
4423	404	2239	PF640	8.0	Ta	16657	1.508	3265	9.567	25.4			38	
4424	404	2207	PF640	8.0	Ta	16618	1.528	3248	2.510	25.5			37	
4425	404	2230	PMMA	6.4	W	19289	1.502	3248	2.507	25.5			41	
4426	404	1160	PF139	8.0	PMMA	1186	2.004	3258	10.184	25.2				
4427	404	860	PF139	7.9	PMMA	1186	1.991	3221	9.552	25.5				
4428	404	2215	PF640	8.0	Ta	16642	1.526	3248	4.183	31.9			37	
4429	404	2262	PF640	8.0	AlN	3250	4.181	3250	4.182	37.8				
4430	405	1490	Air	---	Al	2703	12.7	3236	4.343	18.9				
4431	405	2008	Air	---	Cu	8930	9.408	3219	4.34	25.4				
4432	405	2370	PMMA	6.77	Ta	16669	3.898	3236	4.34	19.1				

Test 4419-4432: the test data is from work by Grady. Material #404 is hot pressed Aluminum Nitride manufactured by Coors, having a nominal initial density = 3254kg/m³. Material #405 is Aluminum Nitride manufactured by Sumitomo Electric Industries Co. having a initial density = 3236kg/m³. The above table primarily provides the initial conditions for the plate impact experiments, although the elastic and plastic stress-density states are provided when available.
Test 4423-4425,4428: the peak hugoniot stress is from Ref. 53, 54.
The HEL ~ 8 GPa from Ref. 54
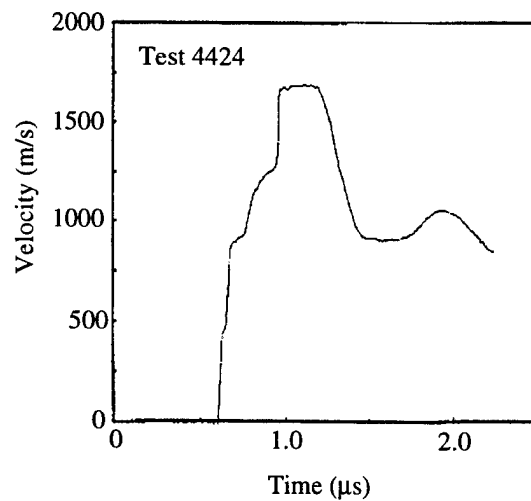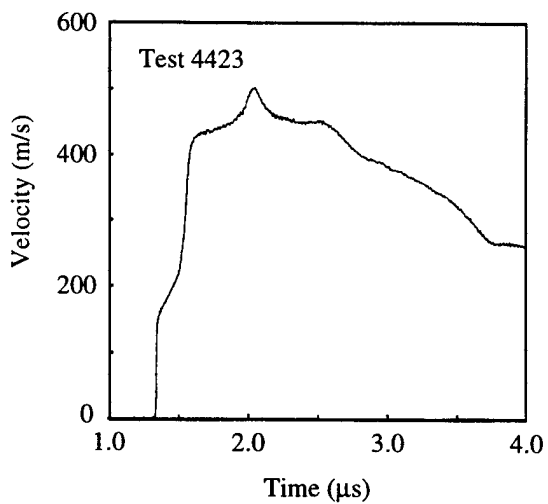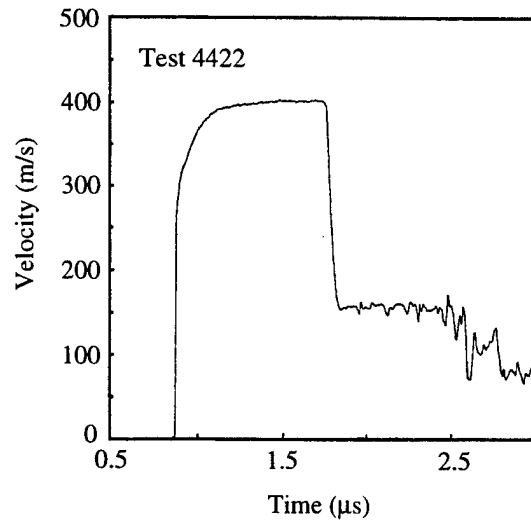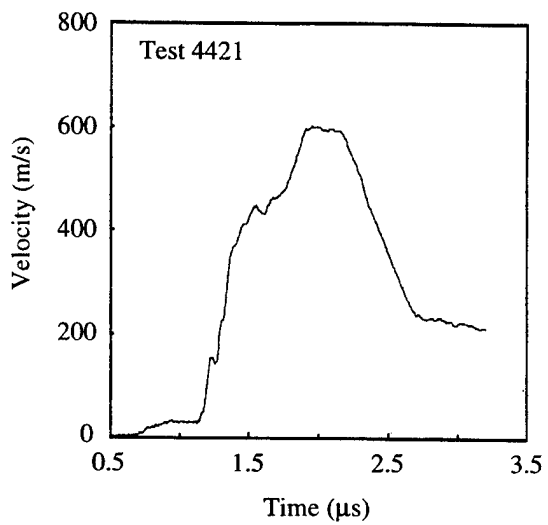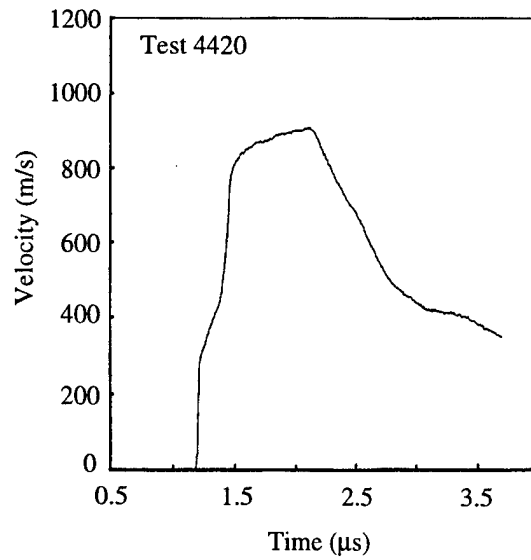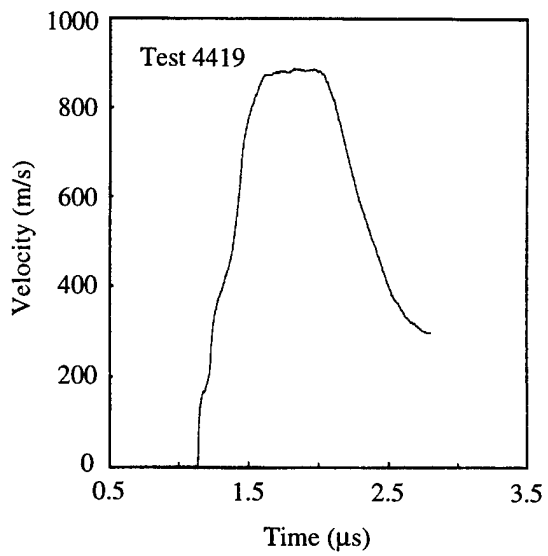
Figure 2.4.4.4 Ceramic-Window Interface Velocity Profiles from Grady and Moody [52] for Tests 4419-4424.
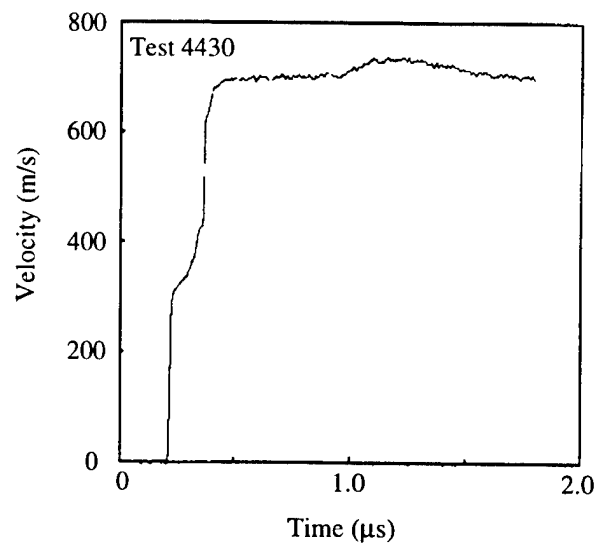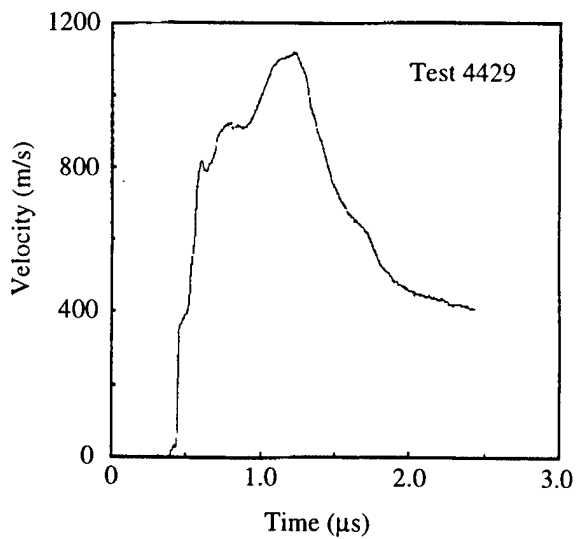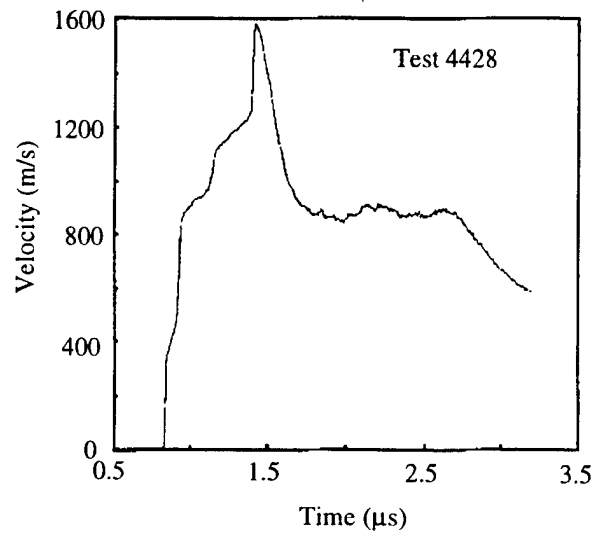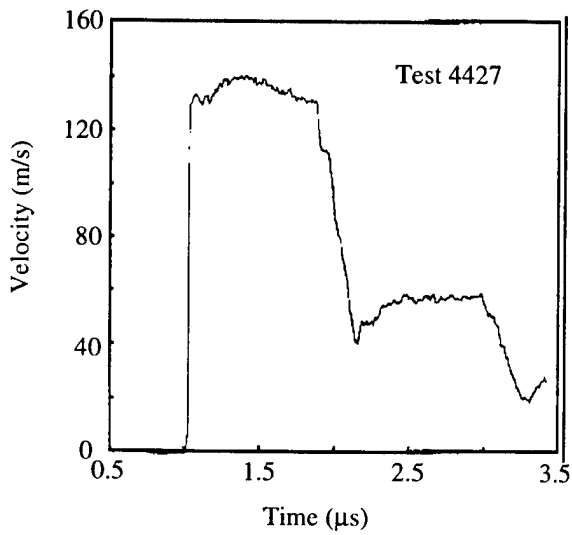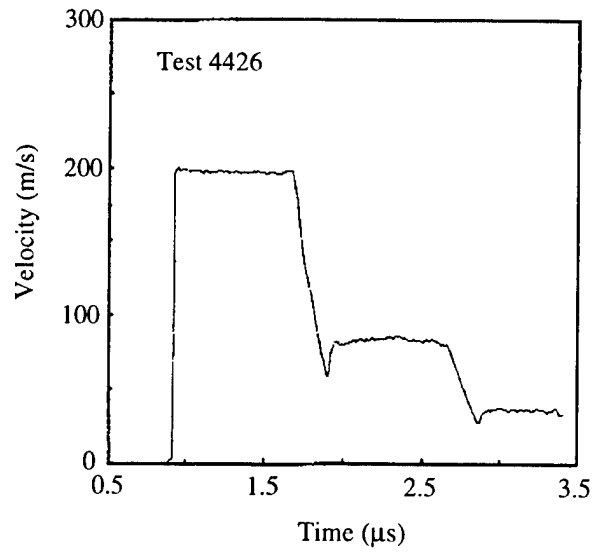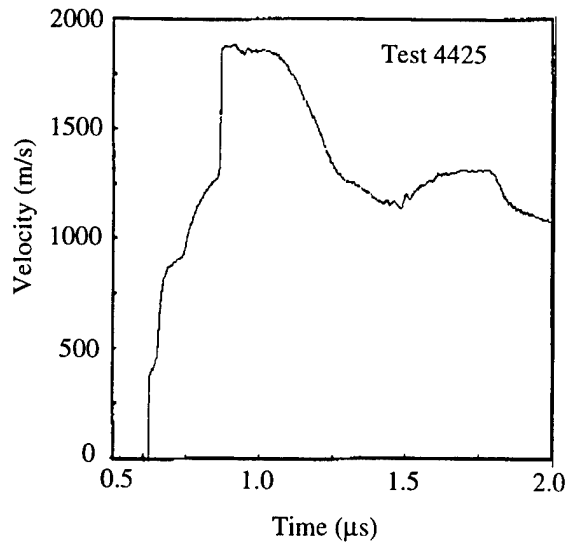
Figure 2.4.4.5 Ceramic-Window Interface Velocity Profiles from Grady and Moody [52] for Tests
4425-4430.
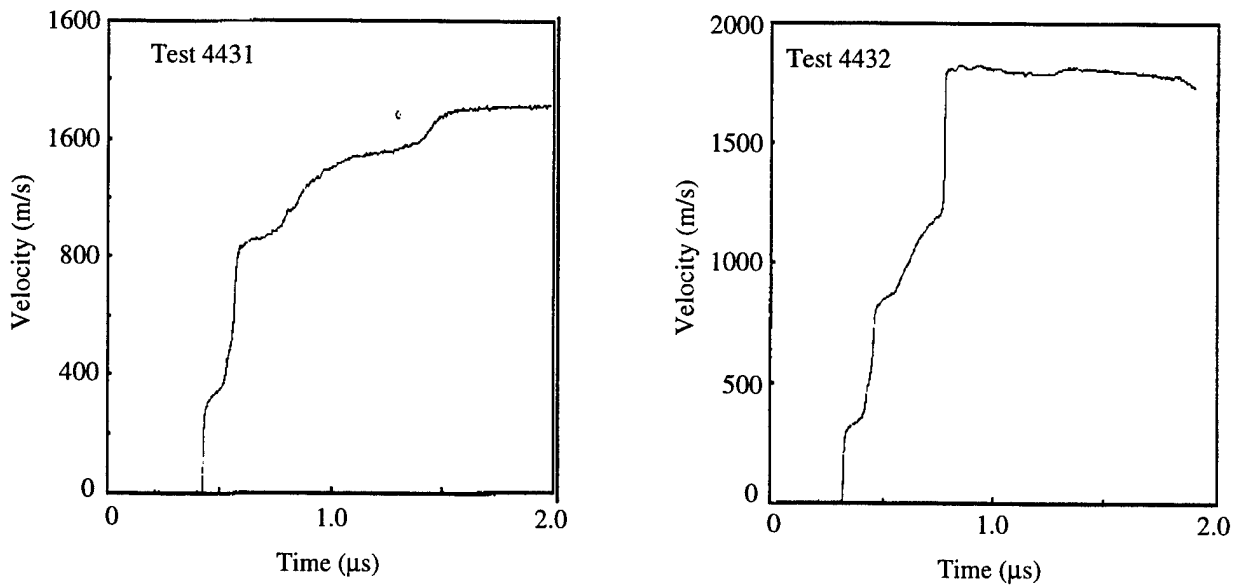
Figure 2.4.4.6 Ceramic-Window Interface Velocity Profiles from Grady and Moody [52] for Tests 4431-4432.

Table 2.4.4.3 Summary of Experimental Plate Impact Results, Nakamura *et al.*[72].

Aluminum Nitride										
Test Number	Material Number	Initial Density ρ_o (kg/m^3)	Elastic Regime (HEL)				Plastic Regime			
			Shock Velocity (m/s)	Particle Velocity (m/s)	σ_z (GPa)	ρ (kg/m^3)	Shock Velocity (m/s)	Particle Velocity (m/s)	σ_z (GPa)	ρ (kg/m^3)
4433	406	3200	10800	230	7.9	3270	6010	360	10.5	3340
4434	406	3200	11000	230	8.1	3270	5890	400	11.4	3370
4435	406	3200	10400	230	7.6	3270	7060	720	18.9	3510
4436	406	3200	11400	250	9.1	3270	7550	1080	29.4	3670
4437	406	3200	11700	250	9.4	3270	7530	1170	32.1	3730

Test 4433-4437: the test data is from work by Nakamura *et al.*[72]. The shock and particle velocities were obtained from Figure 2 in Reference 72.

2.4.5 Penetration (semi-infinite) Test Data for Aluminum Nitride

This section presents ballistic penetration results into semi-infinite Aluminum Nitride targets. Orphal *et al.* [21] performed penetration experiments into Aluminum Nitride over a velocity range of 1500m/s to 4500m/s. The targets and penetrators used are described in Figure 2.4.5.1. The penetration results are presented graphically in Figure 2.4.5.2 and summarized in Table 2.4.5.1. Both primary and total penetration are given. Primary penetration is the depth penetrated when the penetrator is just consumed. Total penetration is the total depth penetrated when the penetration event is complete.
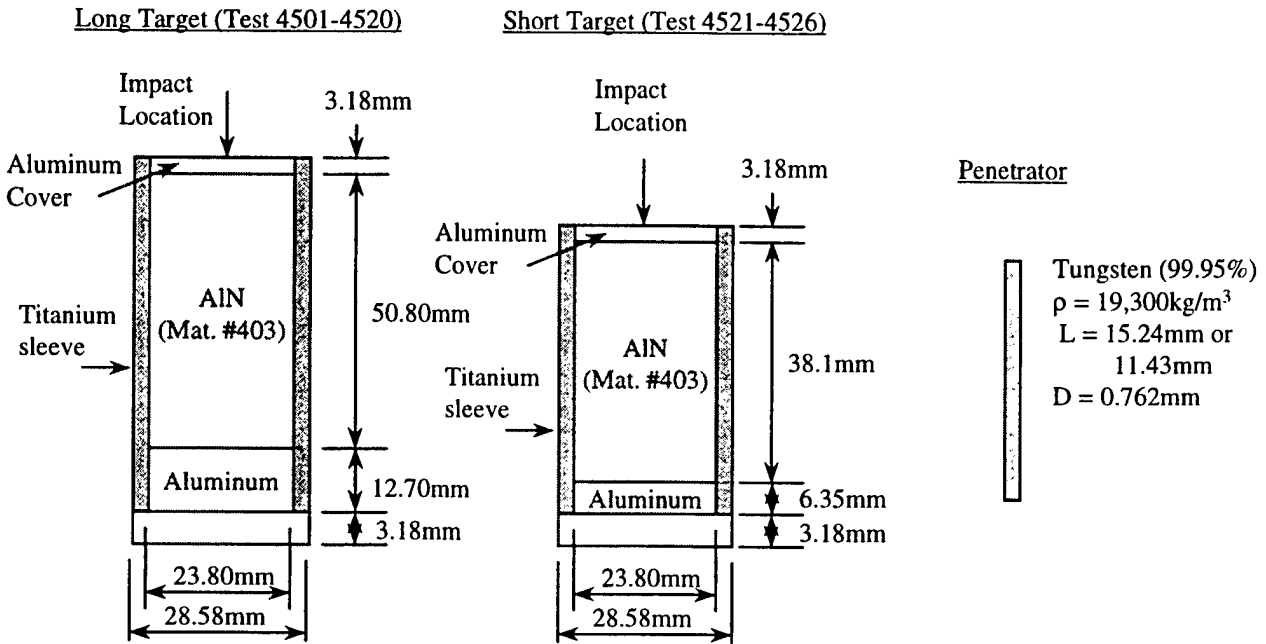
Figure 2.4.5.1 Aluminum Nitride Target and Penetrator Descriptions, Orphal *et al.* [21].
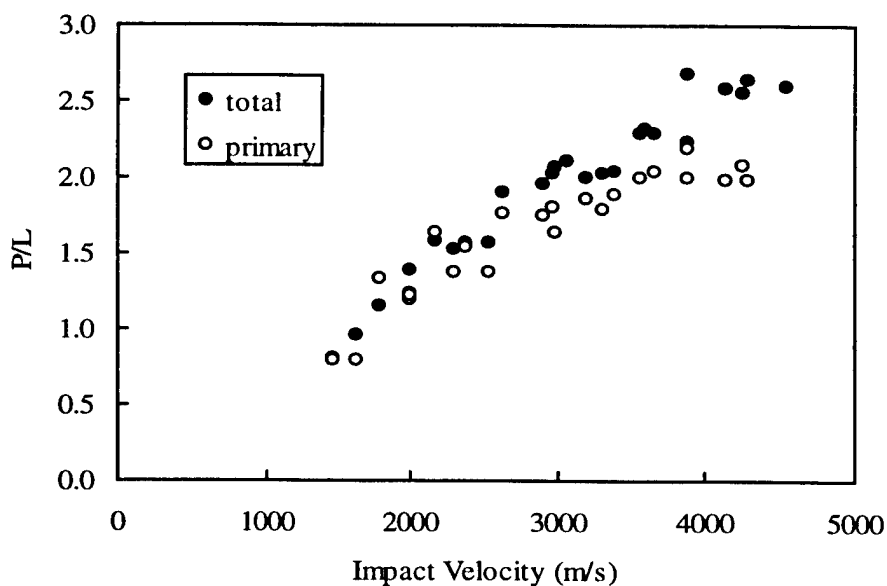
Figure 2.4.5.2   Total and Primary Penetration Depths vs. Impact Velocity for Tungsten Penetrators Impacting Confined Aluminum Nitride Targets, Orphal *et al.* [21].

Table 2.4.5.1 Summary of Penetration Results from Orphal *et al.* [21].

Test Number	Material Number	Penetrator		Target Configuration	Impact Velocity (m/s)	$P_{primary}/L$	P_{total}/L
		D (mm)	L (mm)				
4501	403	0.762	15.24	Long	1490	0.78	0.79
4502	403	0.762	15.24	Long	1650	0.78	0.95
4503	403	0.762	15.24	Long	1810	1.32	1.14
4504	403	0.762	15.24	Long	2010	1.18	1.22
4505	403	0.762	15.24	Long	2010	1.21	1.37
4506	403	0.762	15.24	Long	2190	1.63	1.57
4507	403	0.762	15.24	Long	2310	1.36	1.51
4508	403	0.762	15.24	Long	2400	1.53	1.56
4509	403	0.762	15.24	Long	2550	1.36	1.55
4510	403	0.762	15.24	Long	2650	1.75	1.89
4511	403	0.762	15.24	Long	2920	1.74	1.95
4512	403	0.762	15.24	Long	2980	1.79	2.01
4513	403	0.762	15.24	Long	3000	1.63	2.06
4514	403	0.762	15.24	Long	3080		2.10
4515	403	0.762	15.24	Long	3210	1.85	1.99
4516	403	0.762	15.24	Long	3320	1.78	2.02
4517	403	0.762	15.24	Long	3410	1.87	2.03
4518	403	0.762	15.24	Long	3580	1.99	2.28
4519	403	0.762	15.24	Long	3610		2.30
4520	403	0.762	11.43	Long	3670	2.03	2.28
4521	403	0.762	11.43	Short	3900	2.18	2.67
4522	403	0.762	11.43	Short	3900	1.98	2.22
4523	403	0.762	11.43	Short	4160	1.97	2.57
4524	403	0.762	11.43	Short	4270	2.07	2.54
4525	403	0.762	11.43	Short	4290	1.97	2.63
4526	403	0.762	11.43	Short	4550		2.58

Test 4501-4526: the test data is from work by Orphal *et al.* [21]. Two penetrator lengths and two target configurations were used. The impact velocity and P/L listed here were obtained from Figure 7 in Ref. 21. The primary, P_{primar}, and total, P_{total}, penetration measured includes the 3.18mm cover.

2.4.6 Depth-Of-Penetration (DOP) Test Data for Aluminum Nitride

This section presents depth-of-penetration (DOP) experiments for numerous Aluminum Nitride materials. The DOP test has been used to investigate the effectiveness of ceramics for a number of years. The typical DOP configuration consists of a ceramic tile place on, or within, a steel or aluminum base target. A penetrator impacts and perforates the ceramic tile and continues into the base target. The penetration into the base target is generally referred to as the residual penetration, P_r, and is used to determined the ceramic mass efficiency as discussed in Section 2.0.

The target and penetrator descriptions for the DOP experiments by Franzen *et al.* [33] are presented in Figure 2.4.6.1. The objective of the experiments was to investigate the ballistic effectiveness of Aluminum Nitride as a function of impact velocity and ceramic thickness. The results are summarized in Table 2.4.6.1. No material information was provided for the Aluminum Nitride used in these experiments.

The target and penetrator description for the DOP experiments by Reaugh *et al.* [85] is presented in Figure 2.4.6.2. The results are summarized in Table 2.4.6.2. Also included in the table are penetration results into the 4340 Steel with no ceramic .

The target and penetrator description for the DOP experiments by Rosenberg *et al.* [91] is presented in Figure 2.4.6.3. The objective of the experimental program was to investigate the ballistic efficiency of Aluminum Nitride as a function of ceramic thickness and lateral dimensions. The results are presented graphically in Figure 2.4.6.4 and summarized in Table 2.4.6.3. Also included in the table are penetration results into the steel base target with no ceramic .

Target Configuration
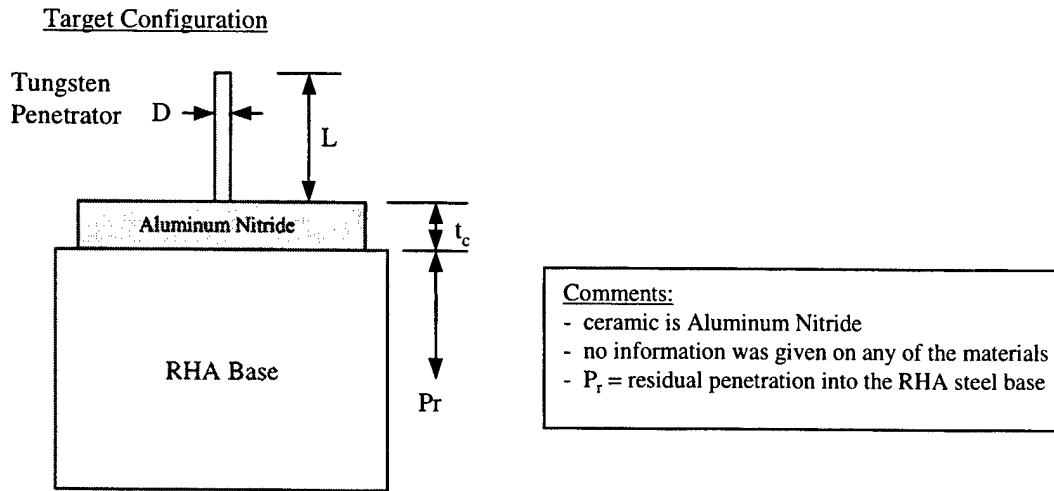
Figure 2.4.6.1   Target and Penetrator Descriptions for Aluminum Nitride DOP
Experiments, Franzen *et al.* [33].

Table 2.4.6.1   Tabulated Experimental Results for Aluminum Nitride, Franzen *et al.* [33].

Aluminum Nitride						
Test Number	Material Number	Impact Velocity (m/s)	Penetrator		Ceramic Thickness t_c (mm)	P_r (mm)
			L (mm)	D (mm)		
4601		1502	81.8	8.18	30.7	39.4
4602		1504	81.8	8.18	30.7	42.6
4603		1499	81.8	8.18	30.7	36.1
4604		1506	81.8	8.18	30.7	41.1
4605		1491	81.8	8.18	30.7	39.1
4606		1499	81.8	8.18	30.7	39.3
4607		1506	81.8	8.18	30.7	37.9
4608		1482	81.8	8.18	30.7	29.1
4609		1457	81.8	8.18	30.2	36.7
4610		1505	81.8	8.18	30.2	41.8
4611		1499	107.4	7.16	45.9	42.4
4612		1510	107.4	7.16	46.1	41.9
4613		2054	62.0	6.20	70.0	9.0
4614		2001	62.0	6.20	70.0	10.0
4615		2467	62.0	6.20	80.0	15.2
4616		2510	62.0	6.20	80.0	9.5
4617		2035	75.0	7.50	80.0	15.4
4618		1995	75.0	7.50	80.0	21.4
4619		2479	75.0	7.50	90.0	22.0
4620		2449	75.0	7.50	90.0	21.6
4621		2027	75.0	7.50	50.0	37.5
Test 4601-4621: The ceramic material is aluminum nitride, no information on the material was given.						
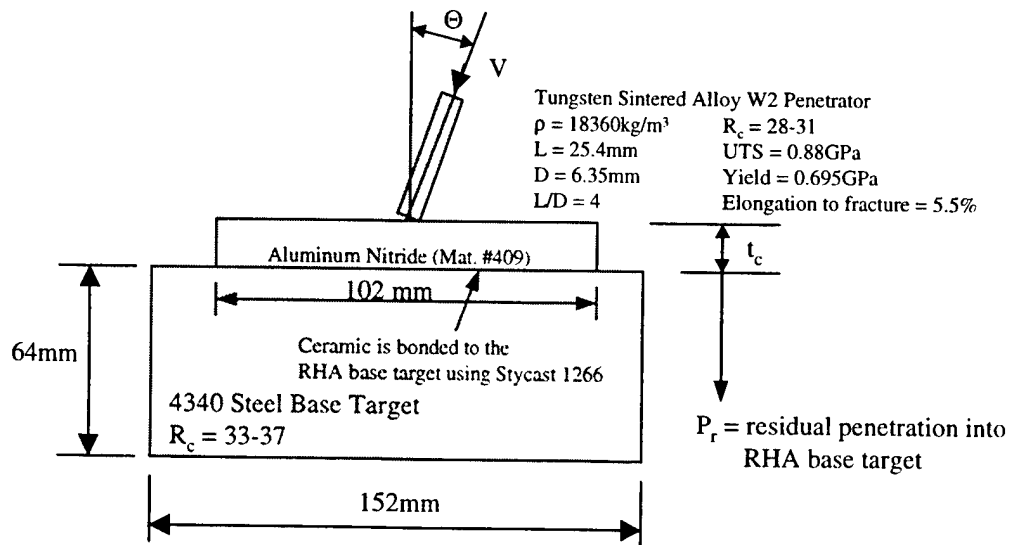
Figure 2.4.6.2 Target and Penetrator Description for DOP Experiment, Reaugh *et al.* [85].

Table 2.4.6.2 Summary of Experimental DOP Results, Reaugh *et al.* [85].

Aluminum Nitride					
Test Number	Material Number	Impact Velocity (m/s)	Ceramic t_c (mm)	Impact Angle# Θ (degrees)	P_r& (mm)
4622	409	1250	9.7	0	10.1
4623	409	1300	14.3	0	8.9
4624	409	1310	19.6	0	4.3
4625	409	1790	9.9	0	27.5
4626	409	1790	19.7	0	14.3
4627	409	1800	28.8	0	8.5
4628	409	1790	37.0	0	0.0
4629	409	1760	28.2	30	1.6
4630	409	1780	17.5	60	0.0
4631	409	2610	30.3	0	19.3
4632	409	2580	39.5	0	8.3
4633		1340	0	0	27.0
4634		1350	0	0	27.8
4635		1350	0	0	28.5
4636		1770	0	0	36.0
4637		2500	0	0	43.8

Test 4622-4637: the test data is from work by Reaugh *et al.* [85].
#the angle between the penetrator flight axis and the normal to the tile.
& the residual penetration measured normal to the impact surface.
Test 4633-4637: tests into 4340 steel target only (no ceramic used).
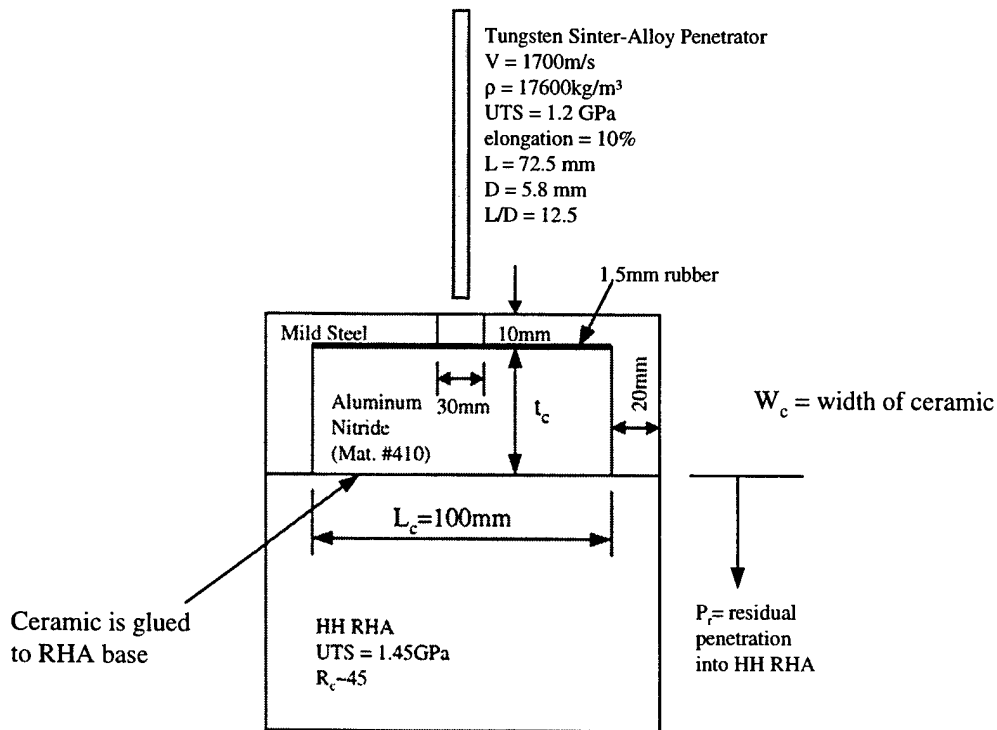
Figure 2.4.6.3 Target and Penetrator Description for DOP Experiment, Rosenberg *et al.* [91].
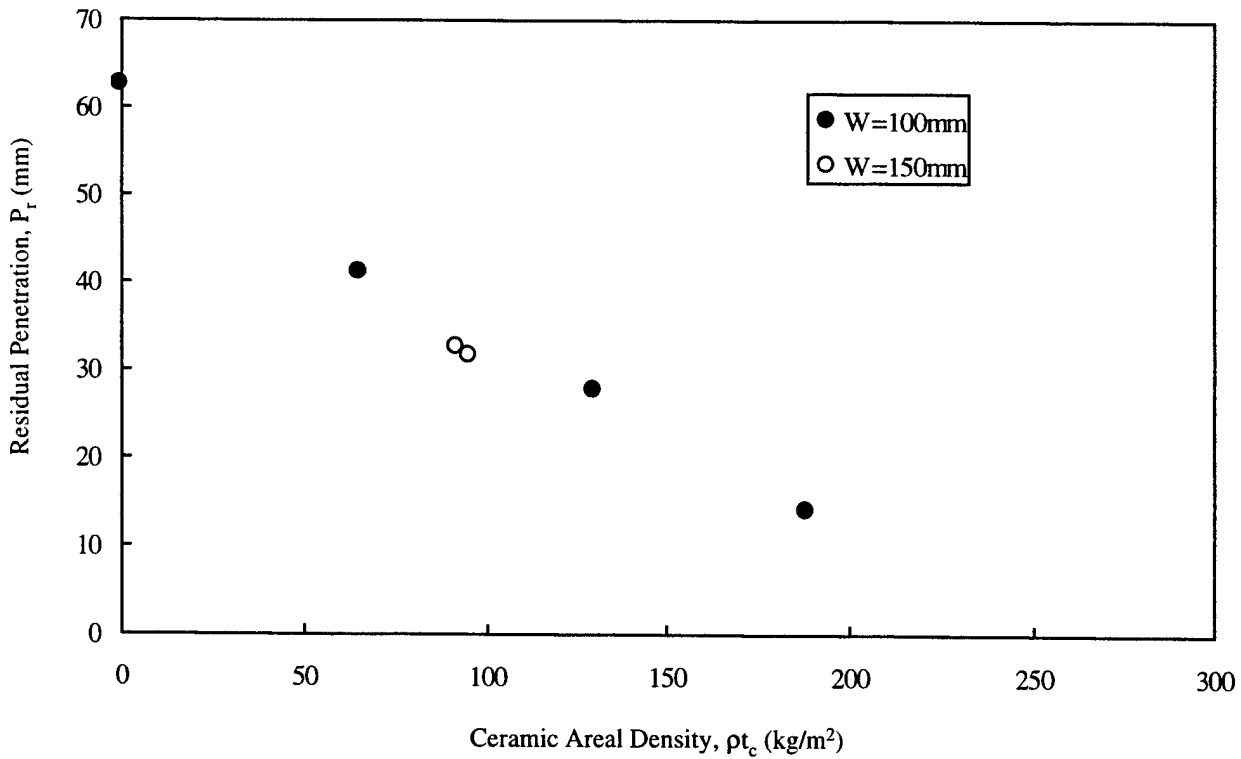
Figure 2.4.6.4 Residual Penetration as a Function of Ceramic Areal Density and Ceramic Tile Width, W, Rosenberg *et al.* [91].

Table 2.4.6.3 Summary of Experimental DOP Results, Rosenberg *et al.* [91].

Aluminum Nitride							
Test Number	Material Number	Impact Velocity (m/s)	Ceramic Dimensions			ρt_c (kg/m^2)	P_r (mm)
			Thickness t_c (mm)	Length L_c, (mm)	Width W_c, (mm)		
4638	410	1700	20	100	100	64.9	41.0
4639	410	1700	40	100	100	129.8	27.5
4640	410	1700	58.1	100	100	187.8	14.0
4641	410	1700	28.5	100	150	92.2	32.4
4642	410	1700	29.6	100	150	95.6	31.5
4643		1700	0			0	62.4

Test 4638-4643: the test data is from work by Rosenberg *et al.* [91]. The tabulated data listed above was obtained from Figure 1 in Reference [91].
$\rho = 3230$kg/m^3 (density of ceramic)
Test 4643: test into steel base target only (no ceramic used).

2.5 SILICON NITRIDE

2.5.1 Material Description for Silicon Nitride

The purpose of this section is to provide as much information as possible on the materials tested. Descriptions for each of the Silicon Nitride materials used in Section 2.5 are presented in Table 2.5.1.1. Each material is given a material number. The material numbers are used throughout Section 2.5 to identify the specific material being tested. The data listed in Table 2.5.1.1 were obtained directly from the corresponding reference. When specific information was not available it was left blank. The strength values listed, (Compressive, Tensile, HEL and Spall), are nominal values and are included for comparison purposes.

Table 2.5.1.1   Description of the Silicon Nitride Materials Tested

	Material Number						
	501	502	503	504	505		
Reference	3, 10	3	44, 49	44, 49	52		
Manufacturer	Norton	Norton			Kyocera		
Trade Name/Description	NC 132	NC 350			SN-220		
Processing	Hot Pressed	Reaction bonded			Sintered		
Average Grain Size (μm)	0.5-3				0.4-0.7		
Density (kg/m³)			3150	2280	3152		
Void Fraction							
Longitudinal Velocity (m/s)			10660	8660	10310		
Shear Velocity (m/s)					5810		
Bulk Velocity (m/s)					7830		
Young's Modulus, E (GPa)					269		
Shear Modulus, G (GPa)					106		
Bulk Modulus, K (GPa)					193		
Poisson Ratio					0.267		
Compressive Strength (GPa)	3.4	2.1					
Tensile Strength (GPa)	0.81						
HEL (GPa)			12.1	1.9			
Spall Strength (GPa)			0.5-0.8	0.25			

2.5.2 Mechanical Test Data for Silicon Nitride

The following section presents mechanical test results for Silicon Nitride. A typical test specimen showing the stress configuration is shown in Figure 2.5.2.1. Loading is generally uniaxial in the z direction and is increased until the material fails, although some researchers use more complex loading techniques to vary the stress state at failure.

Mechanical test data performed by Lankford [3, 10] are presented in Table 2.5.2.1. Two materials were investigated. The stress state at failure is given as a function of average strain rate, $\dot{\varepsilon}$, and temperature. Compression is taken as positive and tension as negative.
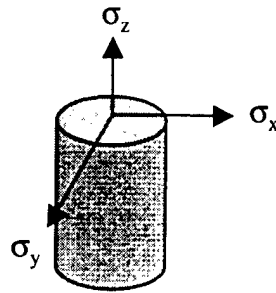
Figure 2.5.2.1 Description of a Typical Mechanical Test Specimen

Table 2.5.2.1 Summary of Experimental Results for Silicon Nitride, Lankford [3, 10].

Silicon Nitride						
Test Number	Material Number	σ_z (GPa)	σ_x (GPa)	σ_y (GPa)	$\sim \dot{\varepsilon}$ (s^{-1})	Temperature Degrees (C)	Ref.
5201	501	3.44	0	0	7×10^{-5}	Ambient	3 (Lankford)
5202	501	3.29	0	0	7×10^{-5}	Ambient	
5203	501	3.29	0	0	6×10^{-1}	Ambient	
5204	501	3.51	0	0	6×10^{-1}	Ambient	
5205	501	3.94	0	0	1×10^{3}	Ambient	
5206	501	4.43	0	0	2×10^{3}	Ambient	
5207	502	2.05	0	0	7×10^{-5}	Ambient	3 (Lankford)
5208	502	2.09	0	0	7×10^{-5}	Ambient	
5209	502	2.48	0	0	6×10^{-1}	Ambient	
5210	502	2.54	0	0	6×10^{-1}	Ambient	
5211	502	2.00	0	0	2×10^{3}	Ambient	
5212	502	2.09	0	0	2×10^{3}	Ambient	
5213	501	3.16	0	0	7×10^{-5}	400	10 (Lankford)
5214	501	1.84	0	0	7×10^{-5}	800	

Test 5201-5214: the test data is from work by Lankford. Compressive strength was investigated for both quasi-static and Hopkinson bar experiments. Quasi-static experiments were also performed as a function of temperature.

2.5.4 Plate Impact Test Data for Silicon Nitride

This section presents plate impact results using various Silicon Nitride materials. A typical plate impact test configuration is presented in Figure 2.5.4.1. The peak stress, σ_z, occurs in the z-direction and is generally measured for both the elastic and plastic response. The lateral stresses, σ_x and σ_y, occur due to the uniaxial strain configuration of the experiment, and are typically not measured. The peak stress for the elastic regime is referred to as the Hugoniot Elastic Limit (HEL) and has become a fundamental property of ceramics. The peak stress for the plastic response is generally referred to as the peak Hugoniot stress. The particle velocity and wave velocity for both the elastic and plastic waves are typically measured and documented herein. In some cases the entire particle velocity time history is measured using laser velocity interferometry techniques (VISAR). VISAR traces provide direct information on the material response and are included in this section when available.

The results from Nahme *et al.* [44, 49] are summarized in Table 2.5.4.1. Two materials were investigated in this study, a dense and porous material. The shock velocity, particle velocity, peak stress, σ_z, and density, ρ, for both the elastic and plastic waves are presented. The experiments did not use a window material as shown in Figure 2.5.4.1, but rather left the rear surface free. The free surface velocity time histories, for selected tests, are presented in Figure 2.5.4.2. The initial conditions of the experiments were not given in the references.

A description of the plate impact test configuration by Grady and Moody [52] is presented in Figure 2.5.4.3. The specific test dimensions are summarized in Table 2.5.4.2. Compression and release behavior was measured by monitoring the ceramic-window interface velocity using laser velocity interferometry techniques (VISAR). The interface velocity profiles reflect the uniaxial strain loading and unloading behavior of the material and are presented in Figures 2.5.4.4-5.
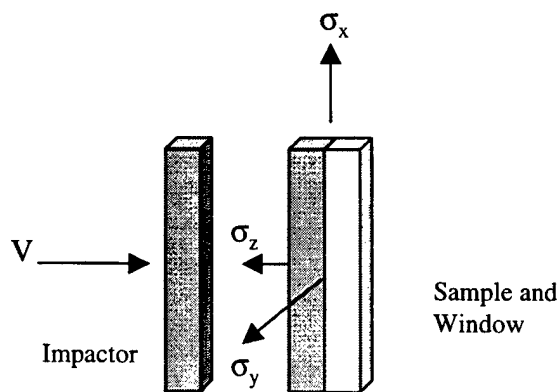
Figure 2.5.4.1 Description of a Typical Plate Impact Test Configuration including Stress Orientations

Table 2.5.4.1 Summary of Experimental Plate Impact Results, Nahme *et al.*[44, 49].

Silicon Nitride										
Test Number	Material Number	Initial Density ρ_o (kg/m^3)	Elastic Regime (HEL)				Plastic Regime			
			Shock Velocity (m/s)	Particle Velocity (m/s)	σ_z (GPa)	ρ (kg/m^3)	Shock Velocity (m/s)	Particle Velocity (m/s)	σ_z (GPa)	ρ (kg/m^3)
5401	503	3150	10660	360	12.1	3265	9000	465	15.2	3304
5402	503	3150	10660	360	12.1	3265	9130	510	16.6	3320
5403	504	2280	8600	97	1.9	2305	5080	200	3.1	2353
5404	504	2280	8600	97	1.9	2305	4760	301	4.1	2408
5405	504	2280	8600	97	1.9	2305	4650	329	4.4	2426
5406	504	2280	8600	97	1.9	2305	4760	553	6.9	2549

Test 5401-5406: The HEL data was not given for each test and as shown here was assumed to be constant for each material. The shock velocity and particle velocity for the plastic wave was obtained from Figure 3 in Reference 44. The peak stress and density for the plastic regime were calculated using the conservation equations. Two Silicon Nitride materials were investigated, a dense material #503 and a porous material #504.
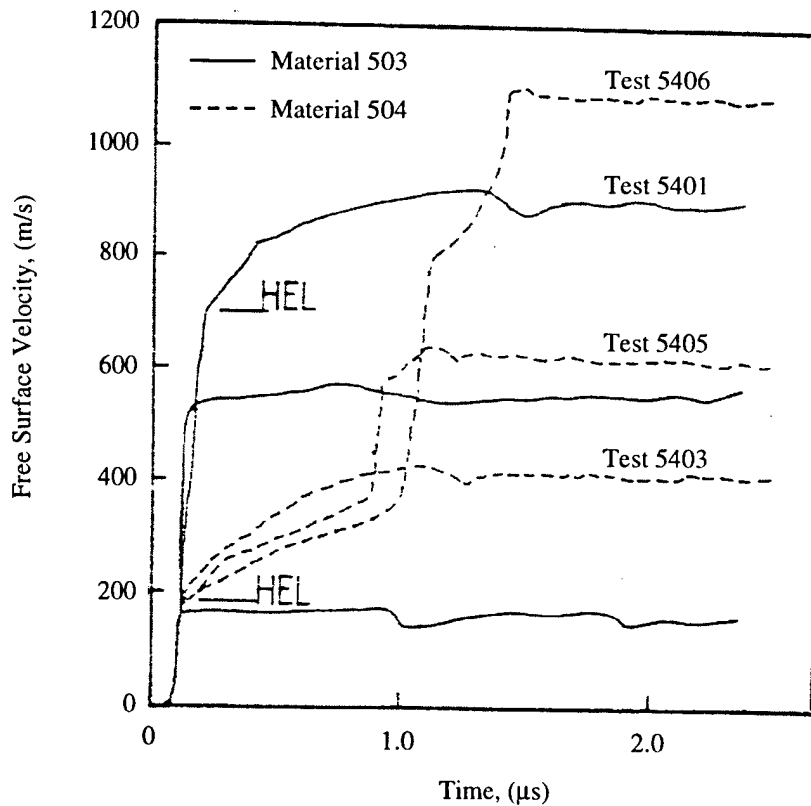
Figure 2.5.4.2 Free Surface Velocity Time Histories for Selected Plate Impact Experiments, Nahme *et al.*[44, 49].

112
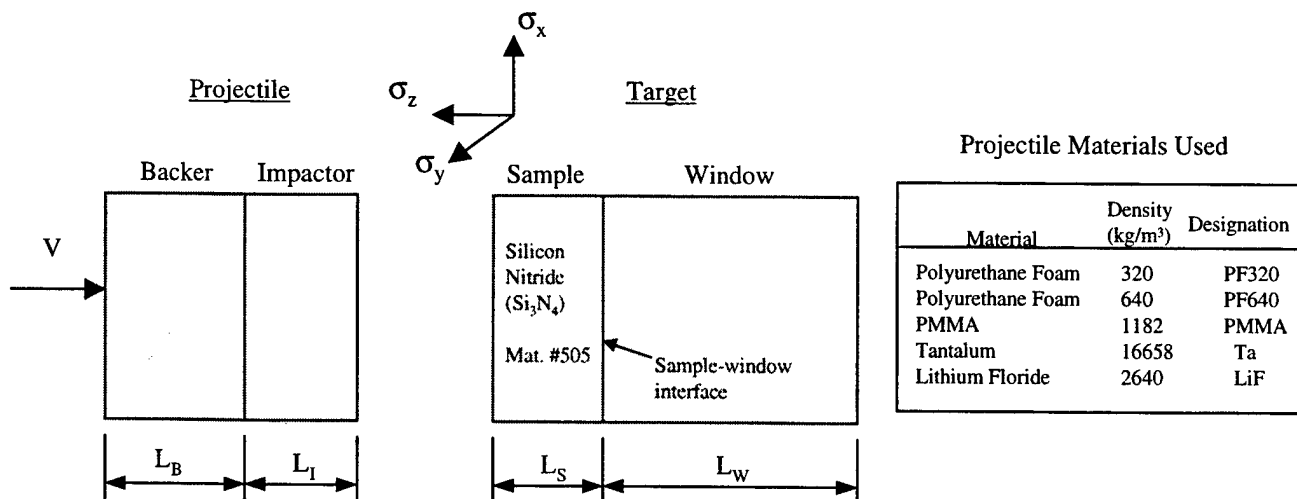
Figure 2.5.4.3 Description of Grady and Moody [52] Plate Impact Test Configuration.

Projectile Materials Used

Material	Density (kg/m³)	Designation
Polyurethane Foam	320	PF320
Polyurethane Foam	640	PF640
PMMA	1182	PMMA
Tantalum	16658	Ta
Lithium Floride	2640	LiF

Table 2.7.4.2 Summary of Experimental Plate Impact Results by Grady and Moody [52].

Silicon Nitride													
		Projectile				Target				Hugoniot Results			
			Backer		Impactor		Sample		Window		Elastic Compression		Plastic Compression	
Test Number	Material Number	V (m/s)	Material	L_B (mm)	Material	L_I (mm)	Density (kg/m³)	L_S (mm)	Material	L_W (mm)	σ_z (GPa)	ρ (kg/m³)	σ_z (GPa)	ρ (kg/m³)
5407	505	1057	PF320	12.8	Si_3N_4	5.005	3156	10.013	LiF	25.6				
5408	505	1478	PF320	12.7	Si_3N_4	5.003	3158	10.026	LiF	25.6				
5409	505	2080	PF320	12.7	Si_3N_4	5.004	3156	10.011	LiF	25.6				
5410	505	2487	PF640	8.0	Si_3N_4	5.000	3156	10.023	LiF	25.4				
5411	505	2284	PMMA	5.904	Ta	1.520	3156	10.023	LiF	25.4				
5412	505	1047	PF320	6.3	Si_3N_4	4.984	3126	15.007	LiF	25.4				
5413	505	1059	PF320	6.3	Si_3N_4	5.039	3126	10.016	LiF	25.4				
5414	505	1049	PF320	7.8	Si_3N_4	5.008	3130	5.013	LiF	25.6				

Test 5407-5414: the test data is from work by Grady. Material #505 is Silicon Nitride manufactured by Kyocera Industrial Ceramics Corporation having a nominal initial density = 3152kg/m³. The above table primarily provides the initial conditions for the plate impact experiments. No elastic and plastic stress-density states were provided. The documented HEL for this material is 9.2 GPa from Ref. 54.

113
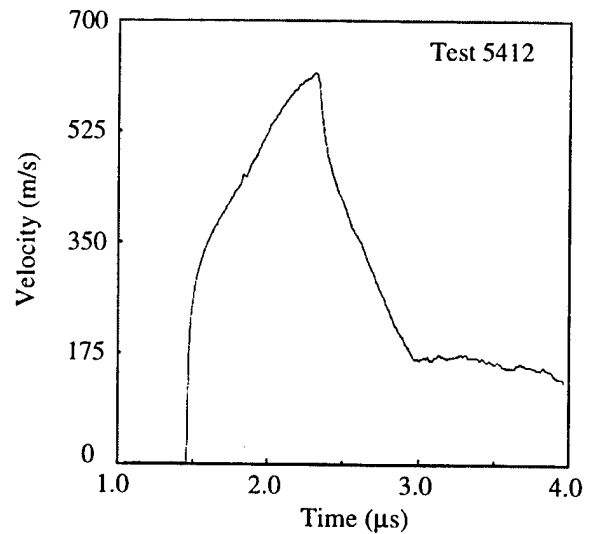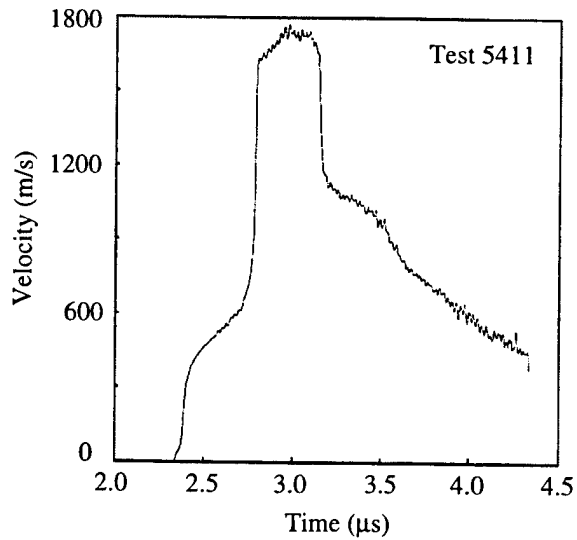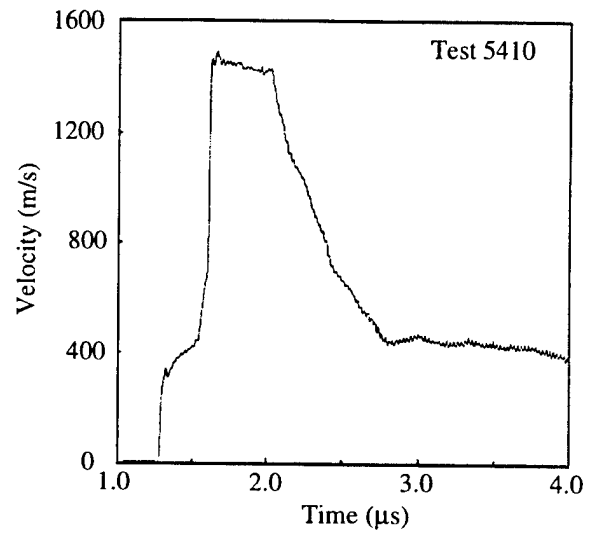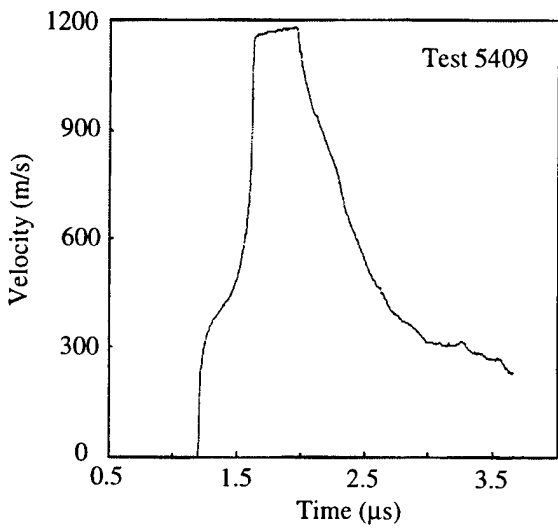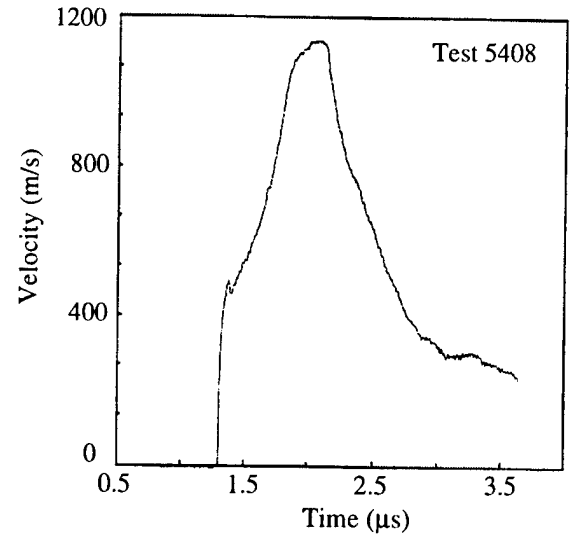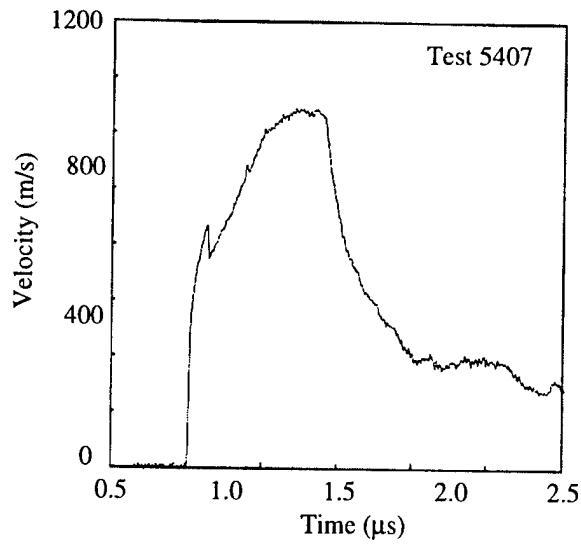
Figure 2.5.4.4 Ceramic-Window Interface Velocity Profiles from Grady and Moody [52] for Tests
5407-5412.

114
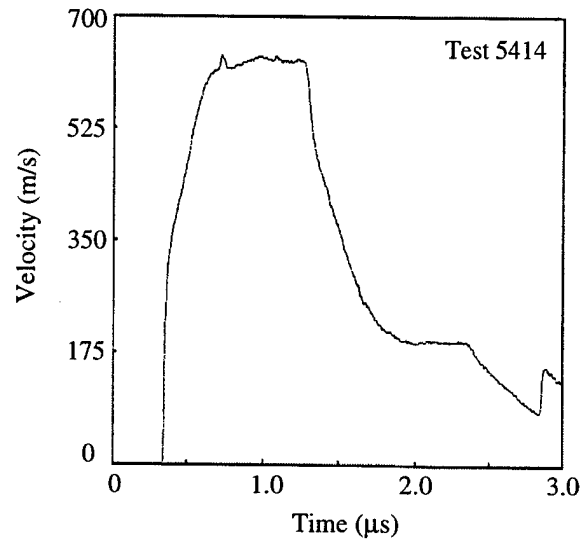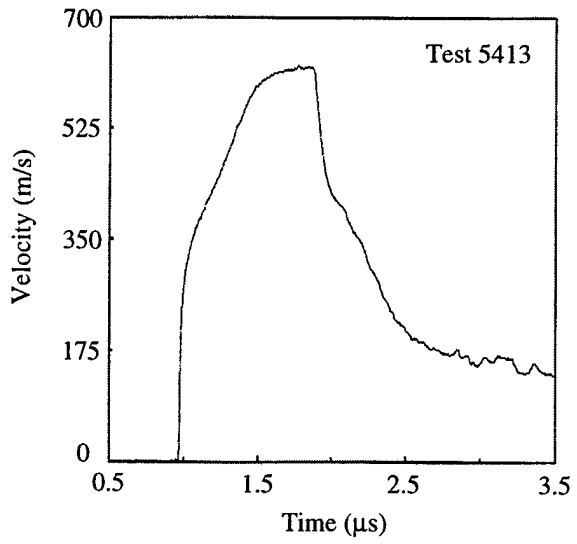
Figure 2.5.4.5 Ceramic-Window Interface Velocity Profiles from Grady and Moody [52] for Tests 5413-5414.

2.5.6 Depth-Of-Penetration (DOP) Test Data for Silicon Nitride

This section presents depth-of-penetration (DOP) experiments for Silicon Nitride materials. The DOP test has been used to investigate the effectiveness of ceramics for a number of years. The typical DOP configuration consists of a ceramic tile place on, or within, a steel or aluminum base target. A penetrator impacts and perforates the ceramic tile and continues into the base target. The penetration into the base target is generally referred to as the residual penetration, P_r, and is used to determined the ceramic mass efficiency as discussed in Section 2.0.

The target and penetrator descriptions for the DOP experiments by Nahme et al.[44] are presented in Figure 2.5.6.1. Two Silicon Nitride materials were investigated. The results are presented graphically in Figure 2.5.6.2 where residual penetration is plotted vs. ceramic areal density for impact velocity of 1700 m/s. The results are also presented in tabular from in Table 2.5.6.1.

Tungsten-Sintered Penetrator
$\rho = 17600 kg/m^3$
D = 5.8mm
L = 72.5mm
UTS = 1.2GPa
Elongation at failure = 10%

Silicon Nitride
(Mat # 503 - #504)

t_c

High Strength German
Steel $R_c = 44$

Pr

Comments:
- Two grades of Silicon Nitride ceramic were used.
  (See material #503 and #504)
- P_r = residual penetration into the RHA steel base
- V_s = Penetrator impact velocity = nominally 1700m/s
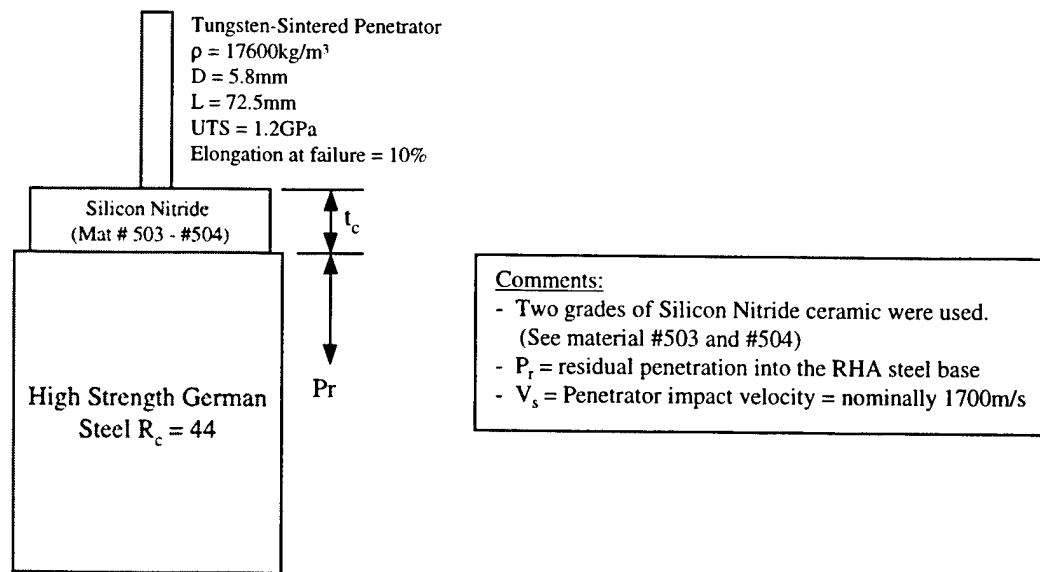
Figure 2.5.6.1   Target and Penetrator Descriptions for Silicon Nitride DOP Experiments, Nahme et al. [44].

116
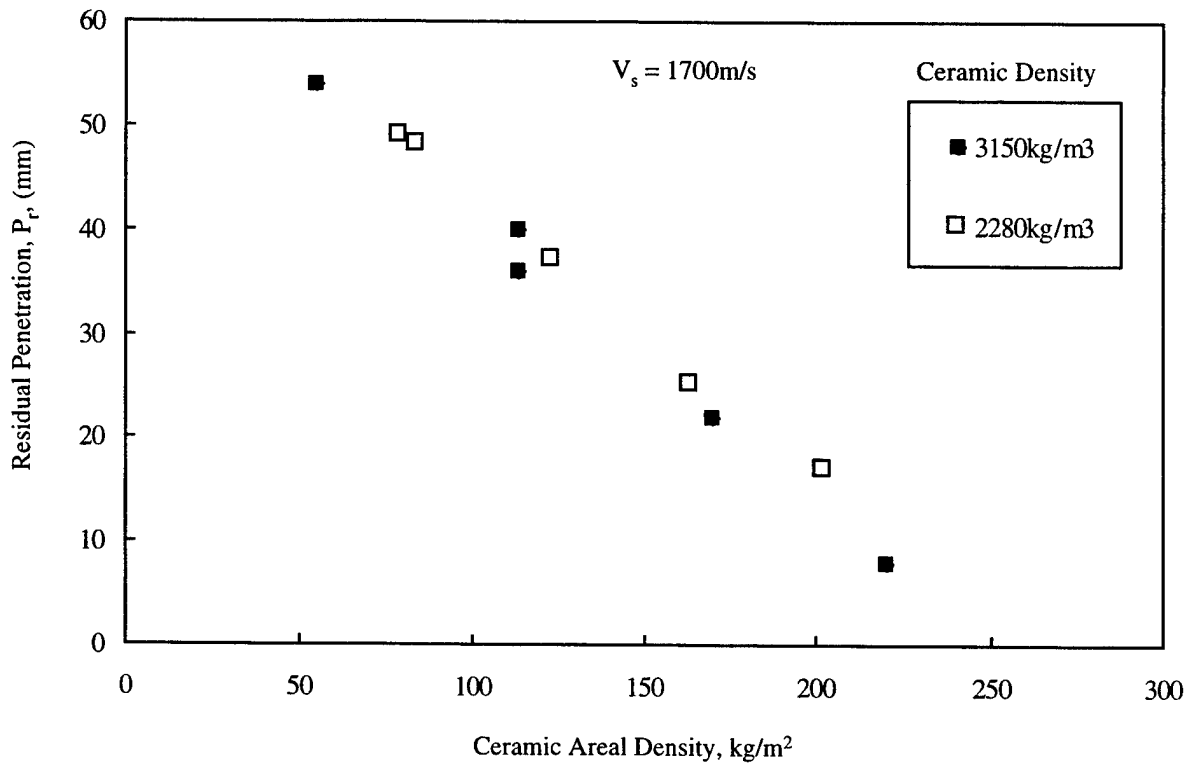
Figure 2.4.6.2   Residual Penetration vs. Ceramic Areal Density for Impact Velocity = 1700m/s,
Nahme *et al.* [44].

Table 4.5.6.1   Tabulated Experimental Results for Silicon Nitride DOP Tests, Nahme et al. [44].

Silicon Nitride						
Test Number	Material Number	Impact Velocity (m/s)	Ceramic Thickness t_c (mm)	Ceramic Areal density (kg/m^2)	P_r (mm)	P_r/P_{st}
5601	503	1700	17	55	54	0.744
5602	503	1700	36	114	36	0.496
5603	503	1700	36	114	40	0.546
5604	503	1700	54	170	22	0.305
5605	503	1700	70	220	8	0.110
5606	504	1700	35	79	49	0.667
5607	504	1700	37	84	48	0.667
5608	504	1700	54	124	37	0.511
5609	504	1700	72	164	25	0.348
5610	504	1700	89	202	17	0.230

P_{st} = 72.5mm = penetration into the steel base target with no ceramic material [45].
Test 5601-5610: The data was obtained from Reference 44, Figure 6. Ceramic performance
was investigated as a function of material and thickness. Material #503 density = 3150kg/m^3
and Material #504 is more porous with a density = 2280kg/m^3.
Areal Density = t_c x ρ_c where ρ_c = ceramic density

117

2.6 ALUMINUM OXIDE (85% pure)

2.6.1 Material Description for Aluminum Oxide (85% pure)

The purpose of this section is to provide as much information as possible on the Aluminum Oxide materials tested. Descriptions for each of the Aluminum Oxide materials used in Section 2.6 are presented in Table 2.6.1.1. Each material is given a material number which is used throughout Section 2.6 to identify it. The data listed in Table 2.6.1.1 were obtained directly from the corresponding reference. When specific information was not available it was left blank. The strength values listed, (Compressive, Tensile, HEL and Spall), are nominal values and are included for comparison purposes. The material defined in the first column (with no material number) is Coors AD-85 alumina [74] and is included here for reference. Coors AD-85 Aluminum Oxide is the most common material tested. Occasionally researchers will determine the chemical composition of the material being tested, Table 2.6.1.1 includes this data when available.

Table 2.6.1.1   Description of Aluminum Oxide (85% pure) Materials Tested

		Material Number					
		601	602	603	604	605	606
Reference	74	11	26	30	32	38, 39, 50	39
Manufacturer	Coors	Coors	Coors	Coors	Coors	Coors	Coors
Trade Name/Description	AD-85	AD-85	AD-85	AD-85	AD-85	AD-85	BC90G
Processing							
Average Grain Size (μm)	6						
Density (kg/m³)	3410		3430	3420		3410	3560
Void Fraction				0.066			
Longitudinal Velocity (m/s)	8700		8800	8840		8900	
Shear Velocity (m/s)	5140		4920	5060		5300	
Bulk Velocity (m/s)	6360		6700	6630		6360	
Young's Modulus, E (GPa)	221		211	221		234	
Shear Modulus, G (GPa)	90		83	88		96	
Bulk Modulus, K (GPa)	138		154	150		138	
Poisson's Ratio	0.22		0.272	0.256		0.22	
Compressive Strength (GPa)	1.93	2.14				1.93	
Tensile Strength (GPa)	0.155						
HEL (GPa)			6.0	6.2	6.0	6.0	7.0
Spall Strength (GPa)						0.3	
Purity (%)	85					~84	
Impurities (%wt)							
SiO₂	9.7			15.0			
MgO	2.7			3.3			
CaO	1.2			2.1			
K₂O	<1.0						
Na₂O	<1.0			0.07			
BaO	<1.0			0.9			
Fe₂O₃	<1.0			0.4			
ZrO₂	<1.0						
TiO₂	<1.0			0.3			

Table 2.6.1.1   Description of Aluminum Oxide (85% pure) Materials Tested, Concluded.

	Material Number						
	607	608	609	610			
Reference	41	65	73	85			
Manufacturer	Coors	Babcock &Wilcox	Coors	Dow			
Trade Name/Description	AD-85		AD-85	AD-85			
Processing		Sintered					
Average Grain Size (µm)			5				
Density (kg/m³)	3430	3700	3421	3400			
Void Fraction							
Longitudinal Velocity (m/s)		9320	8800	8800			
Shear Velocity (m/s)			5190	5070			
Bulk Velocity (m/s)			6000	6570			
Young's Modulus, E (GPa)	224		221	218			
Shear Modulus, G (GPa)			92	87			
Bulk Modulus, K (GPa)			123	147			
Poisson's Ratio			0.20	0.25			
Compressive Strength (GPa)	2.175						
Tensile Strength (GPa)							
HEL (GPa)		4.8-6.3	5.9				
Spall Strength (GPa)			0.30				
Purity (%)		~76					

2.6.2 Mechanical Test Data for Aluminum Oxide (85% pure)

The following section presents mechanical test data for 85% pure Aluminum Oxide. A typical test specimen showing the stress configuration is shown in Figure 2.6.2.1. Compression is taken as positive and tension as negative. Loading is generally uniaxial compression in the z direction and is increased until the material fails, although some researchers use more complex loading techniques to vary the stress state at failure.

Mechanical test data performed by Arrowood and Lankford [11] are presented in Table 2.6.2.1. The stress state at failure is given as a function of confining pressure and average strain rate, $\dot{\varepsilon}$.
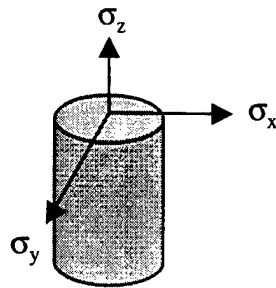
Figure 2.6.2.1 Description of a Typical Mechanical Test Specimen.

Table 2.6.2.1 Summary of Experimental Results, Arrowood and Lankford [11].

Aluminum Oxide (85% pure)					
Test Number	Material Number	σ_z (GPa)	σ_x (GPa)	σ_y (GPa)	$\sim \dot{\varepsilon}$ (s^{-1})
6201	601	2.14	0	0	0.11×10^{-3}
6202	601	2.95	0.041	0.041	0.11×10^{-3}
6203	601	3.29	0	0	0.81
Test 6201-6203: Compression tests were performed to obtain the compressive strength as a function of strain rate and confining pressure. The material is Coors AD-85 Aluminum Oxide.					

2.6.4 Plate Impact Test Data for Aluminum Oxide (85% pure)

This section presents plate impact results, performed by numerous researchers, using various 85% pure Aluminum Oxide materials. A typical plate impact test configuration is presented in Figure 2.6.4.1. The peak stress, σ_z, occurs in the z-direction and is generally measured for both the elastic and plastic response. The lateral stresses, σ_x and σ_y, occur due to the uniaxial strain configuration of the experiment, and are typically not measured. The peak stress for the elastic regime is referred to as the Hugoniot Elastic Limit (HEL) and has become a fundamental property of ceramics. The peak stress for the plastic response is generally referred to as the peak Hugoniot stress. The particle velocity and wave velocity for both the elastic and plastic waves are typically measured and documented herein. In some cases the entire particle velocity time history is measured using laser velocity interferometry techniques (VISAR). VISAR traces provide direct information on the material response and are included in this section when available.

The results from Gust and Royce [30] are summarized in Table 2.6.4.1. The shock velocity, particle velocity, peak stress, σ_z, and density, ρ, for both the elastic and plastic waves are presented.

A description of the plate impact configuration used by Rosenberg and Yeshurun [38] is presented in Figure 2.6.4.2. The longitudinal stress was measured for both the elastic and plastic response using an in-material Manganin gauge. The results are summarized in Table 2.6.4.2.

A description of the plate impact configuration used by Rosenberg *et al.* [50] is presented in Figure 2.6.4.3. The longitudinal and transverse stresses were measured using in-material Manganin gauges. The results are summarized in Table 2.6.4.3.

A description of the plate impact experiments by Rosenberg *et al.* [65] are presented in Figure 2.6.4.4. The HEL was measured using in-material Manganin gauges. The objective of this work was to evaluate precurser decay as a function of target thickness. The results are summarized in Table 2.6.4.4.

A description of the plate impact experiment by Bless *et al.* [73] is presented in Figure 2.6.4.5. The objective of this work was to evaluate spall strength as a function of precurser stress. The experiments used both in-material Manganin gauges and Visar to obtain stress measurements. The results are summarized in Table 2.6.4.5.
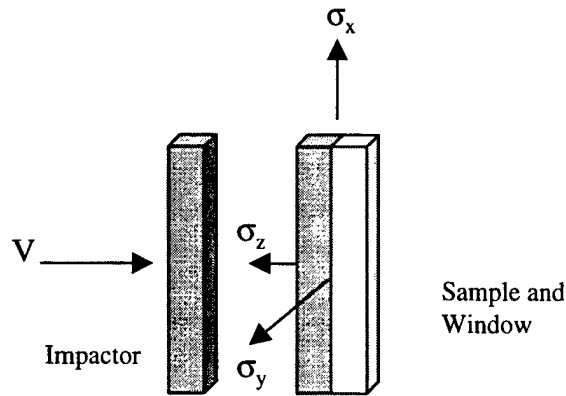
Figure 2.6.4.1 Description of a Typical Plate Impact Test Configuration including Stress Orientations

Table 2.6.4.1 Summary of Experimental Plate Impact Results, Gust and Royce [30].

Aluminum Oxide (85% pure)											
Test Number	Material Number	Initial Density ρ_o (kg/m^3)	Elastic Regime (HEL)				Plastic Regime				Ref.
			Shock Velocity (m/s)	Particle* Velocity (m/s)	σ_z (GPa)	ρ (kg/m^3)	Shock Velocity (m/s)	Particle# Velocity (m/s)	σ_z (GPa)	ρ (kg/m^3)	
6401	603	3403	8420	235	6.7	3501	5060	770	23.2	3941	30 (Gust)
6402	603	3392	8450	226	6.4	3484	4850	800	23.0	3982	
6403	603	3424	8690	192	5.7	3501	5080	790	16.0	3993	
6404	603	3430	8790	221	6.7	3519	5020	790	16.3	3993	
6405	603	3401	8190	216	6.0	3494	5390	650	13.9	3813	
6406	603	3394	8390	222	6.3	3487	5310	735	15.1	3880	
6407	603	3433	8950	189	5.8	3508	5820	980	21.8	4084	
6408	603	3427	8680	213	6.3	3514	5420	1020	21.1	4162	
6409	603	3433	8900	186	5.7	3506	6600	1365	32.2	4296	
6410	603	3426	8890	205	6.2	3508	6730	1355	32.4	4255	
6411	603	3432	8770	192	5.8	3509	7200	1570	39.9	4377	
6412	603	3395	8650	222	6.5	3484	7060	1580	38.8	4349	
6413	603	3441	8840		6.1		8330	2090	59.8	4561	
6414	603	3428					8640	2340	69.6	4692	
6415	603	3427					9390	2785	89.7	4866	
Test 6401-6415: the test data is from work by Gust and Royce [30]. * The elastic particle velocity presented here is half the measured free surface velocity ($U_p=1/2U_{fs}$). # In Reference 30 the plastic particle velocity was calculated by $U_p=1/2U_{fs}$ and by impedance matching. The particle velocity presented here is an average of the two.											
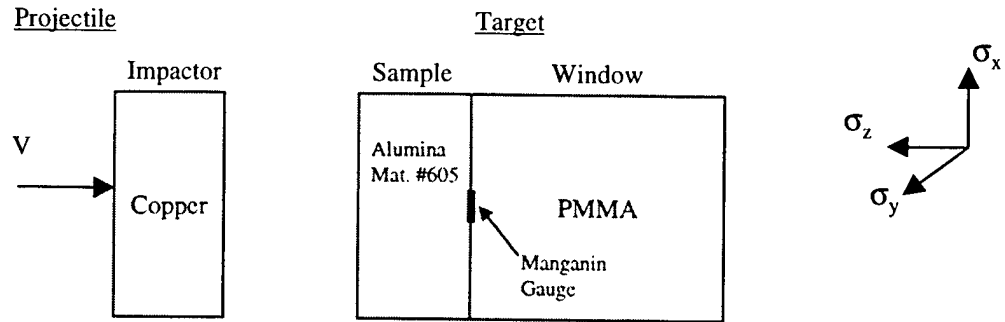
Figure 2.6.4.2 Description of Plate Impact Test Configuration, Rosenberg and Yeshurun [38].

Table 2.6.4.2 Summary of Experimental Plate Impact Results, Rosenberg and Yeshurun [38].

			Aluminum Oxide (85% pure)								
Test Number	Material Number	Initial Density ρ_o (kg/m³)	Elastic Regime (HEL)				Plastic Regime				Ref.
			Shock Velocity (m/s)	Particle* Velocity (m/s)	σ_z (GPa)	ρ (kg/m³)	Shock Velocity (m/s)	Particle# Velocity (m/s)	σ_z (GPa)	ρ (kg/m³)	
6416	605	3410	8900	110	3.3	3453					38 (Rosenberg)
6417	605	3410	8900	152	4.5	3469					
6418	605	3410	8900	194	5.7	3486					
6419	605	3410	8900	198	6.0	3488	2660	214	6.2	3506	
6420	605	3410	8900	198	6.0	3488	3300	220	6.3	3509	
6421	605	3410	8900	198	6.0	3488	4570	227	6.5	3509	
6422	605	3410	8900	198	6.0	3488	8940	217	6.6	3495	
6423	605	3410	8900	198	6.0	3488	4760	250	6.9	3525	
6424	605	3410	8900	198	6.0	3488	8950	233	7.1	3501	
6425	605	3410	8900	198	6.0	3488	6510	263	7.5	3522	
6426	605	3410	8900	198	6.0	3488	5100	331	8.4	3580	
6427	605	3410	8900	198	6.0	3488	3530	519	10.0	3834	

Test 6416-6427: the test data is from work by Rosenberg and Yeshurun [38]. In-material Manganin gauges were used to determine the stress state in the material. The above data were obtained from Figure 3 in Reference 38. The documented HEL for this work = 6.0+-0.1 GPa.
The documented spall stress from this work = 0.3 - 0 GPa as the shock stress increases from 4.0 GPa to the HEL. The elastic shock velocity was assumed constant at 8900m/s.
Test 6419-6427: the HEL particle velocity was assumed constant at 198m/s.

124
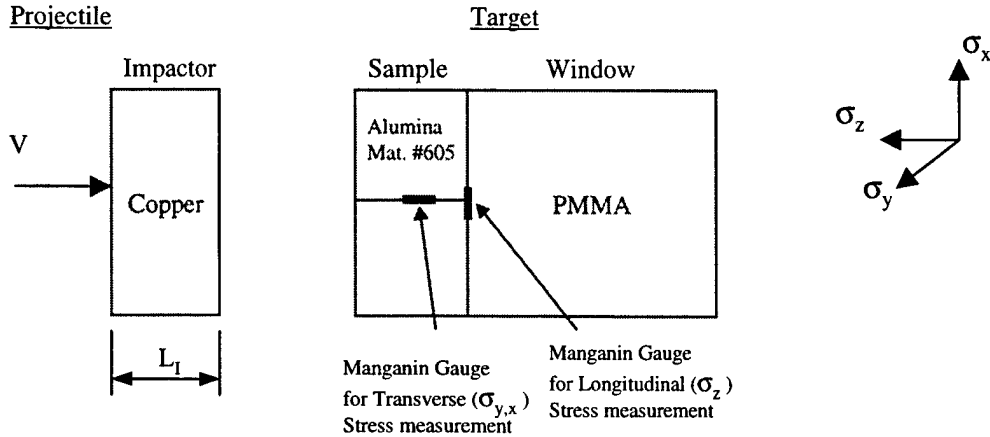
Figure 2.6.4.3 Description of Plate Impact Test Configuration, Rosenberg *et al.* [50]

Table 2.6.4.3   Summary of Experimental Plate Impact Results, Rosenberg *et al.* [50].

Aluminum Oxide (85% pure)									
Test Number	Material Number	Impact Velocity (m/s)	L_I (mm)	Elastic Regime			Plastic Regime		
				σ_z (GPa)	σ_y (GPa)	σ_x (GPa)	σ_z (GPa)	σ_y (GPa)	σ_x (GPa)
6428	605	220	10.0	3.65	0.9	0.9			
6429	605	291	3/3.6	4.9	0.9	0.9			
6429b	605			6.0			6.4	1.4	1.4
6430	605	325	4.0	5.5	1.2	1.2			
6431	605	723	10.0	6.0			9.6	4.2	4.2
6432	605	767	10.0	6.0			9.9	4.3	4.3
6433	605	1045	10.0	6.0			14.2	8.7	8.7

Test 6428-6433: the test data is from work by Rosenberg *et al.* [50]. In-material Manganin gauges were used to determine the stress state of the material in both the longitudinal and transverse directions. The above data was obtained from Tabel I in Reference 50.
Test 6428, 6430: Peak stress below the HEL
Test 6429 used an impactor of copper (3mm)backed by tungsten(3.6mm). The impactor configuration produced a dual level stress pulse. The first stress level is documented under test 6429 (below the HEL)and the second level is under test 6429b(above the HEL).
The documented HEL for this work = 6.0+-0.1 GPa

125
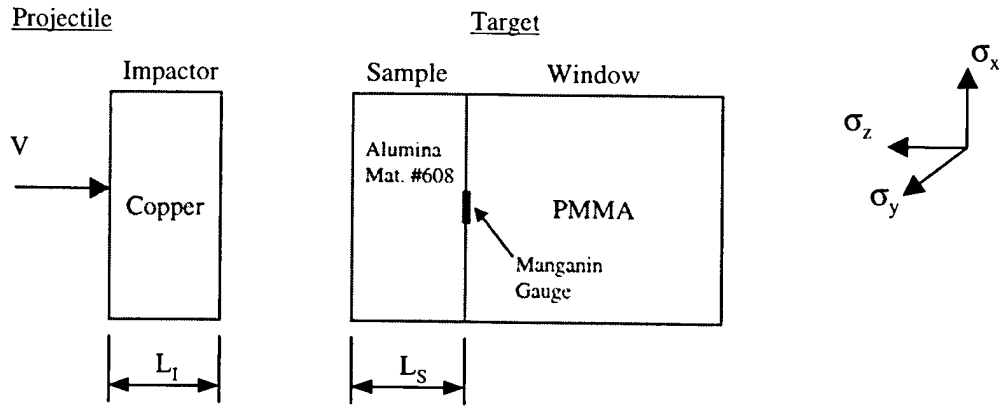
Figure 2.6.4.4 Description of Plate Impact Test Configuration, Rosenberg *et al.* [65]

Table 2.6.4.4 Summary of Experimental Plate Impact Results, Rosenberg *et al.* [65].

Aluminum Oxide (~ 76% purity)					
Test Number	Material Number	Projectile		Target	HEL (GPa)
		V (m/s)	L_I (mm)	L_S (mm)	
6434	608	938	4	5.0	6.27
6435	608	873	4	9.95	4.85
6436	608	859	6	14.1	4.85
Test 6434-6436: In-material Manganin gauges were used to measure the HEL as a function of target thickness. The material was manufactured by Babcock and Wilcox with an initial density = 3700kg/m³.The results of this work demonstrates precurser decay.					
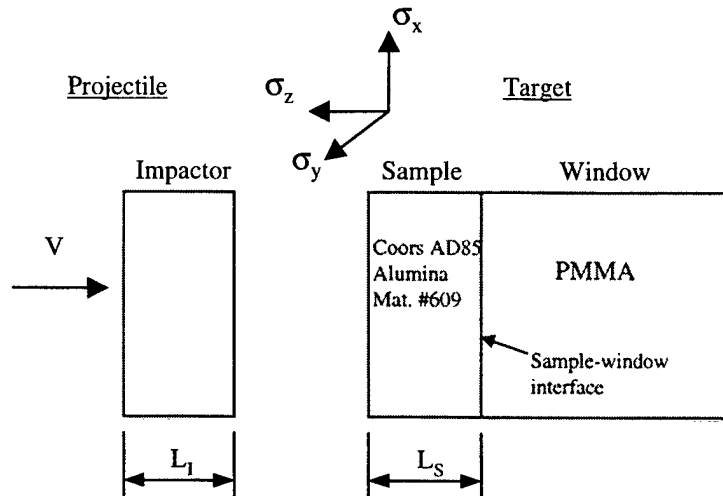
Figure 2.6.4.5 Description of the Plate Impact Test Configuration used to Investigate AD85
Alumina Spall Behavior, Bless *et al.* [73]

Table 2.6.4.5 Summary of Experimental Plate Impact Initial Conditions and Results to Investigate
AD85 Alumina Spall Behavior, Bless *et al.* [73]

Aluminum Oxide (85% pure)						
		Initial Conditions				Results
		Projectile			Target	
Test Number	Material Number	V (m/s)	Material	Thickness L_I (mm)	Sample thickness L_S (mm)	Shock Stress σ_z (GPa)
Test Number	Material Number	V (m/s)	Material	Thickness L_I (mm)	Sample thickness L_S (mm)	Spall Stress σ_{spall} (GPa)
6437	609	119	Aluminum	2.0	6.4	1.2
6438	609	156	Aluminum	2.03	6.4	1.5
6439	609	198	Aluminum	0.9	6.4	2.05
6440	609	203	Aluminum	1.95	6.4	2.05
6441	609	253	Aluminum	1.90	6.45	2.6
6442	609	282	Aluminum	2.03	6.4	2.95
6443	609	293	Aluminum	2.0	6.4	3.1
6444	609	335	Aluminum	2.0	6.4	3.1
6445	609	345	Copper	1.95	6.4	5.6
6446	609	805	Copper	3.0	6.4	10.3

Note: The table above has a final "Spall Stress σ_{spall} (GPa)" column with the following values per test: 6437: 0.275; 6438: 0.33; 6439: 0.275; 6440: 0.32; 6441: ------; 6442: 0.28; 6443: 0.30; 6444: ------; 6445: 0.10; 6446: 0.0

Test 6437-6446: the test data is from work by Bless *et al.* [73]. Material #609 is AD85 alumina manufactured by Coors Ceramic Co., having a initial density = 3421kg/m³. The HEL = 5.9 +- 0.2 GPa for a 6.4mm sample. The HEL decays in thicker samples.
Test 6437, 6444, 6446: Measurements were made using manganin gauges.
Test 6438-6443, 6445: measurements were made using VISAR.

127

2.6.6 Depth-Of-Penetration (DOP) Test Data for Aluminum Oxide (85% pure)

This section presents depth-of-penetration (DOP) experiments using approximately 85% pure Aluminum Oxide. The DOP test has been used to investigate the effectiveness of ceramics for a number of years. The typical DOP configuration consists of a ceramic tile place on, or within, a steel or aluminum base target. A penetrator impacts and perforates the ceramic tile and continues into the base target. The penetration into the base target is generally referred to as the residual penetration, P_r, and is used to determined the ceramic mass efficiency as discussed in Section 2.0.

The target and penetrator descriptions for the DOP experiments by Bless *et al.* [32] are presented in Figure 2.6.6.1. The objective of the experimental program was to investigate ceramic performance as a function of target geometry, penetrator geometry and penetrator velocity. The results are presented graphically in Figure 2.6.6.2 where total penetration is plotted vs. impact velocity for three different penetrator geometry's. The results are summarized in Table 2.6.6.1.

The target and penetrator descriptions for the DOP experiments by Rosenberg and Tsaliah [39] are presented in Figure 2.6.6.3. The objective of the experiments was to investigate ceramic performance as a function of target configuration and impact velocity for two ceramic materials. The results are presented graphically in Figure 2.6.6.4 where the residual penetration is plotted vs. impact velocity for four target configurations. The results are also presented in tabular from in Table 2.6.6.2.

The target and penetrator descriptions for the DOP experiments by Woodward *et al.* [41] are presented in Figures 2.6.6.5. The objective of the experiments was to investigate ceramic performance as a function of ceramic confinement. The results are summarized in Table 2.6.6.3.

The target and penetrator descriptions for the DOP experiments by Yaziv and Partom [66] are presented in Figures 2.6.6.6. The objective of the experiments was to investigate ceramic performance as a function of ceramic thickness and confinement. No information was provided on the material other than defining it as AD85 Alumina manufactured by Coors. The results are summarized in Table 2.6.6.4.

The target and penetrator description for the DOP experiments by Reaugh *et al.* [85] is presented in Figure 2.6.6.7. The objective of the experiments was to investigate ceramic performance as a function of ceramic thickness and impact velocity. The results are summarized in Table 2.6.6.5. Also included in the table are penetration results into the 4340 Steel with no ceramic.
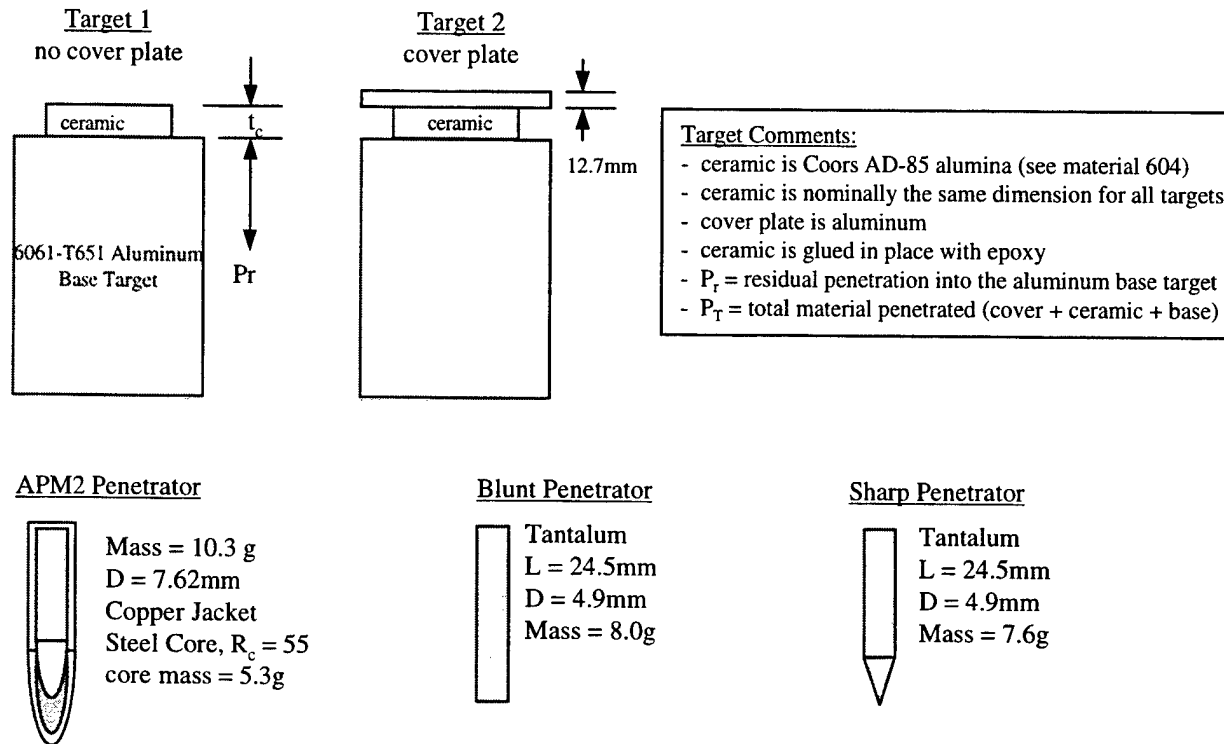
Figure 2.6.6.1 Target and Penetrator Descriptions for DOP Experiments, Bless *et al.* [32].
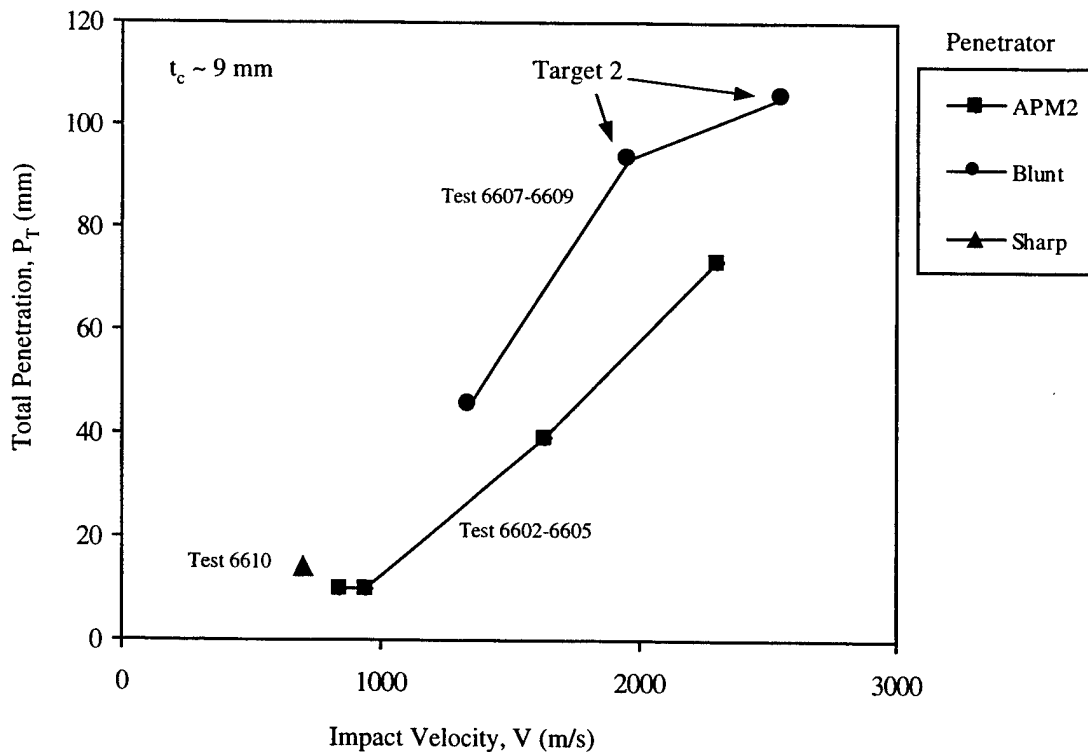
Figure 2.6.6.2 Experimental Results for DOP Tests, Bless *et al.* [32]. Shown here is the total penetration vs. impact velocity for three penetrator configurations and nominally a constant ceramic thickness of 9mm.

Table 2.6.6.1   Tabulated Experimental Results for DOP Tests, Bless *et al.* [32].

Coors AD-85 Alumina							
Test Number	Material Number	Impact Velocity (m/s)	Penetrator	Target Configuration		P_r (mm)	P_T (mm)
				Target	t_c (mm)		
6601	604	780	APM2	1	6.35	1	7.35
6602	604	840	APM2	1	9.14	1	10.14
6603	604	940	APM2	1	9.14	1	10.14
6604	604	1640	APM2	1	9.14	30	39.14
6605	604	2300	APM2	1	9.14	64	73.14
6606	604	610	Blunt	1	6.3	4.8	11.1
6607	604	1350	Blunt	1	9.3	36	45.3
6608	604	1960	Blunt	2	9.3	84*	93.3
6609	604	2550	Blunt	2	9.3	96*	105.3
6610	604	700	Sharp	1	9.19	5.3	14.19

Test 6601-6610: the test data is from work by Bless et al.[32]. The ceramic material used is Coors AD-85. Two target configurations and three different penetrators were used to investigate ceramic performance as a function of impact velocity.
*Test 6608-6609: P_r includes the aluminum cover plate thickness of 12.7mm.
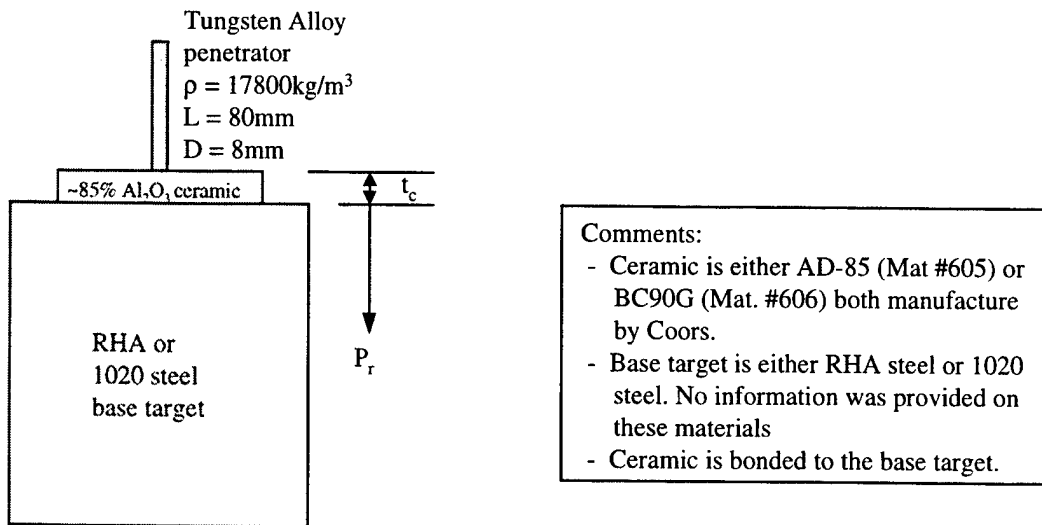
Figure 2.6.6.3 Target and Penetrator Descriptions for DOP Experiments, Rosenberg and Tsaliah [39].
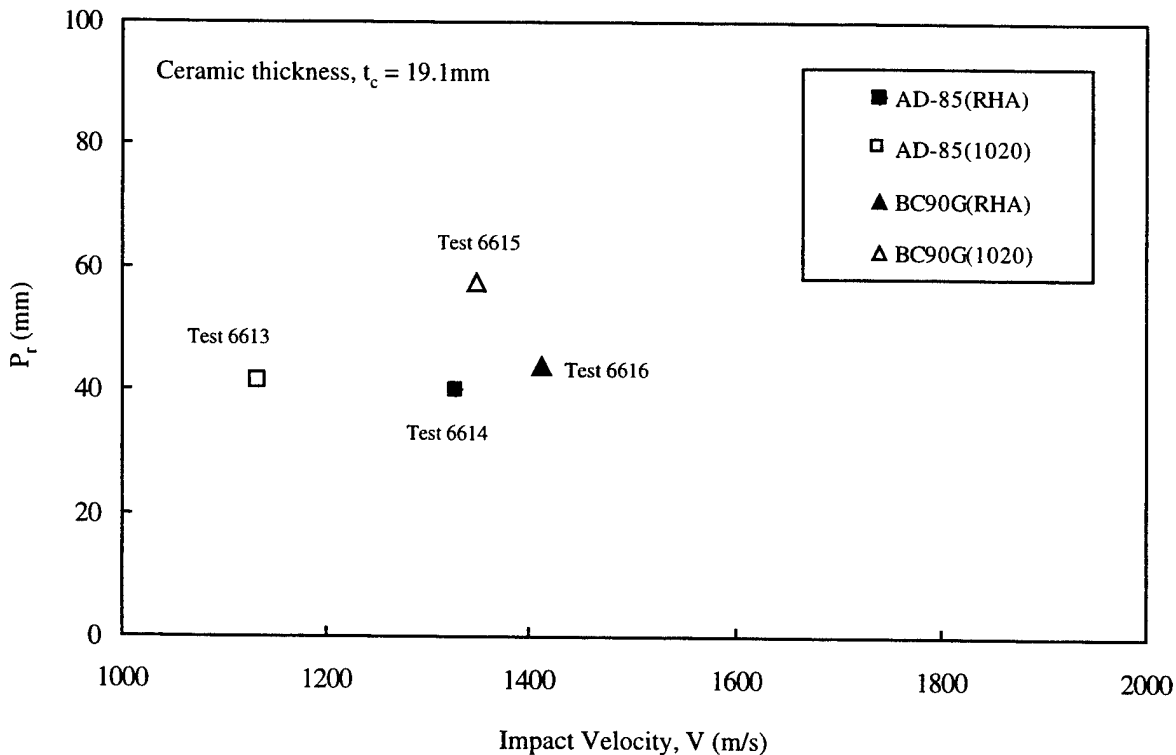
Figure 2.6.6.4 Experimental Results for DOP Tests, Rosenberg and Tsaliah [39]. Shown here is the residual penetration vs. impact velocity for four target configurations and a constant ceramic thickness of 19.1mm.

131

Table 2.6.6.2 Tabulated Experimental Results for DOP Tests, Rosenberg and Tsaliah [39].

~85% Pure Alumina					
Test Number	Material Number	Impact Velocity (m/s)	Target Configuration		P_r (mm)
			t_c (mm)	Base Target	
6611	605	1122	12.7	1020	51
6612	605	1400	12.7	1020	82
6613	605	1135	19.1	1020	41
6614	605	1330	19.1	RHA	40
6615	606	1350	19.1	1020	57.5
6616	606	1412	19.1	RHA	44
Test 6611-6616: the test data is from work by Rosenberg and Tsaliah [39]. The ceramic materials used are AD-85 (Mat. #605) and BC90G (Mat. #606) both manufactured by Coors. Two ceramic thicknesses and two base target materials were used.					
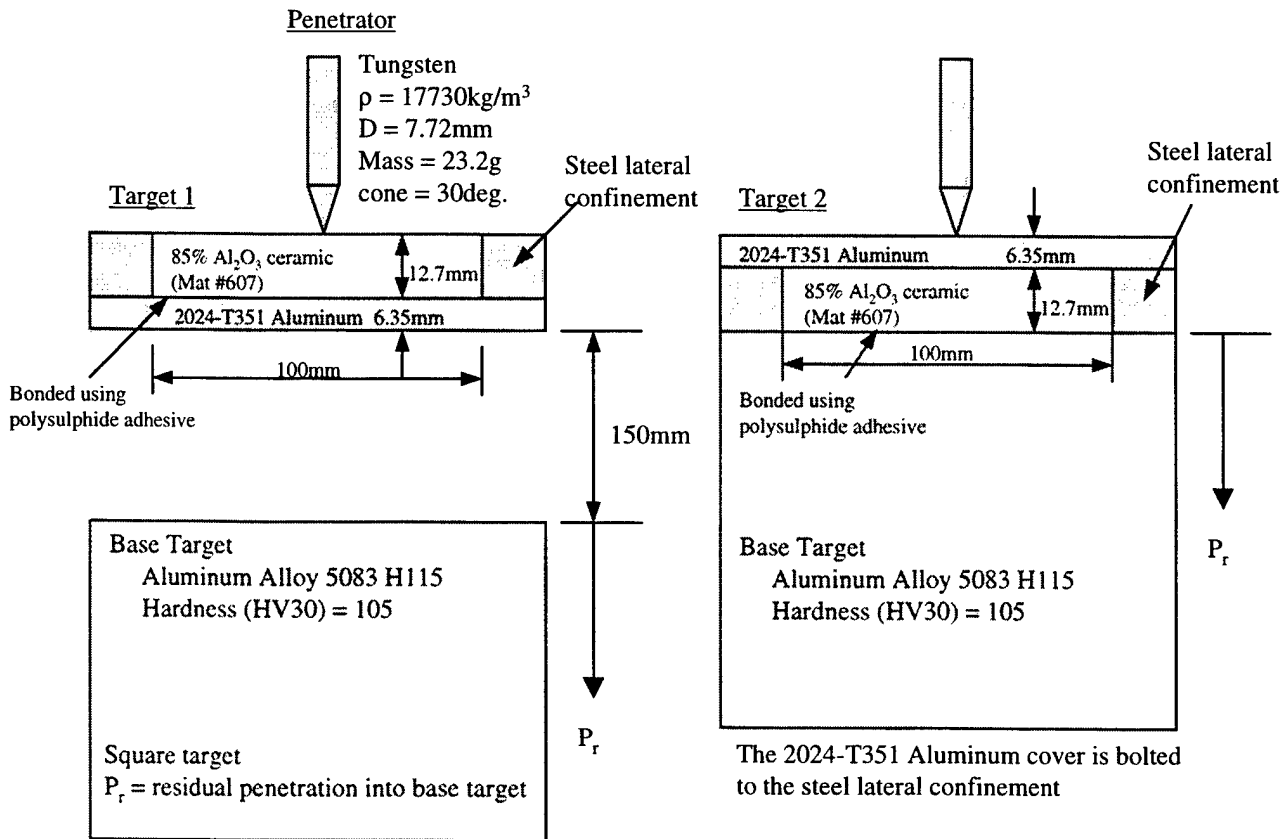
Figure 2.6.6.5 Target and Penetrator Descriptions for DOP Experiments, Woodward *et al.* [41].

Table 2.6.6.3 Tabulated Experimental Results for DOP Tests, Woodward *et al.* [41].

Aluminum Oxide (85% pure)					
Test Number	Material Number	Impact Velocity (m/s)	Target Configuration	P_r (mm)	P* (mm)
6617	607	1209+-15	Target 1	37.1	265
6618	607	1209+-15	Target 2	122.0	265

* This is the semi-infinite penetration into Aluminum.

Test 6617-6618: the test data is from work by Woodward *et al.* [41]. The ceramic material used is 85% Al_2O_3 with an initial density = 3430 kg/m³. One penetrator geometry and two target configurations were investigated.

Test 6617: the penetrator fractured and tumbled on exit from the back-up plate resulting in lower than expected residual penetration.

Configuration 1   Configuration 2

Tungsten Alloy
L/D=20
L=120 or 240mm
D=6 or 12mm

Tungsten Alloy
L/D=20
L=120mm
D=6mm

6.3mm

6.3mm

RHA cover

Coors AD85 Alumina
$\rho = 3420kg/m^3$

t_c

Coors AD85 Alumina
$\rho = 3420kg/m^3$

t_c

L_c

220mm

38mm Steel
Confinement

P_r

P_r

RHA Base Target

RHA Base Target
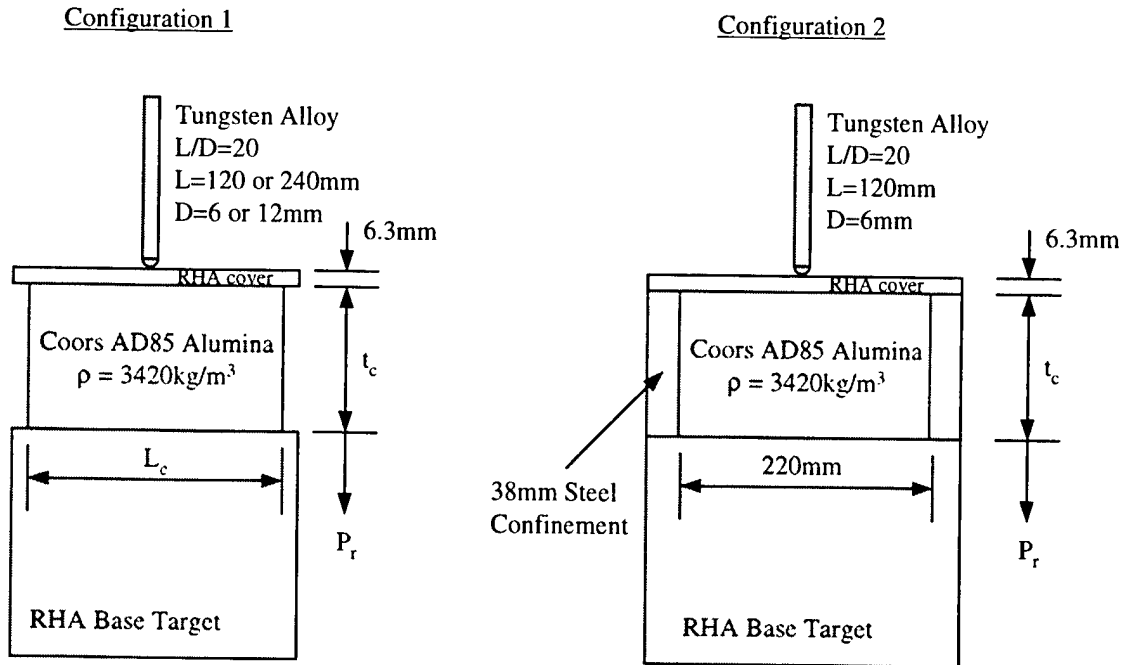
Figure 2.6.6.6 Target and Penetrator Descriptions for DOP Experiments, Yaziv and Partom [66].

Table 2.6.6.4 Tabulated Experimental Results for DOP Tests, Yaziv and Partom [66].

Aluminum Oxide (85% pure)								
Test Number	Material Number	Impact Velocity (m/s)	Penetrator Length (mm)	Target Configuration			P_r (mm)	P_r/L
				Target	t_c (mm)	L_c (mm)		
6619		1346	120	1	12.7	305	48	0.40
6620		1386	120	1	38.1	305	40	0.33
6621		1376	120	1	95.3	305	8.5	0.07
6622		1411	120	2	38.1	220	32	0.26
6623		1359	240	1	25.4	305	122	0.51
6624		1362	240	1	76.2	220	96	0.40
Test 6619-6624: the test data is from work by Yaziv and Partom [66]. The ceramic material used is AD-85 manufactured by Coors with an initial density = 3420kg/m³. No other material information was provided.								

134

Tungsten Sintered Alloy W2 Penetrator

$\rho = 18360 kg/m^3$ $R_c = 28\text{-}31$
L = 25.4mm   UTS = 0.88GPa
D = 6.35mm   Yield = 0.695GPa
L/D = 4   Elongation to fracture = 5.5%

Aluminum Oxide (Mat. #610)

102 mm

t_c

64mm

Ceramic is bonded to the
RHA base target using Stycast 1266

4340 Steel Base Target
$R_c = 33\text{-}37$

P_r = residual penetration into
RHA base target

152mm
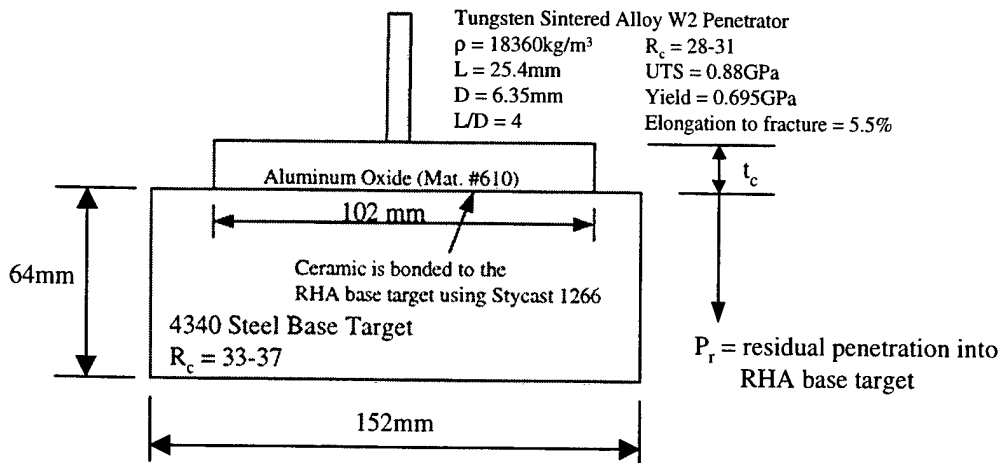
Figure 2.6.6.7 Target and Penetrator Description for DOP Experiment, Reaugh *et al.* [85].

Table 2.6.6.5 Summary of Experimental DOP Results, Reaugh *et al.* [85].

Aluminum Oxide (85% pure)				
Test Number	Material Number	Impact Velocity (m/s)	Ceramic t_c (mm)	P_r (mm)
6625	610	1330	6.2	18.5
6626	610	1350	14.0	11.8
6627	610	1350	22.1	7.5
6628	610	1370	32.0	3.8
6629	610	1750	6.2	31.0
6630	610	1750	14.0	22.0
6631	610	1750	29.9	10.0
6632	610	1770	42.5	2.7
6633	610	2500	20.5	33.6
6634	610	2500	39.3	20.6
6635	610	2500	59.1	2.6
6636		1340	0	27.0
6637		1350	0	27.8
6638		1350	0	28.5
6639		1770	0	36.0
6640		2500	0	43.8
Test 6625-6640: the test data is from work by Reaugh *et al.* [85]. Test 6636-6640: tests into 4340 steel target only (no ceramic used).				

2.6.7 Perforation Test Data for Aluminum Oxide (85% pure)

This subsection presents perforation experiments using approximately 85% pure Aluminum Oxide where the target is usually perforated by the penetrator. Targets are typically comprised of a ceramic front layer and a metallic rear layer and are commonly used in light armor applications. The most common piece of data extracted from perforation experiments is the target ballistic limit, V_{bl}, previously defined in Section 2.0.

The target and penetrator descriptions for the perforation experiments by Wilkins *et al.* [23-28], using a solid ceramic front plate, are presented in Figure 2.6.7.1. The objective of the experiments was to determine the ballistic limit velocity as a function of ceramic front plate thickness and penetrator geometry. The results are presented graphically in Figures 2.6.7.2-4. Figure 2.6.7.2 presents the ballistic limit velocity vs. aluminum rear plate thickness for various front plate thicknesses using the sharp penetrator. Figures 2.6.7.3 and 4 present the ballistic limit velocity as a function of penetrator geometry and rear plate material respectively. The results are summarized in Table 2.6.7.1.

Wilkins also investigated the effect of one and two piece ceramic front plates. Figure 2.6.7.5 presents the target and penetrator descriptions used to investigate this effect. Figure 2.6.7.6 presents the results graphically and shows that one plate is more effective armor than two pieces of total equivalent thickness. The results are also summarized in Table 2.6.7.1.

Target Configuration

Impact location

| Coors AD85 Alumina Front Plate | Δ |
| Aluminum Back Plate | δ |

Bonded using polyurethane
(Scotchcast 221)

Sharp Penetrator

Allegheny Steel 609
$R_c = 54\text{-}56$
M = 8.32g
L ~ 29 mm
D = 7.62 mm
cone angle = 55°

Blunt Penetrator

Allegheny Steel 609
$R_c = 54\text{-}56$
M = 8.32g
L ~ 24 mm
D = 7.62 mm
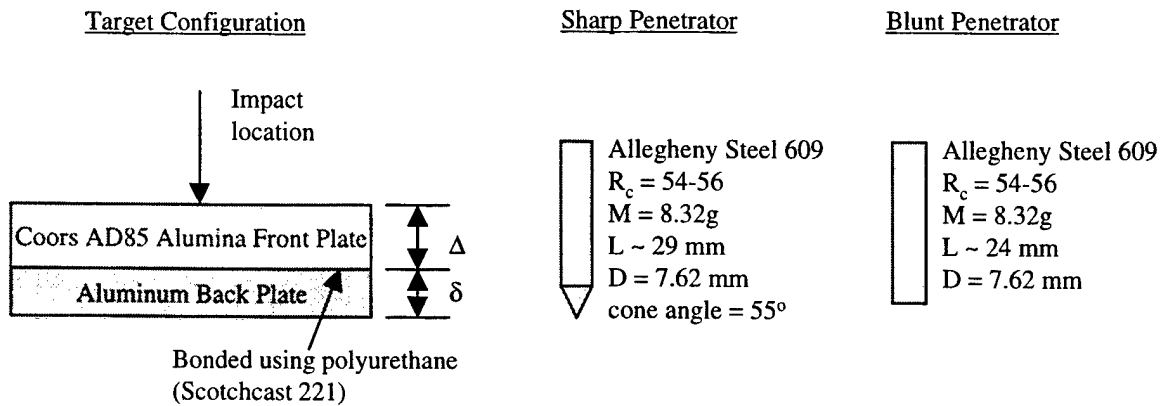
Figure 2.6.7.1 Target and Penetrator Descriptions for Perforation Experiments, Wilkins *et al.* [23-28].
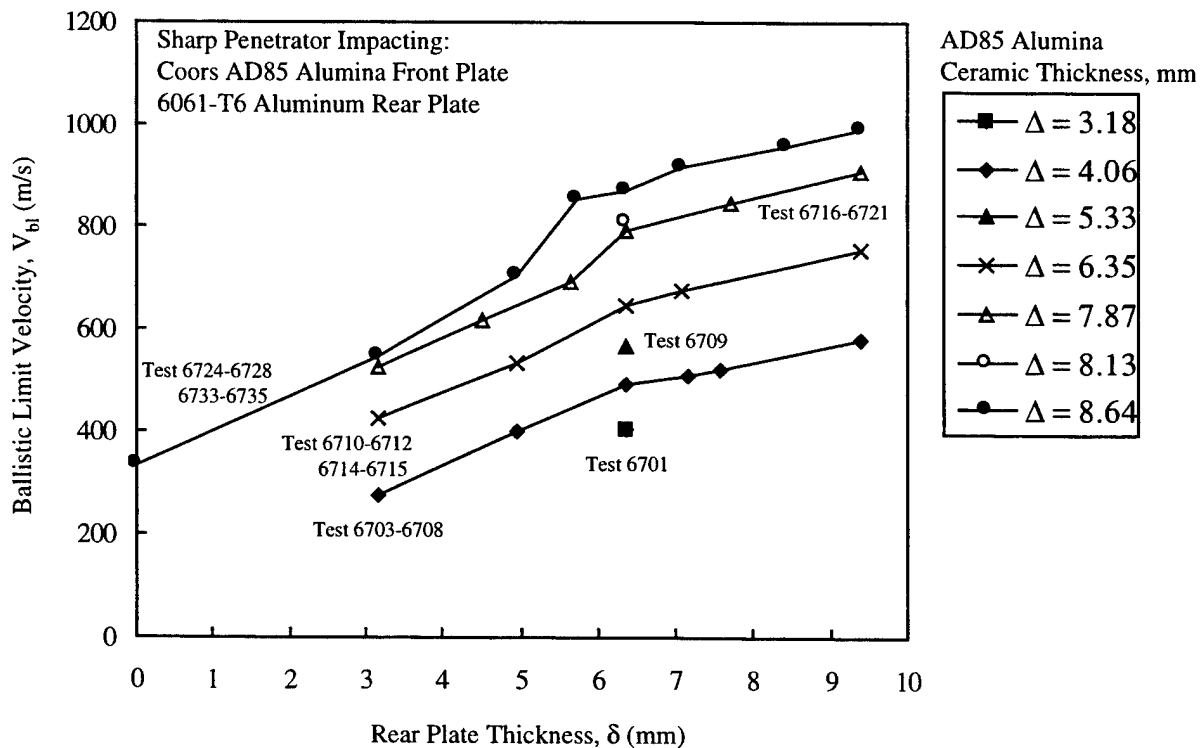
Figure 2.6.7.2   Sharp Penetrator Ballistic Limit Velocity as a function of AD85 Alumina ceramic Thickness and 6061-T6 Aluminum Rear Plate Thickness, Wilkins *et al.* [23-28].

137
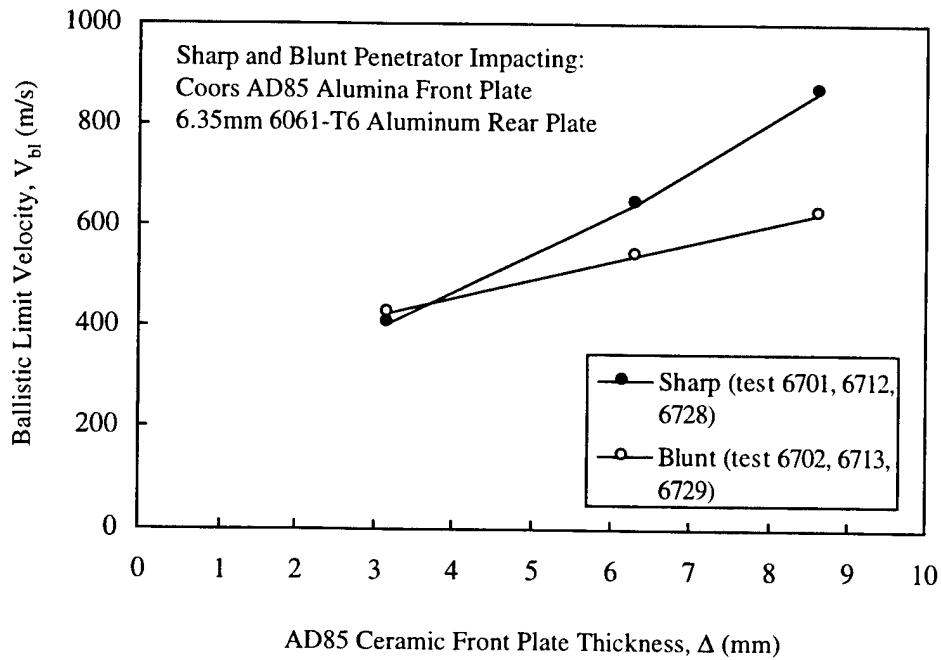
Figure 2.6.7.3 Ballistic Limit Velocity for Sharp and Blunt Projectile as a function of AD85 Alumina Front Plate Thickness. Rear Plate is 6.35mm Thick 6061-T6 Aluminum. Wilkins *et al.* [23-28].
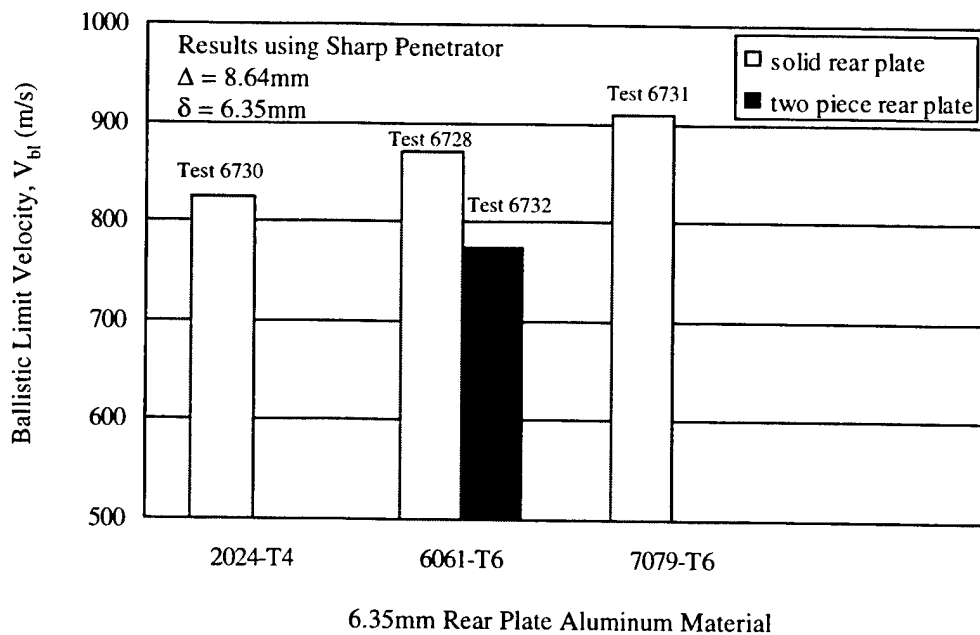
Figure 2.6.7.4 Ballistic Limit Velocity for Sharp Penetrator Impacting 8.64mm AD85 Alumina Backed by 6.35mm of Various Grades of Aluminum. Also shown is a two piece Aluminum Rear Plate (3.175mm each). Wilkins *et al.* [23-28].

Solid Front Plate Target   Two Piece Front Plate Target

Test 6722   Test 6723

Coors AD85 Alumina Front Plate   8.13mm   Coors AD85 Alumina   8.13mm
                                             Coors AD85 Alumina
Aluminum Back Plate   6.35mm   Aluminum Back Plate   6.35mm

Bonded using polyurethane   Bonded using polyurethane
(Scotchcast 221)   (Scotchcast 221)
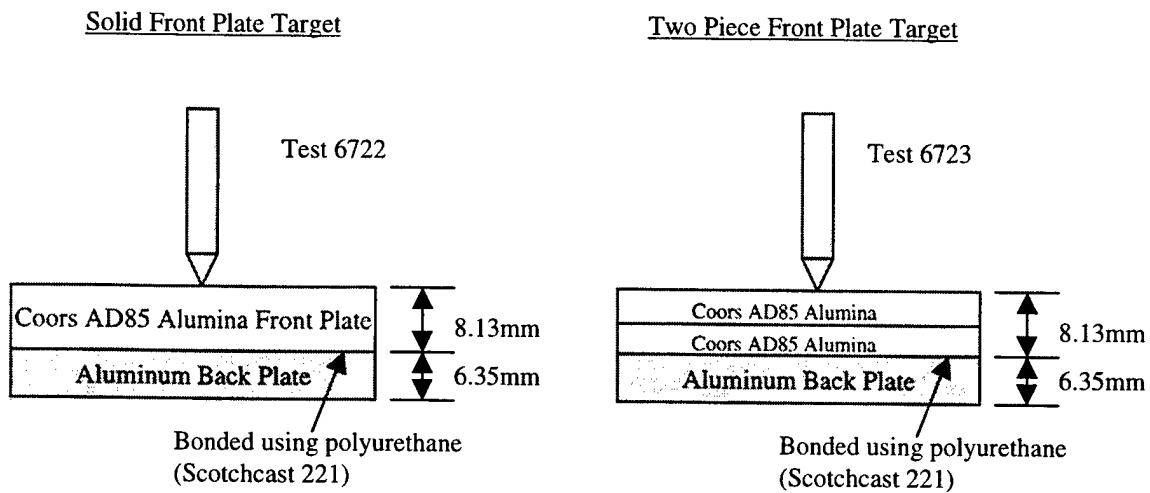
Figure 2.6.7.5   Target and Penetrator Descriptions for Perforation Experiments investigating one and two piece ceramic front plate, Wilkins *et al.* [23-28].
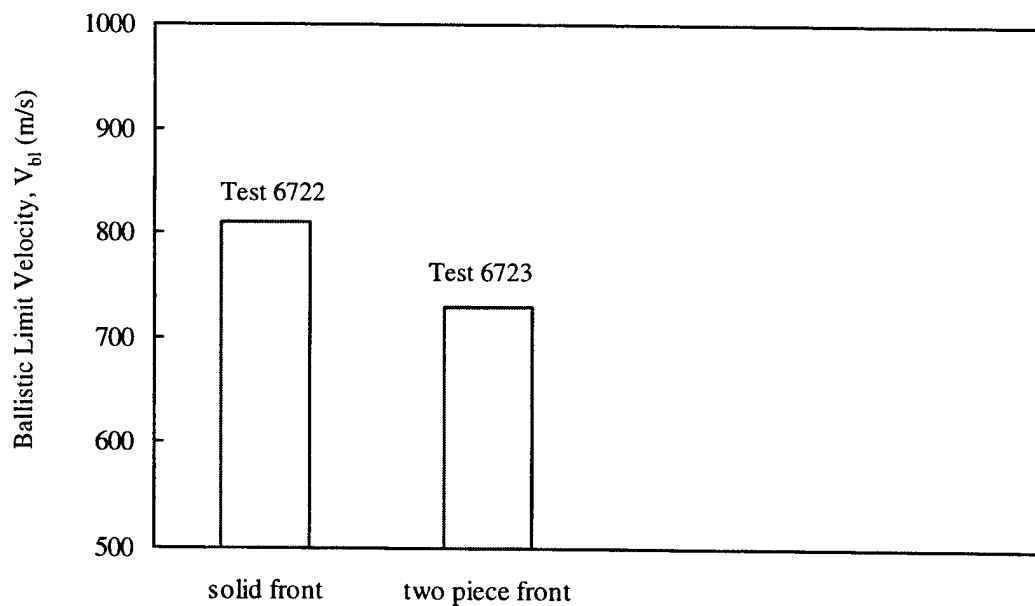
Figure 2.6.7.6 Ballistic Limit Velocity for Sharp Projectile Impacting a Solid Front Plate target and a Two Piece Front Plate Target, Wilkins *et al.* [23-28].

Table 2.6.7.1   Summary of Ballistic Limit Velocities for Two Penetrator types against Various Target Configurations, Wilkins *et al.* [23-28].

Aluminum Oxide (85% pure)						
Test Number	Material Number	Penetrator	Target Configuration			Ballistic Limit Velocity, V_{bl} (+- 15m/s)
			Δ (mm)	δ (mm)	Rear Plate Material	
6701	602	Sharp	3.18	6.35	6061-T6	405
6702	602	Blunt	3.18	6.35	6061-T6	425
6703	602	Sharp	4.06	3.18	6061-T6	275
6704	602	Sharp	4.06	4.95	6061-T6	400
6705	602	Sharp	4.06	6.35	6061-T6	490
6706	602	Sharp	4.06	7.16	6061-T6	510
6707	602	Sharp	4.06	7.57	6061-T6	520
6708	602	Sharp	4.06	9.40	6061-T6	580
6709	602	Sharp	5.33	6.35	6061-T6	565
6710	602	Sharp	6.35	3.18	6061-T6	425
6711	602	Sharp	6.35	4.95	6061-T6	535
6712	602	Sharp	6.35	6.35	6061-T6	645
6713	602	Blunt	6.35	6.35	6061-T6	540
6714	602	Sharp	6.35	7.09	6061-T6	675
6715	602	Sharp	6.35	9.40	6061-T6	755
6716	602	Sharp	7.87	3.18	6061-T6	525
6717	602	Sharp	7.87	4.52	6061-T6	615
6718	602	Sharp	7.87	5.66	6061-T6	690
6719	602	Sharp	7.87	6.35	6061-T6	790
6720	602	Sharp	7.87	7.72	6061-T6	845
6721	602	Sharp	7.87	9.40	6061-T6	910
6722	602	Sharp	8.13	6.35	6061-T6	810
6723	602	Sharp	8.13*	6.35	6061-T6	730
6724	602	Sharp	8.64	0	6061-T6	335
6725	602	Sharp	8.64	3.18	6061-T6	545
6726	602	Sharp	8.64	4.95	6061-T6	705
6727	602	Sharp	8.64	5.74	6061-T6	855
6728	602	Sharp	8.64	6.35	6061-T6	870
6729	602	Blunt	8.64	6.35	6061-T6	625
6730	602	Sharp	8.64	6.35	2024-T4	825
6731	602	Sharp	8.64	6.35	7079-T6	905
6732	602	Sharp	8.64	6.35*	6061-T6	775
6733	602	Sharp	8.64	7.09	6061-T6	915
6734	602	Sharp	8.64	8.43	6061-T6	960
6735	602	Sharp	8.64	9.40	6061-T6	990

Test 6701-6735: the test data is from work by Wilkins *et al.* [23-28]. Two penetrator configurations were used, a sharp and blunt. Target configurations consisted of an AD85 alumina front plate bonded to a aluminum rear plate.The ballistic limit velocity was experimentally determined for each target configuration within a +-15m/s error.
Test 6723: the AD85 alumina front consisted of two 4.06mm alumina plates.
Test 6732: the aluminum rear consisted of two 3.18mm 6061-T6 aluminum plates.

2.7 ALUMINUM OXIDE (high purity)

2.7.1 Material Description for Aluminum Oxide (high purity)

The purpose of this section is to provide as much information as possible on the high purity Aluminum Oxide materials tested. Descriptions for each of the Aluminum Oxide materials used in Section 2.7 are presented in Table 2.7.1.1. Each material is given a material number which is used throughout Section 2.7 to identify it. The data listed in Table 2.7.1.1 were obtained directly from the corresponding reference. When specific information was not available it was left blank. The strength values listed, (Compressive, Tensile, HEL and Spall), are nominal values and are included for comparison purposes. The material defined in the first column (with no material number) is Coors AD-99.5 alumina [74] and is included here for reference. Coors AD-99.5 Aluminum Oxide is the most common material tested. Occasionally researchers will determine the chemical composition of the material being tested, Table 2.7.1.1 includes this data when available.

Table 2.7.1.1 Description of High Purity Aluminum Oxide Materials Tested

		Material Number					
		701	702	703	704	705	706
Reference	74	13	14	26	26	26	29, 30
Manufacturer	Coors		Western Gold	Carborundum	Western Gold	Coors	Western Gold
Trade Name/Description	AD-99.5		AL-995		WESGO 995	AD-99.9	AL-995
Processing		Hot Pressed	Isostat. Pressed	Hot Pressed			
Average Grain Size (μm)	17		20				
Density (kg/m³)	3890	3920	3850	3920	3810	3950	3810
Void Fraction		<0.02					0.040
Longitudinal Velocity (m/s)	10520			10700	10300	10900	10340
Shear Velocity (m/s)	6250			6170	6080	6320	6210
Bulk Velocity (m/s)	7660			7990	7490	8050	7450
Young's Modulus, E (GPa)	372			373	347	392	358
Shear Modulus, G (GPa)	152			149	141	158	147
Bulk Modulus, K (GPa)	228			250	214	256	211
Poisson's Ratio	0.22			0.25	0.23	0.24	0.218
Compressive Strength (GPa)	2.62		3.1	1.3			
Tensile Strength (GPa)	0.26		0.2				
HEL (GPa)				14.0	8.4		8.3
Spall Strength (GPa)							
Purity (%)	99.5	>99					>99.5
Impurities (%wt)							
B							
SiO$_2$							0.4
CaO							0.04
MgO							0.5
Fe$_2$O$_3$							0.1
V$_2$O$_3$							0.01
TiO$_2$							0.015
Na$_2$O							
Ga							

Table 2.7.1.1 Description of High Purity Aluminum Oxide Materials Tested Continued

	Material Number						
	707	708	709	710	711	712	713
Reference	30	31	34, 35	37	40	41	42
Manufacturer	Carborundum	Coors	Ifo Ceramics	Hoechst	Ceramic Oxide	Coors	Coors
Trade Name/Description		AD-99.5(CAP3)		A1898		AD-99.5	AD-99.5
Processing	Hot Pressed		Isostat. Pressed				
Average Grain Size (μm)				6-12			
Density (kg/m³)	3920	3900	3809	3800	3930	3900	3890
Void Fraction	0.008						0.02
Longitudinal Velocity (m/s)	10590		10020	10670			
Shear Velocity (m/s)	6170		5950	6160			
Bulk Velocity (m/s)	7830		7250	7950			
Young's Modulus, E (GPa)	370		330	360		383	
Shear Modulus, G (GPa)	149		135	144			
Bulk Modulus, K (GPa)	240		200	240			
Poisson's Ratio	0.243		0.224	0.24-0.26			
Compressive Strength (GPa)				4.0		2.785	
HEL (GPa)	12.5		8.3	5.3-7.5			
Spall Strength (GPa)							
Purity (%)			99.7		99.5		
Impurities (%wt)							
B	<0.02						
SiO₂	0.6						
CaO	0.03						
MgO	0.3						
Fe₂O₃	0.04						
Na₂O	0.4						
Ga	0.02						

Table 2.7.1.1 Description of High Purity Aluminum Oxide Materials Tested Continued

	Material Number						
	714	715	716	717	718	719	720	721
Reference	48	52	52	65	67	69	70	78
Manufacturer	Coors	Coors	Coors	Babcock/Wilcox	Coors	Hoechst	Coors	*
Trade Name/Description	AD-99.5	AD-99.5	AD-99.9		AD-99.5	A1898	AD-99.5	Hilcox 973
Processing				Sintered	Sintered			
Average Grain Size (μm)						9		1-20
Density (kg/m³)	3880+-3	3890	3948	3900	3895	3790	3892	3810
Void Fraction		0.023	0.006		0.023			
Longitudinal Velocity (m/s)	10560+-30	10560	10850	10520	10700	10440	10591	10820
Shear Velocity (m/s)	6250+-80	6240	6380		6330		6244	6337
Bulk Velocity (m/s)	7710	7720	7970		7780		7758	7970
Young's Modulus, E (GPa)	374	375	398		383	360	375	378
Shear Modulus, G (GPa)	152	152	161		156		152	153
Bulk Modulus, K (GPa)	231	232	251		236		234	242
Poisson's Ratio	0.23	0.232	0.236		0.23		0.2336	0.24
Compressive Strength (GPa)					2.785	4		1.7
Tensile Strength (GPa)					0.262			
HEL (GPa)	6.71	6.2		8.5-10.8			6.16	
Spall Strength (GPa)	0.43-0.46							
Purity (%)	99.5			~99		98		

* Morgan-Matroc

142

Table 2.7.1.1 Description of Aluminum Oxide Materials Tested Concluded

	Material Number								
	722	723							
Reference	86	36							
Manufacturer	Morgan-Matroc	Ceradyne							
Trade Name/Description	Deranox 975								
Processing									
Average Grain Size (μm)									
Density (kg/m³)	3780								
Void Fraction									
Longitudinal Velocity (m/s)									
Shear Velocity (m/s)									
Bulk Velocity (m/s)									
Young's Modulus, E (GPa)	340								
Shear Modulus, G (GPa)									
Bulk Modulus, K (GPa)									
Poisson's Ratio									
Compressive Strength (GPa)									
Tensile Strength (GPa)									
HEL (GPa)									
Spall Strength (GPa)									
Purity (%)		99.5							

2.7.2 Mechanical Test Data for Aluminum Oxide (high purity)

The following section presents mechanical test results, performed by numerous researchers, for various High Purity Aluminum Oxide materials. A typical test specimen showing the stress configuration is shown in Figure 2.7.2.1. Loading is generally uniaxial in the z direction and is increased until the material fails, although some researchers use more complex loading techniques to vary the stress state at failure. Compression is taken as positive and tension as negative.

Mechanical test data performed by Heard and Cline [13] are presented in Table 2.7.2.1. The stress state at failure is given as a function of average strain rate, $\dot{\varepsilon}$. For all the tests a triaxial state of stress was achieved by jacketing the ceramic specimen with a copper or lead jacket. An axial load was applied, σ_z, to the specimen and increased until material failure. The lateral stress, σ_x, σ_y is induced by the jacket and is a function of the axial stress, σ_z. The stress states at failure are summarized in Table 2.7.2.1. All the tests were performed quasi-statically, $\dot{\varepsilon}$ = 10^{-4} s^{-1}.

Mechanical test data performed by Adams and Sines [14] are presented in Table 2.7.2.2 where the stress state at failure is given. For the majority of tests a biaxial state of stress was achieved by applying radial fluid pressure to an axially restrained specimen. The test specimens were typically tubes. Strain rates were not given, but a quasi-static loading rate was implied.

Mechanical test data performed by Wilkins *et al.* [26] are presented in Table 2.7.2.3. The stress state at failure is given as a function of average strain rate, $\dot{\varepsilon}$. All the tests were performed quasi-statically, $\dot{\varepsilon}$ = 10^{-4} s^{-1}. For all but one test a triaxial state of stress was achieved. The specimens were loaded until the material failed and a decrease in axial stress, σ_z, occurred. The stress state, before and after fracture, were measured and are documented in Table 2.2.2.3. The tests documenting the stress state after fracture are identified by an "f" after the test number.

Mechanical test data performed by Meyer and Faber [88] are presented in Table 2.7.2.4. The objective of this work was to determine the strength of fractured ceramic as a function of pressure and strain rate. These tests were performed using "prefactured" ceramic. The prefractured ceramic was obtained from plate impact debris having an average particle size of 2.0 mm. The ceramic particles were placed inside a steel tube providing confinement in the radial and tangential directions, σ_x = σ_y. An axial load, σ_z, was applied until yielding of the steel tube occurred. Different combinations of tube wall thickness and strength were used to vary the confining stress. The stress states listed in Table 2.7.2.4 are the maximum stress states obtained. The bulk density of the ceramic when placed in the tube was approximately 50%. The material was 98% pure, no other information on the Aluminum Oxide material was provided in Reference [88] and thus it was not given a material number.
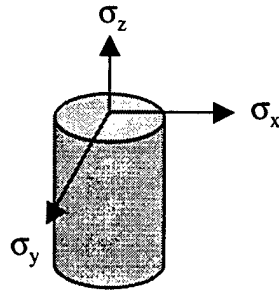
Figure 2.7.2.1 Description of a Typical Mechanical Test Specimen.

Table 2.7.2.1 Summary of Experimental Results, Heard and Cline [13].

Aluminum Oxide (high purity)					
Test Number	Material Number	σ_z (GPa)	σ_x (GPa)	σ_y (GPa)	$\sim \dot{\varepsilon}$ (s^{-1})
7201	701	4.42	0.10	0.10	1.0×10^{-4}
7202	701	5.33	0.10	0.10	1.0×10^{-4}
7203	701	4.84	0.20	0.20	1.0×10^{-4}
7204	701	5.30	0.20	0.20	1.0×10^{-4}
7205	701	6.08	0.20	0.20	1.0×10^{-4}
7206	701	5.53	0.35	0.35	1.0×10^{-4}
7207	701	5.83	0.55	0.55	1.0×10^{-4}
7208	701	6.96	0.83	0.83	1.0×10^{-4}
7209	701	7.04	0.83	0.83	1.0×10^{-4}
7210	701	6.23	0.92	0.92	1.0×10^{-4}
7211	701	7.26	1.10	1.10	1.0×10^{-4}
7212	701	7.17	1.25	1.25	1.0×10^{-4}

Tests 7201-7212: Confining stress (σx, σy) is induced by jacketing the ceramic specimen with a copper or lead jacket. Thus the lateral confining stress (σx, σy) is a function of the axial stress (σz). The stress states documented here are from Ref. 13, Figure 5 and represent the ultimate stress state at failure.

Table 2.7.2.2 Summary of Experimental Results, Adams and Sines [14].

Aluminum Oxide (high purity)					
Test Number	Material Number	σ_z (GPa)	σ_x (GPa)	σ_y (GPa)	$\sim \dot{\varepsilon}$ (s^{-1})
7213	702	-0.22	0	0	6.0x10^{-5}
7214	702	0	0	-0.20	N. A.
7215	702	0	0	-0.18	N. A.
7216	702	0	0	-0.18	N. A.
7217	702	0	0	-0.21	N. A.
7218	702	3.09	0	0	N. A.
7219	702	1.82	0	3.65	N. A.
7220	702	1.81	0	3.61	N. A.
7221	702	1.81	0	3.63	N. A.
7222	702	1.64	0	3.29	N. A.
7223	702	2.02	0	4.03	N. A.
7224	702	1.95	0	3.91	N. A.
7225	702	1.97	0	3.94	N. A.
7226	702	1.95	0	3.90	N. A.
7227	702	0.03	0	3.19	N. A.
7228	702	0.03	0	3.45	N. A.
7229	702	0.04	0	3.50	N. A.
7230	702	0.03	0	3.46	N. A.
7231	702	0.37	0	3.70	N. A.
7232	702	0.37	0	3.66	N. A.
7233	702	0.38	0	3.81	N. A.
7234	702	0.38	0	3.83	N. A.
7235	702	2.92	0	3.70	N. A.
7236	702	2.92	0	3.73	N. A.
7237	702	2.84	0	3.50	N. A.
7238	702	2.91	0	3.63	N. A.

Test 7213: uniaxial tension test.
Test 7214-7217: tension test on cylinders where fluid pressure was applied to the inner diameter untill tensile failure occurred on the outer diameter.
Test 7218: uniaxial compression test.
Test 7219-7234: biaxial stress state on tubes. Fluid pressure is applied to the outer surface along with an axial stress. Failure occurrs on the inner radius of the tube where the radial stress is zero. σ_z = axial stress, σ_x = radial stress σ_y = hoop stress. The strain rate for the tests were not documented

146

Table 2.7.2.3 Summary of Experimental Results, Wilkins *et al.* [26].

Aluminum Oxide (high purity)					
Test Number	Material Number	σ_z (GPa)	σ_x (GPa)	σ_y (GPa)	$\sim \dot{\varepsilon}$ (s^{-1})
7239	703	1.33	0	0	1.0×10^{-4}
7240	703	5.33	0.10	0.10	1.0×10^{-4}
7241	703	4.39	0.10	0.10	1.0×10^{-4}
7242	703	5.27	0.20	0.20	1.0×10^{-4}
7243	703	4.62	0.20	0.20	1.0×10^{-4}
7244	703	6.08	0.20	0.20	1.0×10^{-4}
7245	703	5.51	0.35	0.35	1.0×10^{-4}
7246	703	5.83	0.56	0.56	1.0×10^{-4}
7247	703	7.14	0.83	0.83	1.0×10^{-4}
7248	703	6.97	0.83	0.83	1.0×10^{-4}
7249	703	6.22	0.92	0.92	1.0×10^{-4}
7250	703	7.26	1.10	1.10	1.0×10^{-4}
7251	703	7.15	1.25	1.25	1.0×10^{-4}
7239f	703	0	0	0	1.0×10^{-4}
7240f	703	1.42	0.10	0.10	1.0×10^{-4}
7241f	703	1.10	0.10	0.10	1.0×10^{-4}
7242f	703	1.94	0.20	0.20	1.0×10^{-4}
7243f	703	1.76	0.20	0.20	1.0×10^{-4}
7244f	703	1.34	0.20	0.20	1.0×10^{-4}
7245f	703	3.29	0.35	0.35	1.0×10^{-4}
7246f	703	3.60	0.56	0.56	1.0×10^{-4}
7247f	703	4.37	0.83	0.83	1.0×10^{-4}
7248f	703	4.95	0.83	0.83	1.0×10^{-4}
7249f	703	3.34	0.92	0.92	1.0×10^{-4}
7250f	703	4.98	1.10	1.10	1.0×10^{-4}
7251f	703	3.67	1.25	1.25	1.0×10^{-4}

Test 7239: uniaxial compression test
Test 7240-7251: compressive strength as a function of confining pressure
Test 7239f-7251f: these tests are continuations of test 7239-7251. These results measure the residual ceramic strength after fracture.

Table 2.7.2.4 Summary of Experimental Results, Meyer and Faber[88].

Aluminum Oxide (high purity)						
Test Number	Material Number	σ_z (GPa)	σ_x (GPa)	σ_y (GPa)	$\sim \dot{\varepsilon}$ (s^{-1})	Ref.
7252		0.93	0.11	0.11	5x10^{-4}	88
7253		1.68	0.40	0.40	5x10^{-4}	(Meyer)
7254		2.49	0.59	0.59	5x10^{-4}	
7255		0.96	0.28	0.28	7.7x10^1	
7256		1.77	0.57	0.57	7.7x10^1	
7257		2.88	0.72	0.72	7.7x10^1	

Test 7252-7257: This work was performed by Meyer and Faber [88]. The above data was obtained from Figures 5-6 in Reference [88]. Confinement was provided by steel cylinders of various thickness and strength. Axial loads were applied until the cylinder yielded. The axial stress, σ_z, was measured directly and the lateral stresses, $\sigma_x = \sigma_y$ were obtained using strain gauges. The axial stress, σ_z, listed above is the maximum stress obtained for the corresponding confining stress, $\sigma_x = \sigma_y$. No information was given for the material in Reference [88] and thus was not given a material number.

2.7.3 Hydrostatic Test Data for Aluminum Oxide (high purity)

This section presents the hydrostatic response for High Purity Aluminum Oxide. The experimental data from three researchers [15-17], are summarized in Table 2.7.3.1 and presented graphically in Figure 2.7.3.1. Table 2.7.3.1 presents the pressure, P, the relative volume, V/V_o, and V_o/V -1 where V is the measured volume and V_o is the initial volume. Very little information was provided in Ref. 15-17 on the materials tested, thus the materials were not given a specific material number. All the material information is presented in the comment section directly following the tabulated data for each reference in Table 2.7.3.1.
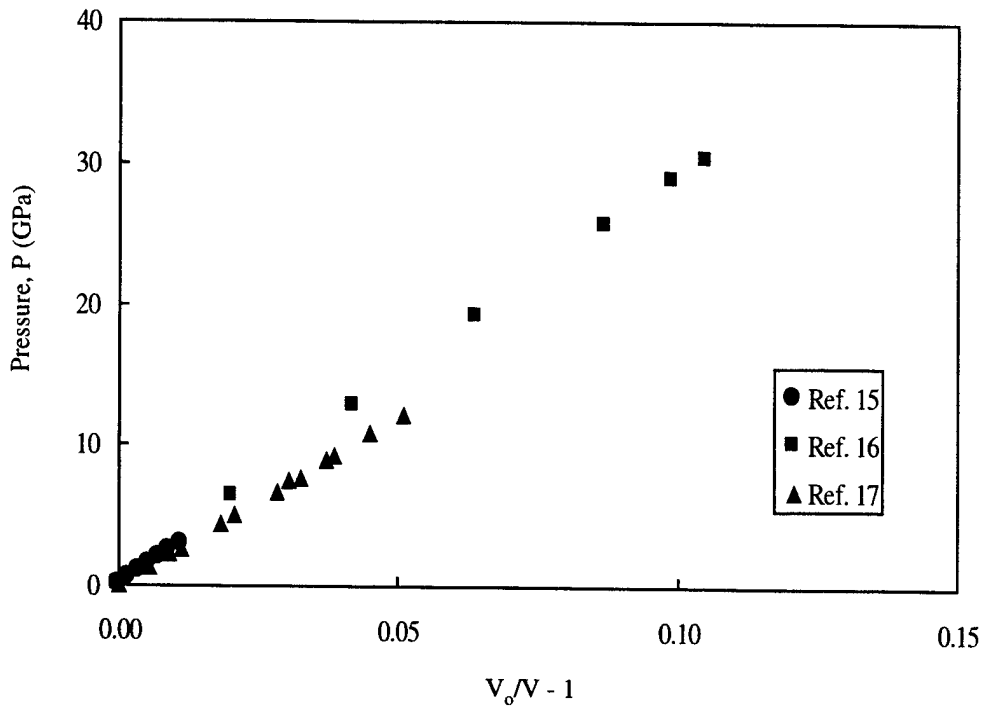

Figure 2.7.3.1 Pressure vs. Volume Relationship for Aluminum Oxide from Ref. 15-17.

Table 2.7.3.1 Summary of Experimental Results Documenting the Hydrostatic Response of Aluminum Oxide

Aluminum Oxide (high purity)					
Test Number	Material Number	P (GPa)	V/V_o	$V_o/V-1$	Ref.
7301		0	1.0	0	15
7302		0.49	0.9982	0.0018	(Bridgman)
7303		0.98	0.9965	0.0035	
7304		1.47	0.9946	0.0054	
7305		1.96	0.9930	0.0070	
7306		2.45	0.9911	0.0090	
7307		2.94	0.9893	0.0108	
Test 7301-7307: this data was obtained using a Lever Piezometer. The Al_2O_3 specimen was from Linde Air Products Co.					
7308		0	1.0	0	16
7309		6.3	0.98	0.020	(Pagannone)
7310		12.8	0.96	0.042	
7311		19.2	0.94	0.064	
7312		25.6	0.92	0.087	
7313		28.8	0.91	0.099	
7314		30.4	0.905	0.105	
Test 7308-7314: this data was obtained using a Lever Piezometer. The Al_2O_3 powder was from the Union Carbide Co.					
7315		0	1.0	0	17
7316		1.24	0.9948	0.0052	(Sato)
7317		2.24	0.9914	0.0087	
7318		2.63	0.9891	0.0110	
7319		4.35	0.9822	0.0181	
7320		5.05	0.9799	0.0205	
7321		6.69	0.9724	0.0284	
7322		7.34	0.9704	0.0305	
7323		7.61	0.9686	0.0324	
7324		8.47	0.9655	0.0357	
7325		8.88	0.9640	0.0373	
7326		9.13	0.9628	0.0386	
7327		10.85	0.9571	0.0448	
7328		12.08	0.9517	0.0508	
Test 7315-7328: this data was obtained using a cubic-anvil high pressure apparatus in conjunction with an x-ray diffraction system. A 4:1 solution of methanol to ethanol was used as the pressure medium. The $\alpha-Al_2O_3$ sample was a commercial reagent-grade powder.					

2.7.4 Plate Impact Test Data for Aluminum Oxide (high purity)

This section presents plate impact results, performed by numerous researchers, using various High Purity Aluminum Oxide materials. A typical plate impact test configuration is presented in Figure 2.7.4.1. The peak stress, σ_z, occurs in the z-direction and is generally measured for both the elastic and plastic response. The lateral stresses, σ_x and σ_y, occur due to the uniaxial strain configuration of the experiment, and are typically not measured. The peak stress for the elastic regime is referred to as the Hugoniot Elastic Limit (HEL) and has become a fundamental property of ceramics. The peak stress for the plastic response is generally referred to as the peak Hugoniot stress. The particle velocity and wave velocity for both the elastic and plastic waves are typically measured and documented herein. In some cases the entire particle velocity time history is measured using laser velocity interferometry techniques (VISAR). VISAR traces provide direct information on the material response and are included in this section when available.

The results from Wilkin's [25] are summarized in Table 2.7.4.1. Two materials were investigated. The peak stress, σ_z, and density, ρ, for both the elastic and plastic response are presented.

The results from Ahrens [29] and Gust and Royce [30] are presented in Table 2.7.4.2. The shock velocity, particle velocity, peak stress, σ_z, and density, ρ, for both the elastic and plastic response are presented.

A description of the plate impact test configuration used by Dandekar and Bartkowski [48] is presented in Figure 2.7.4.2. The objective of this work was to obtain information about the compressive, release, and spall strength of AD995 alumina complimenting the shock wave experiments conducted by Grady and Moody [52]. The shock velocity, particle velocity, peak stress, σ_z, and density, ρ, for both the elastic and plastic response are summarized in Table 2.7.4.3. Selected particle velocity time histories of the sample-window interface are presented in Figure 2.7.4.3.

A description of the plate impact test configuration used by Grady and Moody [52] is presented in Figure 2.7.4.4. The specific test dimensions and some limited results are summarized in Table 2.7.4.4. Compression and release behavior was measured by monitoring the ceramic-window interface velocity using laser velocity interferometry techniques (VISAR). The interface velocity profiles reflect the uniaxial strain loading and unloading behavior of the material and are presented in Figures 2.7.4.5-7.

A description of the plate impact test configuration used by Rosenberg et al. [65] is presented in Figure 2.7.4.8. The objective of the experimental program was to use in-material Manganin gauges to measure the HEL as a function of target thickness. The results are summarized in Table 2.7.4.5.

σ_x

V → Impactor
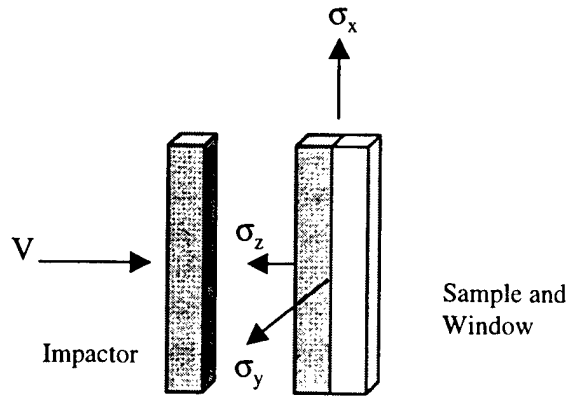
σ_z

σ_y

Sample and Window

Figure 2.7.4.1 Description of a Typical Plate Impact Test Configuration including Stress Orientations

Table 2.7.4.1 Summary of Experimental Plate Impact Results by Wilkins[25].

Aluminum Oxide (high purity)										
Test Number	Material Number	Initial Density ρ_o (kg/m³)	Elastic Regime (HEL)				Plastic Regime				Ref.
			Shock Velocity (m/s)	Particle Velocity (m/s)	σ_z (GPa)	ρ (kg/m³)	Shock Velocity (m/s)	Particle Velocity (m/s)	σ_z (GPa)	ρ (kg/m³)	
7401	703	3920			13.2	4045			21.1	4134	25
7402	703	3920			13.6	4041			22.9	4167	(Wilkins)
7403	703	3920			14.6	4050			30.4	4288	
7404	704	3810			6.8	3877			9.2	3928	
7405	704	3810			7.8	3880			11.4	3940	
7406	704	3810			8.0	3890			27.5	4260	
7407	704	3810			8.4	3885			28.4	4274	
7408	704	3810			8.6	3897			42.6	4458	
7409	704	3810							43.4	4454	

Test 7401-7403: the test data is from work by Wilkins [25]. The material is a hot pressed alumina. The data were obtained from Figure A5 in Reference 25. The HEL data does not necessarily correspond to the associated peak hugoniot stress shown here.

Test 7404-7409: the test data is from work by Wilkins [25]. The data were obtained from Figure A6 in Reference 25. The HEL data does not necessarily correspond to the associated peak Hugoniot stress shown here.

Table 2.7.4.2 Summary of Experimental Plate Impact Results by Ahrens [29] and Gust and Royce [30].

Aluminum Oxide (high purity)											
Test Number	Material Number	Initial Density ρ_o (kg/m³)	Elastic Regime (HEL)				Plastic Regime				Ref.
			Shock Velocity (m/s)	Particle# Velocity (m/s)	σ_z (GPa)	ρ (kg/m³)	Shock Velocity (m/s)	Particle* Velocity (m/s)	σ_z (GPa)	ρ (kg/m³)	
7410	706	3814	10070	260	10.0	3915	6750	290	10.8	3932	29 (Ahrens)
7411	706	3810	10380	210	8.4	3888	7830	310	11.4	3939	
7412	706	3814	10320	200	7.9	3888	7260	870	26.9	4282	
7413	706	3809	9820	180	6.7	3879	7540	850	26.2	4260	
7414	706	3810	10070	220	8.5	3896	8620	1280	43.4	4453	
7415	706	3809	10050	210	8.1	3891	8590	1260	42.6	4443	
7416	706	3808						1960	73.6	4748	
7417	706	3837					11030	2677	112.1	5066	
7418	706	3839					10900	2687	113.1	5094	

Test 7410-7418: the test data is from work by Ahrens [29]. The material is AL-995 manufactured by Western Gold Co.
Test 7416: elastic regime not measured
Test 7417-7418: elastic regime overdriven.
#, * particle velocity obtained assuming $U_p = 1/2U_{fs}$.

7419	707	3919	10720	371	15.6	4060	9470	590	23.8	4164	30 (Gust)
7420	707	3910	10730	473	19.8	4091	8410	610	24.3	4164	
7421	707	3919	10690	316	13.2	4040	9160	600	23.0	4175	
7422	707	3918	10630	341	14.2	4049	9310	565	21.7	4151	
7423	707	3909	10570	278	11.5	4014	9120	605	23.1	4169	
7424	707	3909	10570	264	10.9	4010	9120	600	23.0	4170	
7425	707	3910	10750	209	8.8	3989	9560	580	22.7	4155	
7426	707	3910	10530	232	9.5	3998	9290	580	22.1	4159	
7427	707	3912	10430	416	16.9	4075	9110	780	29.9	4254	
7428	707	3912	10490	383	15.7	4060	8980	780	29.7	4258	
7429	707	3920	10630	293	12.2	4024	8480	770	27.9	4274	
7430	707	3918	10640	323	13.4	4040	8800	805	30.2	4280	
7431	707	3913	10640	251	10.5	4008	9570	1170	44.9	4446	
7432	707	3913	10440	260	10.6	4013	9770	1260	48.7	4483	
7433	707	3913	10660	308	12.8	4031	9720	1300	50.2	4487	
7434	707	3912					10440	1800	73.7	4728	
7435	707	3914					10940	2190	94.1	4889	
7436	707	3915					11260	2310	101.9	4927	

Test 7419-7436: the test data is from work by Gust and Royce [30]. The material is hot pressed alumina manufactured by Carborundum.
Test 7434-7436: elastic regime overdriven
elastic particle velocity obtained using $U_p = 1/2U_{fs}$
* plastic particle velocity obtained using $U_p = 1/2U_{fs}$ and by impedance matching. The particle velocity listed here is the average of the two.
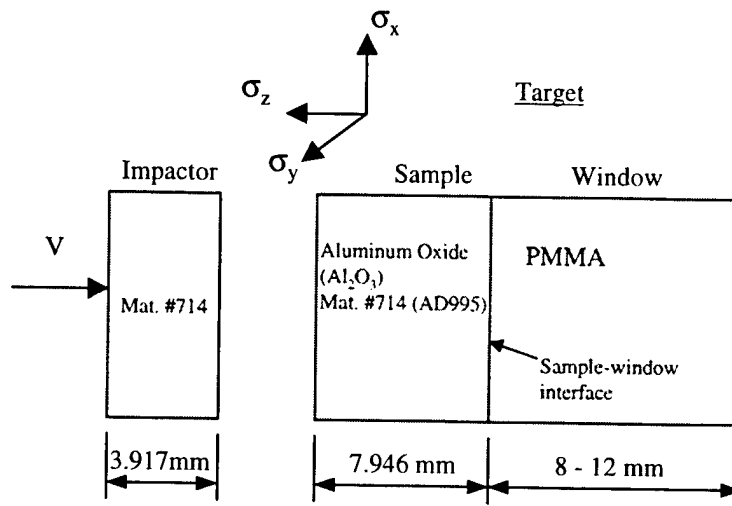
Figure 2.7.4.2 Description of Dandekar and Bartkowski [48] Plate Impact Test Configuration.

Table 2.7.4.3 Summary of Experimental Plate Impact Results by Dandekar and Bartkowski [48].

Aluminum Oxide (high purity)											
Test Number	Material Number	Impact Velocity V, (m/s)	Elastic Regime (HEL)				Plastic Regime				Spall
			Shock Velocity (m/s)	Particle Velocity (m/s)	σ_z (GPa)	ρ (kg/m^3)	Shock Velocity (m/s)	Particle Velocity (m/s)	σ_z (GPa)	ρ (kg/m^3)	σ_{spall} (GPa)
7437	714	83		41.5	1.699	3897					0.431
7438	714	349		152.8	6.263	3939		174.5	7.03		0.511
7439	714	433		161.6	6.623	3942	7450	216.5	8.2	3972	0.459
7440	714	251		125.5	5.134	3923					0.447
7441	714	512		166.5	6.825	3944	8350	256	9.71	3987	0
7442	714	604		164.9	6.758	3944	8520	302	11.28	4010	0
7443	714	175		87.5	3.587	3914					0.427
7444	714	193		96.5	3.956	3918					0.497
7445	714	597		158.3	6.488	3941	7850	298.6	10.74	4014	0
7446	714	182		91.0	3.73	3916					0.641
7447	714	465		158.3	6.488	3941	7810	232.7	8.73	3980	0

Test 7437-7447: the test data is from work by Dandekar. The material is Coors AD995 with an initial density 3880kg/m3.
The HEL = 6.71 +- .08 GPa
Spall Strength of the material varies between 0.43 and 0.46GPa when shock compressed to 8.3GPa. The Spall strength becomes negligibly small when shocked above 8.8GPa.
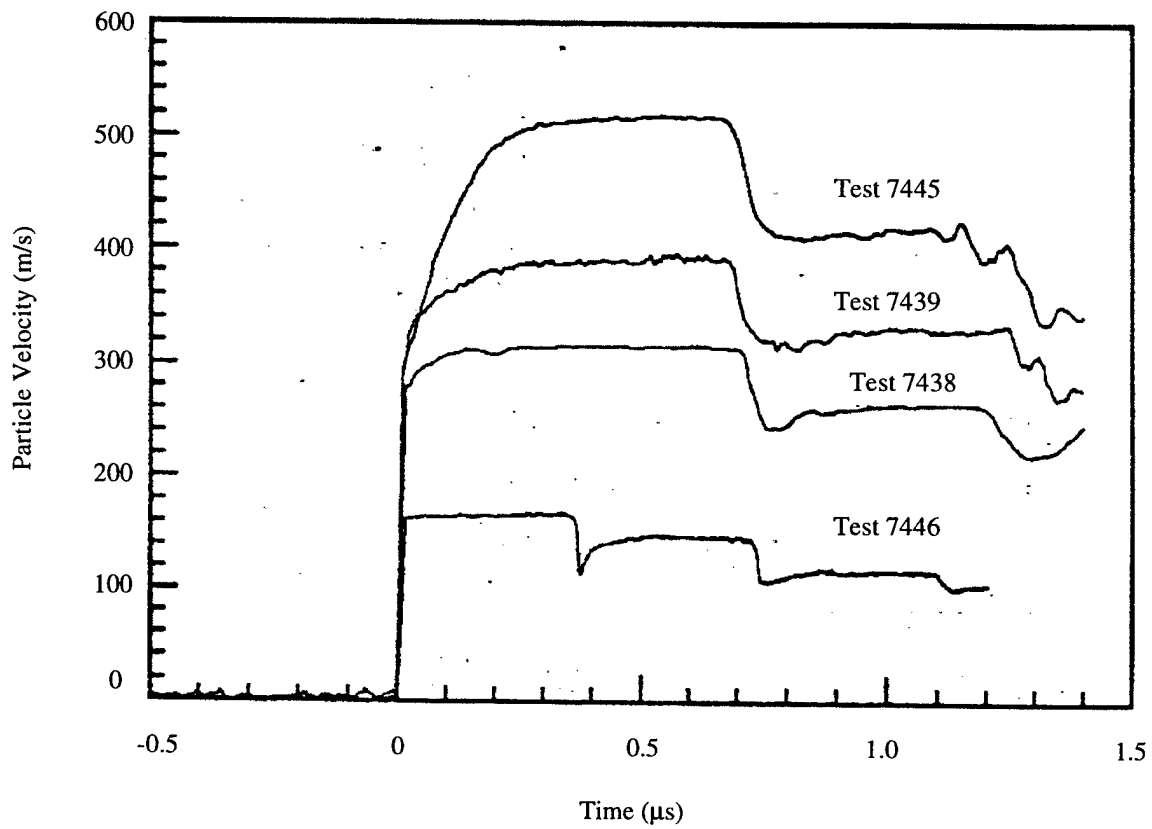
Figure 2.7.4.3 Particle Velocity Time Histories for Selected Plate Impact Experiments, Dandekar and Bartowski [48].
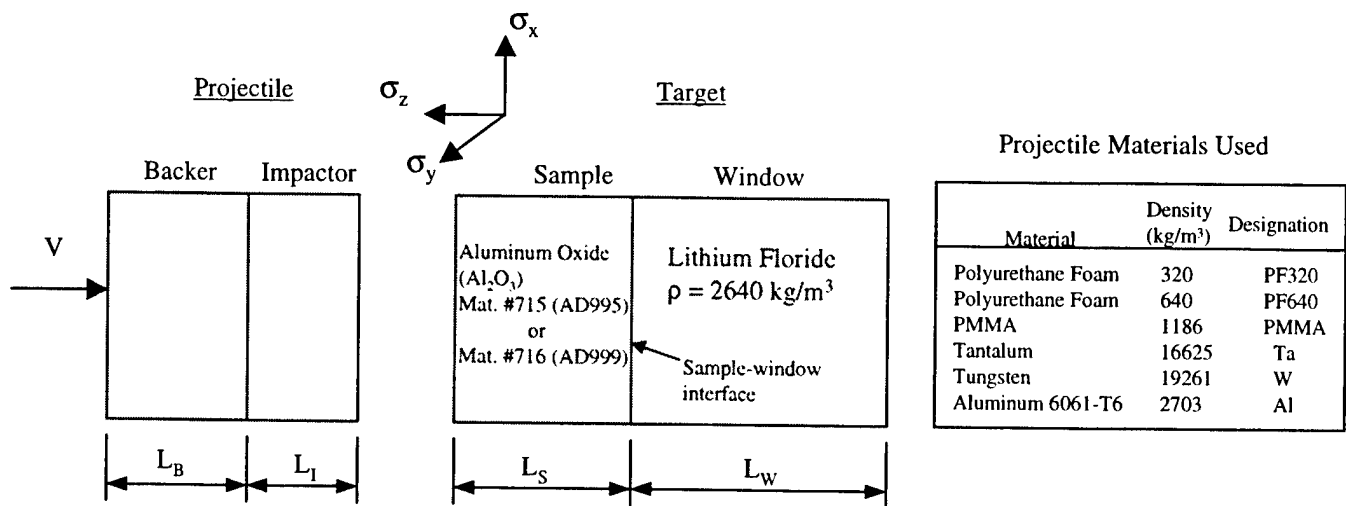
Projectile σ_z σ_x Target

σ_y

Backer   Impactor   Sample   Window

V

Aluminum Oxide (Al₂O₃) Mat. #715 (AD995) or Mat. #716 (AD999)

Lithium Floride $\rho = 2640\ kg/m^3$

Sample-window interface

L_B L_I L_S L_W

Projectile Materials Used

Material	Density (kg/m³)	Designation
Polyurethane Foam	320	PF320
Polyurethane Foam	640	PF640
PMMA	1186	PMMA
Tantalum	16625	Ta
Tungsten	19261	W
Aluminum 6061-T6	2703	Al

Figure 2.7.4.4 Description of Grady and Moody [52] Plate Impact Test Configuration.

Table 2.7.4.4 Summary of Experimental Plate Impact Results by Grady and Moody [52].

Test Number	Material Number	Projectile						Target			Hugoniot State (Plastic Compression)			
		V (m/s)	Backer Material	L_B (mm)	Impactor Material	Density (kg/m³)	L_I (mm)	Sample Density (kg/m³)	L_S (mm)	Window L_W (mm)	U_S (m/s)	U_P (m/s)	σ_z (GPa)	ρ (kg/m³)
7448	715	544	PF320	8.0	Al₂O₃	3888	5.008	3890	10.007	25.4				
7449	715	1070	PF320	8.0	Al₂O₃	3890	5.019	3890	10.006	25.4	8540	535	19.1	4132
7450	715	1573	PF320	8.0	Al₂O₃	3890	5.008	3890	10.008	25.4	8290	786	27.6	4274
7451	715	1943	PF320	8.0	Al₂O₃	3890	5.013	3890	10.007	25.4	8560	972	34.1	4367
7452	715	2329	PF640	8.0	Al₂O₃	3890	5.005	3890	9.998	25.4	8800	1165	41.7	4464
7453	715	561	PF320	8.0	Al₂O₃	3890	4.989	3890	9.987	25.4	9180	281	11.0	4000
7454	715	2241	PF640	5.0	Ta	16625	1.555	3890	5.008	25.5				
7455	715	2260	PMMA	6.34	W	19261	1.501	3890	5.008	25.6				
7456	715	1564	PF320	8.0	Al₂O₃	3890	2.475	3890	4.762	25.4				
7457	715	1551	PF320	8.0	Al₂O₃	3890	2.477	3890	2.478	25.4				
7458	715	549	PMMA	6.37	Al	2688	1.493	3890	4.698	25.3				
7459	716	2033	PMMA	2.0	Ta	16561	1.497	3948	9.909	25.6				
7460	716	2183	PMMA	2.0	W	19274	1.414	3948	10.009	25.4				
7461	716	1290	PF320	12.7	Al₂O₃	3948	5.118	3948	10.026	25.6				
7462	716	1911	PF320	12.7	Al₂O₃	3948	5.059	3948	10.019	25.4				

Alumina Oxide (high purity)

Test 7448-7462: the test data is from work by Grady and Moody [52]. Two high purity alumina materials were investigated. AD99.5 (Mat. #715), having a nominal initial density = 3890kg/m³ and AD99.9 (Mat. #716), having a nominal initial density = 3948kg/m³, both materials were manufactured by Coors Co. The above table primarily provides the initial conditions for the plate impact experiments, although the Hugoniot state is provided when available. The documented HEL for AD99.5 (Mat. #715) is 6.2 +-0.4 GPa (Ref. 54)

Test 7449-7453: the Hugoniot stress state including the shock velocity (U_S) and partilce velocity (U_P) are from Ref. 54.
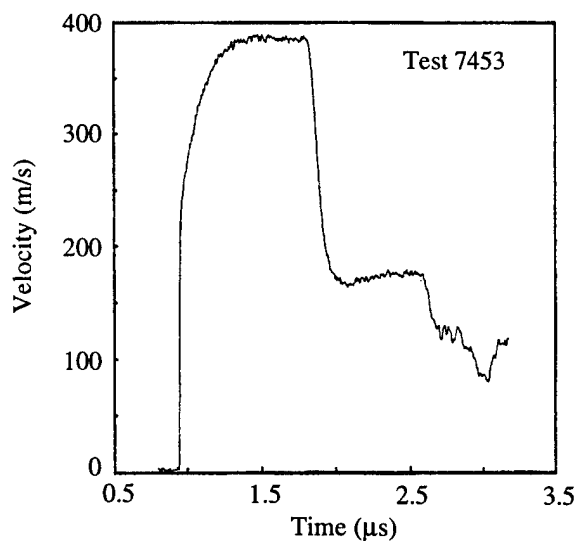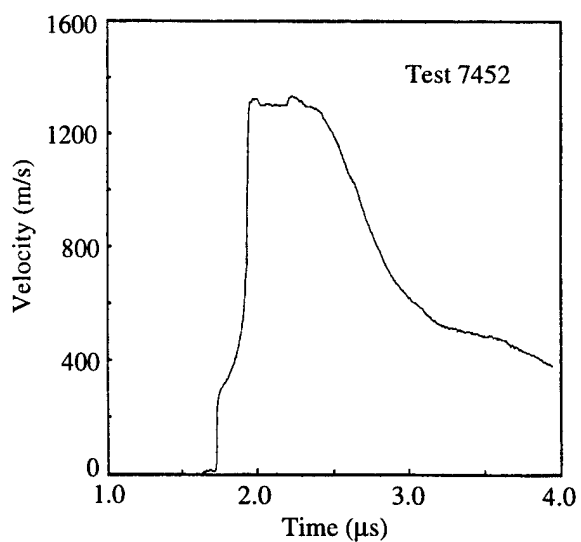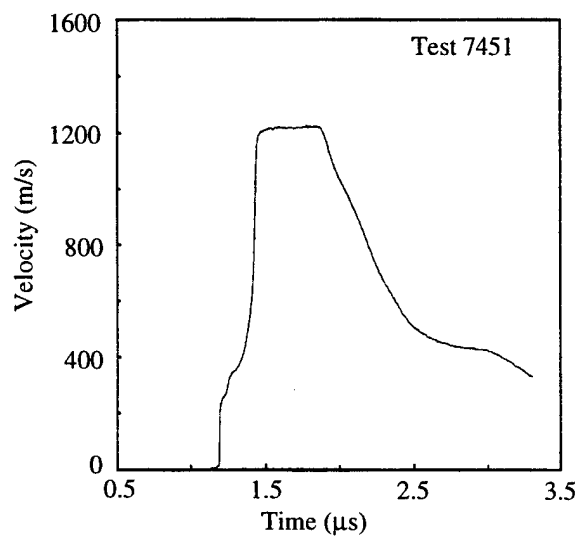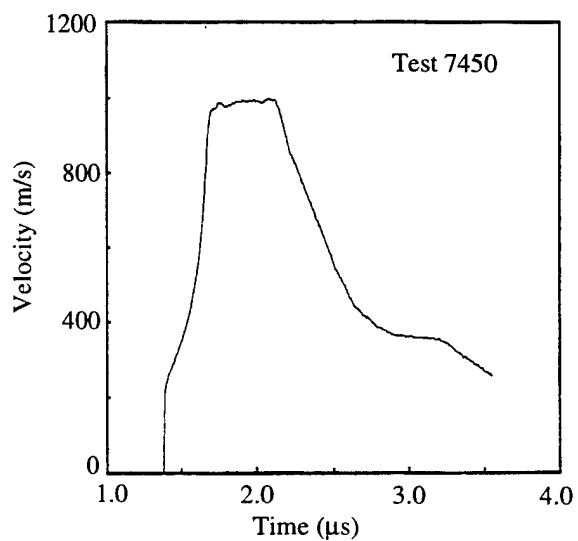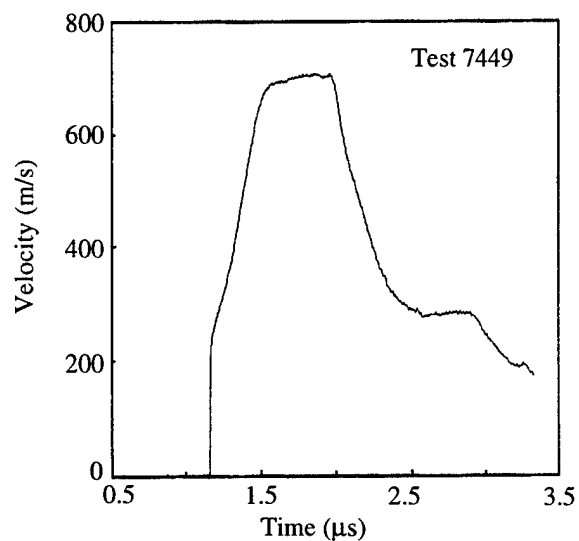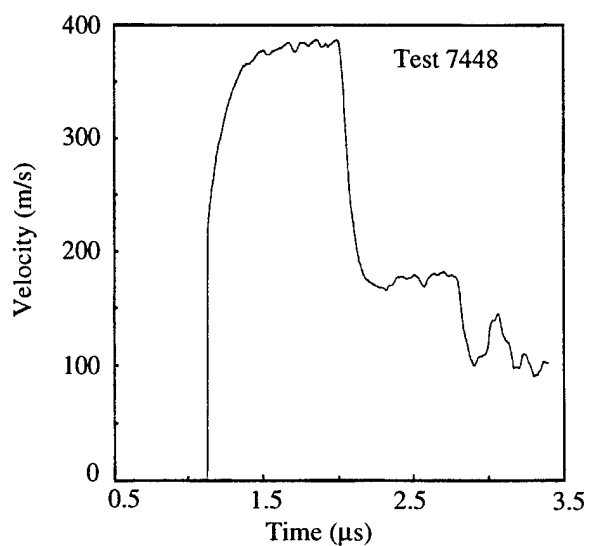
Figure 2.7.4.5 Ceramic-Window Interface Velocity Profiles from Grady and Moody [52] for Tests 7448-7453.

157
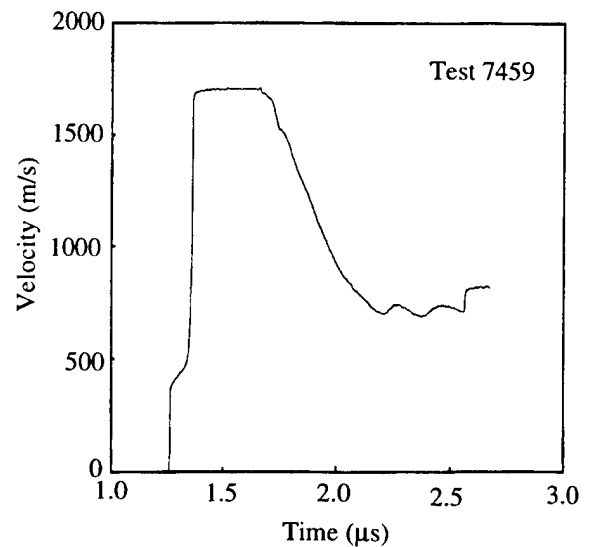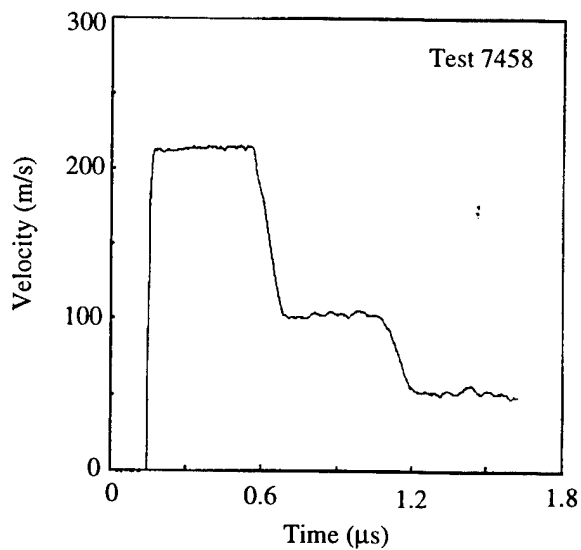
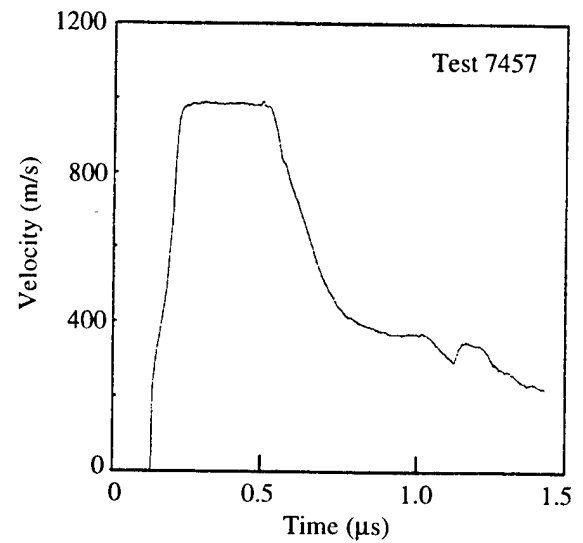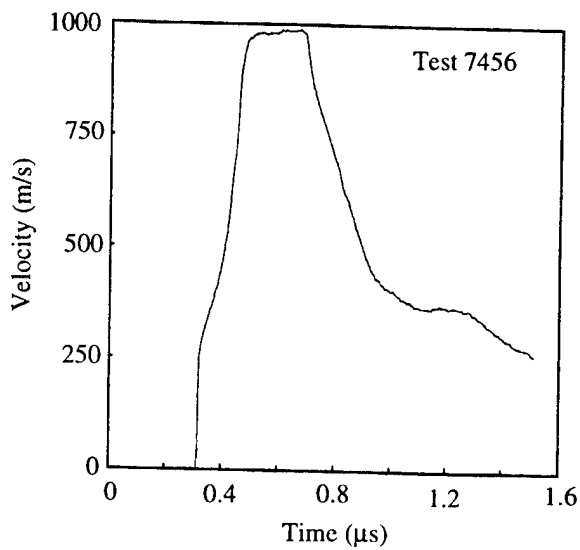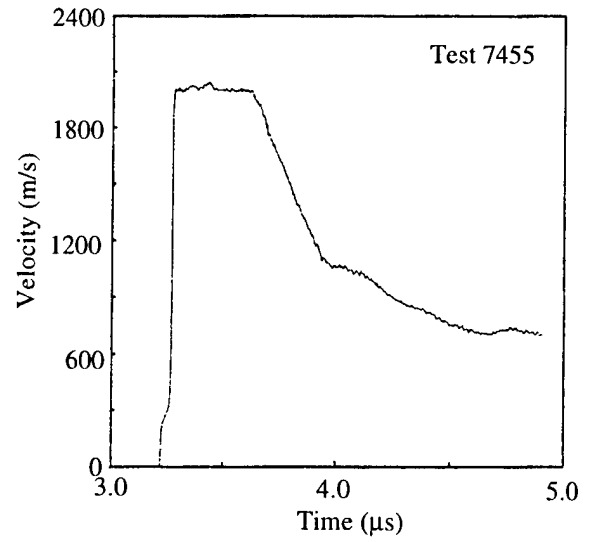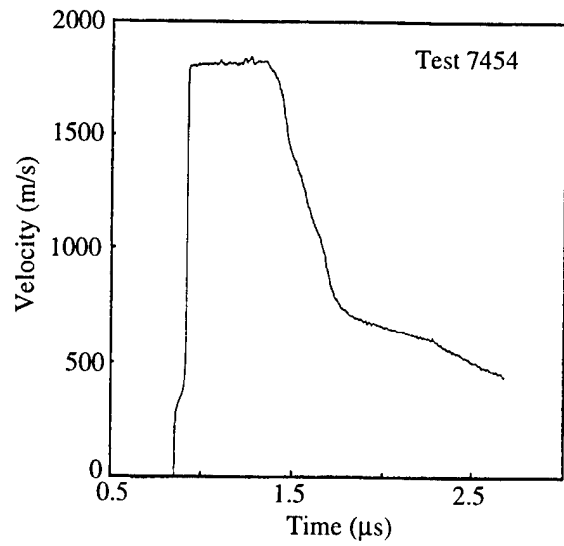Figure 2.7.4.6 Ceramic-Window Interface Velocity Profiles from Grady and Moody [52] for Tests
7454-7459.

158
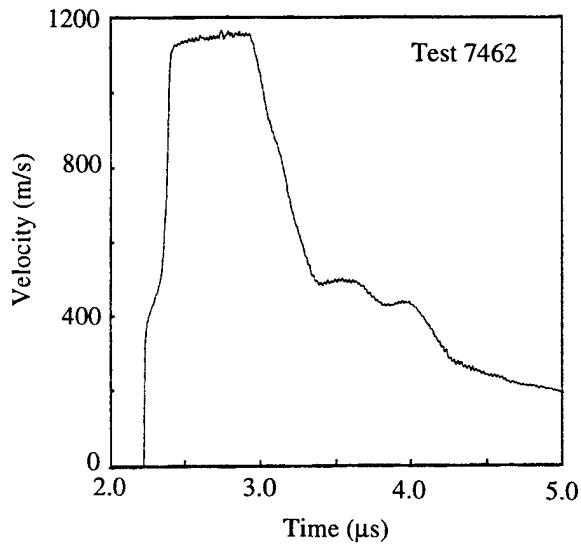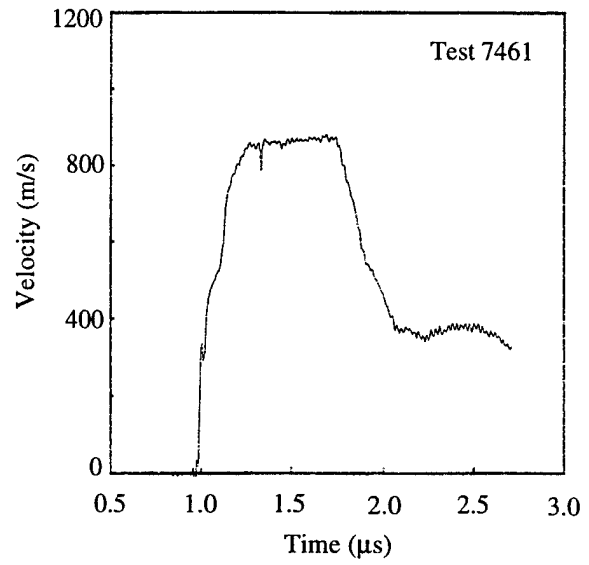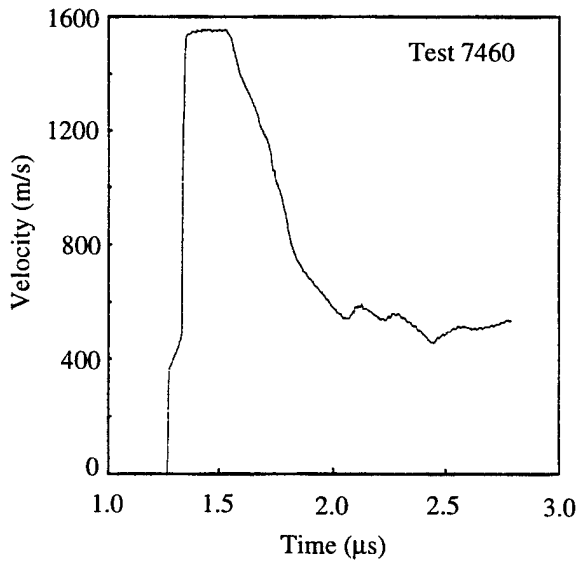
Figure 2.7.4.7 Ceramic-Window Interface Velocity Profiles from Grady and Moody [52] for Tests 7460-7462.
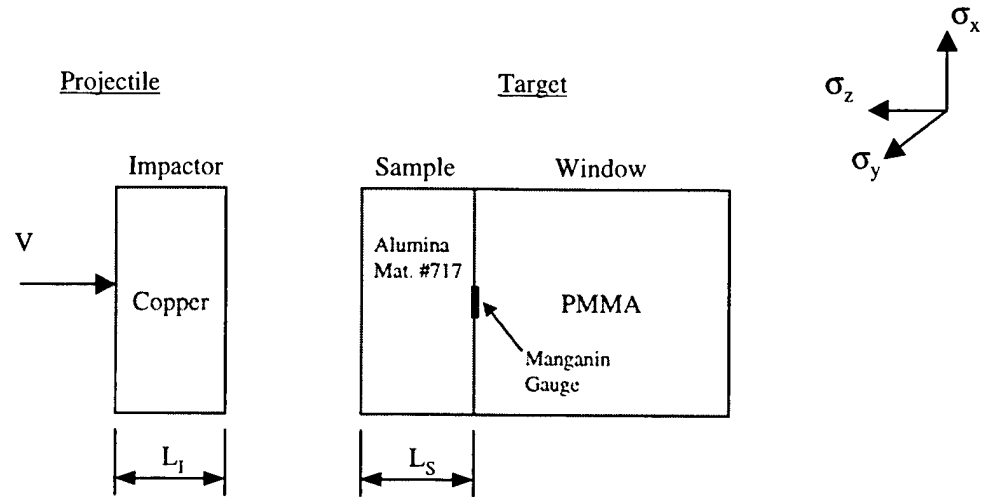
Figure 2.7.4.8 Description of Rosenberg *et al.* [65] Plate Impact Test Configuration.

Table 2.7.4.5 Summary of Experimental Plate Impact Results by Rosenberg *et al.* [65].

Aluminum Oxide (high purity)						
Test Number	Material Number	Projectile		Target	Results	Ref.
		V (m/s)	L_I (mm)	L_S (mm)	HEL (GPa)	
7463	717	905	2	5.1	10.8	65
7464	717	1007	4	9.95	8.6	(Rosenberg)
7465	717	953	3	14.95	8.5	
Test 7463-7465: the test data is from work by Rosenberg *et al.* [65]. In-material Manganin gauges were used to measure the HEL as a function of target thickness. The material was manufactured by Babcock and Wilcox with an initial density = 3900kg/m^3.						

2.7.5 Penetration (semi-infinite) Test Data for Aluminum Oxide (high purity)

Penetration results, into semi-infinite High Purity Aluminum Oxide, are presented in this section. Westerling *et al.* [35] performed penetration experiments into Aluminum Oxide over a velocity range of 2500m/s to 3000m/s. The objective of the experimental program was to investigate penetration performance for novel penetrator geometry's. The target and penetrators used are described in Figure 2.7.5.1. The penetration results are presented graphically in Figure 2.7.5.2 and summarized in Table 2.7.5.1.

Penetration results by Subramanian and Bless [42] investigated penetrator geometry, target geometry and impact velocity. The target and penetrator configurations are presented in Figure 2.7.5.3. The penetration results are presented graphically in Figure 2.7.5.4 and are summarized in Table 2.7.5.2.
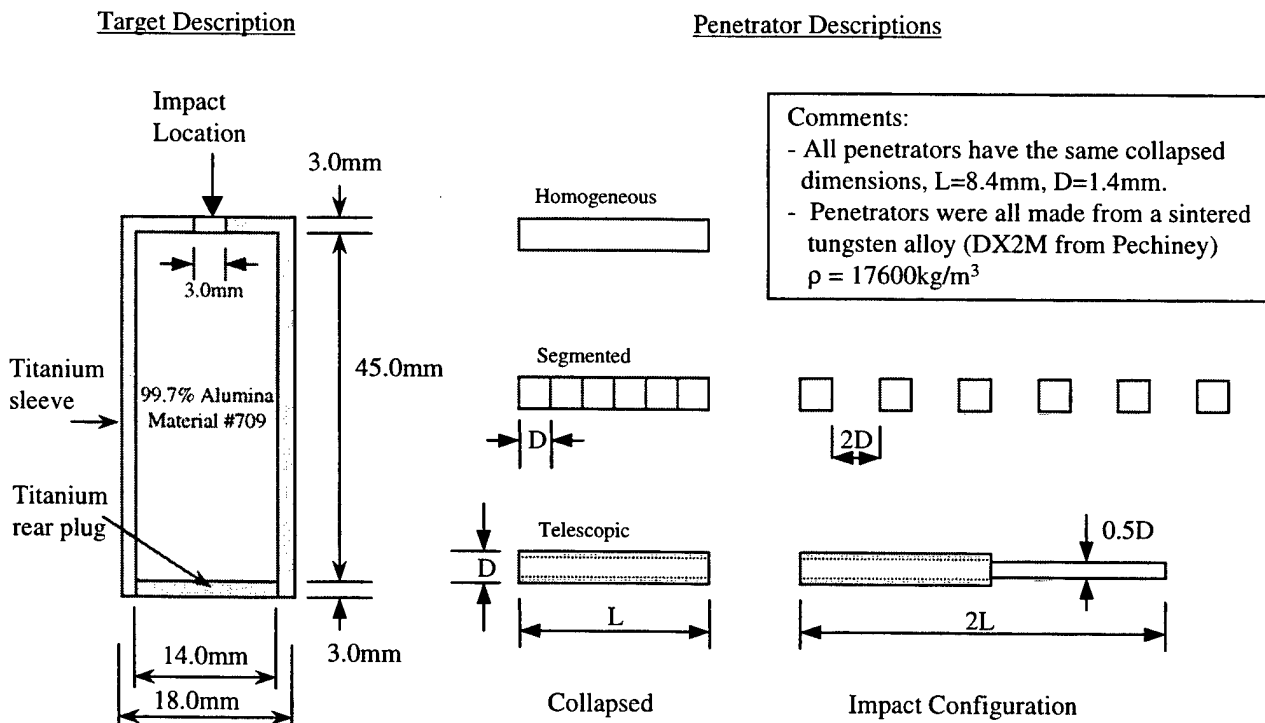
Figure 2.7.5.1 Aluminum Oxide Target and Penetrator Descriptions, Westerling *et al.* [35].
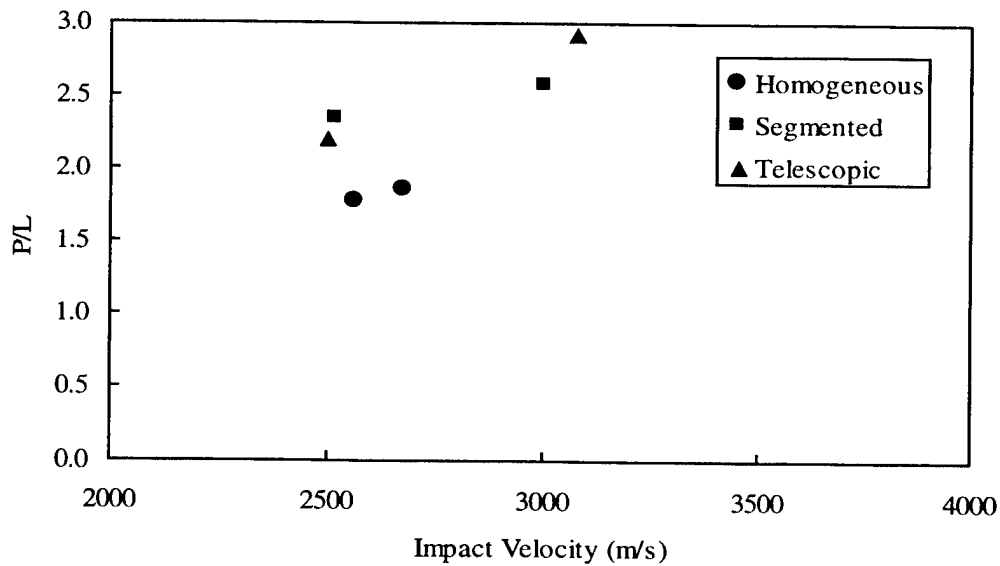
Figure 2.7.5.2 Total Penetration Depth Divided by Collapsed Penetrator Length (P/L) vs. Impact Velocity, Westerling *et al.* [35].

Table 2.7.5.1 Summary of Experimental Results by Westerling *et al.* [35].

Aluminum Oxide (high purity)				
Test Number	Material Number	Penetrator Configuration	Impact Velocity (m/s)	P/L
7501	709	Homogeneous	2570	1.77
7502	709	Homogeneous	2680	1.85
7503	709	Segmented	2520	2.34
7504	709	Segmented	3010	2.57
7505	709	Telescopic	2500	2.19
7506	709	Telescopic	3080	2.91
Test 7501-7506: the test data is from work by Westerling *et al.* [35]. The Alumina used was cold-isostaticly pressed using 99.7% Al_2O_3 powder to an initial density=3809kg/m³. Three penetrator configurations were used. The impact velocity and P/L listed here were obtained from Figure 8 in Ref. 35. The penetration measured is the total penetration into the alumina.				

162

Target Configuration

Impact
Location

Cover
Plate

3.18mm

Titanium
sleeve

99.5% Al₂O₃
(Mat #713)

38.1mm
or
50.8mm

Aluminum

6.35mm or
12.7mm

Aluminum

3.18mm

23.80mm

28.58mm

Penetrator Configurations

Penetrator 2

99.95% Tungsten
ρ = 19300kg/m³
D = 1.52mm
L = 30.4mm
L/D = 20

Penetrator 3

99.95% Tungsten
ρ = 19300kg/m³
D = 1.52mm
L = 22.8mm
L/D = 15

Penetrator 1

99.95% Tungsten
ρ = 19300kg/m³
D = 0.76mm
L = 15.2mm
L/D = 20

Comments:
- Two axi-symmetric target geometries were used
    short: ceramic length=38.1mm, aluminum back=6.35mm, (only used for lower impact velocities)
    long: ceramic length=50.8mm, aluminum back=12.7mm
- Ceramic was slip fit into titanium sleeve, ceramic OD=23.6mm, titanium ID=23.8mm
- In all experiments the final penetration depth was at least 15 penetrator diameters from the ceramic rear surface
- Two cover plate materials were used, 6061-T651 aluminum or RHA (BHN=230)

Figure 2.7.5.3 Target and Penetrator Descriptions, Subramanian and Bless [42].
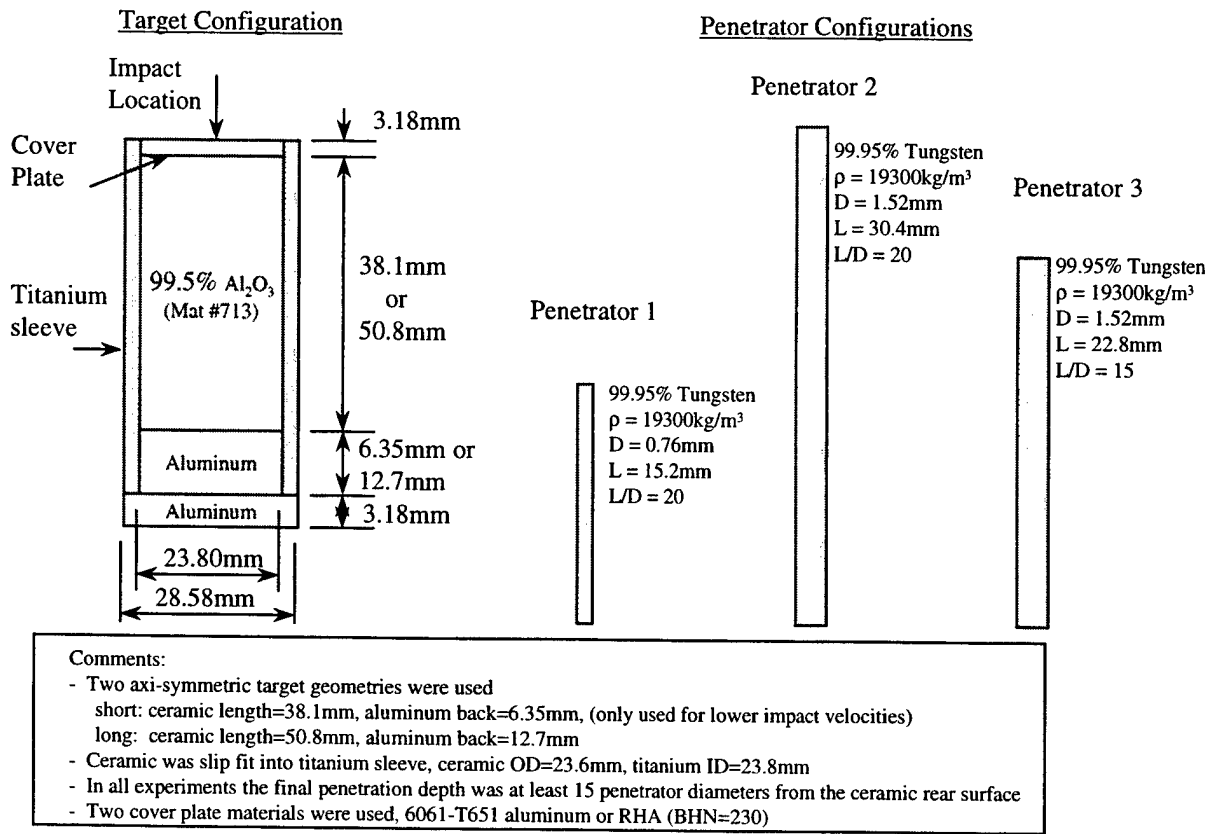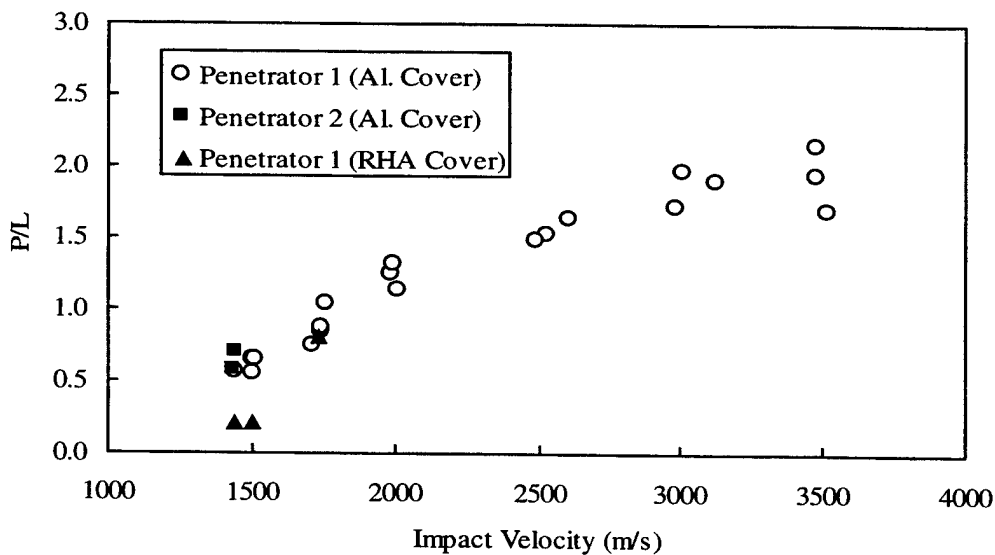

Figure 2.7.5.4 Total Penetration Depth Divided by Penetrator Length (P/L) vs. Impact Velocity
for Two Tungsten Penetrator Configurations Impacting Coors AD-99.5 Alumina
Targets with Two Types of Cover Plates, Subramanian and Bless [42].

163

Table 2.7.5.2 Sumary of Experimental results for Subramanian and Bless [42].

Aluminum Oxide (high purity)								
Test Number	Material Number	Penetrator Configuration	Impact Velocity (m/s)	Cover Plate Material	Penetration Velocity (m/s)	Penetrator Consumption Velocity (m/s)	P_P/L	P_T (mm)
7507	713	1	1989	Aluminum	892	----	------	18.7
7508	713	1	2519	Aluminum	1550	----	------	-----
7509	713	1	3012	Aluminum	1908	1143	1.669	29.8
7510	713	1	2018	Aluminum	920	----	------	17.0
7511	713	1	2018	Aluminum	888	1139	0.780	17.0
7512	713	1	2612	Aluminum	1391	1017	1.368	24.8
7513	713	1	3128	Aluminum	1808	923	1.959	28.7
7514	713	1	2533	Aluminum	1416	1020	1.388	23.0
7515	713	1	2000	Aluminum	896	----	------	19.9
7516	713	1	3529	Aluminum	2036	1316	1.547	25.5
7517	713	1	1448	Aluminum	667	692	0.964	8.4
7518	713	1	1750	Aluminum	724	933	0.776	12.8
7519	713	1	1512	Aluminum	389	1042	0.373	8.2
7520	713	1	1764	Aluminum	809	907	0.892	15.6
7521	713	1	1750	Aluminum	694	920	0.754	13.1
7522	713	1	1510	Aluminum	508	798	0.637	9.7
7523	713	1	2990	Aluminum	1785	1133	1.575	26.0
7524	713	1	2498	Aluminum	1316	1032	1.275	22.4
7525	713	1	3488	Aluminum	2140	1175	1.821	29.4
7526	713	1	3488	Aluminum	2279	1111	2.051	32.6
7527	713	1	1518	Aluminum	494	875	0.565	9.7
7528	713	1	1723	Aluminum	614	937	0.655	11.1
7529	713	2	1442	Aluminum	667	669	0.997	17.4
7530	713	2	1447	Aluminum	684	723	0.946	21.4
7531	713	3	3080	Aluminum	1954	952	2.053	-----
7532	713	1	1443	RHA	n/a	n/a	n/a	3.2
7533	713	1	1736	RHA	661	----	------	12.2
7534	713	1	1500	RHA	n/a	n/a	n/a	3.2

P_T = total penetration depth including the 3.2 mm cover plate.
P_P = primary penetration= depth penetrated when penetrator is just consumed, including the 3.2 mm cover plate. Test 7507-7534: the test data is from work by Subramanian and Bless [42]. The Alumina is AD99.5 manufactured by Coors with an initial density=3890kg/m³. The experiments investigate semi-infinite penetration as a function of confinement, cover plate material and impact velocity. Four radiographs were obtained for each experiment and used to determine the average penetration velocity and average penetrator consumption velocity.

2.7.6 Depth-Of-Penetration (DOP) Test Data for Aluminum Oxide (high purity)

This section presents depth-of-penetration (DOP) experiments performed by numerous researchers using various High Purity Aluminum Oxide materials. The DOP test has been used to investigate the effectiveness of ceramics for a number of years. The typical DOP configuration consists of a ceramic tile place on, or within, a steel or aluminum base target. A penetrator impacts and perforates the ceramic tile and continues into the base target. The penetration into the base target is generally referred to as the residual penetration, P_r, and is used to determined the ceramic mass efficiency as discussed in Section 2.0.

The target and penetrator descriptions for the DOP experiments by Anderson and Royal-Timmons [31] are presented in Figure 2.7.6.1. The objective of these experiments was to investigate ceramic performance as a function of confinement. The results are presented graphically in Figure 2.7.6.2 where total penetration is plotted vs. impact velocity for various degrees of ceramic confinement. The results are also presented in tabular from in Table 2.7.6.1.

The target and penetrator descriptions for the DOP experiments by Lundberg *et al.* [34] are presented in Figures 2.7.6.3-4. The objective of the experiments was to investigate scaling effects as a function of velocity. The results are presented graphically in Figure 2.7.6.5 where normalized total penetration is plotted vs. experimental scale for the two velocity regimes. The results are also presented in tabular from in Table 2.7.6.2.

The target and penetrator descriptions for the DOP experiments by Hohler *et al.* [37] are presented in Figures 2.7.6.6. The objective of the experiments was to investigate ceramic performance as a function of ceramic thickness, ceramic lateral dimension, number of ceramic tiles and impact velocity. The results are presented graphically in Figures 2.7.6.7-9 where residual penetration is plotted vs. ceramic lateral dimension, number of ceramic tiles and impact velocity respectively. The results are also presented in tabular from in Table 2.7.6.3.

The target and penetrator descriptions for the DOP experiments by Woodward and Baxter [40] are presented in Figures 2.7.6.10. The objective of the experiments was to investigate ceramic performance as a function of penetrator geometry, penetrator material and base target material. The results are presented graphically in Figures 2.7.6.11 where residual penetration is plotted as a function of base target material for each of the penetrators tested. The results are also presented in tabular from in Table 2.7.6.4.

The target and penetrator descriptions for the DOP experiments by Woodward *et al.* [41] are presented in Figures 2.7.6.12. The objective of the experiments was to investigate ceramic performance as a function of ceramic rear surface support. Only two experiments were documented in Reference 41 and are presented in tabular from in Table 2.7.6.5.

The target and penetrator descriptions for the DOP experiments by Rupert and Grace [67] are presented in Figure 2.7.6.13. The objective of the experiments was to investigate ceramic performance as a function of ceramic thickness. The results are presented graphically in Figure 2.7.6.14 where residual penetration is plotted vs. ceramic thickness. The results are also presented in tabular from in Table 2.7.6.6.

The target and penetrator descriptions for the DOP experiments by Lynch [86] are presented in Figure 2.7.6.15. The objective of the experiments was to investigate ceramic performance as a function of constant energy projectiles. Two velocities were investigated at nominally the same energy. The results are presented in tabular from in Table 2.7.6.7. Also included in the table are penetration results into the steel base target with no ceramic.
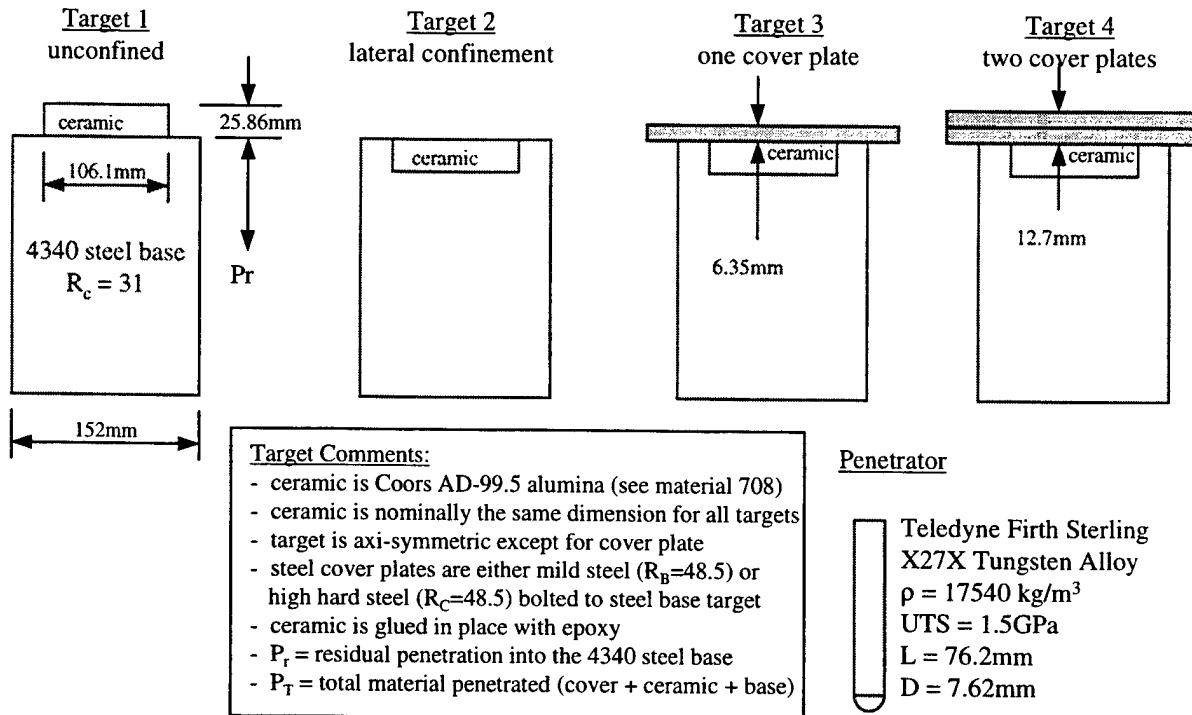
Figure 2.7.6.1 Target and Penetrator Descriptions for DOP Experiments, Anderson and Royal-Timmons [31].
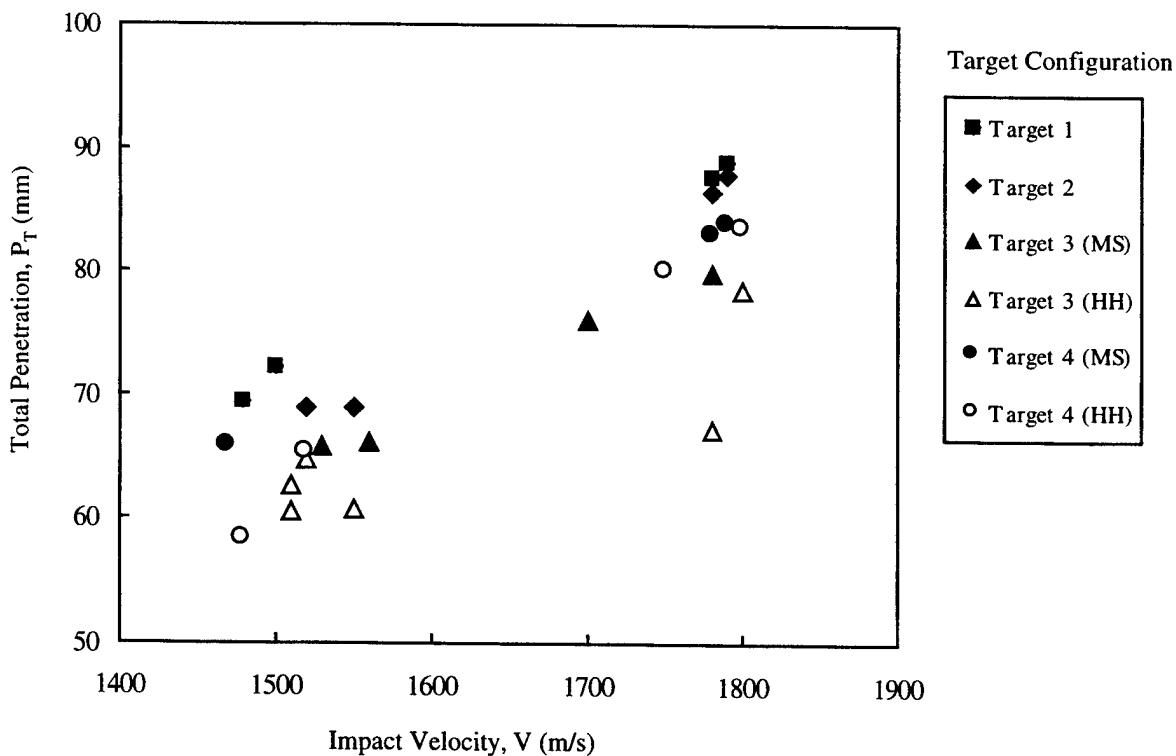

Figure 2.7.6.2 Total Penetration, P_T, vs. impact velocity for the four target configurations, Anderson and Royal-Timmons [31].

167

Table 2.7.6.1   Summary of Results for DOP Tests, Anderson and Royal-Timmons [31]

Aluminum Oxide (high purity)						
Test Number	Material Number	Impact Velocity (m/s)	Target Configuration		P_r (mm)	P_T (mm)
			Target	Cover Plate Material		
7601	708	1550	2		43.2	69.0
7602	708	1520	2		43.2	69.0
7603	708	1780	2		60.6	86.5
7604	708	1790	2		62.0	87.8
7605	708	1560	3	Mild Steel	34.0	66.2
7606	708	1530	3	Mild Steel	33.7	65.8
7607	708	1700	3	Mild Steel	43.8	76.0
7608	708	1780	3	Mild Steel	47.8	79.9
7609	708	1520	3	High Hard	32.5	64.7
7610	708	1510	3	High Hard	30.5	62.7
7611	708	1550	3	High Hard	28.6	60.8
7612	708	1510	3	High Hard	28.4	60.6
7613	708	1780	3	High Hard	35.1	67.2
7614	708	1800	3	High Hard	46.2	78.4
7615	708	1500	1		46.5	72.3
7616	708	1480	1		43.6	69.4
7617	708	1780	1		61.8	87.7
7618	708	1790	1		63.0	88.9
7619	708	1470	4	Mild Steel	27.2	65.8
7620	708	1780	4	Mild Steel	44.5	83.0
7621	708	1790	4	Mild Steel	45.2	83.8
7622	708	1520	4	High Hard	26.7	65.2
7623	708	1480	4	High Hard	19.7	58.3
7624	708	1800	4	High Hard	45.0	83.5
7625	708	1750	4	High Hard	41.4	80.0

Test 7601-7625: the test data is from work by Anderson (Ref. 31). The ceramic material used is Coors AD-99.5 (CAP3) with an initial density = 3900 kg/m³. Four target configurations were used to investigate ceramic performance as a function of confinement and impact velocity.
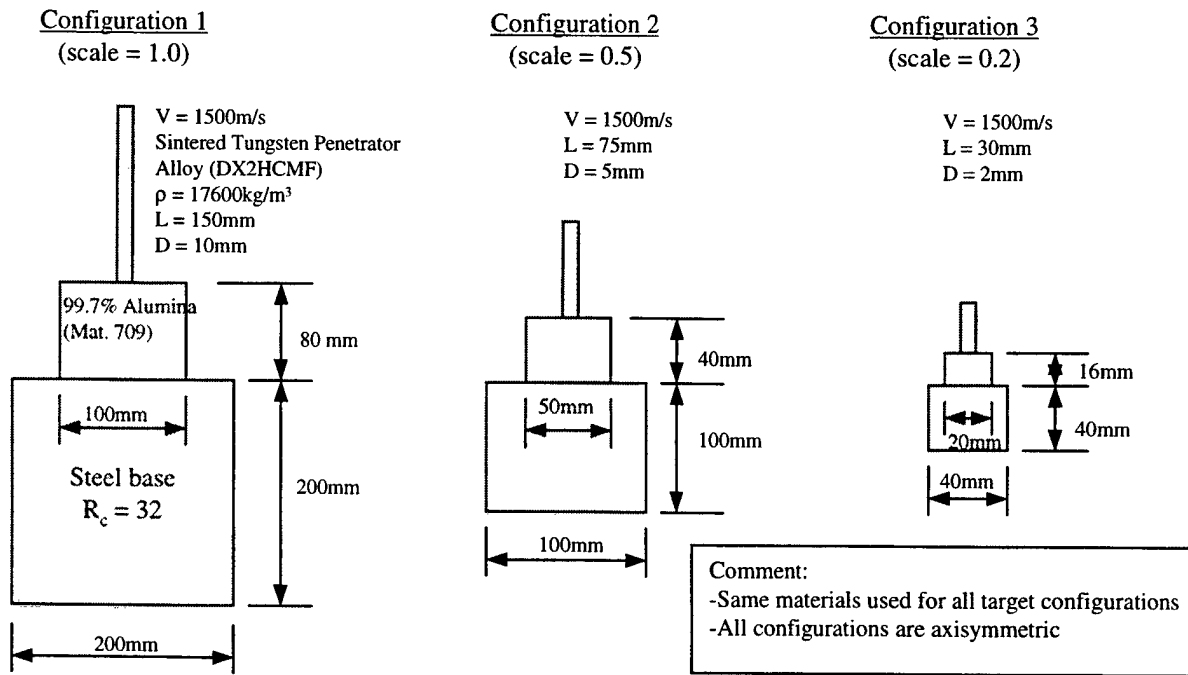
168

Configuration 1
(scale = 1.0)

V = 1500m/s
Sintered Tungsten Penetrator
Alloy (DX2HCMF)
ρ = 17600kg/m³
L = 150mm
D = 10mm

99.7% Alumina
(Mat. 709)

80 mm

100mm

Steel base
R_c = 32

200mm

200mm

Configuration 2
(scale = 0.5)

V = 1500m/s
L = 75mm
D = 5mm

40mm

50mm

100mm

100mm

Configuration 3
(scale = 0.2)

V = 1500m/s
L = 30mm
D = 2mm

16mm

20mm

40mm

40mm

Comment:
-Same materials used for all target configurations
-All configurations are axisymmetric

Figure 2.7.6.3 Target and Penetrator Descriptions for DOP Experiments Investigating Scaling for Impact Velocity = 1500m/s, Lundberg *et al.* [34].

Configuration 4
(scale = 1.0)

V = 2500m/s
Sintered Tungsten Penetrator
Alloy (DX2HCMF)
ρ = 17600kg/m³
L = 150mm
D = 10mm

99.7% Alumina
(Mat. 709)

160 mm

100mm

Steel base
R_c = 32

400mm

200mm

Configuration 5
(scale = 0.5)

V = 2500m/s
L = 75mm
D = 5mm

80mm

50mm

200mm

100mm

Configuration 6
(scale = 0.2)

V = 2500m/s
L = 30mm
D = 2mm

32mm

20mm

80mm

40mm

Comment:
-Same materials used for all target configurations
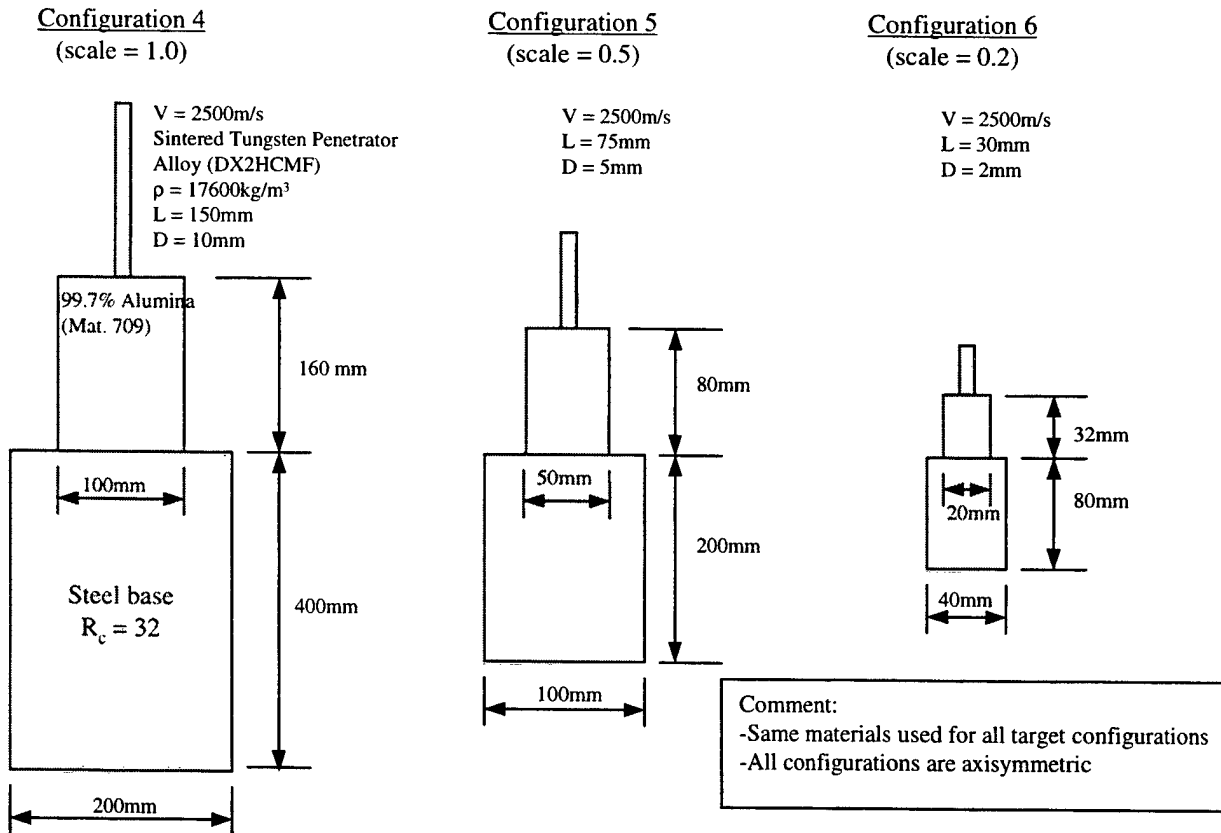-All configurations are axisymmetric

Figure 2.7.6.4 Target and Penetrator Descriptions for DOP Experiments Investigating Scaling for Impact Velocity = 2500m/s, Lundberg *et al.* [34].
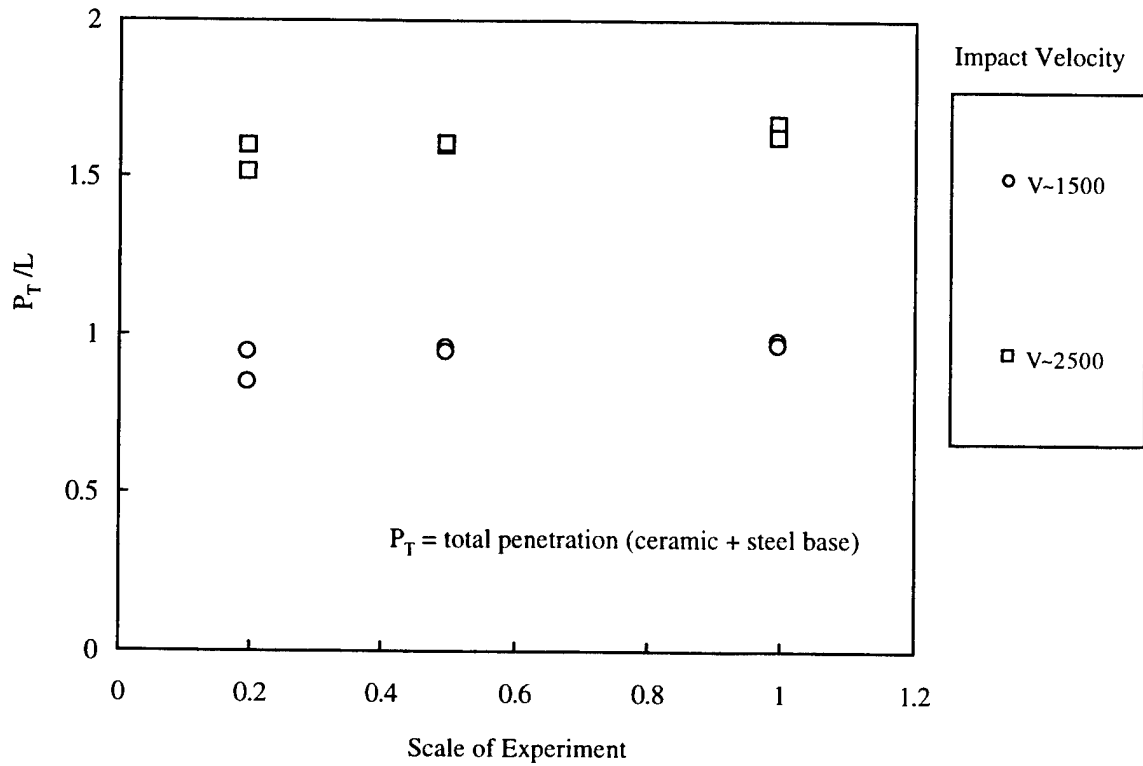
169

Figure 2.7.6.5 Total penetration divided by penetrator length, P_T/L, as a function of scale and impact velocity, Lundberg *et al.* [34].

Table 2.7.6.2 Summary of Experimental DOP Results, Lundberg et al. [34]

Aluminum Oxide (high purity)					
Test Number	Material Number	Impact Velocity (m/s)	Test Configuration	Scale	P_T (mm)
7626	709	1417	3	0.2	25.1
7627	709	1582	3	0.2	28.3
7628	709	2409	6	0.2	47.6
7629	709	2475	6	0.2	45.4
7630	709	1488	2	0.5	71.4
7631	709	1503	2	0.5	70.3
7632	709	2505	5	0.5	119.6
7633	709	2521	5	0.5	119.7
7634	709	1502	1	1.0	145.3
7635	709	1471	1	1.0	143.3
7636	709	2505	3	1.0	249.0
7637	709	2485	3	1.0	243.0

Test 7626-7637: the test data is from work by Lundberg (Ref. 34). The ceramic material used is 99.7% Alumina CIP processed to an initial density =3809kg/m³. Six target configurations were used to investigate scaling effects as a function of impact velocity.
P_T = total penetration (ceramic + steel base)

Configuration 1

Tungsten Sinter-Alloy
Penetrator
$\rho = 17600\text{kg/m}^3$
UTS = 1.2 GPa
elongation = 10%
L = 72.5 mm
D = 5.8 mm
L/D = 12.5

1,5mm rubber

Mild Steel   10mm

Al_2O_3 30mm h_c 20mm
Ceramic tiles
(Mat. #710)

L_c

HH RHA
UTS = 1.45GPa
R_c~45

P_r= residual
penetration
into HH RHA

Configuration 2

Tungsten Sinter-Alloy
Penetrator
$\rho = 17600\text{kg/m}^3$
UTS = 1.49 GPa
elongation = 8.8%
L = 50 mm
D = 5 mm
L/D = 10

1,5mm rubber

Mild Steel   10mm

Al_2O_3 50mm h_c 10mm
Ceramic tiles
(Mat. #710)

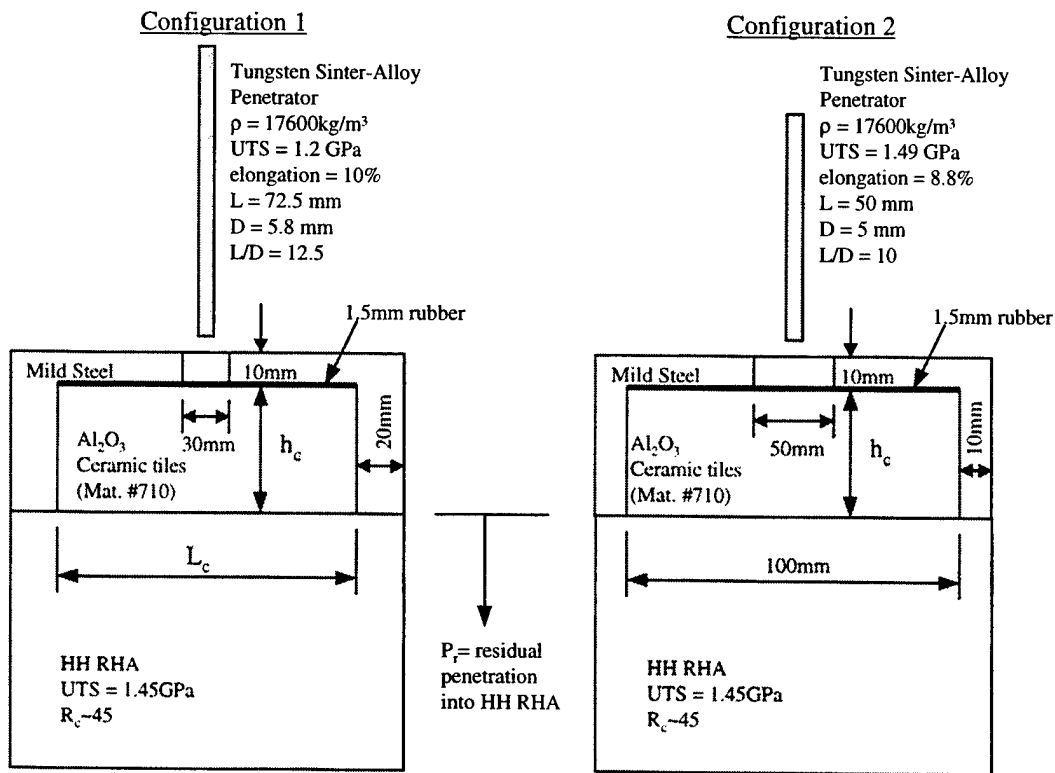100mm

HH RHA
UTS = 1.45GPa
R_c~45

Figure 2.7.6.6 Target and Penetrator Descriptions for DOP Experiments, Hohler *et al.* [37].
Configuration 1 is used for impact velocities 1250m/s - 1700m/s, Configuration 2 is
used for impact velocities 2500m/s - 3000m/s. Same target materials used for both
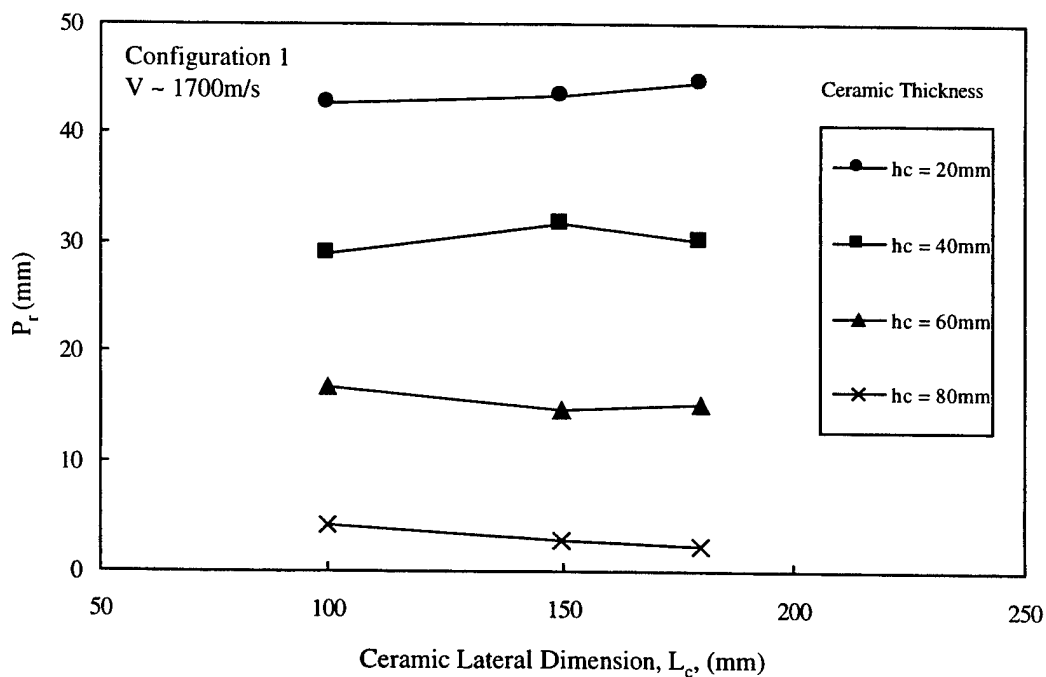configurations and both targets are generally square.

Figure 2.7.6.7 Residual Penetration as a Function of the Ceramic Lateral Dimension
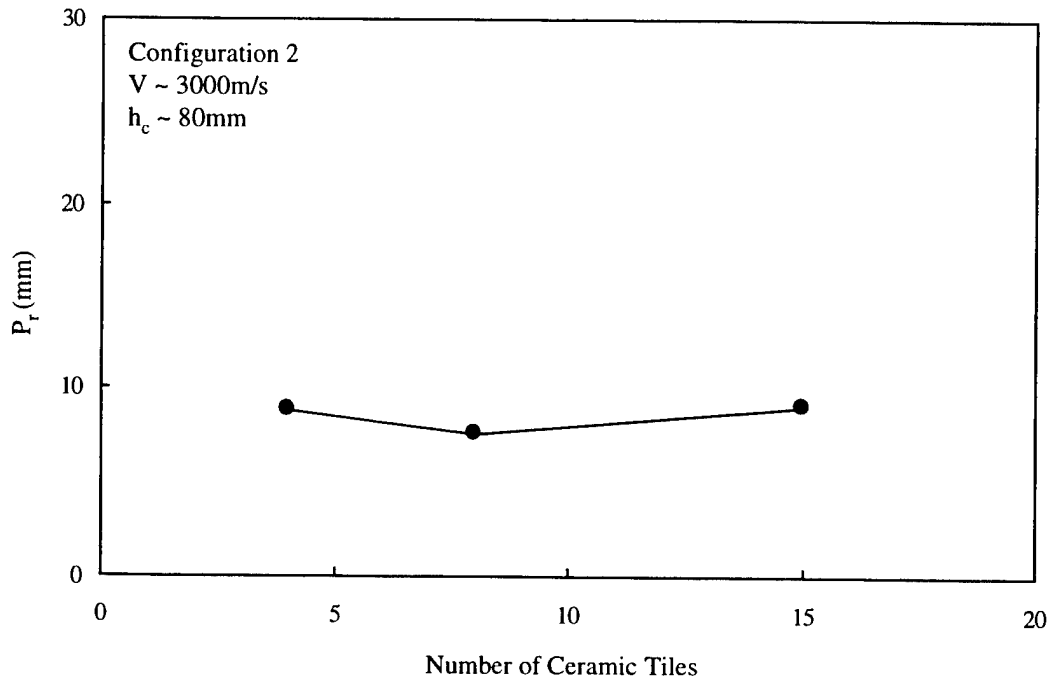and Ceramic Thickness, Hohler *et al.* [37].

171

Figure 2.7.6.8 Experimental Results for DOP Tests, Hohler *et al.* [37]. Shown here is the residual penetration as a function the number of ceramic tiles for constant impact velocity and total ceramic thickness.
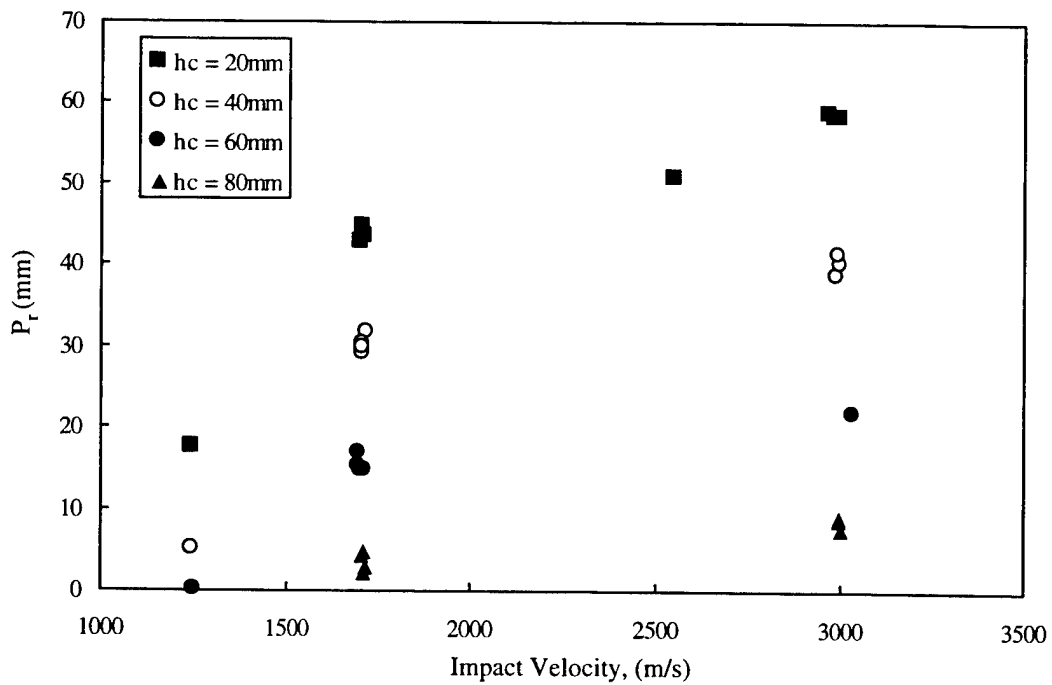

Figure 2.7.6.9 Experimental Results for DOP Tests, Hohler *et al.* [37]. Shown here is the residual penetration as a function of ceramic thickness and impact velocity.

172

Table 2.7.6.3 Tabulated Experimental Results for DOP Tests, Hohler *et al.* [37].

Test Number	Material Number	Impact Velocity (m/s)	Test Config.	No. of ceramic tiles			h$_c$ (mm)	L$_c$ (mm)	Yaw (deg.)	Pitch (deg.)	P$_r$ (mm)
				5mm	10mm	20mm					
7638	710	1246	1			1	19.8	180	1.0	<1.0	17.5
7639	710	1246	1			2	39.6	180	1.0	<1.0	5.0
7640	710	1252	1			3	59.8	180	0.0	<1.0	0.0
7641	710	1705	1			1	20.2	100	0.3	<1.0	42.6
7642	710	1709	1			2	40.1	100	1.8	<1.0	28.9
7643	710	1702	1			3	61.1	100	1.5	<1.0	16.7
7644	710	1705	1			4	81.4	100	4.8	<1.0	4.2
7645	710	1717	1			1	20.0	150	0.8	<1.0	43.4
7646	710	1721	1			2	40.0	150	<0.5	<1.0	31.7
7647	710	1717	1			3	60.0	150	0.8	<1.0	14.7
7648	710	1716	1			4	80.0	150	1.0	<1.0	2.8
7649	710	1710	1			1	19.9	180	0.3	<1.0	44.6
7650	710	1711	1			2	39.5	180	0.5	<1.0	30.2
7651	710	1698	1			3	59.6	180	1.0	<1.0	15.2
7652	710	1708	1			4	79.0	180	1.0	<1.0	2.2
7653	710	1711	*			2	40.6	100	0.7	<1.0	29.7
7654	710	1691	*		1	2	51.0	100	0.8	<1.0	19.4
7655	710	1706	*			3	60.0	100	0.5	<1.0	14.5
7656	710	1710	*			4	80.7	100	<1.0	<1.0	4.6
7657	710	2552	2		1		10	100	0.2	1.7	60.2
7658	710	2552	2		2		20	100	1.0	6.4	50.7
7659	710	2537	2		3		30	100	0.1	<0.5	39.1
7660	710	2550	2		5		50	100	0.1	1.9	23.9
7661	710	2516	2		7		70	100	0.5	0.2	10.2
7662	710	3024	2		1		10	100	<2.0	3.1	66.8
7663	710	3023	2		1		10	100	<1.0	4.8	67.0
7664	710	2994	2		1		10	100	0.2	1.4	68.0
7665	710	2984	2		2		20.5	100	2.0	<1.0	58.1
7666	710	3002	2		2		19.9	100	0.5	1.5	58.3
7667	710	2968	2		2		19.6	100	3.0	1.6	58.8
7668	710	3025	2		3		30	100	0.5	0.2	50.0
7669	710	3000	2		3		30.8	100	0.0	3.0	50.2
7670	710	2991	2		4		40.8	100	0.3	<1.0	38.6
7671	710	3000	2		4		41.1	100	0.2	<1.0	40.1
7672	710	2995	2		4		40.4	100	4.8	0.2	41.3
7673	710	3037	2		6		62.0	100	0.3	<1.0	21.6
7674	710	2980	2		7		69.8	100	<1.0	<1.0	18.7
7675	710	3003	2		8		82.0	100	<1.0	<1.0	7.5
7676	710	2998	2			4	81.1	100	<1.0	<1.0	8.8
7677	710	2995	2	15			80.8	100	<1.0	0.0	9.0
7678	710	2964	2		10		101.2	100	<1.0	0.1	0
7679	710	2963	2		10		100.5	100	<1.0	1.5	0

Test 7638-7679: the test data is from work by Hohler *et al.* [37] The ceramic material used is A1898 Al$_2$O$_3$ manufactured by Hoechst CeramTec with an initial density = 3800 kg/m^3. Target configurations were used to investigate ceramic performance as a function of ceramic thickness, ceramic lateral dimensions, number of ceramic tiles and impact velocity.

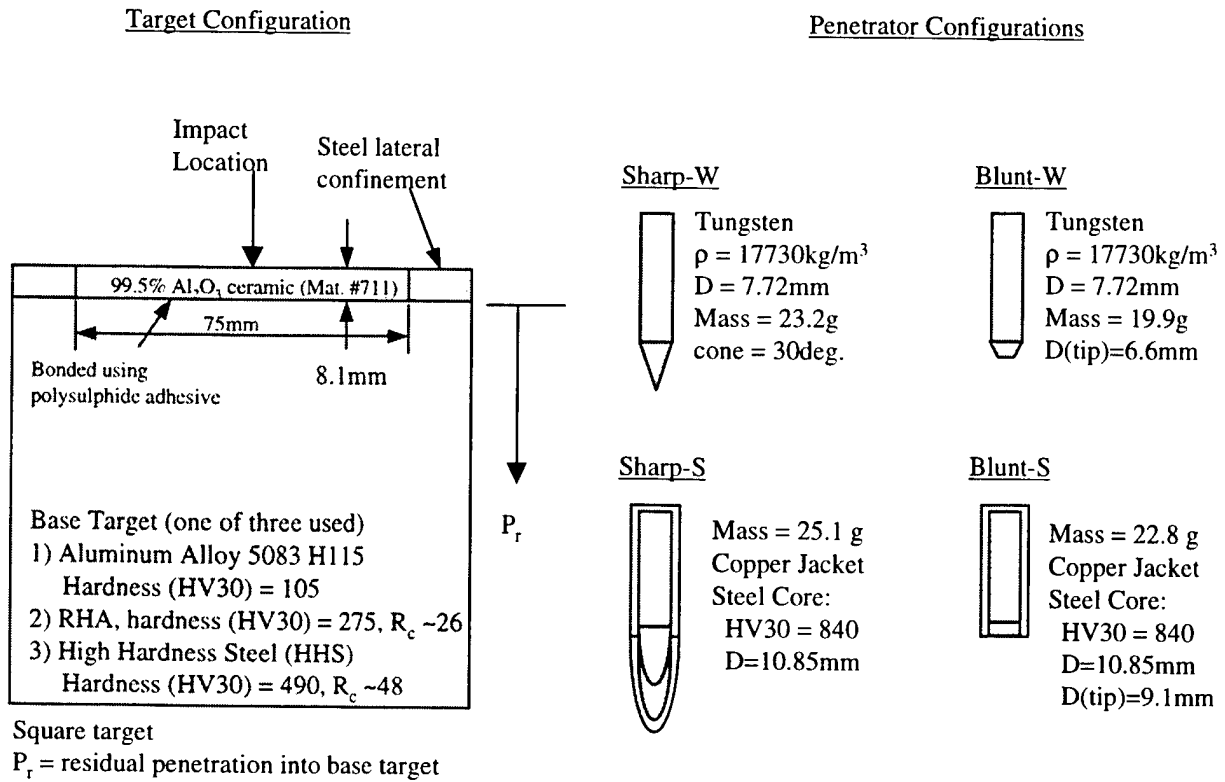*Test 7653-7656 used the target from configuration 2 and the penetrator from configuration 1.

Target Configuration

Impact
Location

Steel lateral
confinement

99.5% Al₂O₃ ceramic (Mat. #711)

75mm

Bonded using
polysulphide adhesive

8.1mm

P_r

Base Target (one of three used)
1) Aluminum Alloy 5083 H115
   Hardness (HV30) = 105
2) RHA, hardness (HV30) = 275, R_c ~26
3) High Hardness Steel (HHS)
   Hardness (HV30) = 490, R_c ~48

Square target
P_r = residual penetration into base target

Penetrator Configurations

Sharp-W
Tungsten
ρ = 17730kg/m³
D = 7.72mm
Mass = 23.2g
cone = 30deg.

Blunt-W
Tungsten
ρ = 17730kg/m³
D = 7.72mm
Mass = 19.9g
D(tip)=6.6mm

Sharp-S
Mass = 25.1 g
Copper Jacket
Steel Core:
  HV30 = 840
  D=10.85mm

Blunt-S
Mass = 22.8 g
Copper Jacket
Steel Core:
  HV30 = 840
  D=10.85mm
  D(tip)=9.1mm

Figure 2.7.6.10 Target and Penetrator Descriptions for DOP Experiments, Woodward and
Baxter [40].
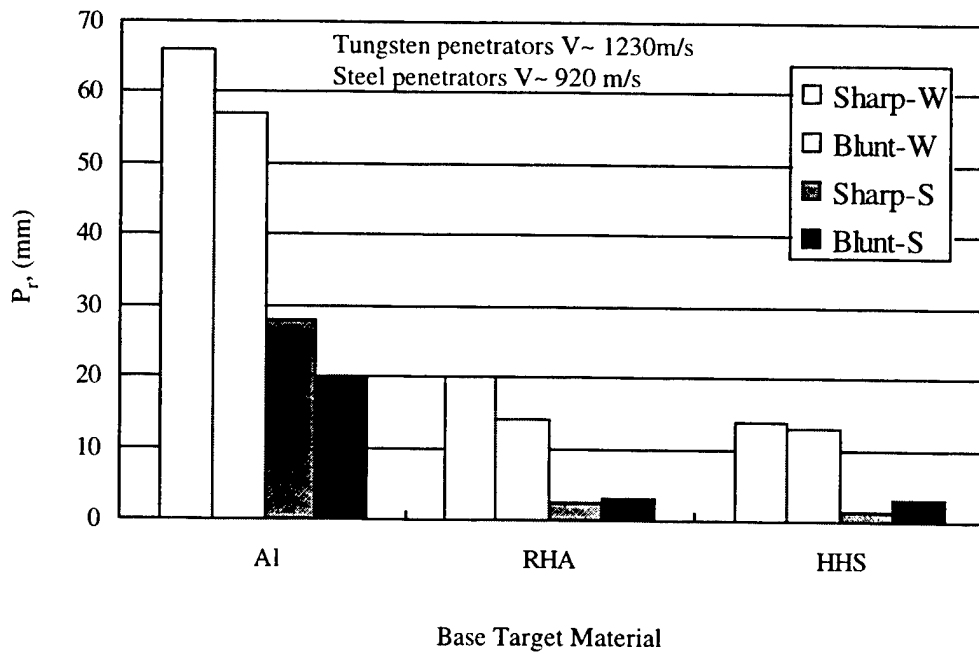
Figure 2.7.6.11 Residual Penetration as a Function of Base Target Material and Penetrator
Configuration, Woodward and Baxter [40].

174

Table 2.7.6.4 Summary of Experimental Results for DOP Tests, Woodward and Baxter [40].

Aluminum Oxide (high purity)						
Test Number	Material Number	Impact Velocity (m/s)	Penetrator	Base Target Material	P_r (mm)	P* (mm)
7679	711	1209+-15	Sharp-W	Aluminum	66	265
7680	711	1243+-15	Blunt-W	Aluminum	57	75
7681	711	899+-10	Sharp-S	Aluminum	28	85
7682	711	937+-11	Blunt-S	Aluminum	20	62
7683	711	1209+-15	Sharp-W	RHA	20	34
7684	711	1243+-15	Blunt-W	RHA	14	23.5
7685	711	899+-10	Sharp-S	RHA	2.5	30
7686	711	937+-11	Blunt-S	RHA	3	10
7687	711	1209+-15	Sharp-W	HHS	13.7	23.5
7688	711	1243+-15	Blunt-W	HHS	13	23
7689	711	899+-10	Sharp-S	HHS	1.5	19
7690	711	937+-11	Blunt-S	HHS	3	11.5

* This is the penetration with no ceramic.
Test 7679-7690: the test data is from work by Woodward and Baxtor [40]. The ceramic material used is 99.5% Al_2O_3 with an initial density = 3809 kg/m³. Four penetrator configurations and three target configurations were investigated.
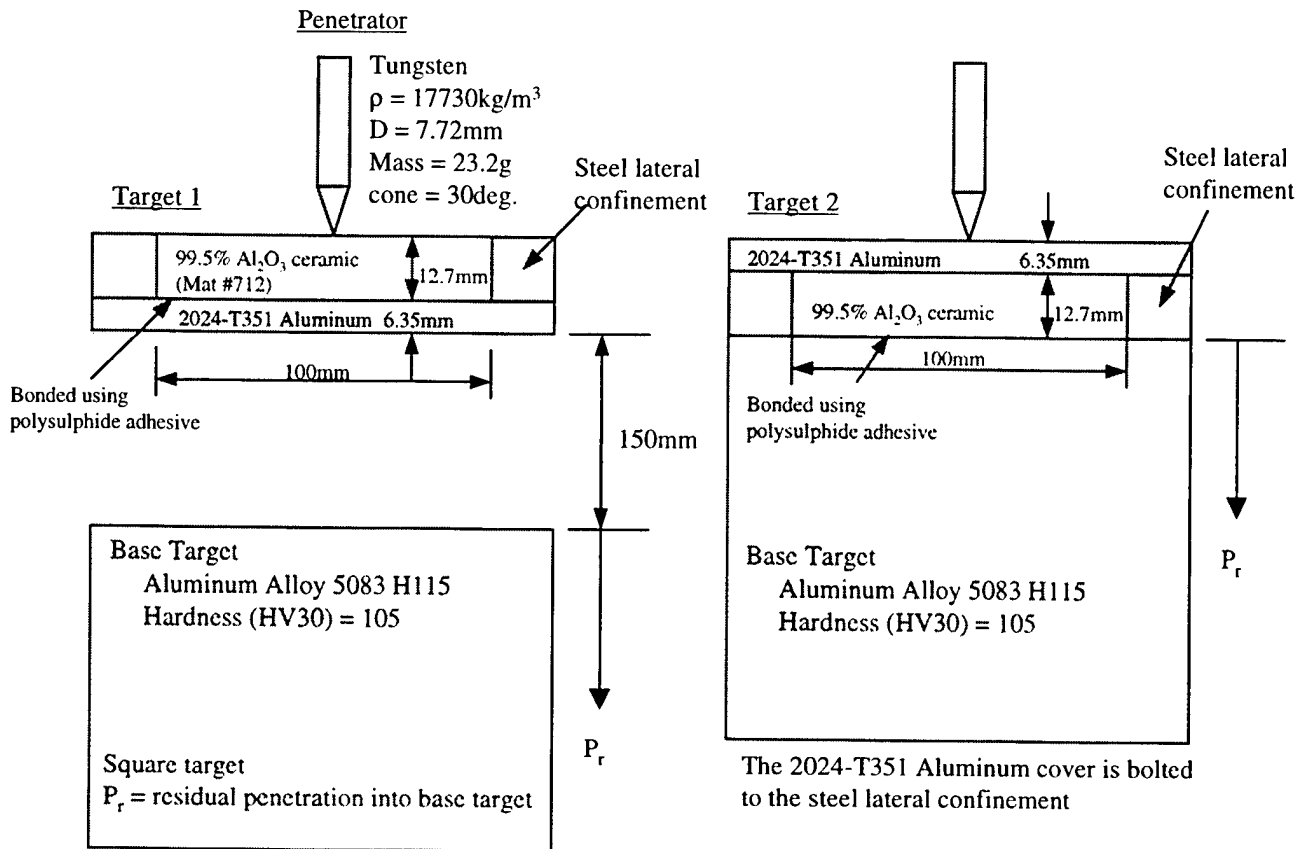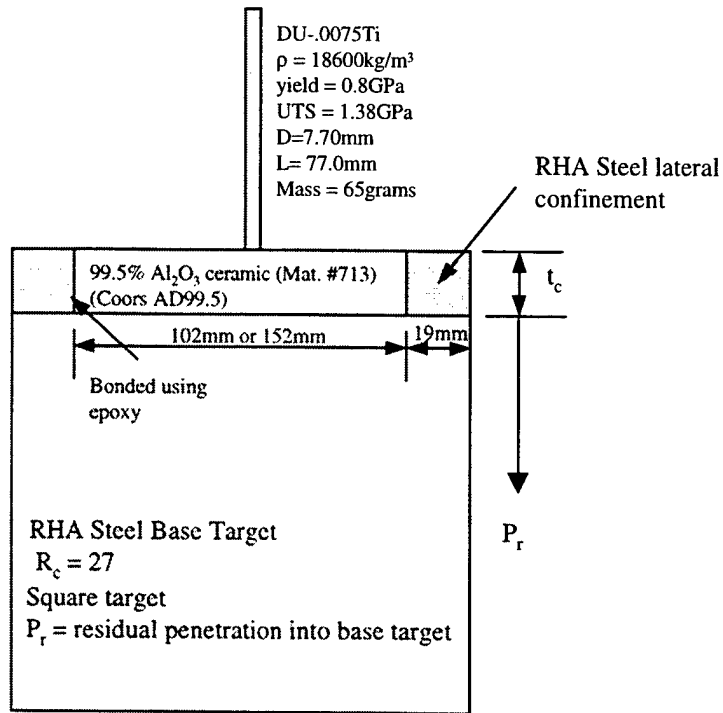
Figure 2.7.6.12   Target and Penetrator Descriptions for DOP Experiments, Woodward *et al.* [41].

Table 2.7.6.5   Summary of Experimental Results for DOP Tests, Woodward *et al.* [41].

Aluminum Oxide (high purity)					
Test Number	Material Number	Impact Velocity (m/s)	Target Configuration	P_r (mm)	P* (mm)
7691	712	1209+-15	Target 1	53	265
7692	712	1209+-15	Target 2	45.1	265
* This is the semi-infinite penetration into Aluminum. Test 7691-7692: the test data is from work by Woodward *et al.* [41]. The ceramic material used is 99.5% Al_2O_3 with an initial density = 3900 kg/m³. One penetrator geometry and two target configurations were investigated.					

176

Figure 2.7.6.13   Target and Penetrator Descriptions for DOP Experiments, Rupert and Grace [67].
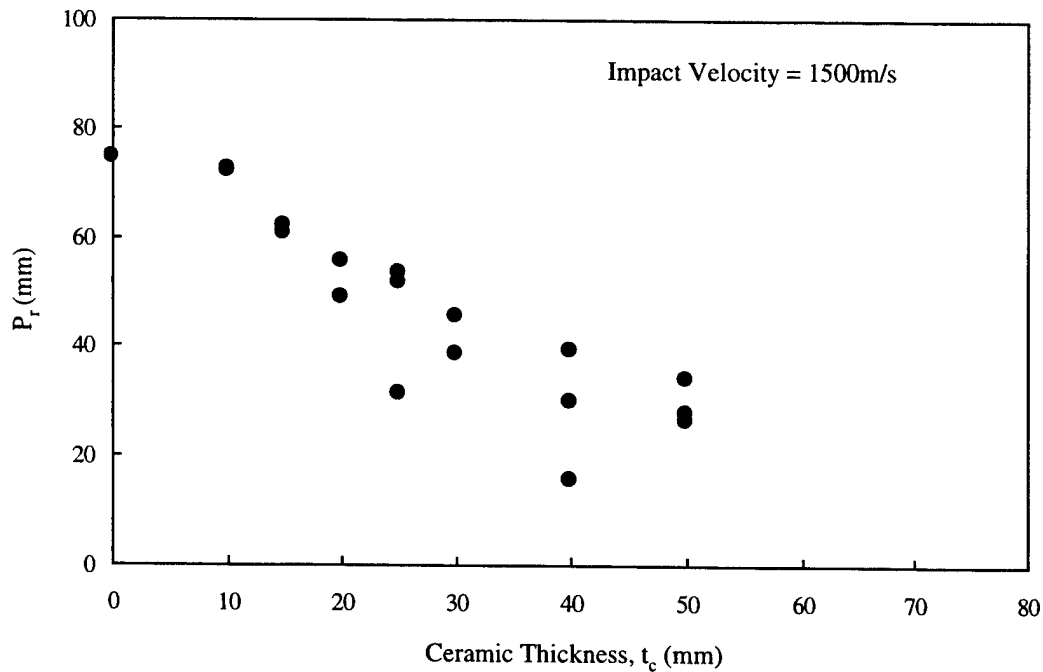

Figure 2.7.6.14   Residual Penetration as a Function of Ceramic Thickness, Rupert and Grace [67].

177

Table 2.7.6.6 Summary of Experimental Results for DOP Tests, Rupert and Grace [67].

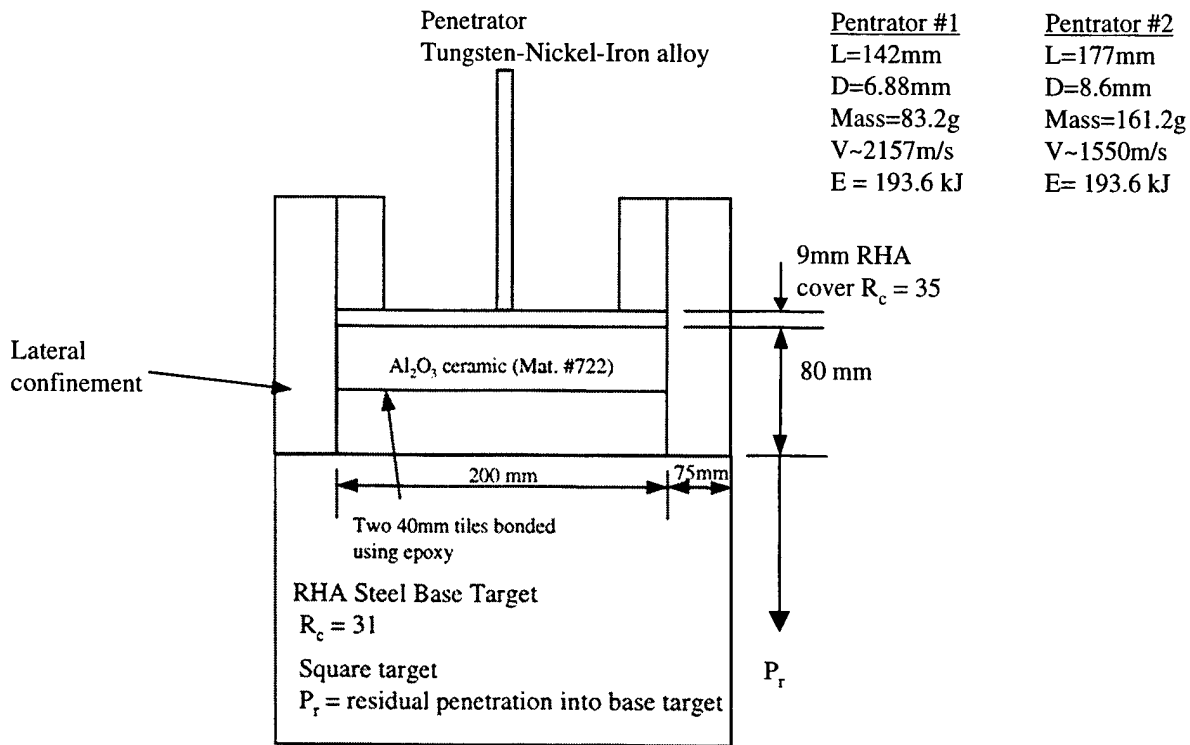| Aluminum Oxide (high purity)				
Test Number	Material Number	Impact Velocity* (m/s)	Ceramic Thickness t_c (mm)	P_r (mm)
7693	718	1500	0	74.7
7694	718	1500	10	72.6
7695	718	1500	10	72.2
7696	718	1500	15	61.9
7697	718	1500	15	60.5
7698	718	1500	20	55.5
7699	718	1500	20	48.7
76100	718	1500	25	53.4
76101	718	1500	25	51.6
76102	718	1500	25	30.9
76103	718	1500	30	45.2
76104	718	1500	30	38.4
76105	718	1500	40	39.1
76106	718	1500	40	29.5
76107	718	1500	40	15.3
76108	718	1500	50	33.8
76109	718	1500	50	27.7
76110	718	1500	50	26.3
* Nominal impact velocity is 1500m/s. No specific velocity data was given. Test 7693-76110: the test data is from work by Rupert and Grace [67]. The ceramic material used is 99.5% Al_2O_3 manufactured by Coors (AD99.5) with an initial density = 3895 kg/m^3. The tabulated residual penetration, P_r, was obtained from Figure 6 in Ref. 67.				

178

Figure 2.7.6.15   Target and Penetrator Descriptions for DOP Experiments, Lynch [86].

Table 2.7.6.7   Summary of Experimental Results for DOP Tests, Lynch [86].

Aluminum Oxide (high purity)						
Test Number	Material Number	Impact Velocity (m/s)	Penetrator Geometry	Ceramic Thickness (mm)	Penetrator yaw at impact (degrees)	P_r (mm)
76111	722	1525	2	80	1.55	60.5
76112	722	1531	2	80	0.8	64.0
76113	722	2120	1	80	1.4	93.0
76114	722	2130	1	80	1.4	91.5
76115		1521	2	0	0.35	137.5
76116		1523	2	0	1.05	131.8
76117		2114	1	0	0.3	177.5
76118		2102	1	0	2.0	169.5
76119		2112	1	0	1.8	166
76120		2147	1	0	1.0	175
Test 76111-76120: the test data is from work by Lynch[86]. Test 76115-76120: test data using no ceramic, performed to calibrate penetrator penetration capability. P_r for these tests is the total RHA penetration. Test 76111-76114: P_r is the measured residual penetration into the RHA steel base target and does not include the 9mm steel cover plate.						

2.7.7 Perforation Test Data for Aluminum Oxide (high purity)

This subsection presents perforation experiments using High Purity Aluminum Oxide where the target is usually perforated by the penetrator. Targets are typically comprised of a ceramic front layer and a metallic rear layer and are commonly used in light armor applications. The most common piece of data extracted from perforation experiments is the target ballistic limit, V_{bl}, previously defined in Section 2.0.

The target and penetrator descriptions for the perforation experiments by Wilkins *et al.* [24, 26] are presented in Figure 2.7.7.1. The objective of the experimental program was to determine the ballistic limit velocity as a function of ceramic front plate thickness and penetrator geometry. The results are presented graphically in Figure 2.7.7.2 where the ballistic limit velocity is plotted vs. ceramic front plate thickness for the two penetrator geometry's. Three different ceramic materials were used for this work. The results are summarized in Table 2.7.7.1.

The target and penetrator descriptions for the perforation experiments by Anderson *et al.* [36] are presented in Figure 2.7.7.3. The objective of the experiments was to determine the ballistic limit velocity as a function of scale. The results are presented graphically in Figure 2.7.7.4 where the ballistic limit velocity is plotted vs. the scale of the experiment for two target configurations. The results are also presented in tabular from in Table 2.7.7.2.

The target and penetrator descriptions for the perforation experiments by Den Reijer [78] are presented in Figure 2.7.7.5. One of the objectives of the experiments was to determine the ballistic limit velocity as a function of aluminum rear plate configuration. Both rear plate thickness and stiffness were investigated. The results are presented graphically in Figure 2.7.7.6 where the ballistic limit velocity is plotted vs. aluminum rear plate thickness and configuration. The results are also presented in tabular from in Table 2.7.7.3. Very little of Den Reijer work is actually presented here. Over 130 experiments were performed to obtain the results presented in Table 2.7.7.3. For many of the experiments, x-rays were taken to investigate the projectile-armor interaction process. X-rays were taken at 2, 4, 6, 8, 10, 12, 14, 16, 20, 25, 30, 35, 40/45 and 60μs after penetrator impact, and are presented in great detail in Reference 78. Much insight into the penetration process can be obtained from studying this work and the reader is urged to obtain this reference if this phenomena is of interest.
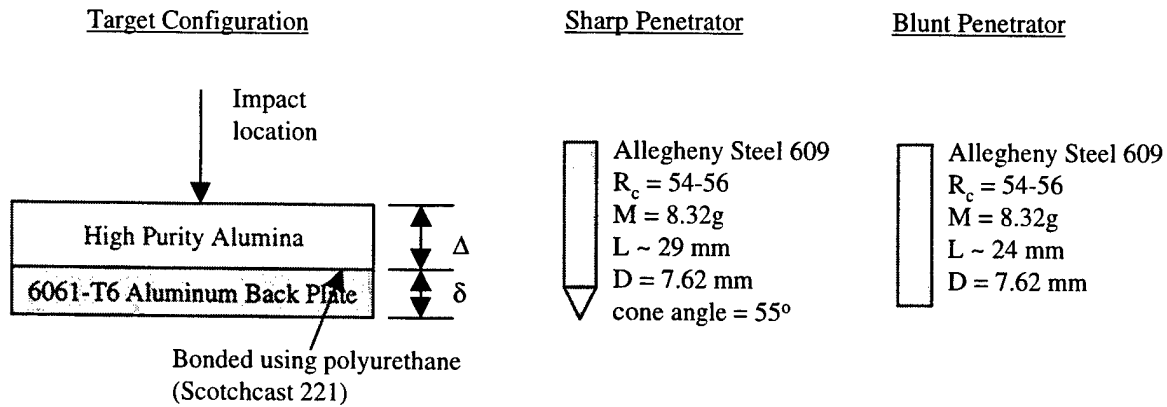
Figure 2.7.7.1   Target and Penetrator Descriptions for Perforation Experiments, Wilkins *et al.* [24, 26].
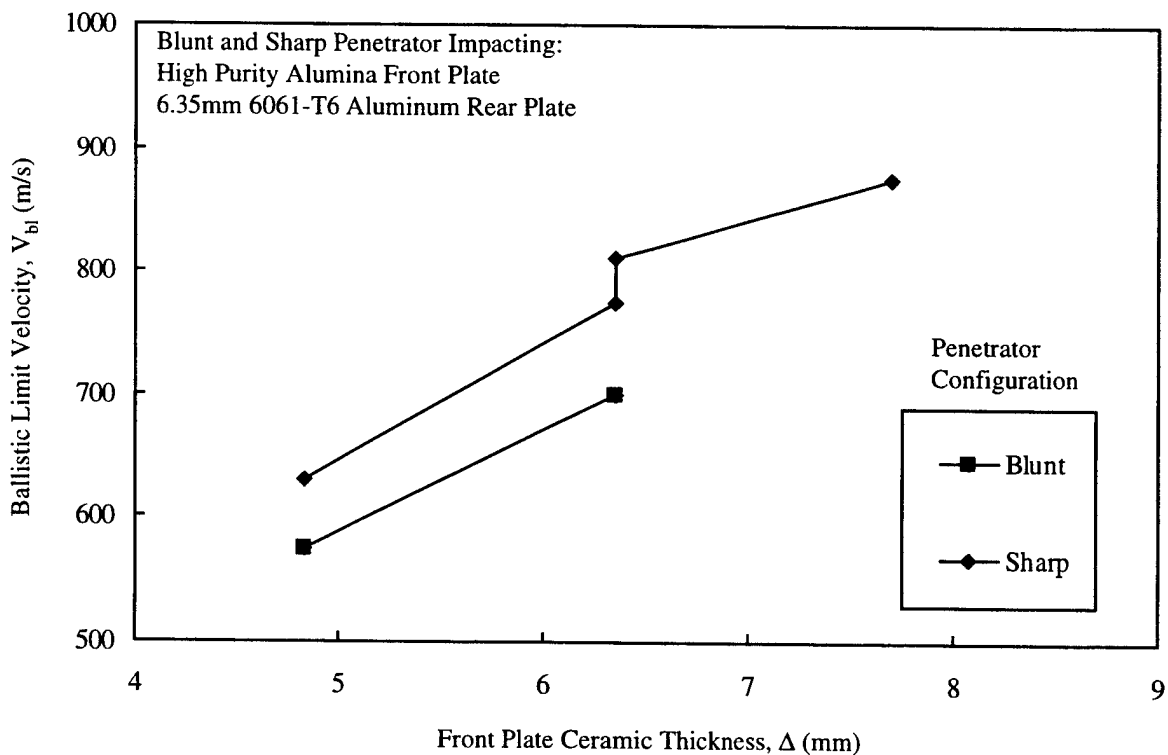

Figure 2.7.7.2   Blunt and Sharp Penetrator Ballistic Limit Velocity as a function of High Purity Alumina Ceramic Front Plate Thickness, Wilkins *et al.* [24, 26].

181

Table 2.7.7.1 Summary of Experimental Results for Perforation Tests, Wilkins *et al.* [24, 26].

| Aluminum Oxide (high purity)					
Test Number	Material Number	Penetrator	Target Configuration		Ballistic Limit Velocity, V_{bl} (+- 15m/s)
			Δ (mm)	δ (mm)	
7701	703	Sharp	4.83	6.35	630
7702	703	Blunt	4.83	6.35	575
7703	703	Sharp	6.35	6.35	775
7704	703	Blunt	6.35	6.35	700
7705	704	Sharp	6.35	6.35	810
7706	705	Sharp	7.70	6.35	875
Test 7701-7706: the test data is from work by Wilkins *et al.* [24, 26]. Two penetrator configurations were used, a sharp and blunt. Target configurations consisted of high purity Alumina front plate bonded to a 6061-T6 aluminum rear plate.The ballistic limit velocity was experimentally determined for each target configuration within a +-15m/s error.					

182
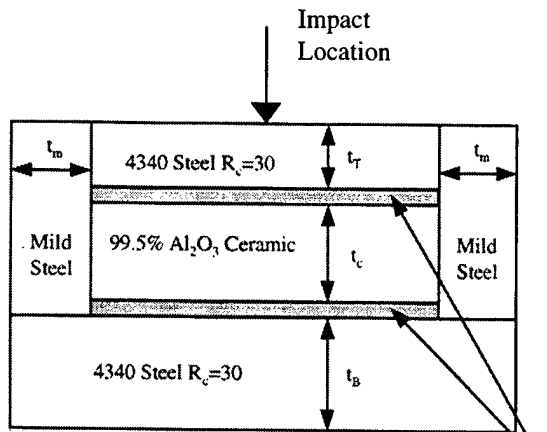
	Target 1			Target 2		
	scale			scale		
	1/3.15	1/6.30	1/12.60	1/3.15	1/6.30	1/12.60
t_T(mm)	38.10	19.05	9.53	57.15	28.58	14.29
t_c (mm)	50.80	25.40	12.70	76.20	38.10	19.05
t_B (mm)	50.80	25.40	12.70	76.20	38.10	19.05
t_i (mm)	6.35	3.18	1.59	6.35	3.18	1.59
t_m (mm)	25.4	12.70	6.35	25.40	12.70	6.35

Fiberfrax (isolator) Manufactured by Carborundum
Density = 100kg/m³ (thickness = t_i)

Tungsten Alloy Penetrator WN008FH manufactured by GTE
(90% W, 8% Ni, 2% Fe), ρ = 17190 kg/m³
UTS = 1.3 GPa, Elongation at failure = 8%, Rc = 43
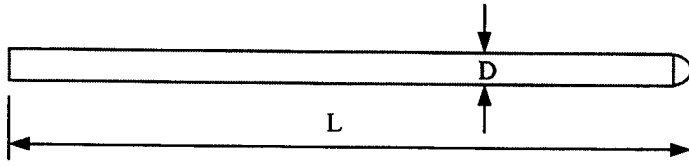
	Penetrator Characteristics		
Scale	D (mm)	L (mm)	Mass (g)
1/3.15	8.063	161.2	158.9
1/6.30	4.032	80.64	19.82
1/12.60	2.016	40.32	2.433

Figure 2.7.7.3   Target and Penetrator Descriptions for Perforation Experiments, Anderson *et al.* [36].
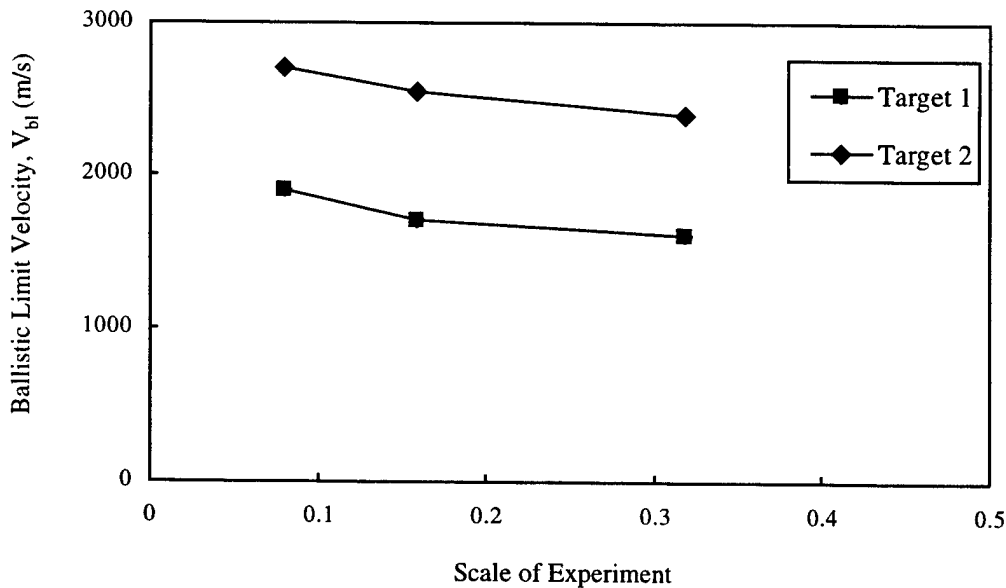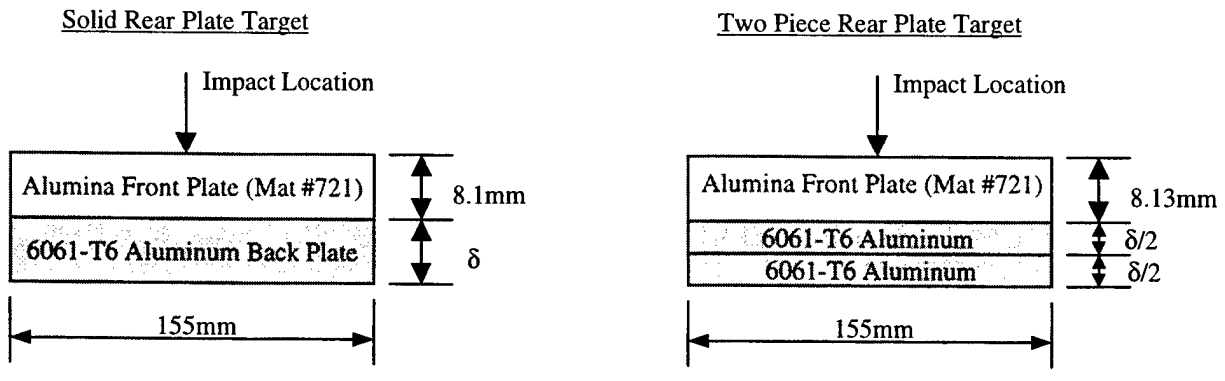

Figure 2.7.7.4   Ballistic Limit Velocity as a function of Experiment Scale and Target Configuration, Anderson *et al.* [36].
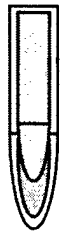
183

Table 2.7.7.2 Tabulated Experimental Results Investigating Scale Effects on Ballistic Limit Velocities, Anderson *et al.* [36].

Aluminum Oxide (high purity)								
Test Number	Material Number	Scale	Target	V_s (m/s)	γ (deg)	V_r/V_s	L_r/L_d	P/L	Ballistic Limit V_{BL} (m/s)
7707	723	1/3.15	1	2180	2.12	0.867	4.16	Perf	
7708	723	1/3.15	1	1920	2.00	0.766	2.90	Perf	
7709	723	1/3.15	1	1670	0.79	0.683	2.65	Perf	1600+-40
7710	723	1/3.15	1	1490	1.50	0.000	0.00	0.72	
7711	723	1/3.15	1	1560	0.56	0.000	0.00	0.97	
7712	723	1/3.15	1	1580	6.52	0.000	0.00	<0.63	
7713	723	1/3.15	1	1640	0.50	0.433	1.64	Perf	
7714	723	1/3.15	1	1610	0.35	0.106	-----	Perf	
7715	723	1/3.15	2	2190	1.50	0.000	0.00	1.40	
7716	723	1/3.15	2	2330	0.79	0.000	0.00	1.33	2400+-100
7717	723	1/3.15	2	2330	0.79	0.000	0.00	1.36	
7718	723	1/3.15	2	2190	2.70	0.000	0.00	1.15	
7719	723	1/6.30	1	2160	6.75	0.588	frag	Perf	
7720	723	1/6.30	1	1870	1.52	0.861	3.91	Perf	
7721	723	1/6.30	1	1630	3.53	0.000	0.00	0.88	
7722	723	1/6.30	1	1730	3.02	0.572	1.70	Perf	1710+-40
7723	723	1/6.30	1	2190	2.91	0.868	4.35	Perf	
7724	723	1/6.30	1	1820	2.55	0.544	0.94	Perf	
7725	723	1/6.30	1	1690	0.75	0.000	0.00	0.85	
7726	723	1/6.30	1	1730	0.56	0.225	1.13	Perf	
7727	723	1/6.30	2	2540	8.25	0.000	0.00	1.00	
7728	723	1/6.30	2	2540	3.29	0.000	0.00	1.31	
7729	723	1/6.30	2	2680	0.75	0.537	0.50	Perf	
7730	723	1/6.30	2	2670	5.52	------	-----	Perf	2550+-40
7731	723	1/6.30	2	2630	1.68	0.567	0.76	Perf	
7732	723	1/6.30	2	2620	6.91	0.000	0.00	0.19	
7733	723	1/6.30	2	2620	1.25	0.214	frag	Perf	
7734	723	1/6.30	2	2600	1.03	0.469	0.76	Perf	
7735	723	1/12.6	1	2140	8.30	0.000	0.00	0.84	
7736	723	1/12.6	1	2210	8.37	0.000	0.00	0.86	
7737	723	1/12.6	1	2460	7.19	0.610	frag	Perf	
7739	723	1/12.6	1	2300	11.86	0.000	0.00	0.85	1900+-160
7740	723	1/12.6	1	2300	5.12	0.739	1.26	Perf	
7741	723	1/12.6	1	2180	0.79	0.358	frag	Perf	
7742	723	1/12.6	1	2040	4.99	0.480	1.26	Perf	
7743	723	1/12.6	2	2390	2.02	0.000	0.00	1.26	
7744	723	1/12.6	2	2600	6.97	0.000	0.00	1.09	
7745	723	1/12.6	2	2690	13.64	0.000	0.00	0.96	2700+40-100
7746	723	1/12.6	2	2720	3.58	0.272	frag	Perf	
7747	723	1/12.6	2	2760	7.44	0.000	0.00	1.04	
7748	723	1/12.6	2	2760	14.10	0.000	0.00	<0.91	
7749	723	1/12.6	2	2720	13.81	0.000	0.00	<0.91	

V_s=strike (impact) velocity, γ = total yaw at impact, V_r=residual velocity, L_r = residual length
Test 7707-7749: the test data is from work by Anderson *et al.* [36]. The Ceramic was 99.5% pure Al_2O_3 manufactured by Ceradyne, no other information on the ceramic was given.
Test 7715: integrity of target was compromised before testing
Test 7712, 7748, 7749: penetration stopped in ceramic, measurement assumes ceramic was fully penetrated

Solid Rear Plate Target

Two Piece Rear Plate Target

Impact Location

Impact Location

| Alumina Front Plate (Mat #721) | 8.1mm |
| 6061-T6 Aluminum Back Plate | δ |

155mm

Alumina Front Plate (Mat #721)	8.13mm
6061-T6 Aluminum	δ/2
6061-T6 Aluminum	δ/2

155mm

7.62mm AP Penetrator

Mass = 9.45 g
L = 28.5mm
D = 7.62mm

Blunt Penetrator

Steel
ρ = 7800 kg/m^3
R_c = 28
Yield = 1.03 GPa
Failure strain = 7%
L = 31.5mm
D = 6.0 mm
Mass = 7.0g

Comments:
-Alumina is bonded to the Aluminum using Scotchdamp BA-9323.
-Targets are square.
-Nine 50mm x 50mm x 8.1mm alumina tiles are used in one target.

Figure 2.7.7.5   Target and Penetrator Descriptions for Perforation Experiments, Den Reijer [78].

Blunt Penetrator Impacting: 8.1mm Alumina Front Plate and various thickness 6061-T6 Aluminum Rear Plate

Rear Plate

—●— One Piece
—○— Two Piece

6061-T6 Aluminum Rear Plate Thickness, δ (mm)
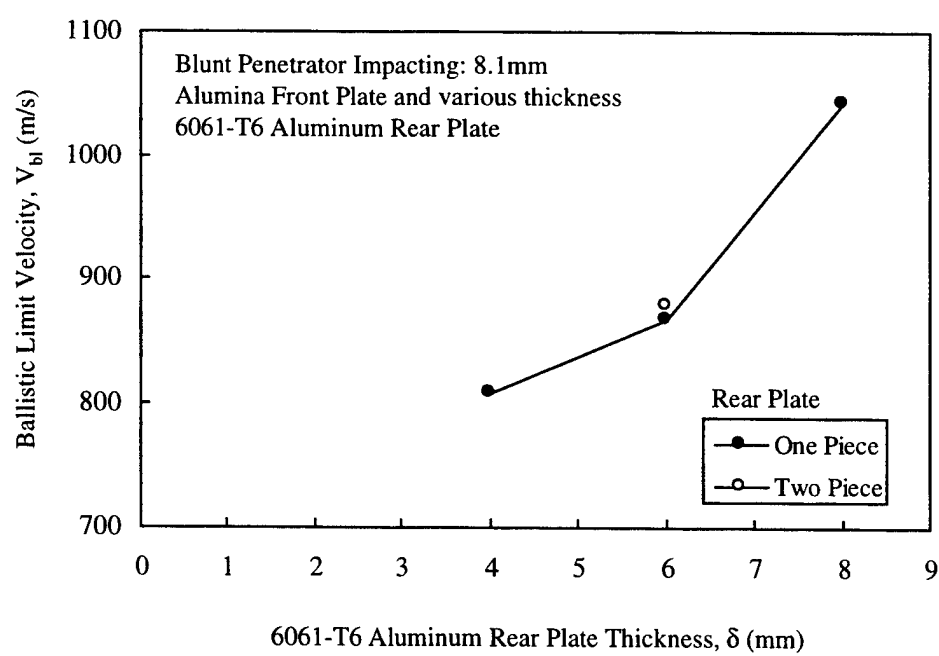
Figure 2.7.7.6   Ballistic Limit Velocity for Blunt Projectile as a function of Rear Plate Thickness and Configuration, Den Reijer [78].

185

Table 2.7.7.3   Summary of Ballistic Limit Velocities for Two Penetrator types against Various Target Configurations, Den Reijer [78].

Aluminum Oxide (high purity)					
Test Number	Material Number	Penetrator	Target Configuration		Ballistic Limit Velocity, V_{bl} (m/s)
			δ (mm)	Rear Plate	
7749	721	Blunt	4.0	One	808 +-21
7750	721	Blunt	6.0	One	866 +-50
7751	721	Blunt	6.0	Two	878 +-60
7752	721	Blunt	8.0	One	1043 +-48
7753	721	AP	6.0	One	841(see below)
7754	721	AP	6.0	Two	841(see below)

Test 7749-7754: the test data is from work by Den Riejer [78]. Two penetrator configurations were used, a blunt and Armor Piercing (AP). Target configurations consisted of alumina front plate bonded to a aluminum rear plate.The ballistic limit velocity was experimentally determined for each target configuration.

Test 7753-7754: the velocity listed is not the ballistic limit velocity, but the velocity at which the target just defeats the AP projectile. Thus, the ballistic limit velocity will be slightly higher.

Test 7751, 7754: the results from these experiment were unexpected. Wilkins et al. [23-28] showed a decrease in target effectiveness when two plates, instead of one, were used, the results from this work did not show this effect.

2.7.8 Other Test Data for Aluminum Oxide (high purity)

This section presents test data for experiments that do not fit into any of the previous sections. Typically the experiments that are reported in this section are more theoretical and unique in design than those reported previously. The following text briefly discusses the experiments presented in this section.

Experiments by Strassberger *et al.* [69] were designed to investigate the fracture propagation in ceramics. The damage velocity, V_d, was measured as a function of projectile impact velocity, V_p. The target and projectile descriptions are presented in Figure 2.7.8.1. The results of the experiments are summarized in Table 2.7.8.1 were the projectile impact velocity and damage velocity are tabulated. Figure 2.7.8.2 presents the results graphically. The damage velocity is defined as the fastest observed fracture velocity in the ceramic. The fracture propagation was observed by means of a Cranz-Schardin camera and photos of this process are presented in Reference 69.

Wise and Grady [70] performed experiments on confined and unconfined ceramic rods where both the axial (longitudinal) and transverse (radial) surface velocities were measured. The velocities were measured by means of a velocity interferometer (VISAR). The initial geometry of the experiment is presented in Figure 2.7.8.3. The initial conditions of the experiments are presented in Table 2.7.8.2. The particle velocity time histories are presented in Figure 2.7.8.4 where both the longitudinal and radial velocities are shown.
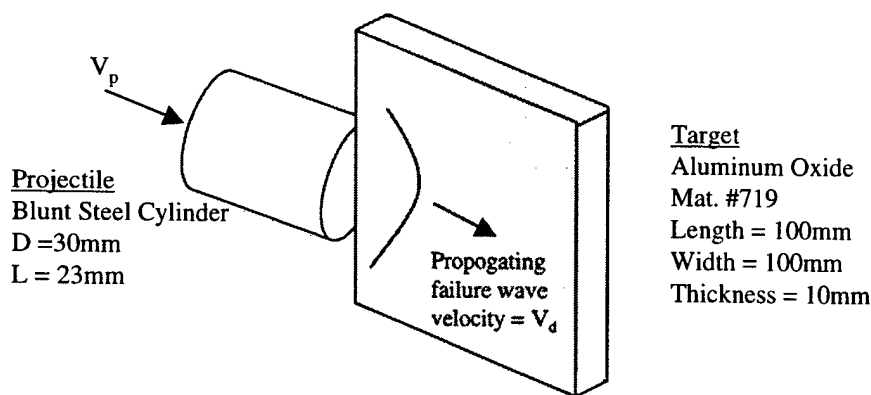

Figure 2.7.8.1 Target and Projectile Description for Fracture Experiment, Strassburger *et al.* [69].
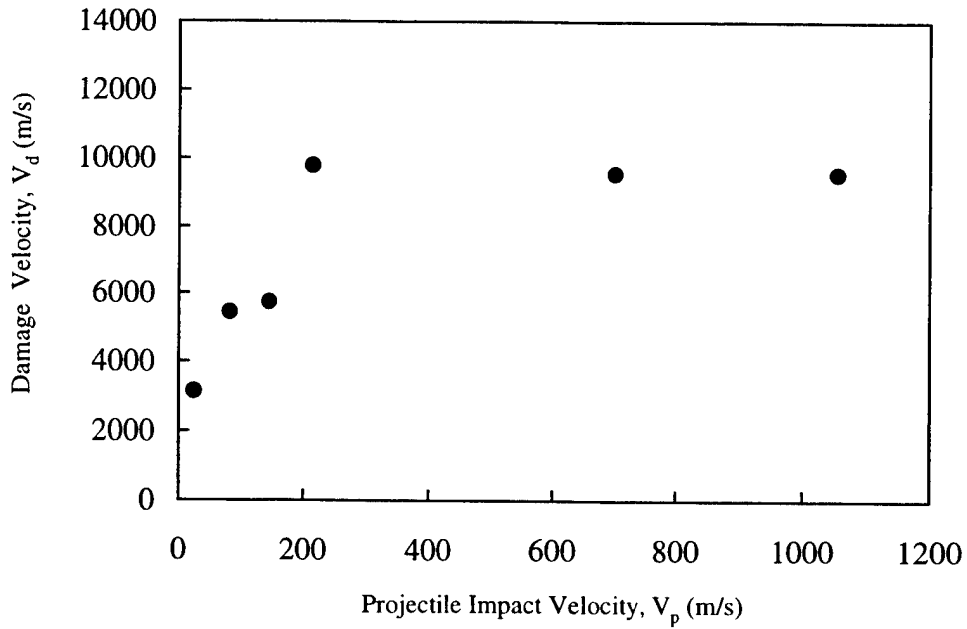
Figure 2.7.8.2 Damage Velocity in Ceramic vs. Projectile Impact Velocity, Strassburger *et al.* [69].

Table 2.7.8.1 Summary of Damage Velocity in Aluminum Oxide as a Function of Projectile Impact Velocity, Strassburger *et al.*[69].

Aluminum Oxide (high purity)			
Test Number	Material Number	Projectile Impact Velocity, V_p (m/s)	Damage Velocity V_d (m/s)
7801	719	27	3090
7802	719	85	5350
7803	719	150	5660
7804	719	219	9680
7805	719	706	9470
7806	719	1060	9470
Test 7801-7806: the test data is from work by Strassburger *et al.*[69]. The data were obtained from Figure 9c in Ref. 69.			

188

Impactor   **Confined or Unconfined Ceramic Target**
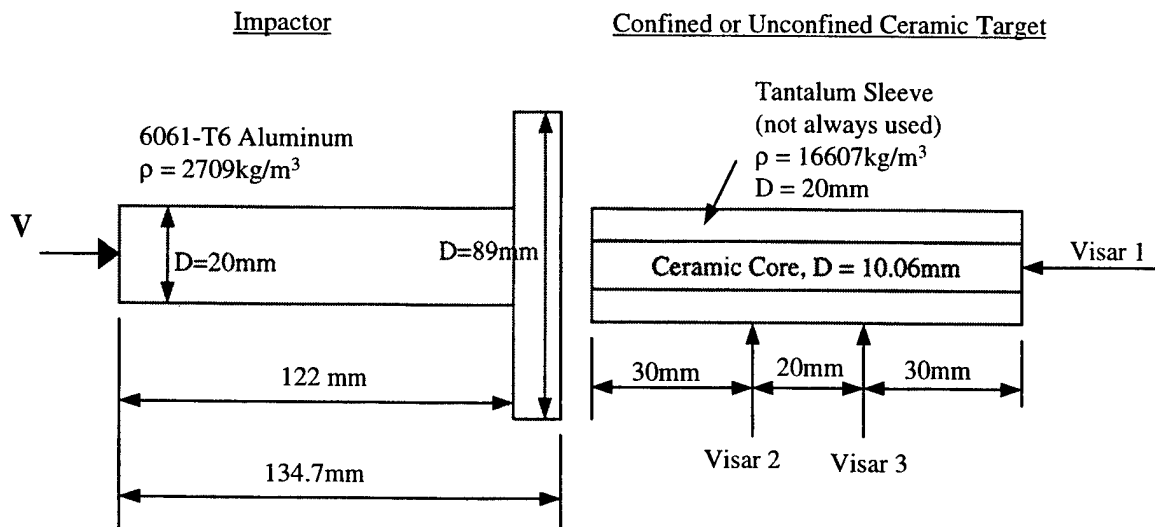
Figure 2.7.8.3 Initial Geometry for Aluminum Impactor and Ceramic Target and the Location of the Three VISARS, Wise and Grady [70].

Table 2.7.8.2 Summary of Intitial Conditions for Wise and Grady Experiments [70].

Aluminum Oxide (high purity)			
Test Number	Material Number	Impact Velocity V, (m/s)	Sleeve Material
7807	720	1035	None used
7808	720	1051	Tantalum
7809	720	2175	None used
7810	720	2182	None used
7811	720	2140	Tantalum
Test 7807-7811: the test data is from work by Wise and Grady [70]. Test 7807, 7809, 7810: no sleeve was used, bare ceramic only.			
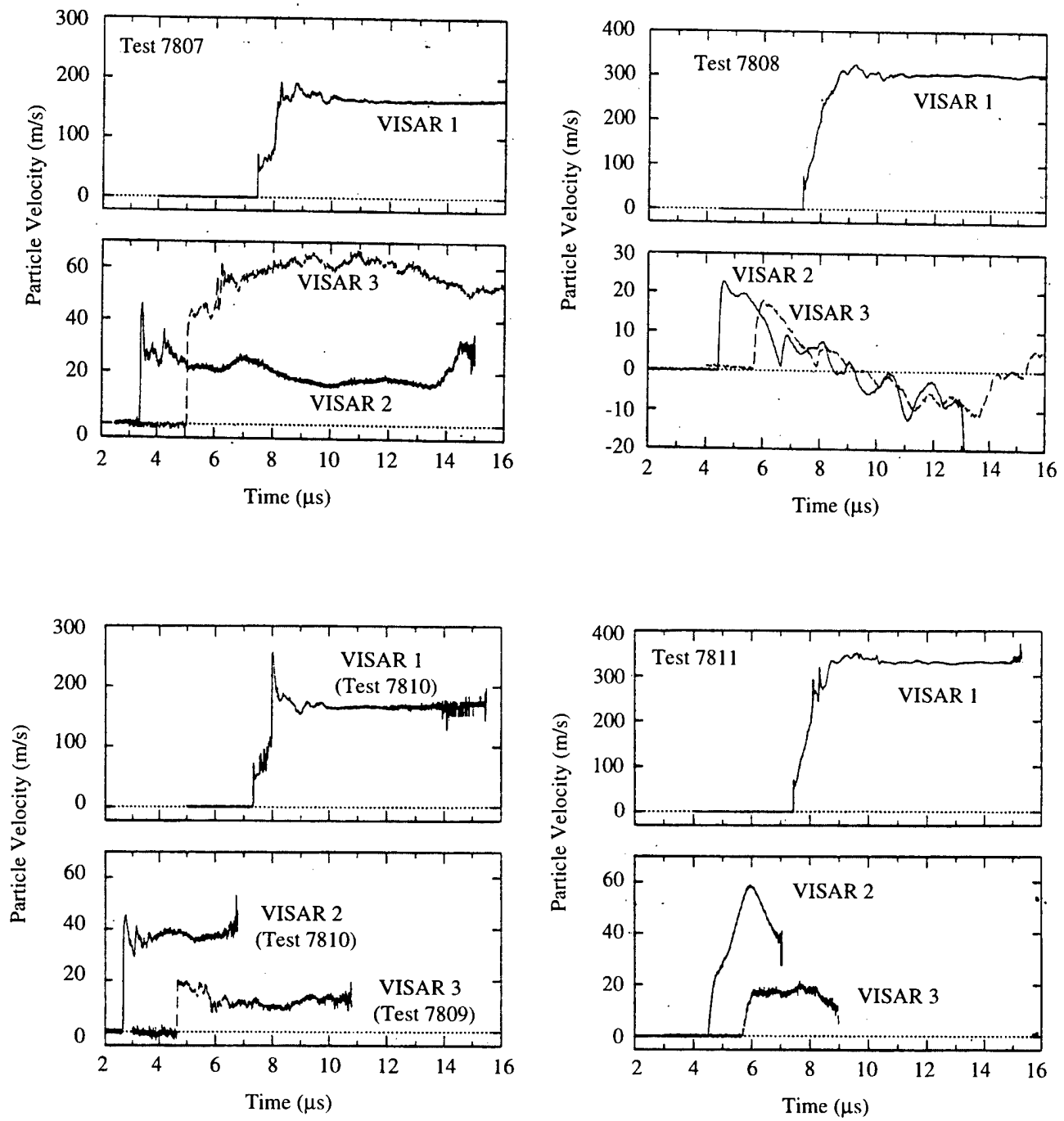
Figure 2.7.8.4 Particle Velocity Time Histories for Test 7807-7811, Wise and Grady [70].

2.8 TUNGSTEN CARBIDE

2.8.1 Material Description for Tungsten Carbide

The purpose of this section is to provide as much information as possible on the Tungsten Carbide materials tested. Descriptions for each of the Tungsten Carbide materials used in Section 2.8 are presented in Table 2.8.1.1. Each material is given a material number which is used throughout Section 2.8 to identify it. The data listed in Table 2.8.1.1 were obtained directly from the corresponding references. When specific information was not available it was left blank. The strength values listed, (Compressive, Tensile, HEL and Spall), are nominal values and are included for comparison purposes. Occasionally researchers will determine the chemical composition of the material being tested to further characterize it, Table 2.8.1.1 includes this data when available.

Table 2.8.1.1 Description of the Tungsten Carbide Materials Tested

	Material Number						
	801	802	803	804	805		
Reference	52, 54	52, 54	52	75	26		
Manufacturer	Kennametal	*	Cercom				
Trade Name/Description	K-68						
Processing	Sintered	Sintered	Hot Pressed				
Average Grain Size (μm)			0.9				
Density (kg/m³)	14930	14910	15560	15013	15240		
Void Fraction							
Longitudinal Velocity (m/s)	6900	6920	7040	6890			
Shear Velocity (m/s)	4170	4150	4300	4180			
Bulk Velocity (m/s)	4940	4990	4990	4917			
Young's Modulus, E (GPa)	630		692	634			
Shear Modulus, G (GPa)	260	257	288	262			
Bulk Modulus, K (GPa)	364	371	387	363			
Poisson's Ratio	0.213	0.219	0.202	0.209			
Compressive Strength (GPa)	5.8	4.4					
Tensile Strength (GPa)		0.25					
HEL (GPa)	~4	~4					
Spall Strength (GPa)	2.7	3.5					
Hardness Rockwell (R$_A$)	93	86-92					
Impurities (%wt)							
Co	5.7	0.05-0.2		5			
Ta	1.9						
Ni		3-4					
Fe		0.4-0.8					
Nb	<0.3						
Ti	<0.3						

* This material was extracted from the 14.5mm AP (BS-41) penetrator

2.8.4 Plate Impact Test Data for Tungsten Carbide

This section presents plate impact results using various Tungsten Carbide materials. A typical plate impact test configuration is presented in Figure 2.8.4.1. The peak stress, σ_z, occurs in the z-direction and is generally measured for both the elastic and plastic response. The lateral stresses, σ_x and σ_y, occur due to the uniaxial strain configuration of the experiment, and are typically not measured. The peak stress for the elastic regime is referred to as the Hugoniot Elastic Limit (HEL) and has become a fundamental property of ceramics. The peak stress for the plastic response is generally referred to as the peak Hugoniot stress. The particle velocity and wave velocity for both the elastic and plastic waves are typically measured and documented herein. In some cases the entire particle velocity time history is measured using laser velocity interferometry techniques (VISAR). VISAR traces provide direct information on the material response and are included in this section when available.

A description of the plate impact test configuration used by Grady and Moody [52] is presented in Figure 2.8.4.2. The specific test dimensions and some limited results are summarized in Table 2.8.4.1. Compression and release behavior of the Tungsten Carbide was measured by monitoring the ceramic-window interface velocity using laser velocity interferometry techniques (VISAR). The interface velocity profiles reflect the uniaxial strain loading and unloading behavior of the material and are presented in Figures 2.8.4.3-4 .

The results from the LASL Shock Hugoniot Data [75] are summarized in Table 2.8.4.2. The shock velocity, particle velocity, peak stress, σ_z, and density, ρ, for the plastic wave is presented.
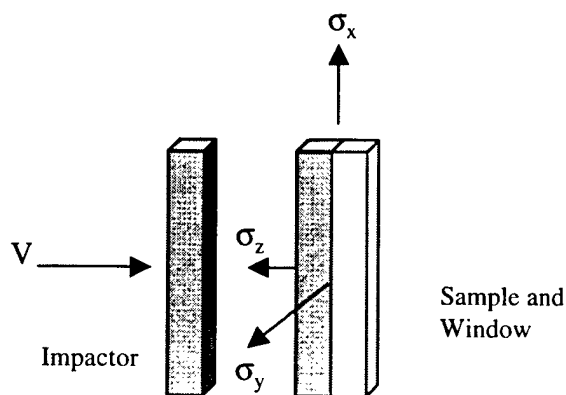

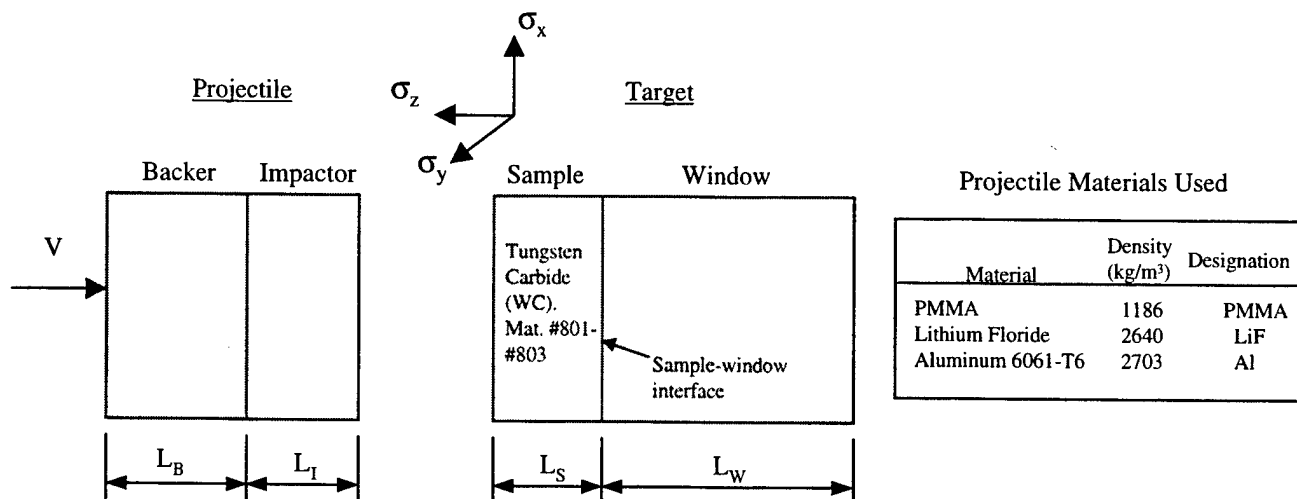Figure 2.8.4.1 Description of a Typical Plate Impact Test Configuration including Stress Orientations

Projectile σ_x Target

σ_z

Backer   Impactor σ_y Sample   Window   Projectile Materials Used

V

Tungsten
Carbide
(WC).
Mat. #801-
#803

Sample-window
interface

Material	Density (kg/m³)	Designation
PMMA	1186	PMMA
Lithium Floride	2640	LiF
Aluminum 6061-T6	2703	Al

L_B L_I L_S L_W

Figure 2.8.4.2 Description of the Plate Impact Test Configuration used by Grady and Moody [52] including the Stress Orientation and Materials used for the Projectile.

Table 2.8.4.1 Summary of Experimental Plate Impact Initial Conditions and Results from Grady and Moody [52].

Tungsten Carbide														
		Projectile				Target				Hugoniot Results				
Test Number	Material Number	V (m/s)	Backer		Impactor		Sample		Window		Elastic Compression		Plastic Compression	
			Material	L_B (mm)	Material	L_I (mm)	Density (kg/m³)	L_S (mm)	Material	L_W (mm)	σ_z (GPa)	ρ (kg/m³)	σ_z (GPa)	ρ (kg/m³)
8401	801	1141	PMMA	5.82	WC	3.370	14930	6.566	LiF	25.4			51.4	16507
8402	801	1566	PMMA	5.91	WC	3.363	14930	6.542	LiF	25.4			72.7	17097
8403	801	405	PMMA	5.90	Al	1.030	14930	3.357	LiF	25.4				
8404	802	1039	Air	-----	Al	12.87	14910	2.985	LiF	9.542			15.3	15318
8405	802	687	Air	-----	Al	12.51	14910	2.994	LiF	9.45				
8406	802	361	PMMA	5.85	Al	1.047	14910	2.986	LiF	9.47				
8407	802	446	PMMA	5.91	Al	1.038	14910	2.980	LiF	9.54				
8408	803	1660	PMMA	5.82	WC	6.200	15560	6.178	LiF	19.0				
8409	803	362	PMMA	5.90	Al	1.507	15560	6.192	LiF	19.0				
8410	803	454	PMMA	5.90	Al	1.500	15560	6.190	LiF	18.9				

Test 8401-8410: the test data is from work by Grady and Moody [52]. Three different materials were tested. The above table provides the initial conditions for the plate impact experiments, and includes when available, the hugoniot stress state. The associated interface wave profiles can be found on the following pages.
Test 8401, 8402, 8404: The Hugoniot stress and density obtained from Figure 8.6 in Ref. 54.
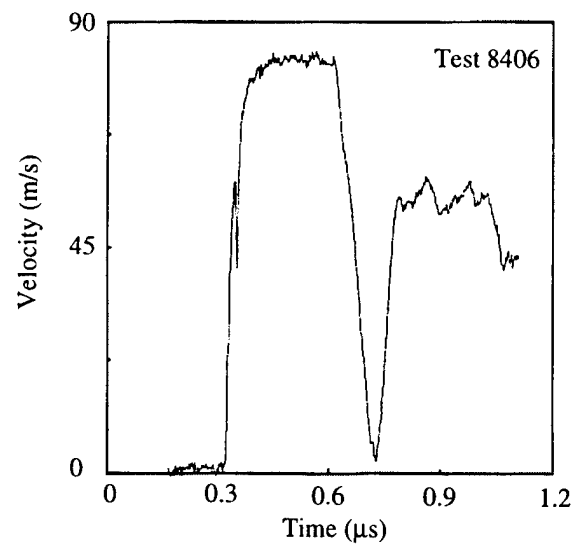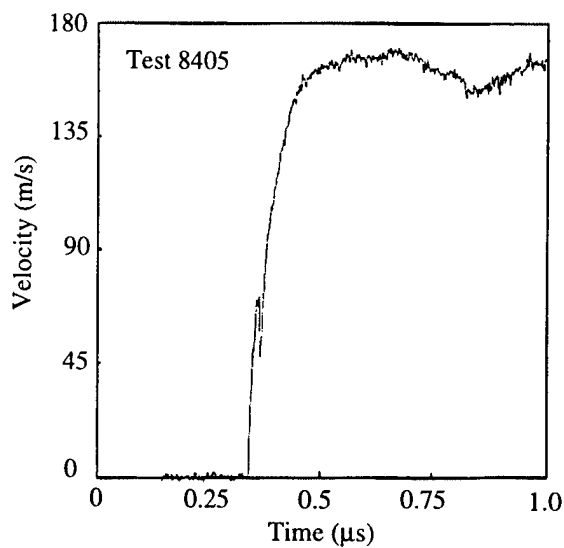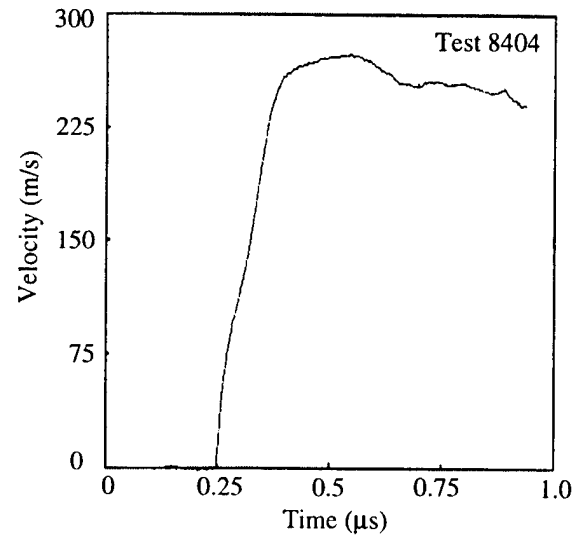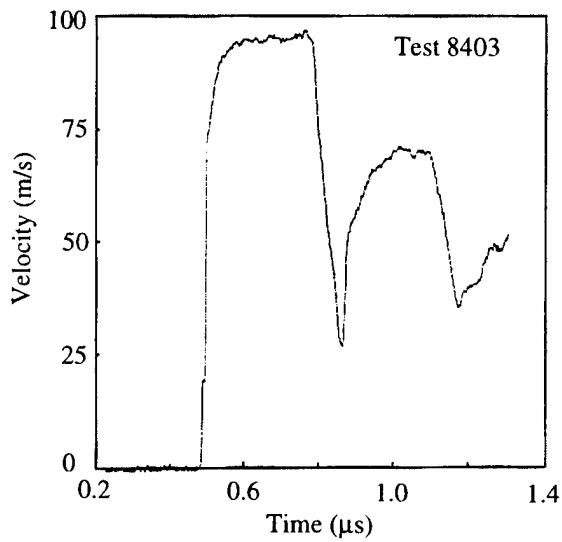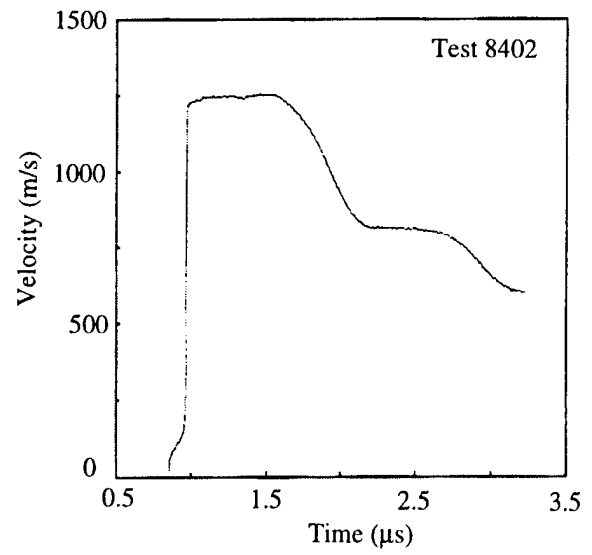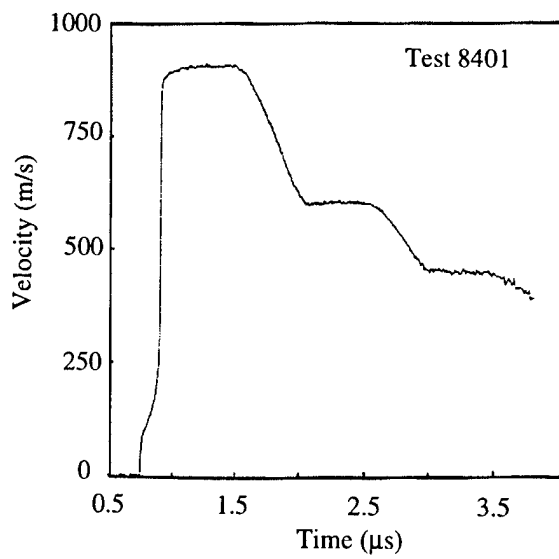
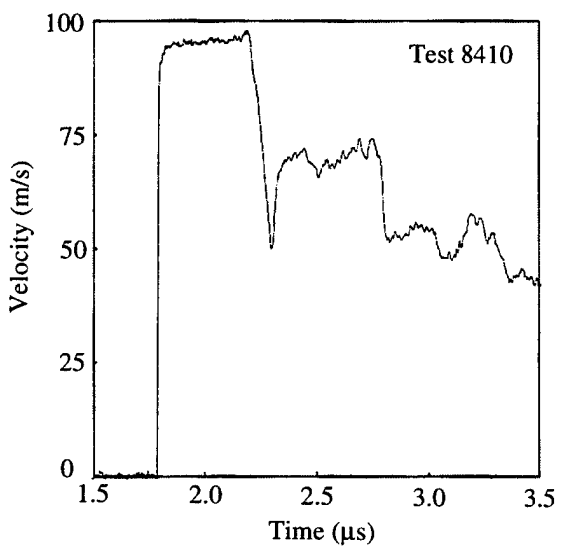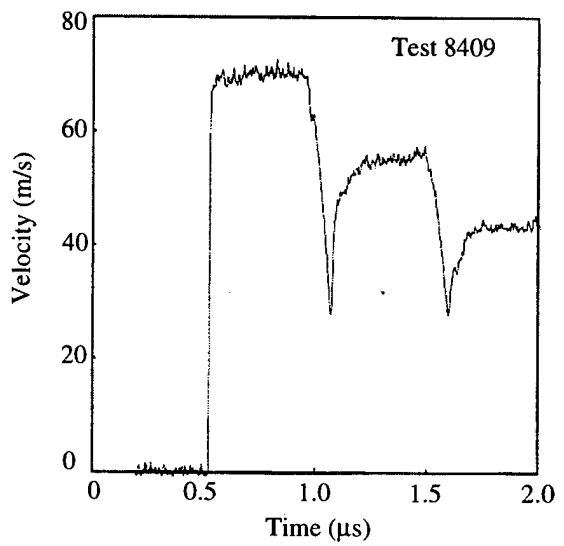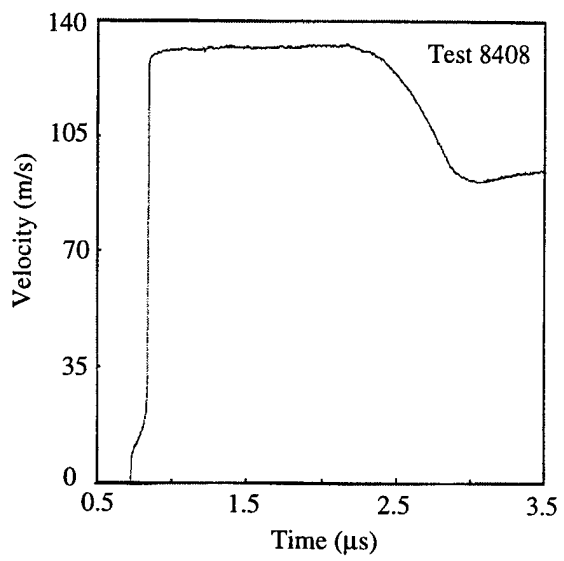Figure 2.8.4.3 Ceramic-Window Interface Velocity Profiles from Grady and Moody [52] for Tests 8401-8406.
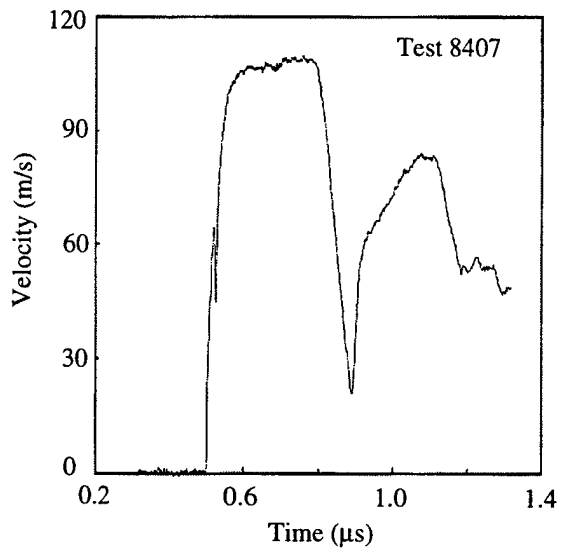
Figure 2.8.4.4 Ceramic-Window Interface Velocity Profiles from Grady and Moody [52] for Tests 8407-8410.

Table 2.8.4.2 Summary of Experimental Plate Impact Results, [75]

Test Number	Material Number	Initial Density ρ_o (kg/m³)	Elastic Regime (HEL)*				Plastic Regime			
			Shock Velocity (m/s)	Particle Velocity (m/s)	σ_z (GPa)	ρ (kg/m³)	Shock Velocity (m/s)	Particle# Velocity (m/s)	σ_z (GPa)	ρ (kg/m³)
8410	804	15050					5569	220	18.439	15669
8411	804	15010					5706	351	30.062	15994
8412	804	15010					5671	369	31.410	16055
8413	804	15000					5734	437	37.586	16237
8414	804	15060					5720	440	37.903	16315
8415	804	15020					5965	679	60.835	16949
8416	804	14990					6008	712	64.123	17005
8417	804	14990					5971	750	67.129	17143
8418	804	14990					6857	1445	148.526	18992
8419	804	15030					6927	1484	154.503	19128
8420	804	15020					6912	1489	154.585	19144
8421	804	15000					7108	1712	182.533	19759
8422	804	15010					7175	1751	188.577	19856
8423	804	15010					7334	1819	200.242	19961

Test 8410-8423: the test data is from LASL Shock Hugoniot Data [75].
* The elastic regime was not documented.

196

2.8.7 Perforation Test Data for Tungsten Carbide

This section presents perforation experiments where the target is usually perforated by the penetrator. Targets are typically comprised of a ceramic front layer and a metallic rear layer and are commonly used in light armor applications. The most common piece of data extracted from perforation experiments is the target ballistic limit, V_{bl}, previously defined in Section 2.0.

The target and penetrator description for the perforation experiments by Wilkins *et al.* [26]. is presented in Figure 2.8.7.1. The results of the experiments are summarized in Table 2.8.7.1 were the ballistic limit velocity, V_{bl}, is provided.

Target Configuration

Sharp Penetrator

Impact location

Tungsten Carbide

$\Delta = 6.35$mm

6061-T6 Aluminum Back Plate

$\delta = 6.35$mm

Allegheny Steel 609
$R_c = 54\text{-}56$
$M = 8.32$g
$L \sim 29$ mm
$D = 7.62$ mm
cone angle $= 55°$
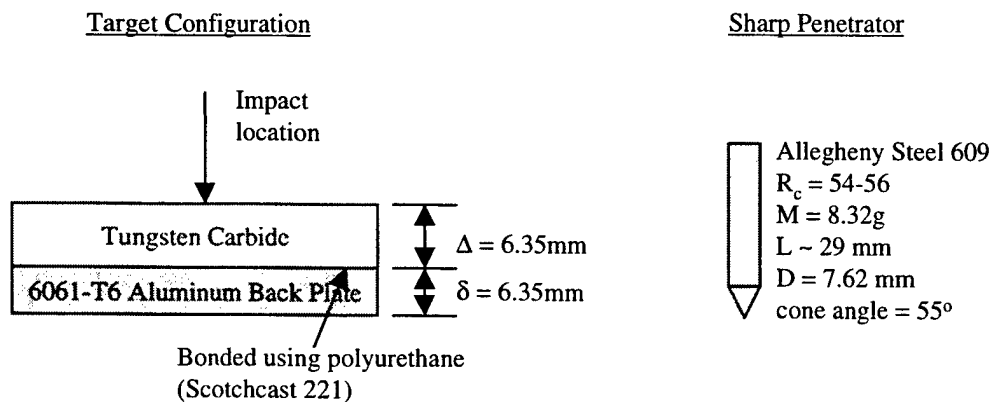
Bonded using polyurethane
(Scotchcast 221)

Figure 2.8.7.1   Target and Penetrator Descriptions for Perforation Experiments, Wilkins *et al.* [26].

Table 2.8.7.1   Ballistic Limit Velocity for a Sharp Penetrator against a Tungsten Carbide Target, Wilkins *et al.* [26].

Tungsten Carbide					
Test Number	Material Number	Penetrator	Target Configuration		Ballistic Limit Velocity, V_{bl} (+- 60m/s)
			Δ (mm)	δ (mm)	
8701	805	Sharp	6.35	6.35	1010
Test 8701: the test data is from work by Wilkins *et al.* [26]. No material information other then the density = 15240kg/m³was given.					

197

2.9 GLASS

2.9.1 Material Description for Glass

The purpose of this section is to provide as much information as possible on the Glass materials tested. Descriptions for each of the Glass materials used in Section 2.9 are presented in Table 2.9.1.1. Each material is given a material number which is used throughout Section 2.9 to identify it. The data listed in Table 2.9.1.1 were obtained directly from the corresponding references. When specific information was not available it was left blank. The strength values listed, (Compressive, Tensile, HEL and Spall), are nominal values and are included for comparison purposes. Occasionally researchers will determine the chemical composition of the material being tested to further characterize it, Table 2.9.1.1 includes this data when available.

Table 2.9.1.1   Description of the Glass Materials Tested

	Material Number					
	901	902	903	904	905	906
Reference	7	41	43	47	62	80
Manufacturer	Schott Glaswerke		Schott Glaswerke			
Trade Name/Description	Float Glass	Soda Lime Glass	Float Glass	Soda Lime Glass	Glass	Soda Lime Glass
Processing						
Average Grain Size (μm)						
Density (kg/m^3)	2530	2500	2500	2500	2480	2500
Void Fraction						
Longitudinal Velocity (m/s)	5828		5860	5840	5850	5750
Shear Velocity (m/s)	3468					
Bulk Velocity (m/s)	4234					
Young's Modulus, E (GPa)	74.8	69				
Shear Modulus, G (GPa)	30.4					
Bulk Modulus, K (GPa)	45.4					
Poisson's Ratio	0.23					
Compressive Strength (GPa)	1.02	0.97				
Tensile Strength (GPa)	0.15					
HEL (GPa)	5.95			6.4		
Spall Strength (GPa)				>3.0		
Impurities (%wt)						
SiO$_2$	73.7		70		72.2	
Na$_2$O	10.6		15*		14.1	
CaO	9.4		12#			
MgO	3.1				0.1	
Al$_2$O$_3$	1.8		1		0.5	
K$_2$O	1.1					
Fe$_2$O$_3$	0.2				0.08	
CuO					12.4	
SO$_3$					0.43	

* (Na$_2$O + K$_2$O)
# (CaO + MgO)

199

2.9.2 Mechanical Test Data for Glass

The following section presents mechanical test results for various Glass materials. A typical test specimen showing the stress configuration is shown in Figure 2.9.2.1. Compression is taken as positive and tension as negative. Loading is generally uniaxial in the z direction and is increased until the material fails, although some researchers use more complex loading techniques to vary the stress state at failure.

Mechanical test data performed by Holmquist et al. [7] are presented in Table 2.9.2.1. The stress state at failure is given as a function of average strain rate, $\dot{\varepsilon}$. Compression is taken as positive and tension as negative.
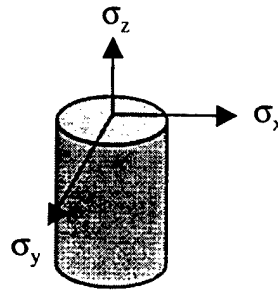

Figure 2.9.2.1 Description of a Typical Mechanical Test Specimen.

Table 2.9.2.1 Summary of Experimental Results, Holmquist *et al.*[7].

Glass					
Test Number	Material Number	σ_z (GPa)	σ_x (GPa)	σ_y (GPa)	$\sim \dot{\varepsilon}$ (s^{-1})
9201	901	1.12	0	0	1×10^{-3}
9202	901	0.92	0	0	1×10^{-3}
9203	901	1.17	0	0	1×10^{-3}
9204	901	0.88	0	0	1×10^{-3}
9205	901	1.45	0	0	2.5×10^2
9206	901	1.10	0	0	2.5×10^2
9207	901	1.05	0	0	2.5×10^2
9208	901	1.00	0	0	2.5×10^2
9209	901	0	0.48	-0.16	1×10^{-3}
9210	901	0	0.52	-0.17	1×10^{-3}
9211	901	0	0.35	-0.12	1×10^{-3}

Test 9201-9211: The test data is from Holmquist *et al.* [7].
Test 9201-9208: Compression tests were performed to obtain the compressive strength as a function of strain rate. The highest strain rate used a Hopkinson bar system.
Tests 9209-9211: Tested in the configuration referred to as the "Brazilian test" [8]. The specimen is compressed in the σ_x direction resulting in tension in the σ_y direction.The specimen fails in tension.

2.9.4 Plate Impact Test Data for Glass

This section presents plate impact results, performed by numerous researchers, using various Glass materials. A typical plate impact test configuration is presented in Figure 2.9.4.1. The peak stress, σ_z, occurs in the z-direction and is generally measured for both the elastic and plastic response. The lateral stresses, σ_x and σ_y, occur due to the uniaxial strain configuration of the experiment, and are typically not measured. The peak stress for the elastic regime is referred to as the Hugoniot Elastic Limit (HEL) and has become a fundamental property of ceramics. The peak stress for the plastic response is generally referred to as the peak Hugoniot stress. The particle velocity and wave velocity for both the elastic and plastic waves are typically measured and documented herein. In some cases the entire particle velocity time history is measured using laser velocity interferometry techniques (VISAR). VISAR traces provide direct information on the material response and are included in this section when available.

The results from Dremin and Adadurov [62] are summarized in Table 2.9.4.1. Plate impact experiments were performed on Glass to obtain peak Hugoniot stress states. No distinction was made between the elastic and plastic stress states and the HEL was not documented. All the data was assumed to have exceeded the HEL and are thus all listed under the plastic regime. The shock velocity, particle velocity, peak stress, σ_z, and density, ρ, for the plastic wave were obtained.

A description of the plate impact experiments performed by Rosenberg et al. [47] is presented in Figure 2.9.4.2. The objective of this work was to investigated spall behavior as a function of peak longitudinal stress. Plate impact experiments were performed on Soda Lime Glass using in-material Manganin gauges to determine spall strength. The results are summarized in Table 2.9.4.2.

A description of the plate impact experiments by Holmquist et al. [7] are presented in Figure 2.9.4.3. The objective of this work was to obtain the HEL, Hugoniot stress-density state and particle velocity time histories from VISAR data. Three plate impact experiments were performed and the results are summarized in Table 2.9.4.3. The particle velocity time history profiles reflect the uniaxial strain loading and unloading behavior of the material and are presented in Figure 2.9.4.4.

A description of the plate impact experiments by Bless et al. [80] are presented in Figure 2.9.4.5. The objective of this work was to determine the lateral and transverse stress using in-material Manganin gauges. By obtaining both stresses the hydrostatic pressure and shear strength can be directly determined. Eight experiments were performed and the results are summarized in Table 2.9.4.4.

σ_x

V →

Impactor
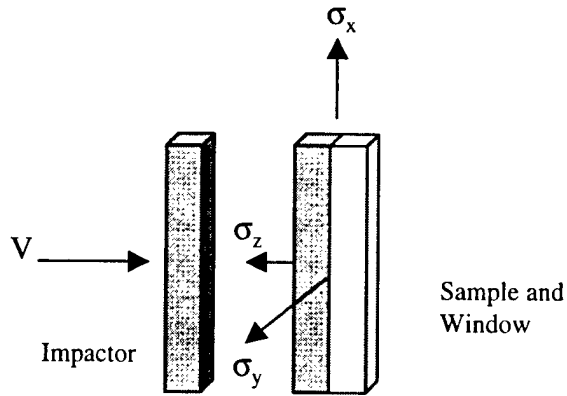
σ_z

σ_y

Sample and
Window

Figure 2.9.4.1 Description of a Typical Plate Impact Test Configuration including Stress Orientations

Table 2.9.4.1 Summary of Experimental Plate Impact Results, Dremin and Adadurov [62].

Glass										
Test Number	Material Number	Initial Density ρ_o (kg/m^3)	Elastic Regime (HEL)*				Plastic Regime			
			Shock Velocity (m/s)	Particle Velocity (m/s)	σ_z (GPa)	ρ (kg/m^3)	Shock Velocity (m/s)	Particle# Velocity (m/s)	σ_z (GPa)	ρ (kg/m^3)
9401	905	2480					3560	370	3.3	2793
9402	905	2480					3740	490	4.6	2882
9403	905	2480					4000	710	7.1	3040
9404	905	2480							8.9	3155
9405	905	2480							9.8	3226
9406	905	2480							10.5	3311
9407	905	2480							10.9	3322
9408	905	2480							11.8	3413
9409	905	2480							14.0	3636
9410	905	2480					4420	1510	16.7	3802
9411	905	2480					4450	1550	17.3	3831
9412	905	2480					5300	1960	26.0	3968
9413	905	2480					5900	2200	32.6	3984
9414	905	2480					6400	2570	41.0	4184
Test 9401-9414: the test data is from Dremin and Adadurov [62]. * The elastic regime was not documented.										

Projectile　　　　　　　Target

Impactor　　　Sample　　Window

V

Glass
Mat. #904

PMMA

Manganin
Gauge

L_I

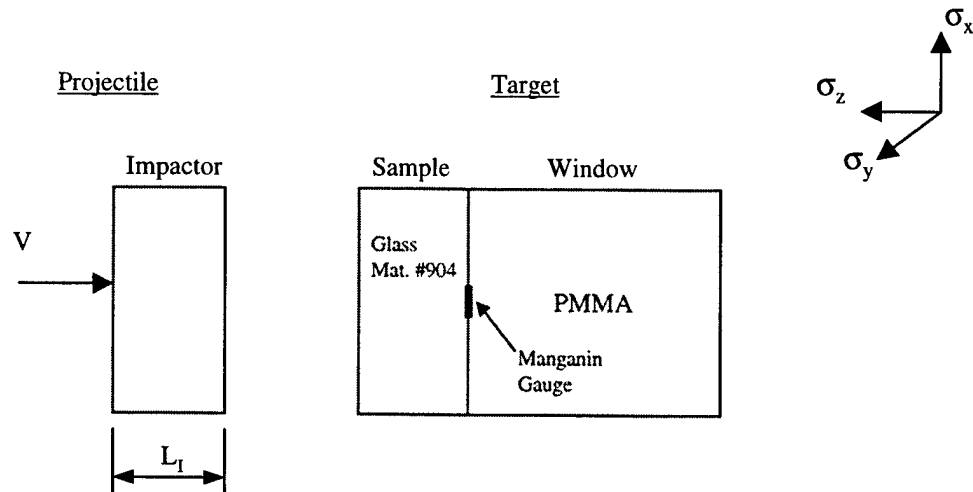σ_x
σ_z
σ_y

Figure 2.9.4.2 Description of Plate Impact Test Configuration, Rosenberg *et al.* [47].

Table 2.9.4.2 Summary of Experimental Plate Impact Results, Rosenberg *et al.* [47].

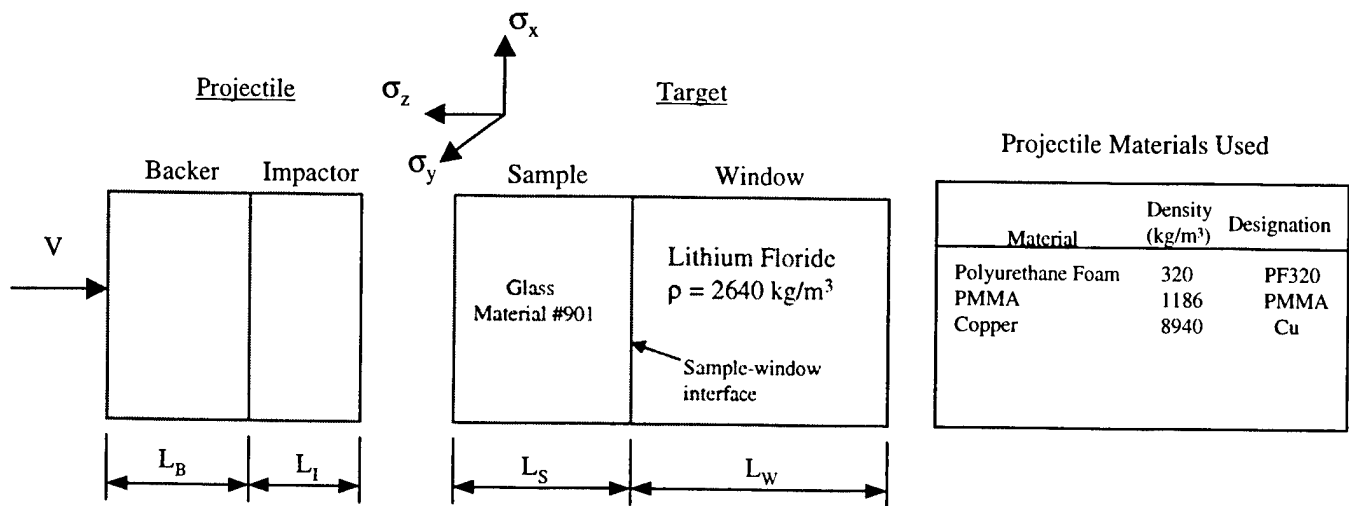| Glass									
Test Number	Material Number	Projectile Initial Conditions			Results				
		V (m/s)	L_I (mm)	Material	Elastic Regime		Plastic Regime		Spall (GPa)
					σ_z (GPa)	ρ (kg/m^3)	σ_z (GPa)	ρ (kg/m^3)	
9415	904	277	2.0	Aluminum	2.1				>1.2
9416	904	745	3.14	Aluminum	5.7				>3.0
9417	904	906	3.9	Aluminum	6.4		6.8		0.0
9418	904	746	3.0	Steel	6.4		7.3		0.0
Test 9404-9407: the test data is from work by Rosenberg *et al.* [47]. Plate impact experiments were performed on Soda Lime Glass using in-material manganin gauges to determine spall strength. Test 9415: Peak stress below HEL, no spall, peak tension in glass = 1.2 GPa Test 9416: Peak stress below HEL, no spall, peak tension in glass = 3.0 GPa Test 9417: Peak stress above HEL, spall signal with zero strength Test 9418: Peak stress above HEL, spall signal with zero strength									

Figure 2.9.4.3 Description of Plate Impact Test Configuration, Holmquist *et al.* [7].

Table 2.9.4.3 Summary of Experimental Plate Impact Results, Holmquist *et al.* [7].

Glass											
		Projectile Initial Conditions				Target Initial Conditions		Results			
Test Number	Material Number	V (m/s)	Backer		Impactor		Sample	Window	Elastic Regime		Plastic Regime	
			Material	L_B (mm)	Material	L_I (mm)	L_S (mm)	L_W (mm)	σ_z (GPa)	ρ (kg/m³)	σ_z (GPa)	ρ (kg/m³)
9419	901	1990	PF320	6.0	Glass	6.0	6.0	25.4	5.95	2718	11.46	3285
9420	901	2380	PF320	6.0	Glass	6.0	6.0	25.4	5.95	2718	14.25	3408
9421	901	1940	PF320	12.8	Copper	2.4	6.0	25.4	5.95	2718	18.76	3617

Test 9419-9421: the test data is from work by Holmquist *et al.* [7]. Plate impact experiments were performed on Float Glass (density = 2530kg/m³) to obtain Hugoniot and wave profiles.
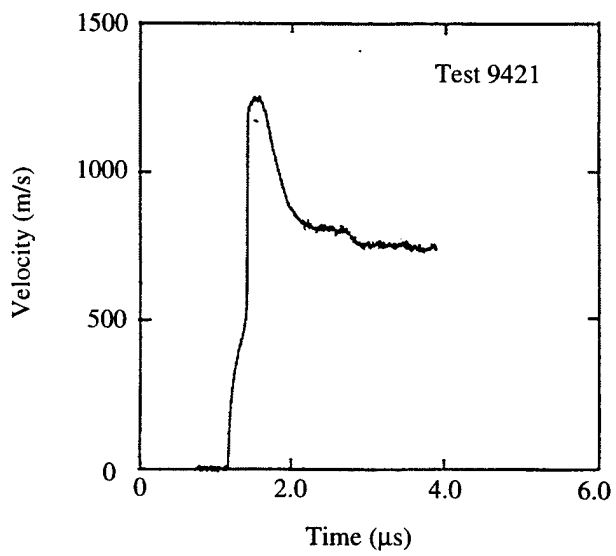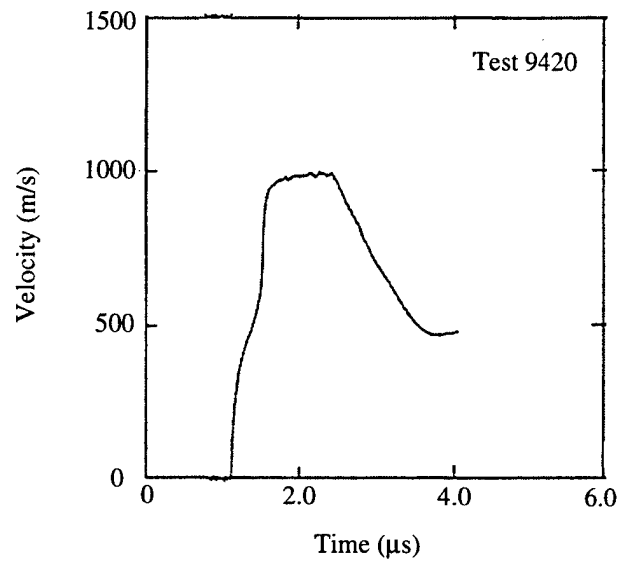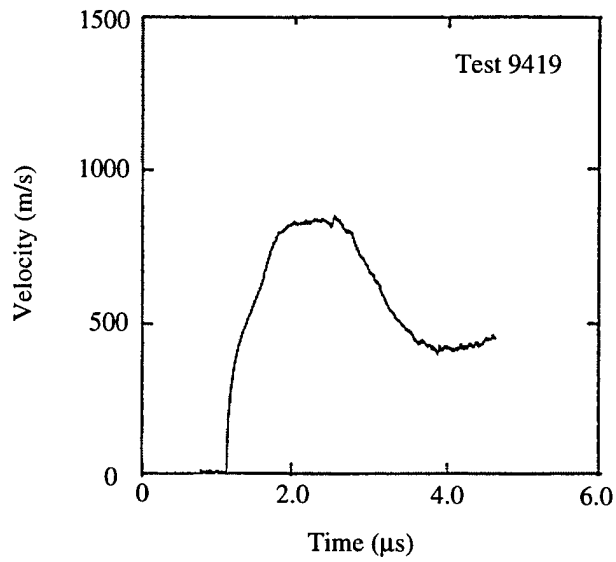
204

Figure 2.9.4.4 Ceramic-Window Interface Velocity Profiles from Holmquist *et al*. [7] for Tests 9419-9421.
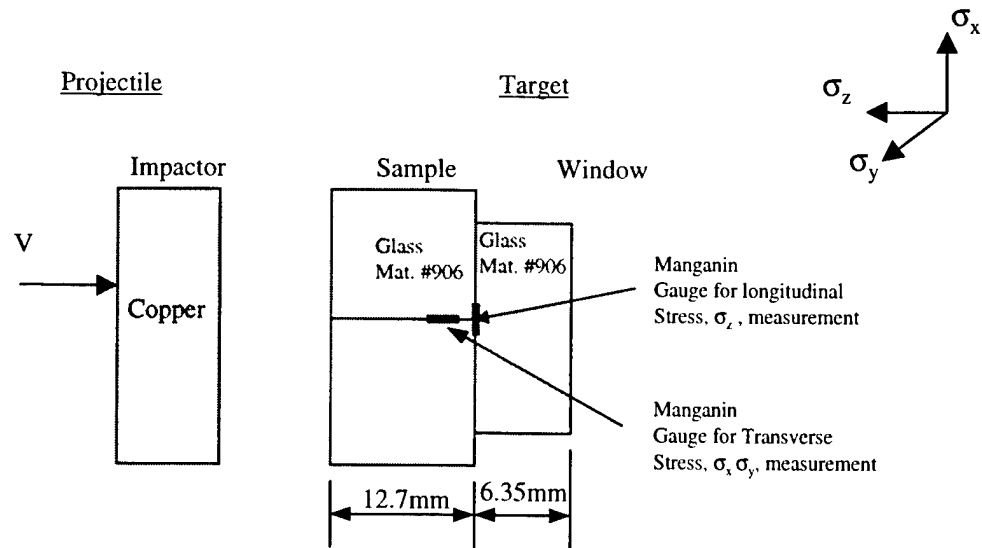
Figure 2.9.4.5 Description of Plate Impact Test Configuration, Bless *et al.* [80].

Table 2.9.4.4 Summary of Experimental Plate Impact Results by Bless *et al.* [80].

Glass						
Test Number	Material Number	Elastic Regime (HEL)			Plastic Regime (peak Hugoniot stress)		
		σ_z (GPa)	$\sigma_y = \sigma_x$ (GPa)	ρ (kg/m^3)	σ_z (GPa)	$\sigma_y = \sigma_x$ (GPa)	ρ (kg/m^3)
9422	906	2.8	0.9				
9423	906	5.4	1.9				
9424	906	6.0	2.0		7.0	3.3	
9425	906	6.0	2.0		9.2	5.1	
9426	906	6.0	2.0		11.3	8.5	
9427	906	6.0	2.0		12.4	9.9	
9428	906	6.0	2.0		12.6	9.7	
9429	906	6.0	2.0		13.1	9.8	

Test 9422-9429: The test data is from work by Bless *et al.*[80]. The material is Soda Lime Glass having an initial density = 2500kg/m3. Both longitudinal and transverse stresses were measured using in-material manganin gauges. The above tabulated data was obtained from Figure 3, Reference 80.
Test 9422, 9423: Peak stress did not exceed the HEL, but remained in the elastic regime.
Test 9424-9429: Peak stress exceeded the HEL. The Documented HEL for this material is 6.0 +-0.5GPa.

2.9.5 Penetration (semi-infinite) Test Data for Glass

Penetration results, into semi-infinite Glass, are presented in this section. Anderson *et al.* [9] performed penetration experiments into Glass at two impact velocities, 1250m/s and 1700m/s. The penetrator tip and tail positions were measured as a function of time and the final penetration depths were also obtained. The target and penetrator used are described in Figure 2.9.5.1. The penetration time histories are presented graphically in Figure 2.9.5.2 and in tabular form in Table 2.9.5.1.

Taylor *et al.* [79] performed penetration experiments of spheres of various diameter and material into a soda lime glass target at a nominal impact velocity of 5000 m/s. The experiments investigated soda lime glass penetration as a function of sphere diameter and material. The target and sphere configuration is presented in Figure 2.9.5.3. The penetration results are presented graphically in Figure 2.9.5.4 where the normalized penetration is shown as a function of projectile density. The results are also summarized in Table 2.9.5.2.

Target   Penetrator

Impact Location

Glass
(stacked 19mm sheets)
Material 701

200mm

Mild Steel Backing

150mm

Tungsten-sintered alloy
ρ = 17600kg/m3
UTS = 1.20 GPa
Elongation to failure = 10%
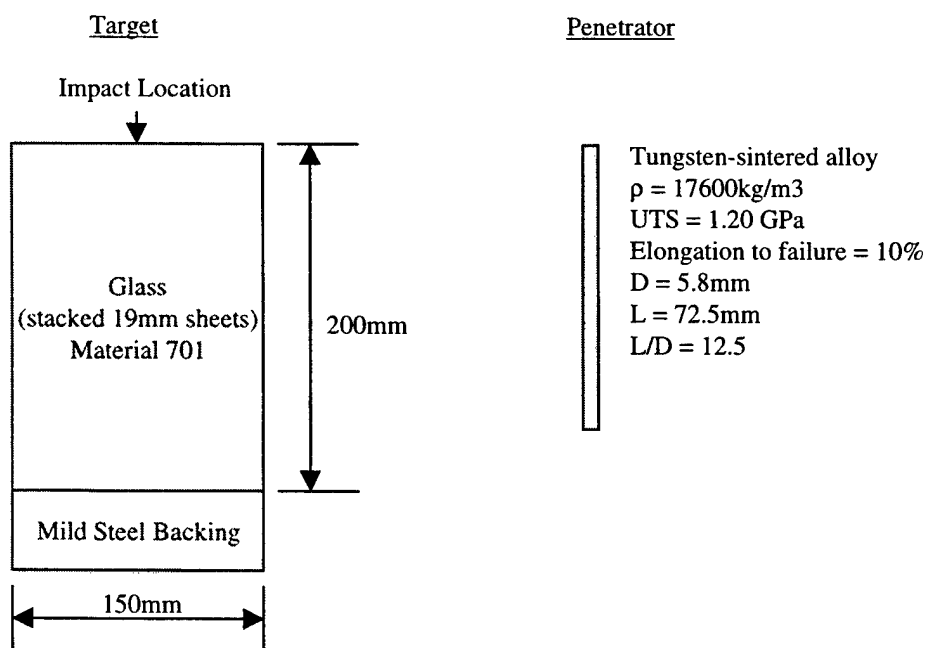D = 5.8mm
L = 72.5mm
L/D = 12.5

Figure 2.9.5.1 Glass Target and Penetrator Description, Anderson *et al.* [9].
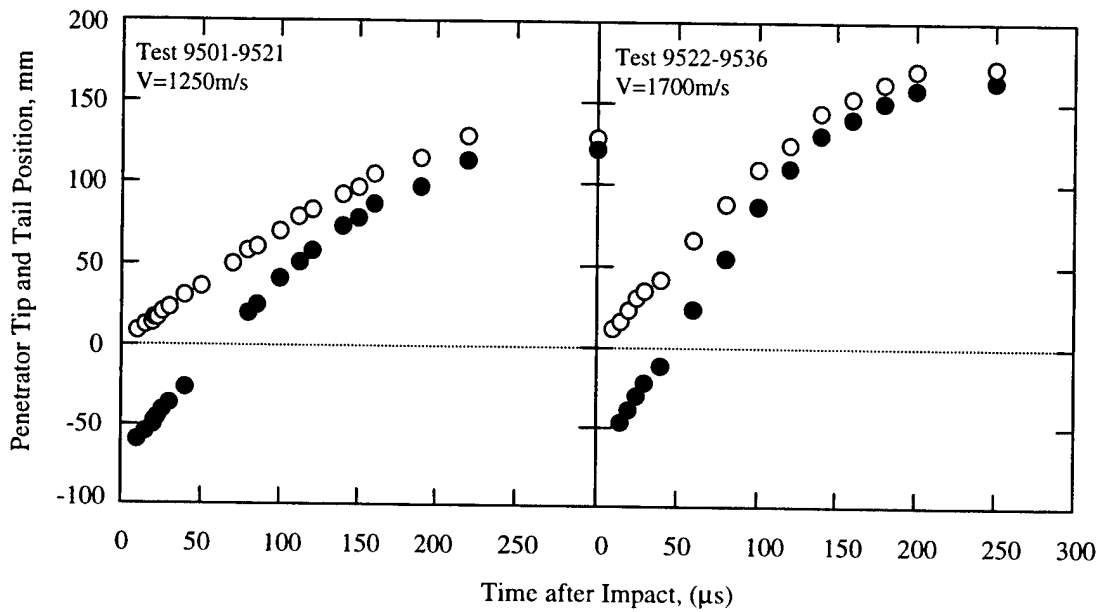
Figure 2.9.5.2 Penetrator Tip and Tail Position as a Function of Time for Two
Impact Velocities, Anderson *et al.* [9].

Table 2.9.5.1 Summary of Experimental Results, Anderson *et al.* [9].

Glass					
Test Number	Material Number	Impact Velocity (m/s)	Time after Penetrator impact (μs)	Penetrator Position	
				Tip (mm)	Tail (mm)
9501	901	1250	10	8	-60
9502	901	1250	16	12	-53
9503	901	1250	18	13	-50
9504	901	1250	21	16	-48
9505	901	1250	23	16	-45
9506	901	1250	26	20	-41
9507	901	1250	30	23	-36
9508	901	1250	40	30	-26
9509	901	1250	50	36	N.A.
9510	901	1250	70	50	N.A.
9511	901	1250	80	57	20
9512	901	1250	86	60	25
9513	901	1250	100	70	42
9514	901	1250	112	78	52
9515	901	1250	122	83	58
9516	901	1250	140	92	73
9517	901	1250	150	97	78
9518	901	1250	160	105	87
9519	901	1250	190	115	97
9520	901	1250	220	129	114
9521	901	1250	300	128	121
9522	901	1700	10	12	N.A.
9523	901	1700	15	16	-47
9524	901	1700	20	23	-39
9525	901	1700	25	30	-30
9526	901	1700	30	35	-22
9527	901	1700	40	42	-11
9528	901	1700	60	66	24
9529	901	1700	80	88	55
9530	901	1700	100	109	87
9531	901	1700	120	124	110
9532	901	1700	140	144	130
9533	901	1700	160	153	140
9534	901	1700	180	163	151
9535	901	1700	200	170	158
9536	901	1700	250	172	164

Test 9501-9536: The test data is from work by Anderson *et al.* [9]. The target material is Float Glass. The penetration data listed here were obtained from Figure 15 & 16 in Ref. 9.
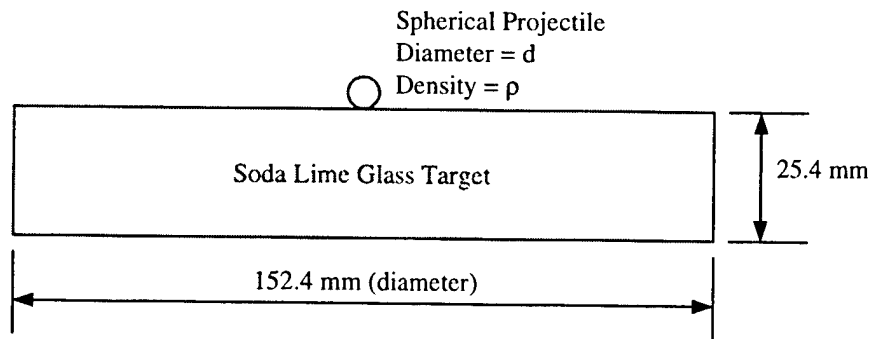
Figure 2.9.5.3 Glass Target and Penetrator Description, Tayler *et al.* [79].
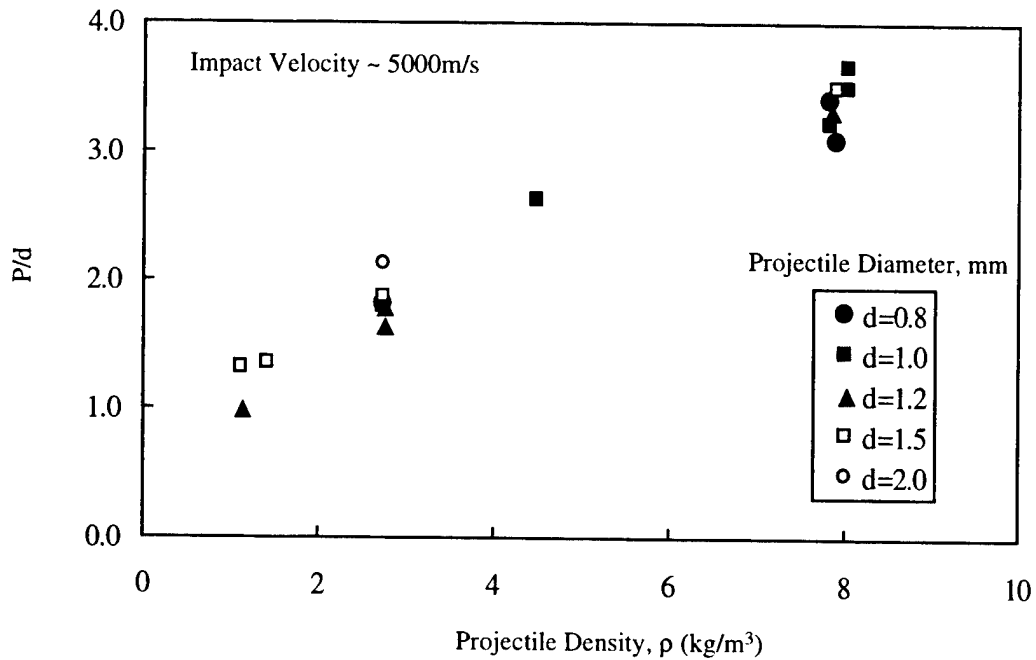

Figure 2.9.5.4 Total Penetration Divided by Projectile Diameter (P/d) vs.
Projectile Density for Various Diameters, Tayler *et al.* [79].

210

Table 2.9.5.2 Summary of Experimental Results, Taylor *et al*. [79].

Glass							
Test Number	Material Number	Impact Velocity (m/s)	Projectile Characteristics			Penetration (mm)	P/d
			Material	Density, ρ (kg/m³)	Diameter, d (mm)		
9537		5370	Nylon	1150	1.2	1.18	0.98
9538		5340	Nylon	1150	1.5	1.95	1.30
9539		5440	Cellulose Acetate	1450	1.5	2.01	1.34
9540		5000	Aluminum alloy 2017	2780	0.8	1.43	1.79
9541		5050	Aluminum alloy 2017	2780	1.0	1.78	1.78
9542		5070	Aluminum alloy 2017	2780	1.2	1.95	1.63
9543		5420	Aluminum alloy 2017	2780	1.2	2.13	1.78
9544		5180	Aluminum alloy 2017	2780	1.5	2.78	1.85
9545		4440	Aluminum alloy 2017	2780	2.0	4.24	2.12
9546		4990	Titanium	4510	1.0	2.62	2.62
9547		4690	Chrome Steel AISI 52100	7830	0.8	2.71	3.39
9548		5000	Chrome Steel AISI 52100	7830	0.8	2.71	3.39
9549		5200	Chrome Steel AISI 52100	7830	1.0	3.20	3.20
9550		5140	Chrome Steel AISI 52100	7830	1.2	3.97	3.31
9551		5000	Stainless Steel AISI 304	7920	0.8	2.46	3.08
9552		4880	Stainless Steel AISI 304	7920	0.8	2.08	2.60
9553		4900	Stainless Steel AISI 304	7920	1.5	5.22	3.48
9554		5010	Stainless Steel AISI 316	8030	1.0	3.49	3.49
9555		5170	Phosphor Bronze	8420	1.0	3.65	3.65

Test 9537-9555: The test data is from work by Taylor *et al*. [79]. The target material is Soda Lime Glass, no other material information was provided. The penetration data listed here were obtained from Figure 8 in Ref. 79.

2.9.6 Depth-Of-Penetration (DOP) Test Data for Glass

This section presents depth-of-penetration (DOP) experiments for Glass materials. The DOP test has been used to investigate the effectiveness of ceramics for a number of years. The typical DOP configuration consists of a ceramic tile placed on, or within, a steel or aluminum base target. A penetrator impacts and perforates the ceramic tile and continues into the base target. The penetration into the base target is generally referred to as the residual penetration, P_r, and is used to determined the ceramic mass efficiency as discussed in Section 2.0.

The target and penetrator descriptions for the DOP experiments by Woodward *et al.* [41] are presented in Figures 2.9.6.1. The objective of the experiments was to investigate glass performance as a function of penetrator geometry. Two experiments were performed and the results are presented in Table 2.9.6.1.
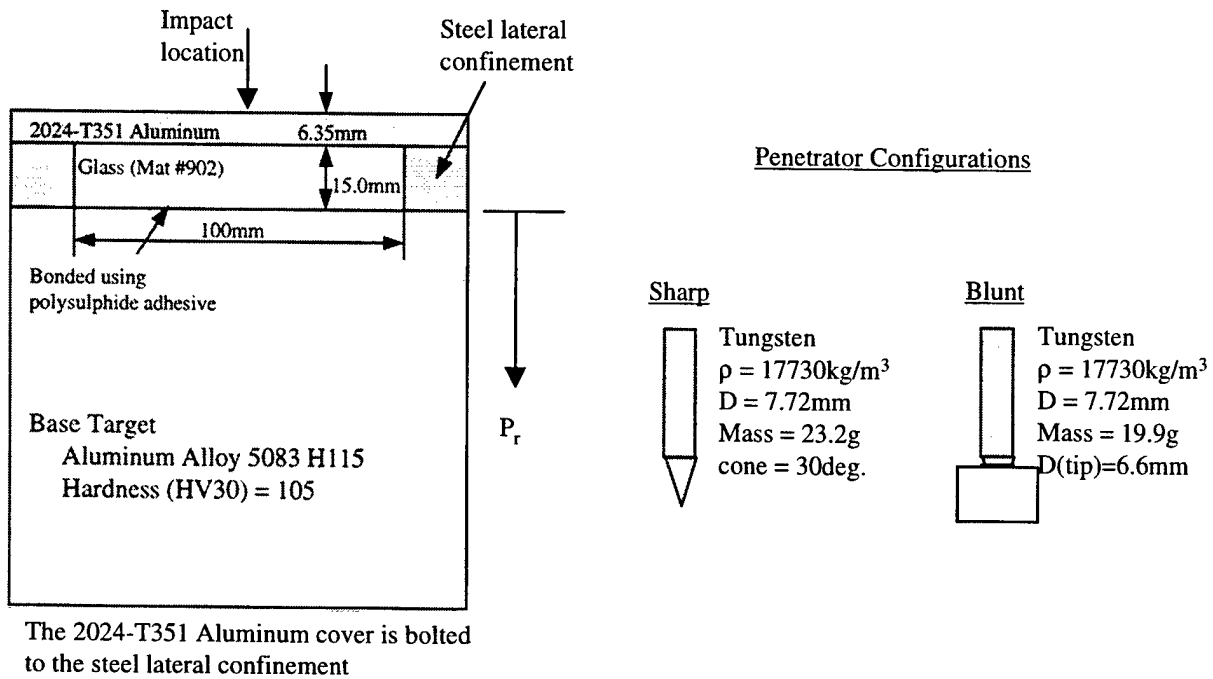
Figure 2.9.6.1 Target and Penetrator Descriptions for DOP Experiments, Woodward *et al.* [41].

Table 2.9.6.1   Tabulated Experimental Results for DOP Tests, Woodward *et al.* [41].

Glass					
Test Number	Material Number	Impact Velocity (m/s)	Penetrator Geometry	P_r (mm)	P* (mm)
9601	902	1209	Sharp	200.0	265
9602	902	1243	Blunt	46.0	75
* This is the semi-infinite penetration into Aluminum. Test 9601-9602: the test data is from work by Woodward *et al.* [41]. The material used is Soda Lime Glass with an initial density = 2500 kg/m³. Two penetrator geometries and one target configuration were investigated.					

2.9.7 Perforation Test Data for Glass

This section presents perforation experiments where the target is usually perforated by the penetrator. Targets are typically comprised of a ceramic front layer and a metallic rear layer and are commonly used in light armor applications. The most common piece of data extracted from perforation experiments is the target ballistic limit, V_{bl}, previously defined in Section 2.0.

The target and penetrator descriptions for the perforation experiments by Senf *et al.* [43] are presented in Figure 2.9.7.1. The objective of the experiments was to determine the effectiveness of glass as a function of glass thickness. Sharp projectiles were shot, at a constant velocity, against a glass target of varying glass thickness. The projectile velocity exiting the target (residual velocity, V_r) was obtained. The results are presented graphically in Figure 2.9.7.2 and summarized in Table 2.9.7.1.
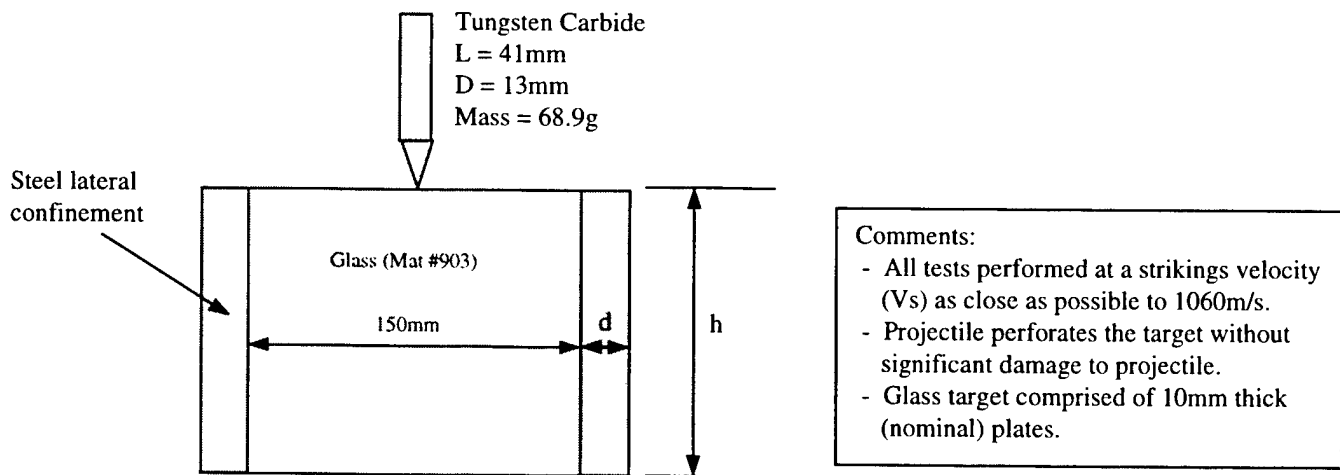
Tungsten Carbide
L = 41mm
D = 13mm
Mass = 68.9g

Steel lateral confinement

Glass (Mat #903)

150mm

d

h

Comments:
- All tests performed at a strikings velocity (Vs) as close as possible to 1060m/s.
- Projectile perforates the target without significant damage to projectile.
- Glass target comprised of 10mm thick (nominal) plates.

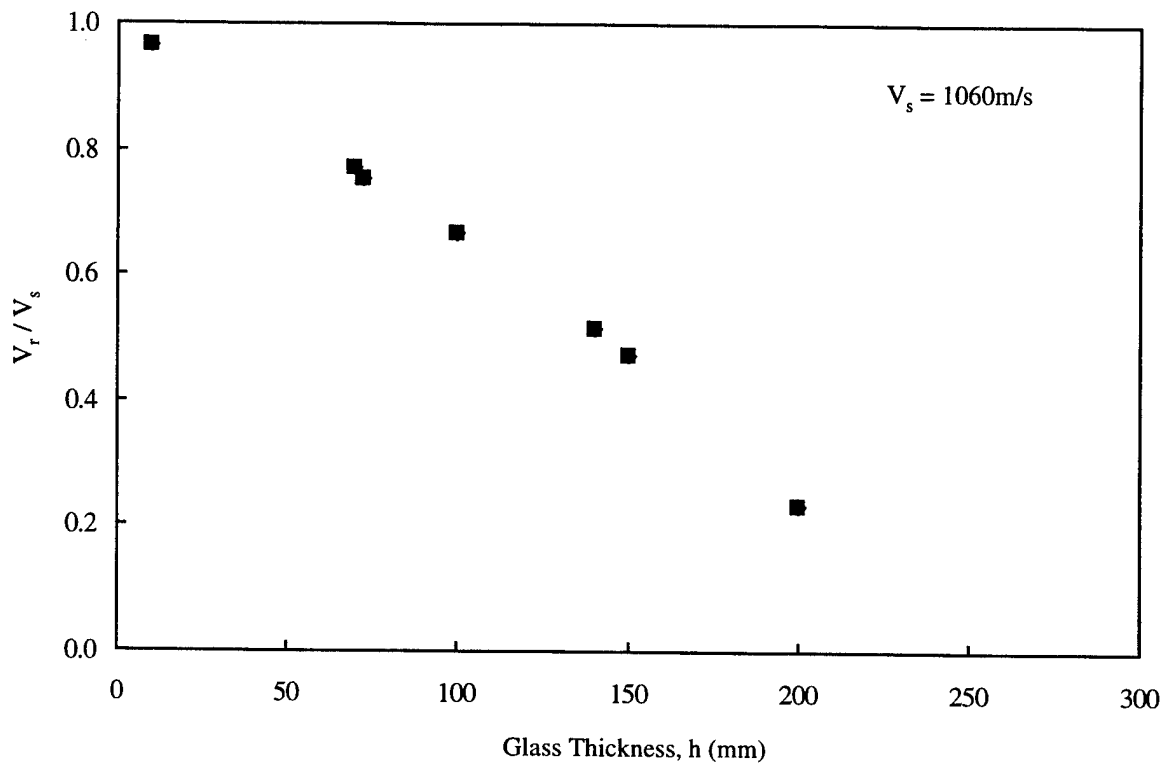Figure 2.9.7.1 Target and Penetrator Descriptions for Perforation Experiments, Senf *et al.* [43].

214

Figure 2.9.7.2 Experimental Results for Perforation Tests Senf *et al.* [43]. Shown here is residual velocity, V_r, divided by the Impact velocity, V_s, as a function of glass thickness, h.

Table 2.9.7.1 Tabulated Experimental Results for Perforation Tests, Senf *et al.* [43].

Glass					
Test Number	Material Number	Impact Velocity V_s (m/s)	Target Configuration		Residual Velocity V_r (m/s)
			h (mm)	d (mm)	
9701	903	1060	10	20	1025
9702	903	1060	70	20	820
9703	903	1060	70	0	820
9704	903	1060	73	20	800
9705	903	1060	100	20	705
9706	903	1060	140	20	545
9707	903	1060	140	0	545
9708	903	1060	150	20	500
9709	903	1060	200	20	245
Test 9701-9709: the test data is from work by Senf *et al.* [43]. The material used is Float Glass with an initial density = 2500 kg/m³. The residual velocity listed here was obtained from Reference 43 Figure 4.					

215

3.0 REFERENCES

1. W. H. Gust, A. C. Holt and E. B. Royce, "Dynamic Yield, Compression, and Elastic Parameters for Several Lightweight Intermetallic Compounds", *Journal of Applied Physics*, Vol. 44, No. 2, February, 1973.

2. W. A. Bassett, M. S. Weathers, T. C. Wu and T. J. Holmquist, "Compressibility of SiC up to 68.4 GPa," *Journal of Applied Physics*, Vol. 74, No. 6, September, 1993.

3. J. Lankford, "The role of Subcritical Tensile Microfracture Processes in Compression Failure of Ceramics," *Fracture Mechanics of Ceramics*, Vol. 5, 1983, pp. 625-637.

4. C. E. Anderson, Jr., P. E. O'Donoghue, J. Lankford and J. D. Walker, "Numerical Simulations of SHPB Experiments for the Dynamic Compressive Strength and Failure of Ceramics," *International Journal of Fracture*, Vol. 55, 1992, pp. 193-208.

5. J. Lankford, "Uniaxial Compressive Damage in a-SiC at Low Homologous Temperatures," *Journal of the American Ceramic Society-Discussions and Notes*, Vol. 62, No. 5-6, 1979, pp. 310-312.

6. D. L. Orphal and R. R. Franzen, "Penetration of Confined Silicon Carbide Targets by Tungsten Long Rods at Impact Velocities from 1.5 to 4.6 km/s," *International Journal of Impact Engineering*, Vol. 19, No. 1, 1997, pp.1-13.

7. T. J. Holmquist, G. R. Johnson, D. E. Grady, C. M. Lopatin and E. S. Hertel Jr., "High Strain Rate Properties and Constitutive Modeling of Glass," *Proceedings of Fifteenth International Symposium on Ballistics*, Jerusalem, Israel, May 1995.

8. J. Rodriguez, C. Navarro and V. Sanchez-Galvez, "Splitting Tests: An Alternative to Determine the Dynamic Tensile Strength of Ceramic Materials," *Journal De Physique IV*, Colloque C8, Vol. 4, September 1994, pp. 101-106.

9. C. E. Anderson, Jr., V. Hohler, J. D. Walker and A. J. Stilp, "Penetration of Long Rods into Steel and Glass Targets: Experiments and Computations," *Proceedings of Fourteenth International Symposium on Ballistics*, Quebec, Canada, September 1993.

10. J. Lankford, "Comparative Study of the Temperature Dependence of Hardness and Compressive Strength in Ceramics," *Journal of Material Science*, Vol. 18, 1983, pp.1666-1674.

11. R. Arrowood and J. Lankford, "Compressive Fracture Processes in an Alumina-Glass Composite," *Journal of Material Science*, Vol. 22, 1987, pp.3737-3744.

12. D. J. Steinberg, "Computer Studies of the Dynamic Strength of Ceramics," *Journal De Physique IV*, Colloque C3, Vol. 1, October 1991, pp. 837-844.

13. H. C. Heard and C. F. Cline, "Mechanical Behaviour of Polycrystalling BeO, Al_2O_3 and AlN at High Pressure," *Journal of Materials Science*, Vol. 15, 1980, pp. 1889-1897.

14. M. Adams and G. Sines, "Determination of Biaxial Compressive Strength of a Sintered Alumina Ceramic," Journal of the American Ceramic Society, Vol. 59, No. 7-8, 1976, pp. 300-304.

15. P. W. Bridgman, "Linear Compressions to 30,000kg.cm2, Including Relatively Incompressible Substances," *Proceedings of the American Academy of Arts and Sciences*, Vol. 77, No. 7, 1949, pp.189-234.

16. H. V. Hart and H. G. Drickamer, "Effect of High Pressure on the Lattice Parameters of Al_2O_3," *Journal of Chemical Physics*, Vol. 43, No. 7, 1965, pp.2265-2266.

17. Y. Sato and S. Akimoto, "Hydrostatic Compression of Four Corundum-Type Coumpounds: α-Al_2O_3, V_2O_3, Cr_2O_3 and α-Fe_2O_3," *Journal of Applied Physics*, Vol. 50, No. 8, 1979, pp. 5285-5291.

18. Q. Xia, H. Xia and A. Ruoff, "Pressure-Induced Rocksalt Phase of Aluminum Nitride: A Metastable Structure at Ambient Condition," *Journal of Applied Physics*, Vol. 73, No. 12, June 1993, pp. 8198-8200.

19. J. Akella, Unpublished Data, Lawrence Livermore National Laboratory, 1991.

20. D. Steinberg, "Computer Studies of the Dynamic Strength of Ceramics (II)," *Journal De Physique IV*, Colloque C8, Vol. 4, September 1994, pp. 183-188.

21. D. L. Orphal, R. R. Franzen, A. J. Piekutowski and M. J. Forrestal, "Penetration of Confined Aluminum Nitride Targets by Tungsten Long Rods at 1.5-4.5 km/s," *International Journal of Impact Engineering*, Vol. 18, No. 4, 1996, pp. 355-368.

22. D. L. Orphal, R. R. Franzen, A. C. Charters, T. L. Menna and A. J. Piekutowski, "Penetration of Confined Boron Carbide Targets by Tungsten Long Rods at Impact Velocities from 1.5 to 5.0 km/s," *International Journal of Impact Engineering*, Vol. 19, No. 1, 1997, pp. 15-29.

23. M. L. Wilkins, C. Honodel and D. Sawle, "An Approach to the Study of Light Armor," *Lawrence Livermore National Laboratory* Report UCRL-50284 (1967).

24. M. L. Wilkins, "Second Progress Report of Light Armor Program," *Lawrence Livermore Laboratory* Report UCRL-50349, Revision 1 (1976).

25. M. L. Wilkins, "Third Progress Report of Light Armor Program," *Lawrence Radiation Laboratory* Report UCRL-50460 (1968).

26. M. L. Wilkins, C. F. Cline and C. A. Honodel, "Fourth Progress Report of Light Armor Program," *Lawrence Radiation Laboratory* Report UCRL-50694 (1969).

27. M. L. Wilkins, R. L. Landingham and C. A. Honodel, "Fifth Progress Report of Light Armor Program," *Lawrence Radiation Laboratory* Report UCRL-50980 (1971).

28. M. L. Wilkins, "Mechanics of Penetration and Perforation," *International Journal of Engineering Science*, Vol. 16, 1978, pp. 793-807.

29. T. J. Ahrens, "Material Strength Effect in the Shock Compression of Alumina," *Journal of Applied Physics,* Vol. 39, No. 10, 1968, pp. 4610-4616.

30. W. H. Gust and E. B. Royce, "Dynamic Yield Strengths of B4C, BeO, and Al_2O_3 Ceramics," *Journal of Applied Physics*, Vol. 42, No. 1, 1971, pp.276-295.

31. C. E. Anderson Jr., and S. A. Royal-Timmons, "Ballistic Performance of Confined 99.5%-Al2O3 Ceramic Tiles," *International Journal of Impact Engineering*, Vol. 19, No. 8, 1997, pp. 703-713.

32. S. J. Bless, Z. Rosenberg and B. Yoon, "Hypervelocity Penetration of Ceramics," *International Journal of Impact Engineering*, Vol. 5, 1987, pp. 165-171.

33. R. R. Franzen, D. L. Orphal and C. E. Anderson Jr., "The Influence of Experimental Design on Depth-Of-Penetration (DOP) Test Results and Derived Ballistic Efficiencies," *International Journal of Impact Engineering*, Vol. 19, No. 8, 1997, pp. 727-737.

34. P. Lundberg, L. Westerling and B. Lundberg, "Influence of Scale on the Penetration of Tungsten rods into Steel-Backed Alumina Targets," *International Journal of Impact Engineering*, Vol. 18, No. 4, 1996, pp. 403-416.

35. L. Westerling, P. Lundberg, L. Holmberg and B. Lundberg, "High Velocity Penetration of Homogeneous, Segmented and Telescopic Projectiles into Alumina Targets," *International Journal of Impact Engineering*, Vol. 20, 1997, pp. 817-827.

36. C. E. Anderson, Jr., S. A. Mullin, A. J. Piekutowski, N. W. Blaylock and K. L. Poormon, "Scale Model Experiments with Ceramic Laminate Targets," *International Journal of Impact Engineering*, Vol. 18, No. 1, 1996, pp. 1-22.

37. V. Hohler, A. J. Stilp and K. Weber, "Hypervelocity Penetration of Tungsten Sinter-Alloy Rods into Alumina," *International Journal of Impact Engineering*, Vol. 17, 1995, pp. 409-418.

38. Z. Rosenberg and Y. Yeshurun, "Determination of the Dynamic Response of AD-85 Alumina with In-Material Manganin Gauges," *Journal of Applied physics*, Vol. 58, No. 8, 1985, pp. 3077-3080.

39. Z. Rosenberg and J. Tsaliah, 'Applying Tate's Model for the Interaction of Long Rod Projectiles with Ceramic Targets," *International Journal of Impact Engineering*, Vol. 9, No. 2, 1990, pp. 241-251.

40. R. L. Woodward and B. J. Baxter, "Ballistic Evaluation of Ceramics: Influence of Test Conditions," *International Journal of Impact Engineering*, Vol. 15, No. 2, 1994, pp. 119-124.

41. R. L. Woodward, W. A. Gooch, Jr, R. G. O'Donnell, W. J. Perciballi, B. J. Baxter and S. D. Pattie, "A Study of Fragmentation in the Ballistic Impact of Ceramics," *International Journal of Impact Engineering*, Vol. 15, No. 5, 1994, pp. 605-618.

42. R. Subramanian and S. J. Bless, "Penetration of Semi-Infinite AD995 Alumina Targets by Tungsten Long Rod Penetrators from 1.5 to 3.5 km/s," *International Journal of Impact Engineering*, Vol. 17, 1995, pp. 807-816.

43. H. Senf, H. Rothenhausler, w. Pavel, H. J. Raatschen and R. Schwarz, "Analysis of Experimental and Numerical Investigations with Rigid Projectiles Impacting Glass Targets of Differing Physical Quality," *Journal De Physique*, Colloque C3, September 1988, pp. 319-325.

44. H. Nahme, V. Hohler and A. Stilp, "Dynamic Material Properties and Terminal Ballistic Behavior of Shock-Loaded Silicon-Nitride Ceramics," *Journal De Physique IV*, Colloque C8, vol. 4, September 1994, pp. 237-242.

45. C. E. Anderson, Jr., B. L. Morris and D. L. Littlefield, "A Penetration Mechanics Database," SwRI Report 3593/001, January 1992.

46. J. Lankford, Unpublished Data, Southwest Research Institute.

47. Z. Rosenberg, D. Yaziv and S. Bless, "Spall Strength of Shock-Loaded Glass," *Journal of Applied Physics*, Vol. 58, No. 8, 1985, pp. 3249-3251.

48. D. P. Dandekar and P. Bartkowski, "Shock Response of AD995 Alumina," *High Pressure Science and Technology-1993*, edited by S. C. Schmidt, J. W. Shaner, G. A. Samara and M. Ross, AIP Press, 1994, pp. 733-736.

49. H. Nahme, V. Hohler and A. Stilp, "Determination of the Dynamic Material Properties of Shock Loaded Silicon-Nitride," *High Pressure Science and Technology-1993*, edited by S. C. Schmidt, J. W. Shaner, G. A. Samara and M. Ross, AIP Press, 1994, pp. 733-736.

50. Z. Rosenberg, D. Yaziv, Y. Yeshurun and S. J. Bless, "Shear Strength of Shock-Loaded Alumina as Determined with Longitudinal and Transverse Manganin Gauges," *Journal of Applied Physics*, Vol. 62, No. 3, 1987, pp. 1120-1122.

51. Z. Rosenberg, N. S. Brar andS. J. Bless, "Dynamic High-Pressure Properties of AlN Ceramic as Determined by Flyer Plate Impact," *Journal of Applied Physics*, Vol. 70, No. 1, 1991, pp. 167-171

52. D. E. Grady and R. L. Moody, "Shock Compression Profiles in Ceramics," Sandia National laboratory Report, SAND96-0551, March 1996.

53. M. E. Kipp and D. E. Grady, "Shock Phase Transformation and Release Properties of Aluminum Nitride," *Journal De Physique IV*, Colloque C8, Vol. 4, September 1994, pp. 249-256.

54. D. E. Grady, "Dynamic Properties of Ceramic Materials," Sandia National laboratory Report, SAND94-3266, February 1995.

55. M. E. Kipp and D. E. Grady, "Shock Compression and Release in High-Strength Ceramics," Sandia National laboratory Report, SAND89-1461, July 1989.

56. D. E. Grady, "Shock-Wave Strength Properties of Boron Carbide and Silicon Carbide," *Journal De Physique IV*, Colloque C8, Vol. 4, September 1994, pp. 385-391.

57. D. E. Grady and J. L. Wise, "Dynamic Properties of Ceramic Materials," Sandia National laboratory Report, SAND93-0610, September 1993.

58. M. E. Kipp, D. E Grady and J. L. Wise, "Planar-Shock and Penetration Response of Ceramics," *Shock Wave and High-Strain-Rate Phenomena in Materials*, 1992.

59. D. P. Dandekar and D. C. Benfanti, "Strength of Titanium Diboride Under Shock Wave Loading," *Journal of Applied Physics*, Vol. 73, No. 2, 1993, pp. 673-679.

60. D. P. Dandekar, "Shear Strength of Aluminum Nitride and Titanium Diboride under Plane Shock Wave Compression," *Journal De Physique IV*, Colloque C8, Vol. 4, September 1994, pp. 379-384.

61. D. P. Dandekar, "Response of Ceramics Under Shock Wave Loading," *High Pressure Science and Technology-1993*, edited by S. C. Schmidt, J. W. Shaner, G. A. Samara and M. Ross, AIP Press, 1994, pp. 729-732.

62. A. N. Dremin and G. A. Adadurov, "The Behavior of Glass Under Dynamic loading," *Soviet Physics-Solid State*, Vol. 6, No. 6, December 1964, pp. 1379-1384.

63. D. P. Dandekar, A. Abbate and J. Frankel, "Equation of State of Aluminum Nitride and its Shock Response," *Journal of Applied Physics*, Vol. 76, No. 7, 1994, pp. 4077-4085.

64. D. Yaziv and N. S. Brar, "Shock Wave Study of Titanium Diboride," *Journal De Physique*, Colloque C3, September 1988, pp. 683-687.

65. Z. Rosenberg, N. S. Brar and S. J. Bless, "Elastic Precurser Decay in Ceramics as Determined with Manganin Stress Gauges," *Journal De Physique*, Colloque C3, September 1988, pp. 707-711.

66. D. Yaziv and Y. Partom, "The Ballistic Efficiency of Thick Alumina Targets against Long Rod Penetrators," *Proceedings of Fourteenth International Symposium on Ballistics*, Quebec, Canada, September 1993, pp. 331-340.

67. N. L. Rupert and F. I. Grace, "Penetration of Long Rods into Semi-Infinite, Bi-Element Targets," *Proceedings of Fourteenth International Symposium on Ballistics*, Quebec, Canada, September 1993, pp. 469-478.

68. D. Yaziv, G. Rosenberg and Y. Partom, "Differential Ballistic Efficiency of Applique Armor," *Proceedings of 9th International Symposium on Ballistics*, Royal Military College of Science, Shrivenham, April 1986, pp. 315-319.

69. E. Strassburger, H. Senf and H. Rothenhausler, "Fracture Propagation During Impact in Three Types of Ceramics," *Journal De Physique IV*, Colloque C8, Vol. 4, September 1994, pp. 653-658.

70. J. L. Wise and D. E. Grady, "Dynamic, Multiaxial Impact Response of Confined and Unconfined Ceramic Rods," *High Pressure Science and Technology-1993*, edited by S. C. Schmidt, J. W. Shaner, G. A. Samara and M. Ross, AIP Press, 1994, pp. 777-780.

71. M. Ueno, A. Onodera, O. Shimomura and K. Takemura, "X-Ray Observation of the Structural Phase Transition of Aluminum Nitride Under High Pressure," *Physical Review B*, Vol. 45, No. 17, 1992, pp. 10123-10126.

72. A. Nakamura, T. Mashimo and M. Kodama, "Shock Compression of AlN Ceramics," *Mechanical Behaviour of Materials-VI*, edited by M. Jono and T. Inoue, Pergamon Press, 1992, pp. 395-400.

73. S. J. Bless, d. Yaziv and Z. Rosenberg, "Spall Zones in Polycrystalline Ceramics," *Shock Waves in Condensed Matter*, edited by Y. M. Gupta, Plenum Press, 1986, pp.419-424.

74. Material Properties Standard 990, Coors Ceramics Company, Golden Colorado, 1989.

75. *LASL Shock Hugoniot Data*, edited by S. P. Marsh, University of California Press, 1980.

76. M. E. Kipp and D. E. Grady, "Elastic Wave Dispersion in High-Strength Ceramics," *Shock Compression of Condensed Matter*, edited by S. C. Schmidt, R. D. Dick, J. W. Forbes and D. G. Tasker, Elsevier Science , 1992, pp. 456-462.

77. M. E. Kipp and D. E. Grady, "Shock Compression and Release in High-Strength Ceramics," *Shock Compression of Condensed Matter-1989*, edited by S. C. Schmidt, J. N. Johnson and L. W. Davison, Elsevier Science , 1990, pp. 377-380.

78. P. C. den Reijer, "Impact on Ceramic Faced Armour," PhD Thesis, Technical University, Delft, Netherlands, November, 1991.

79. E. A. Taylor, K. Tsembelis, C. J. Hayhurst, L. Kay and M. J. Burchell, "Hydrocode Modeling of hypervelocity Impact on Brittle Materials: Depth of Penetration and Conchoidal Diameter," *International Journal of Impact Engineering*, to be published in 1999.

80. S. J. Bless, N. S. Brar and A. Rosenberg, "Strength of Soda Lime Glass under Shock Compression," *Shock Waves in Condensed Matter-1987*, edited by S. C. Schmidt and N. C. Holmes, Elsevier Science , 1988, pp. 309-312.

81. W. Winkler and A. J. Stilp, "Spallation Behavior of TiB$_2$, SiC, and B$_4$C under Planar Impact Tensile Stresses," *Shock Compression of Condensed Matter-1991*, edited by S. C. Schmidt, R. D. Dick, J. W. Forbes and D. G. Tasker, Elsevier Science Publishers, 1992, pp. 475-478.

82. W. Winkler and A. J. Stilp, "Pressure Induced Macro- and Micromechanical Phenomena in Planar Impacted TiB$_2$," *Shock Compression of Condensed Matter-1991*, edited by S. C. Schmidt, R. D. Dick, J. W. Forbes and D. G. Tasker, Elsevier Science Publishers, 1992, pp. 555-558.

83. W. Chen and G. Ravichandran, "Static and Dynamic Compressive Behavior of Aluminum Nitride under Moderate Confinement," *Journal of the American Ceramic Society*, Vol. 79, No. 3, 1996, pp. 579-584.

84. G. Subhash and G. Ravichandran, "Mechanical Behaviour of a Hot Pressed Aluminum Nitride under Uniaxial Compression", *Journal of Material Science*, Vol. 33, 1998, pp. 1933-1939.

85. J. E. Reaugh, A. C. Holt, M. L. Wilkins, B. J. Cunningham, B. L. Hord and A. S. Kusubov, "Impact Studies of Five Ceramic Materials and Pyrex," to be published in *International Journal of Impact Engineering*, 1999.

86. N. J. Lynch, "Constant Kinetic Energy Impacts of Scale Size KE Projectiles at Ordnance and Hypervelocity," to be published in *International Journal of Impact Engineering*, 1999.

87. Z. Rosenberg, N. S. Brar and S. J. Bless, "Shear Strength of Titanium Diboride Under Shock Loading Measured by Transverse Manganin Gauges," *Shock Compression of Condensed Matter-1991*, edited by S. C. Schmidt, R. D. Dick, J. W. Forbes and D. G. Tasker, Elsevier Science Publishers, 1992, pp. 471-473.

88. L. W. Meyer and I. Faber, "Investigations on Granular Ceramics and Ceramic Powder," *Journal De Physique IV*, Colloque C3, Vol. 7, 1997, pp. 565-570.

89. P. Lundberg, L. Holmberg and B. Janzon, "An Experimental Study of Long Rod Penetration into Boron Carbide at Ordnance and Hyper Velocities," *Proceedings of 17th International Symposium on Ballistics*, Midrand, South Africa, March 1998, pp. 251-258.

90. N. S. Brar, Z. Rosenberg and S. J. Bless, "Applying Steinberg's Model to the Hugoniot Elastic Limit of Porous Boron Carbide Specimens," *Shock Compression of Condensed Matter-1991*, edited by S. C. Schmidt, R. D. Dick, J. W. Forbes and D. G. Tasker, Elsevier Science Publishers, 1992, pp. 467-470.

91. Z. Rosenberg, E. Dekel, V. Hohler, A. J. Stilp and K. Weber, "Penetration of Tungsten-Alloy rods into Composite Ceramic Targets: Experiments and 2-D Simulations," *Shock Compression of Condensed Matter-1997*, edited by S. C. Schmidt, D. Dandekar and J. W. Forbes, The American Institute of Physics, 1998, pp. 917-920.

92. I. M. Pickup and A. K. Barker, "Damage Kinetics in Silicon Carbide," *Shock Compression of Condensed Matter-1997*, edited by S. C. Schmidt, D. Dandekar and J. W. Forbes, The American Institute of Physics, 1998, pp. 513-516.

93. R. Feng, Y. M. Gupta and G. Yuan, "Dynamic Strength and Inelastic Deformation of Ceramics Under Shock Wave loading," *Shock Compression of Condensed Matter-1997*, edited by S. C. Schmidt, D. Dandekar and J. W. Forbes, The American Institute of Physics, 1998, pp. 483-488.

94. R. Feng, G. F. Raiser and Y. M. Gupta, "Shock Response of Polycrystalline Silicon Carbide Undergoing Inelastic Deformation," *Journal of Applied Physics*, Vol. 79, No. 3, February, 1996, pp. 1378-1387.

95. N. Bourne, J. Millett and I. Pickup, "Delayed Failure in Shocked Silicon Carbide," *Journal of Applied Physics*, Vol. 81, No. 9, May, 1997.

96. J. Akella, Personnel Communication, Lawrence Livermore National Laboratory, January, 1999.

4.0 DISTRIBUTION LIST

NO. OF COPIES	ORGANIZATION	NO. OF COPIES	ORGANIZATION
2	DEFENSE TECHNICAL INFORMATION CENTER DTIC DDA 8725 JOHN J KINGMAN RD STE 0944 FT BELVOIR VA 22060-6218	1	DPTY ASSIST SCY FOR R & T SARD TT THE PENTAGON RM 3E479 WASHINGTON DC 20310-0103
1	HQDA DAMO FDQ DENNIS SCHMIDT 400 ARMY PENTAGON WASHINGTON DC 20310-0460	3	DARPA L STOTTS J PENNELLA B KASPAR 3701 N RAIRFAX DR ARLINGTON VA 22203-1714
1	CECOM SP &TRRSTRL COMMCTN DIV AMSEL RD ST MC M H SOICHER FT MONMOUTH NJ 07703-5203	1	DIRECTOR US ARMY RESEARCH LAB AMSRL CS AL TP 2800 POWDER MILL RD ADELPHI MD 20783-1145
1	PRIN DPTY FOR TCHNLGY HQ US ARMY MATCOM AMCDCG T R PRICE 5001 EISENHOWER AVE ALEXANDRIA VA 22333-0001	1	DIRECTOR US ARMY RESEARCH LAB AMSRL CS AL TA 2800 POWDER MILL RD ADELPHI MD 20783-1145
1	PRIN DPTY FOR ACQUSTN HQS US ARMY MATCOM AMCDCG A D ADAMS 5001 EISENHOWER AVE ALEXANDRIA VA 22333-0001	1	DIRECTOR US ARMY RESEARCH LAB AMSRL CI LL 2800 POWDER MILL RD ADELPHI MD 20783-1145
1	DPTY CG FOR RDE HQS US ARMY MATCOM AMCRD 5001 EISENHOWER AVE ALEXANDRIA VA 22333-0001	3	DIRECTOR US ARMY ARDEC AMSTA AR FSA E W P DUNN J PEARSON E BAKER PICATINNY ARSENAL NJ 07806-5000
1	ASST DPTY CG FOR RDE HQS US ARMY MATCOM AMCRD COL S MANESS 5001 EISENHOWER AVE ALEXANDRIA VA 22333-0001	7	US ARMY TARDEC K BISHNOI (5 CPS) D TEMPLETON J THOMPSON AMSTA TR R MS 263 WARREN MI 48397-5000
2	AIR FORCE ARMAMENT LAB AFATL DLJW W COOK D BELK J FOSTER EGLIN AFB FL 32542	1	JET PROPULSION LAB M ADAMS IMPACT PHYSICS GROUP 4800 OAK GROVE DR PASADENA CA 91109

NO. OF COPIES	ORGANIZATION	NO. OF COPIES	ORGANIZATION

1	ALLIANT TECHSYSTEMS INC
	G R JOHNSON MN11 1614
	600 SECOND ST NE
	HOPKINS MN 55343
		14	DIR, USARL
			AMSRL-WM-TD
			  A M DIETRICH
			  M RAFTENBERG
			  M SCHEIDLER
			  T WRIGHT
			  A RAJENDRAN (5 COPIES)
			  D GROVE (5 COPIES)
			ABERDEEN PROVING GROUND
			ABERDEEN MD 21005-5065

1	COMPUTATIONAL MECHANICS CONSULTANTS J A ZUKAS PO BOX 11314 BALTIMORE MD 21239-0314		
4	INST OF ADVANCED TECHNOLOGY UNIVERSITY OF TX AUSTIN S J BLESS J CAZAMIAS S SATAPATHY D LITTLEFIELD 4030-2 W BRAKER LN AUSTIN TX 78759	1	DERA N J LYNCH WEAPON SYSTEMS BUILDING A20 DRA FORT HALSTEAD SEVENOAKS KENT TN14 7BP
		1	APPLIED RESEARCH ASSOCIATES D E GRADY 4300 SAN MATEO BLVD NE SUITE A-220 ALBUQUERQUE NM 87110
1	KAMAN SCIENCES CORP D L JONES 2560 HUNTINGTON AVE SUITE 200 ALEXANDRIA VA 22303		
1	KAMAN SCIENCES CORP J S WILBECK 600 BLVD S SUITE 208 HUNTSVILLE AL 35802	1	INTERNATIONAL RESEARCH ASSOCIATES INC. D L ORPHAL 4450 BLACK AVENUE PLEASANTON CA 94566

12	DIR, USARL
	AMSRL-WM, I. MAY
	AMSRL-WM-TA
	  J DEHN
	  TOM HAVEL
	  MIKE NORMANDIA
	  W A GOOCH
	  H W MEYER
	  E HORWALT
	AMSRL-WM-TC
	  K KIMSEY
	  D SCHEFLER
	  R COATES
	AMSRL-WM-PD G GAZONAS
	AMSRL-WM-WD A PRAKASH
	ABERDEEN PROVING GROUND
	ABERDEEN MD 21005-5069
		4	ERNST MACH INTITUT
			VOLKER HOHLER
			E SCHMOLINSKE
			E SCHNEIDER
			W RIEDEL
			ECKERSTRASSE 4
			D-7800 FREIBURG I BR 791 4
			GERMANY

		1	JET PROPULSION LAB M ADAMS IMPACT PHYSICS GROUP 4800 OAK GROVE DR PASADENA CA 91109
		1	THE DOW CHEMICAL CO M EL-RAHEB CENTRAL RESEARCH ENGINEERING LAB BUILDING 1776 MIDLAND MI 48640

NO. OF
COPIES   ORGANIZATION

1   S R SKAGGS
        BOB SKAGGS CONSULTANT
        79 COUNTY RD 117 SOUTH
        SANTA FE NM 87501

1   J L DING
        SCHOOL OF MECHANICAL
        AND MATERIAL ENGINEERING
        WASHINGTON ST UNIVERSITY
        PULLMAN WA 99164-2920

1   Y M GUPTA
        INSTITUTE FOR SHOCK PHYSIC
        WASHINGTON ST UNIVERSITY
        PULLMAN WA 99164-2814

1   FOA 2
        PATRIK LUNDBERG
        S-14725 TUMBA
        SWEDEN

1   N H MURRAY
        PCS GROUP
        CAVENDISH LABORATORY
        MADINGLEY RD
        CAMBRIDGE
        UNITED KINGDOM

1   COORS CERAMIC COMPANY
        TOM RILEY
        600 NINTH STREET
        GOLDEN CO 80401

1   J Y TRANCHET
        CENTRE D'ETUDES DE GRAMAT
        46500 GRAMAT
        FRANCE

1   D KRAVCINOVIC
        MECHANICAL AND AEROSPACE
        ENGINEERING
        ARIZONA STATE UNIVERSITY
        TEMPE AZ 85287-6106

1   C HARI SIMHA
        UNIVERSITY OF DAYTON
        RESEARCH INSTITUTE
        300 COLLEGE PARK
        MS SPC 1911
        DAYTON OH 45469